# Provenance and palaeoclimate study of Palaeoproterozoic basal Gulcheru Formation of Cuddapah Basin, Andhra Pradesh, India

THESIS SUBMITTED FOR THE DEGREE OF DOCTOR OF PHILOSOPHY (SCIENCE), JADAVPUR UNIVERSITY

**Saurav Jana**

**Department of geological sciences**

**Jadavpur university**

**Kolkata**

**2022**

## CERTIFICATE FROM THE SUPERVISOR(S)

This is to certify that the thesis entitled "**Provenance and palaeoclimate study of Palaeoproterozoic basal Gulcheru Formation of Cuddapah Basin, Andhra Pradesh, India**" submitted by **Shri Saurav Jana**, who got his name registered on 31.03.2014 for the award of **Ph. D (Science) degree of Jadavpur University**, is absolutely based upon his own work under the supervision of **Dr. Gopal Chakrabarti** and **Dr. Debasish Shome** and that neither the thesis nor any part of it has been submitted for either any degree/diploma or any other academic award anywhere before.

Debasish Shome.
29.06.2022

DR. DEBASISH SHOME
Professor (Retd.)
Dept. of Geological Sciences
Jadavpur University, Kolkata - 700 032

29/06/2022

DR. GOPAL CHAKRABARTI, WBES
Joint Director of Public Instruction
Scholarship and Stipend
Government of West Bengal

TO

MY LATE FATHER

# Acknowledgements

I would like to express warmest sense of gratitude to Dr. Debasish Shome, retired Professor in Geology, Jadavpur University and Dr. Gopal Chakrabarti, Associate Professor of Geology, WBES (offering as Joint Director of Public Instruction (S&S), Education Directorate, Govt. Of West Bengal) for their guidance and advice carried me through all stages of my project. Sincere thanks are also being accorded to Dr. C. Manikyamba, Senior Principal Scientist, NGRI and Dr. J.S. Armstrong-Altrin for their valuable support for my Ph.D. work. I would also like to thanks my teachers for their encouragement and assistance. I would also like to special thanks to teaching and non-teaching staff of the Jadavpur University for their kind co-operation and help. Also, I express my gratitude to University Grant Commission [Grant no-5-442007(BSR)] for financial assistance. I would like to extend a big thanks to my fellow labmates (Dr. Subhasish Kumar, Dr. Madhumita Panja, Dr. Suparna Bose, Dr. Rahul Mitra and Miss. Adrika Roy) for their continuous support.

“And speaking of stones, what about
The little ones you can
Hold in your hands, their heartbeats
So secret, so hidden it may take years

Before, finally, you hear them?”
— **Mary Oliver, Swan: Poems and Prose Poems**

# ABSTRACT

The basal Paleoproterozoic Gulcheru Formation (30-200m thick) of Papaghni Group of rocks, Cuddapah Basin, India is composed of thin conglomerate and multi-storey thick quartzite with grey shales as interbeds from base to top. The entire succession sits on the Archaean gneiss with profound unconformity in the Eastern Dharwar Craton (EDC). The present work focuses on sedimentological and geochemical studies on the Palaeoproterozoic Gulcheru Formation, Papaghni Group belonging to Cuddapah Supergroup of the Papaghni Sub-basin of Proterozoic Cuddapah Basin, in an around Kanampalli (78˚05'25.18" E, 14˚25'13.60"N), Pendllimari (78˚36'43" E, 14˚24'55.2"N) and Gandi (14°18´25.34″ N, 78°28´ 36.52″ E) areas, Andhra Pradesh, India. Three stratigraphic sections, each from each aforesaid area are measured for sedimentological and geochemical studies. Eleven facies are identified from the studied sections as under: Facies A: Clast supported poorly sorted breccia; Facies B:Clast supported conglomerate; Facies C: Stacked couplets of clast supported conglomerate and sandstone; Facies D:Medium to coarse grained trough cross stratified sandstone; Facies E: Medium to coarse grained tabular cross-bedded sandstone; Facies F: Fine to medium grained ripple laminated sandstone; Facies G: Fine to medium grained tabular cross-bedded sandstone; Facies H: Fine to medium grained massive sandstone with coarse basal lag; Facies I: Fine grained planar laminated sandstone; Facies J: Fine to Medium grained trough cross-stratified sandstone; Facies K: Rhythmite. Facies associations along with associated sedimentary structures like ripple marks, cross-bedding, pin-stripe lamination, herringbone cross-strata, tidal bundles and double mud drape demonstrate that the Gulcheru Formation lithology is deposited in alluvial-fan, ephemeral braided stream, aeolian and low gradient tidal flat environment under extensional setting in semi-arid climatic set-up. Major oxides, trace and rare earth element (REE) elemental abundance gives significant information about (a) source

rock including paleo-environment condition, (b) tectonic setting during deposition of sediments and (c) condition of deposition of the sediments. The high Chemical Index of Weathering (CIW) [average 97], Plagioclase Index of Alteration (PIA) [average 95] values of the Gulcheru shales suggest strong chemical weathering processes of the source rock. The $Al_2O_3/TiO_2$, $TiO_2$/Ni ratio, LREE/HREE ratios with negative Eu anomaly and Cu/Zn, Ni/Co, U/Th and V/Cr ratio indicate a mixed felsic igneous provenance which seems to be derived from Dharwarian Granite Gneiss. The geochemical components of V, Cr, Ni, Co, U and Th strongly suggest that these clastic rocks are deposited in an oxic condition. The discrimination plot La-Th-Sc and Th-Sc-Zr/10 suggest that the Gulcheru clastic sediments are deposited in continental island arc setting during the process of amalgamation of supercontinent Columbia. Combined, it is concluded that Paleoproterozoic Gulcheru Formation, Cuddapah Basin reveals the saga of deposition of sediments in the Papaghni sub-basin taking place in fluvio-aeolian environmental condition with alluvial fan in the lower part and tidal-flat in the upper region. The clastic sediments having been eroded from mixed source rocks of granite, granodiorite and tonalite felsic igneous rocks of Eastern Dharwar Craton (EDC) of southern India during late Paleoproterozoic time are deposited in the Papaghni sub-basin when the process of amalgamation of supercontinent Columbia is taking place.

# CONTENTS

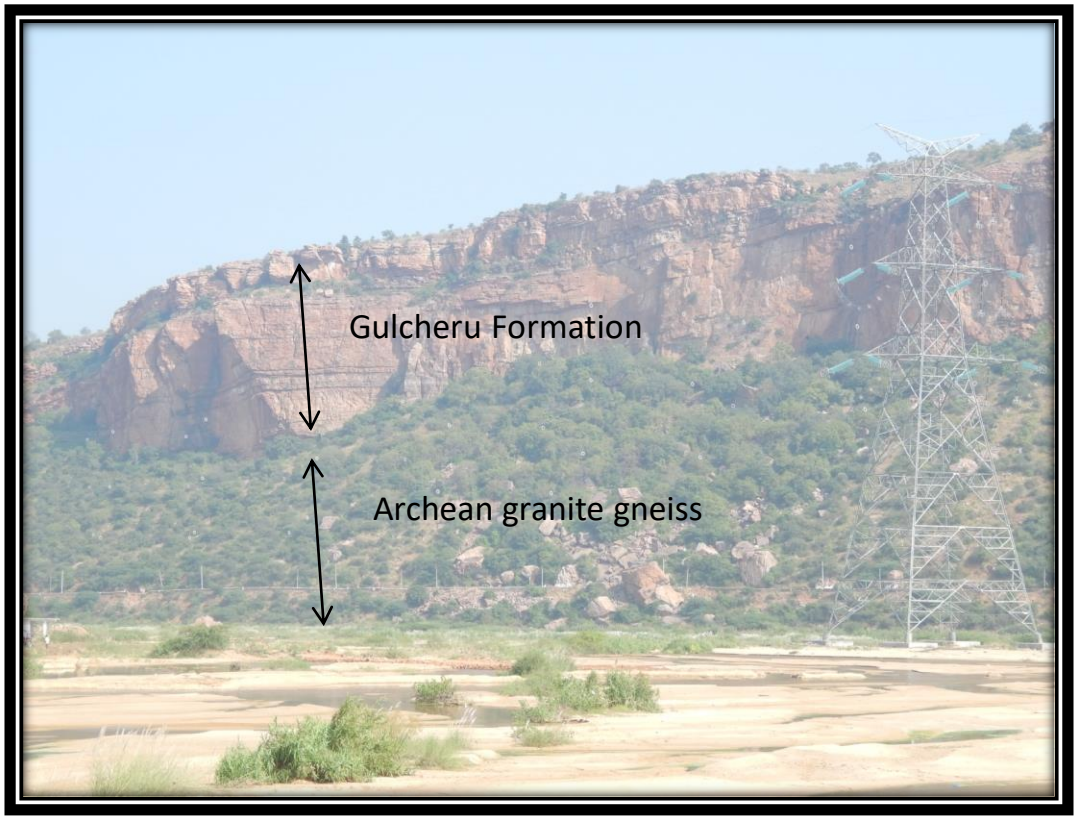


Panoramic view of contact between Gulcheru Formation and Archaean basement of Cuddapah Basin, India

# CHAPTER 1

# INTRODUCTION

## 1.1 PROTEROZOIC SEDIMENTARY BASINS OF INDIA

Mainly two major types of sedimentary basins have been identified within Indian shield during Proterozoic time **(Fig. 1.1)**. These Indian Proterozoic basins are commonly termed as "Purana Basins" and are resting over four distinct Archean nuclei, viz (i) Dharwar craton, (ii) Aravalli-Bundelkhand craton, (iii) Bastar craton and (iv) Singhbhum craton **(Fig. 1.2)**. The older commonly deformed and highly metamorphosed, basins are Aravalli-Delhi-Bijawar-Sausor-Sakoli etc. The other comparatively less metamorphosed as well as less deformed ones, represented by Cuddapah-Vindhyan-Kaladgi-Bhima basin. They are traditionally believed to have been deposited during the mid-Paleoproterozoic to terminal Neoproterozoic-early Cambrian time period **(Ramakrishnan and Vaidyanadhan, 2008)**. These 'purana basins' cover more than $1/5^{th}$ area of the Precambrian exposures of the Indian Peninsular Shield (**Fig. 1.3; Meert and Pandit, 2015)**. Paleomagnetic studies aimed at reconstructing the continental configuration shows that India was also at the tropics during this era like other continents such as Australia, Arabian-Nubian shield, and South China from which overwhelming evidence in support of the Neoproterozoic global glaciations as well as Shuram anomaly have been reported **(Li et al., 2008)**.

**Meert and Pandit (2015)** has treated the term Purana as chronostratigraphic unit and identified Purana-I spanning through 2.5–1.6 Ga, Purana-II covering the period between 1.6 and 1.00 Ga and Purana-III representing the activities between 900 and 541 Ma. Although the original definition of Puranas broadly includes the rocks of Mesoproterozoic-Neoproterozoic ages, in recent revision, rocks of undeformed Paleoproterozoic ages have been included in this domain. Geochronological studies carried out in these intracratonic babins indicate that the deposition may have started nearly 2700 Ma (Cuddapah Basin) age and finished by nearly 750 Ma **(Collins et al., 2015; Conrad et al., 2011; Das et al., 2009; Khelen et al., 2020; Malone**

**et al., 2008; Patranabis-Deb et al., 2007; Rasmussen et al., 2002; Ray et al., 2003; Saha and Patranabis-Deb, 2014).**

Vindhyan Basin is the largest basin among all the Purana basins and it overlies the Bundelkhand craton. The Cuddapah Basin is considered to be the second largest basin which develops over the Eastern Dharwar Craton (EDC). Sediments in these basins vary in thickness from 200m to 10,000m and are constituted predominantly of ortho-quartzite-shale-carbonate suit of rocks. Each basin has a separate orientation and therefore, is likely to have created by the diverse tectonic activities in the Indian subcontinent during early Proterozoic time. The process of generation of such intracratonic basins has been a matter of debate for decades though a relationship between sub crustal heat flow regime and plate tectonics has well been established by **Anderson (1982), Gurnis (1988) and Sloss (1991)**. On the other hand, according to **Hartley and Allen (1994)**, periods of formation of many cratonic basins are coincident with fragmentation of Pre-Proterozoic Supercontinent.

## 1.2 A BRIEF INTRODUCTION OF CUDDAPAH BASIN

On the basis of lithology, degree of metamorphism, magmatism, types of greenstone (schist) belts and ages of rocks, the Dharwar Craton of southern India is divided into two parts: (1) Western Dharwar Craton (WDC) and (2) Eastern Dharwar Craton EDC. Some people consider it as the suture boundary between the WDC and EDC, whereas others suggest the Chitradurga eastern boundary shear zone is the boundary. The WDC and EDC are sutured together by subduction-accretion processes, indicating operation of plate tectonic during the Neoarchean **(Jayananda et al., 2020)**. The EDC is made up of several long NW to N-S to SW trending Neoarchean linear granite-greenstone belts, 2.37-1.8 Ga widespread mafic dykes, Proterozoic (1.8-0.8 Ga) Cuddapah basin, Eastern Ghats granulite belt, 1.1 Ga kimberlite fields, 550 Ma East-African orogenic activity **(Rao and Nara, 2022**). After the

final cratonization event (formation of Closepet granite) within Dharwar craton there is a major tectonic hiatus which is followed by the penetration of mafic dyke swarms into the Eastern Dharwar Craton in and around 2200 Ma **(French et al., 2008; Saha and Patranabis-Deb. 2014)**. This emplacement is followed by the formation of intracratonic Cuddapah Basin which is placed at the south-eastern portion of the Eastern Dharwar Craton and located near to the western margin of Eastern Ghat Mobile Belt (EGMB) **(Chetty, 2011; Saha and Patranabis-Deb. 2014)**. Several workers mark this margin as a "Proterozoic collisional boundary" **(Chetty and Murthy, 1994; Vijaya Kumar and Leelanandam, 2008; Chetty, 2011)**.

Cuddapah Basin is one of the purana basin of India situated in south-eastern part of Indian shield. The crescent-shaped Cuddapah Basin of Andhra Pradesh, south-eastern Peninsular India, is confined between $13^0$15' to $17^0$00' latitude and East $77^0$45' to $80^0$15' longitudes covering area of about of 44,500 sq. Km and has a maximum width of 145 km in the middle **(Fig. 1.4; Kalpana et al., 2010; Kumar et al., 2015)**. This basin is considered as an arcuate, low-amplitude, asymmetrical synclinorium **(King, 1872; Matin, 2015; Sheppard et al., 2017)**. The semi-circular boundary on these three sides is an undisturbed geological contact representing an Eparchean unconformity **(Singh and Mishra, 2002)**.

The Cuddapah Basin's western margin has a convex shape, and is caused by an unconformable relationship between the Proterozoic sediments of Cuddapah Basin and the late Archean granites of Eastern Dharwar Craton **(Fig. 1.4; Kale and Phansalkar, 1991)**. This part of the basin is relatively less tectonically active than the eastern part **(Anand et al., 2003)**. Whereas the Cuddapah Basin's eastern margin has a concave shape, which denoted by a distinct deep crustal, low angle thrust contacted with the Nellore Schist Belt (NSB) and Eastern Ghats Mobile Belt (EGMB) **(Fig. 1.4; Mohanty, 2011; Joy et al., 2015).** In contrast to the western sector, the eastern sector has been folded, metamorphosed, and deformed during

Middle to Late Proterozoic Eastern Ghat Orogeny, leading to the crescent shape of this basin **(Anand et al., 2003; Kumar et al., 2015)**.

Within the Cuddapah Basin there is Cuddapah Supergroup composed of dominant argillaceous and arenaceous sediments along with subordinate calcareous sediments, and the unconformably overlying Kurnool Group composed of Orthoquartzite-shale-carbonate association **(Patranabis-Deb et al., 2012)**. The Cuddapah Supergroup consists of the Papaghni, Chitravati and Nallamalai groups, each separated by regional unconformities **(Table 1.1)**. Each of these groups is composed, broadly, of a fining upward succession from quartzite at the base to shale at the top and is interpreted to representing shallow-marine shelf with periodic transgressive and regressive events **(Patranabis-Deb et al., 2012; Saha and Tripathy, 2012; Chakrabarti et al., 2014, 2015)**. Whereas the relatively undeformed Papaghni and Chitravati groups, exposed in the western part of the basin **(Nagaraja Rao et al., 1987; Saha and Tripathy, 2012)**, likely are deposited during successive thermal upwarping and rifting events **(Chyakrabarti et al., 2015)**. The highly deformed Nallamalai Group exposed in the eastern part of the basin **(Chaudhuri et al., 2002, Sheppard et al., 2017)**, likely represents development of an active convergence along the eastern margin of the basin **(Mishra, 2011)**. Within Cuddapah Supergroup, the sedimentary strata of Papaghni and Chitravati Group are frequently interrupted by numerous mafic-ultramafic sills and dykes. Deposition of the overlying Kurnool Group likely represents resumption of an extensional regime via reactivation of basement normal faults in the western basin **(Collins et al., 2015; Sheppard et al., 2017)**.

Sedimentation in the Cuddapah Basin took place in a series of successively evolved, spatially distributed but interconnected subbsins viz. Papaghni, Nallamalai, Srisailam and Kurnool-Palnad **(Murthy 1981)**. Lithologically, the Gulcheru Formation of the Papaghni Group consists of three units from bottom to top, viz. (a) conglomerate (b) Orthoquartzite and

(c) Rhythmites (Alternation of siltstone/mudstone/sandstone). A number of basic volcanic flows are associated with the upper part of Vempalle Formation conformably overlain by basal siliciclastic strata of Gulcheru Formation **(Murthy et. Al., 1987)**. In the Vempalle Formation, predominantly stromatolitic dolomite and dolomitic shale, are found with subordinate sandstone, and the formation represents a regional carbonate ramp setup **(Nagaraja Rao et al., 1987)**. Similarly, the Chitravati Group is composed of the Pulivendla, Tadpatri, Gandikota Formation, and the Nallamalai Group consists of the Bairenkonda and Cumbum Formation. The Papaghni and Chitravati group of rocks mainly exposed in the western part of the basin which are relatively undeformed in nature **(Nagaraja Rao et al., 1987; Saha and Tripathy, 2012)**. Nallamalai Group of rocks are highly deformed and thrust bounded which occupy the eastern part of the Cuddapah Basin **(Chaudhuri et al., 2002; Saha and Tripathy, 2012; Sheppard et al., 2017)**. All three (Papaghni, Chitravati and Nallamalai) groups show same sediment assemblage indicates similar depositional environment with syn-sedimentation tectonic activity.

Depending on the rock type, lithostratigraphy, and structural distribution the following four sub-basins were developed as a result of the evolution of the Cuddapah Basin, according to **Nagaraja Rao et al. (1987)**.

1. The Papaghni sub-basin, located in the western portion of the basin, which is made up of rocks from the Papaghni and Chitravati Group;
2. The Nallamalai Group of rocks make up the Nallamalai Sub-basin in the eastern portion of the basin;
3. The Srisailam Sub-basin, located in the basin's northwest, is made up of rocks from the Srisailam Formation.
4. the Kurnool Group of rocks, which are found in the Kurnool and Palnad Sub-basin in the basin's central region;

**Murthy (1981)** propose a paleogeographic model for the Cuddapah basin based on aeromagnetic mapping of the basin **(Fig. 1.5)**. Due to the basin's surroundings condition and possible connection to the open sea in the basin's northeast, all of the groups' lithology are quite similar. To explore the evolution of the Cuddapah Basin **Bhattacharji and Singh (1984), Drury (1984) and Bhattacharji (1987)** suggest a thermo-mechanical model of crustal doming, erosion, and subsidence. As a result of geophysical investigation, **Singh and Mishra (2002)** suggested that the Cuddapah Basin originated in a continent – continent collision during the Proterozoic period **(Fig. 1.6)**. As a result of the geochemical analysis and subsidence **Anand et al. (2003)** suggest that this intracratonic basin formed as a result of passive rifting. The formation of the Cuddapah Supergroup can also be explained by **Mishra (2011)** as being linked to rifting, followed by a plate convergence event that led to the formation of the Kurnool Group of rocks.

According to **Chetty (2011)**, the Cuddapah Basin's evolution is likely to have occurred through the following stages based on low angle dipped detachment faults and kinematic history:

1. In the adjacent basement beneath the Cuddapah Basin, collisional events result in the development of mobile belts and thrust zones between 2600-2000 Ma.
2. Cuddapah Basin's formation is triggered by the impending freeze of collisional processes and is associated with the emergence of an extensional tectonic regime. Around 1800 Ma, a period associated with magmatism caused the construction of sills and dykes within the basin.
3. The Nallamalai basin was created by normal faulting of the "domino" type as a result of ongoing extensional tectonics, which was followed by sedimentation (1600-1400Ma).

Papaghni basin is the result of normal faults with a N-S trend that are of the "listric" kind.

4. Due to the intense compression phase, imbricate thrusting and folding have developed in the Nallamalai Basin.
5. Following the establishment of transfer faults, the extensional regime begins (1400-850Ma).
6. With post-Kurnool thrust episodes, transpressional dextral shearing along the mobile belt was reactivated (650-450Ma).

   Based on **Mohanty (2011)**, the morphological fit of the Naiper Complex margin of East Antartica, coupled with the matching tectonic trend lines, along with identical mafic dykes and identical tectonic evolution of the blocks on opposite sides of the matching line, and suggests that the Naiper Complex and SIWA were juxtaposed during early Palaeoproterozoic time. This assembly is separated at ~1950 Ma to give rise to the development of Cuddapah Basin **(Fig. 1.7)**.

According to **Basu and Bickford (2015),** the Papaghni-Chitravati sub-basin of Cuddapah Basin was opened up during the fragmentation of the earliest supercontinent Kenorland in the Palaeoproterozoic (1900-2000 Ma). This earliest Purana Basin is closed at around 1800 Ma, when the fragments of Kenorland reassemble again to form another Supercontinent Columbia **(Basu and Bickford, 2015)**. A Large Igneous Province (LIP) has formed in the Southern Indian Block as a result of this event **(French et al., 2008)**. It is likely that the mafic igneous activity is associated with the breakup of Kenorland, when the Rayner complex separated from India and settled in East Antarctica **(Mohanty, 2011; Basu and Bickford, 2015)**.

The stages of the Cuddapah Basin evolution model provided by **Absar et al. (2016)** are as follows:

1. Due to subduction in a western direction and the eastern Indian continental margin, the Papaghni sub-basin opened as a back-arc basin in an era of about 2000 Ma. During the early stage of Gulcheru sedimentation, the newly opened basin absorbed detritus from the Dharwar craton, and during later stages (Vempalle Formation and Chitravati Group), received detritus and dissolved load from a magmatic arc located southeast of depositional basin.
2. The disappearance of the magmatic arc coincided with the polarity of the subduction zone changing in the area around 1850 Ma, most likely as a result of plume activity. Following this occurrence, Papaghni sub-basin sedimentation may have stopped.
3. At 1600 Ma, Dharwar and Antarctica/Australia cratons clashed, and the remaining Cuddapah basin developed as a foreland basin behind the "collisional" Krishna Orogen (cf. **Dobmeier and Raith, 2003; Henderson et al., 2014**). A post-collisional foreland basin is where the sedimentation of the Nallamalai Group and Srisailam Formation occurs (cf. **Collins et al., 2015; Joy et al., 2015**).

The evolution of this model's stages 1 and 2 was primarily triggered by the breakup of the Kenorland Supercontinent, whereas stages 3 resulted from the amalgamation of the Kenorland fragments. The emplacement of ~2.17 Ga mafic dyke swarms, which are an event that precedes the ~2.0 Ga Kenorland breakup (**Ernst et al., 2013**), suggests massive rifts on a worldwide scale (**Basu and Bickford, 2015**).

**Sesha Sai et al. (2017)** have proposed a continental arc setting during the development of the Papaghni and Chitravati group rocks, based on the mafic-ultramafic sill bodies configuration. According to **Mukherjee et al., (2019)**, the crescent shape of Cuddapah Basin is mainly due to thrusting during the Eastern Ghat Orogeny. Basin fill contains the imprint of progressive stages of rifting and sub-basin development.

The crescent shape of the Cuddapah Basin, according to **Mukherjee et al., (2019)**, is mostly attributable to thrusting associated with the Eastern Ghat Orogeny. The rocks that form the basin fill are engraved with the stages of rifting and sub-basin development. Later stages of deformation have also somewhat altered and formed the basin's ultimate shape. Recently, **Goswami et al. (2020)** proposed a basin development model with active rifting characteristics. During rifting and sedimentation, the model depicts the mechanism of bimodal volcanism. Within the Cuddapah Basin, different sub-basins reflect a combined mechanism of rifting and orogenic events.

## 1.3 GEOCHRONOLOGY

Geochronological studies carried out in these intracratonic basins indicate that the deposition may have started nearly 2700 Ma (Cuddapah Basin) ago and completed by nearly 750 Ma **(Rasmussen et al., 2002; Ray et al., 2002, 2003; Patranabis-Deb et al., 2007; Malone et al., 2008; Das et al., 2009; Conrad et al., 2011; Saha and Patranabis-Deb, 2014; Collins et al., 2015; Khelen et al., 2020)**.

## 1.4 SEDIMENTOLOGY OF GULCHERU FORMATION – PRESENT STATUS

The Gulcheru Formation, the oldest succession of the Cuddapah Supergroup, was deposited in Papaghni Subbasin, is dominated by clastic sedimentary rocks.

**Dasgupta et al., (2005)** identify major eight sedimentary facies from this formation, as follows:

F1- Pebbly conglomerate, F2- Moderately sorted pebble-cobble conglomerate, F3- Disorganised cobble-boulder conglomerate, F4- Medium to coarse grained sandstone, F-5

Massive, very coarse to granule sandstone, F6- Very fine sandstone, F7- Couplet facies, F8- Lensoidal cross stratified sandstone.

**Basu et al., (2014)** also identify twelve distinct sedimentary facies which are as follows:

F1- Sandy matrix supported, poorly sorted, lensoidal breccia, F2- Unsorted sandy conglomerate grading into laminated sandstone, F3- Clast supported conglomerate with sandy matrix, F4- Stacked couplets of conglomerate and sandstone, F5- Unsorted pebbly conglomerate, F6- Medium to coarse-grained, tabular cross-stratified sandstone, F7- Fine to medium grained, trough cross-stratified lenticular sandstone, F8- Fine to medium grained, well-sorted tabular sandstone, F9- Plane laminated siltstone to fine-grained sandstone, F10- Fine to medium grained sheet sandstone with coarse lags, F11- Fine to medium grained, tabular cross-stratified sandstone, F12- Horizontal to slightly concave-up heterolithic unit.

Recently on the basis of grain size, sedimentary structure, bed thickness and bed contacts, six sedimentary facies are identified by **Chakrabarti et al., (2015)** are as follows:

F1- Massive diamictites, F2- Stratified conglomerates, F3- Framework supported imbricated conglomerates, F4- Medium to coarse grained, well sorted multi storeyed sandstone beds, F5- Fine to Medium grained multi-storeyed sandstone beds, F6- Alternating beds of laminated siltstone, laminated calcareous shale and fine-grained lenticular sandstone.

Depositional environment of the Gulcheru Formation is interpreted as ancient shoreline **(Pascoe, 1973)**, Tidal flat **(Nagaraja Rao et al., 1987)**, fluvial **(Dasgupta et al., 1990)**, fluvio-aeolian **(Basu et al., 2014)**, beach **(Reddy et al., 1990)**, fan-delta complex **(Chaudhuri et al., 2002; Chakrabarti and Shome, 2007; Chakrabarti et al., 2015)**.

**Chakrabarti et al., (2009)** perform geochemical analysis to highlight provenance and weathering history of the Gulcheru Formation. Based on the major, trace and REE data

**Chakrabarti et al., (2009)** propose a mixed felsic-mafic provenance with felsic dominancy of the Gulcheru rocks and a cold-arid climatic condition during its evolution.

**Khan et al., (2019)** perform geochemical analysis to highlight provenance and palaeoweathering and crustal evolution. They propose a variable mix of mafic source rock and based on petrochemical tectonic discrimination diagrams quartzites were deposited in active as well as passive tectonic setting.

## 1.5 STATEMENT OF PROBLEM

At a very early stage of mantle perturbation two major trends of lineaments (NE-SW and NW-SE) appeared to have been set in the basement which controlled the initiation of the Proterozoic Cuddapah basin of Peninsular India **(Kale, 2016). Huan et al., (2021)** has offered a combined thermo.-mechanical model for the same on the argument that a thermal "driving load" is a prerequisite for the basin evolution. **Chattarjee and Bhattacharya (2001)** clearly demonstrated the Cuddapah basin as rift basin based on their study of the magmatic components of the basin. **Chaudhury et al. (2002)** too has proposed that the Cuddapad Basin and other intra-cratonic basins in India developed in rift settings. The theory is based on the existence of deep faults within the Cuddapah Basin exposed by gravity data (NGRI, 1975). **Chaudhuri et al. (2002)** suggest the initial rifts may have followed pre-existing lineaments defined either by Archaean greenstone belts of the Dharwar Craton, or belts of crustal convergence. **Hou et al. (2008)** also propose it was a rift-type basin formed during the fragmentation of the Proterozoic Columbia Supercontinent. Recently, Goswami et al. (2020) also proposes a basin evolutional model of the Cuddapah basin with the signature of active rifting.

However, this basin is often interpreted as being a foreland basin to the Eastern Ghats orogen (Dasgupta and Biswas, 2006; Manikyamba et al., 2008) largely due to its position next

to the Eastern Ghats. **Singh and Mishra (2002)** however, have offered an alternative model based on geophysical study. To them, the Cuddapah basin may represent a peripheral foreland basin evolved through Proterozoic continent-continent collision. They conclude that the presence of prominent seismic reflectors in the upper mantle under the Cuddapah Basin may indicate that some crustal rocks might have subducted towards the west suggesting divergent collision along the middle to late Proterozoic Eastern Ghat Mobile Belt.

The basal Gulcheru Formation, lacking any syn-sedimentary deformation features and igneous episodes does not conform to the rift-like set-up of the Cuddapah basin during its initiation. The tell-tale signatures associated with foreland basin have not been documented so far in the Gulcheru Formation of the Cuddapah basin. So, additional sedimentological information needs to be obtained to test the workability of the aforesaid two models during the initiation of the Cuddapah Basin. The proposed work, titled as **"Provenance and palaeoclimate study of Palaeoproterozoic basal Gulcheru Formation of Cuddapah Basin, Andhra Pradesh, India"** is an attempt to highlight the sedimentology during the initial phase of the Cuddapah basin and it comprises various aspects of facies attributes and related sedimentation patterns which are the responses of tectonic or eustatic or both controls operative at the early phase of poly-history, Cuddapah Basin. And the following objectives are summarized as following:

1. Characterization and evalution of the primary facies along three selected sections from north-western part of the basin.
2. Study of the provenance, paleo-weathering and paleoclimatic condition of Gulcheru Formation based on the elemental geochemistry of shale.
3. Construction of a depositional model based on facies attributes, facies association and global correlation of Gulcheru Formation during Paleoproterozoic time.

4. To better understand in respect of the evolution of Papaghni sub-basin during the deposition of Gulcheru Formation in the Paleoproterozoic time.

## 1.6 STUDY AREA

The Gulcheru Formation is well exposed in the southwestern part of the Cuddapah Basin. A detail sedimentological investigation of dispersed sections spreading along the SW rn part of the Cuddapah Basin starting from **Kanampalli (14˚25'13.60" N, 78˚05'25.18" E)** to **Pendllimari (14˚24'55.2" N, 78˚36'43" E)** gorge via **Gandi (14°18´25.34″ N, 78°28´ 36.52" E)** is taken up to shed light on depositional environment. Kanampalli section is exposed beside the Jammalamadugu-Kadiri road, 11.3 Km from the town of Pulivendla, near Lanampalli village towards Kadiri. Gandi section is exposed beside the river bank of Papaghni river, 6.2 Km from town of Vempalle, near Gandi area. And Pendllimari section is exposed beside the Vempalle-Kadapa highway, 23.1 Km from the town of Vempalle, near Pendllimari village and hindu temple. Measured sections **(Fig. 1.8)** provide valuable information on the spatial and vertical variation of lithofacies, bedform geometry and geochemistry that are used to decipher the depositional character of the Gulcheru Formation in this region.

## 1.7 METHODOLOGY

The following methods are adopted for studying the Gulcheru Formation

1. Systematic collection of field data and representative rock samples for Gulcheru Formation.
2. Sample preparation for laboratory work involving chemical analysis and petrographic analysis.

Collection of Field data: The Gulcheru outcrops are studied by lateral mapping and vertical logging of sections across two- and three-dimensional exposures of the formation in and around Kanampalli (78˚05’25.18” E, 14˚25’13.60” N) to Pendllimari (78˚36’43” E, 14˚24’55.2” N) gorge via Gandi (14°18´25.34″ N, 78°28´ 36.52″ E), Andhra Pradesh, India. The locations are plotted by GPS in the Survey of India topo sheet (57 J/3, 57 J/11 and 57 J/7).

c. The field study essentially comprises of the following,

- Construction of lithologs in different areas
- Construction of composite lithologs to delineate the spatial and vertical variation of lithofacies across the area.
- Identification of sedimentary structures.
- Palaeocurrent measurements.
- Organized collection of samples at close intervals up section for geochemical (fresh sample needed), as well as petrological analysis.

2. Laboratory Analysis: Laboratory analysis include,

a) Sample preparation for petrographic as well as for geochemical study.

b) Elemental geochemical studies.

c) Construction of lithologs, composite lithlogs and 3D block diagrams.

a) Sample preparation for petrographic study: The collected samples in the field are grouped for two different analytical purposes.

i) For thin section.

ii) For geochemical analysis.

i) For preparation of thin section samples are crushed into small slices. Section perpendicular to bedding is best suited for this purpose. Each sample is mounted on a glass slide after

preliminary grinding. The sample is then further grounded and polished to bring to a thickness of 0.03 mm. The thin section is covered with a cover slip to avoid dust contamination and oxidation.

i) For geochemical analysis samples are pulverized in a laboratory ball mill to 15pprox.. 200 mesh size and 10 gm. Of each sample are collected for analysis.

b). Analytical methods:

Geochemical analysis

The major elements concentration was acquired by Bruker model S4 Pioneer sequential wavelength-dispersive X-ray fluorescence (XRF) spectrometer. REE and Trace elements were analysed by high resolution inductively coupled plasma mass spectrometer (HR-ICPMS). At the beginning, a mixture of 50 mg sample and 10 ml of 7:3 HF– $HNO_3$ was taken in Savillex vessels. After settling the vessels keep it on the hot plate at $150^0$C for 50 hrs. From that point forward, a solitary drop of $HclO_4$ was added to the mixture, which were additionally vaporised to close dryness at $160^0$C. Whatever is left of every vessel were dissolved by adding 20 ml of 1:1 $HNO_3$– Milli-Q water and putting them on the hot plate for 30– 45 min at $100^0$C to dissolve every single suspended molecule. Further Rhodium solution (5 ml) was mixed as an inside mark to every vessel, and the volume of mixture increased to 250 ml by including Milli-Q water and the solution was stored in High Density Polyethylene (HDPE) bottles. 5 ml of this solution was mixed again with 50 ml Milli-Q water (1:10 proportion) and stored in Eppendorf tubes for examination. The analytical precision for major oxides by XRF is estimated to be better than 8%. Minor and rare earth element analysis with international standard GSR-5 indicated an analytical precision generally better than 6% for all elements.

c) Construction of lithologs, composite lithlogs and 3D block diagrams have been drawn in Coreldraw software.

Composite lithologs have been constructed i) to delineate the spatial and vertical variation of lithofacies in the study area. Ii) to construct 3D block diagram to depict the evolution of the Cuddapah Basin during the deposition of Gulcheru Formation.

# FIGURES AND TABLES

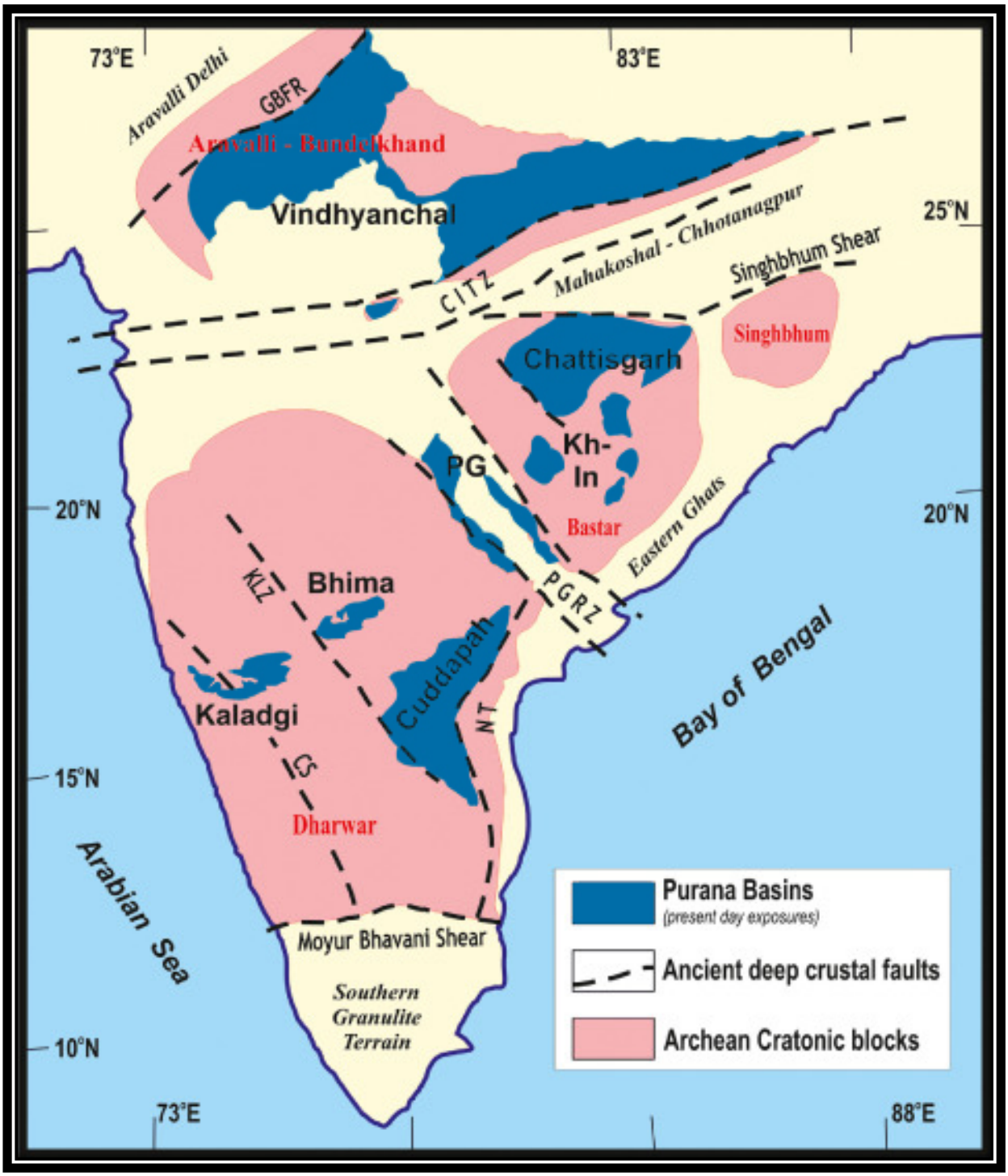


**Fig. 1.1** Purana basins of Peninsular India on the background of the estimated extents of the Archean cratonic blocks (named in red) and Proterozoic mobile belts (named in black italics). Ancient deep crustal faults/shear zones with a Late Archaean-Neoproterozoic heritage have influenced the geometry of the Purana basins adjoining them. CITZ = Central Indian Tectonic Zone; CS= Clospet Suture zone; GBFR= Great Boundary Fault of Rajasthan; Kh-In = Khairiar - Indravati Basin; KLZ = Kurduwadi Lineament Zone; NT = Nallamalai Thrust; PGRZ = Pranhita Godavari Rift Zone (after **Kale and Patil Pillai, 2022**)

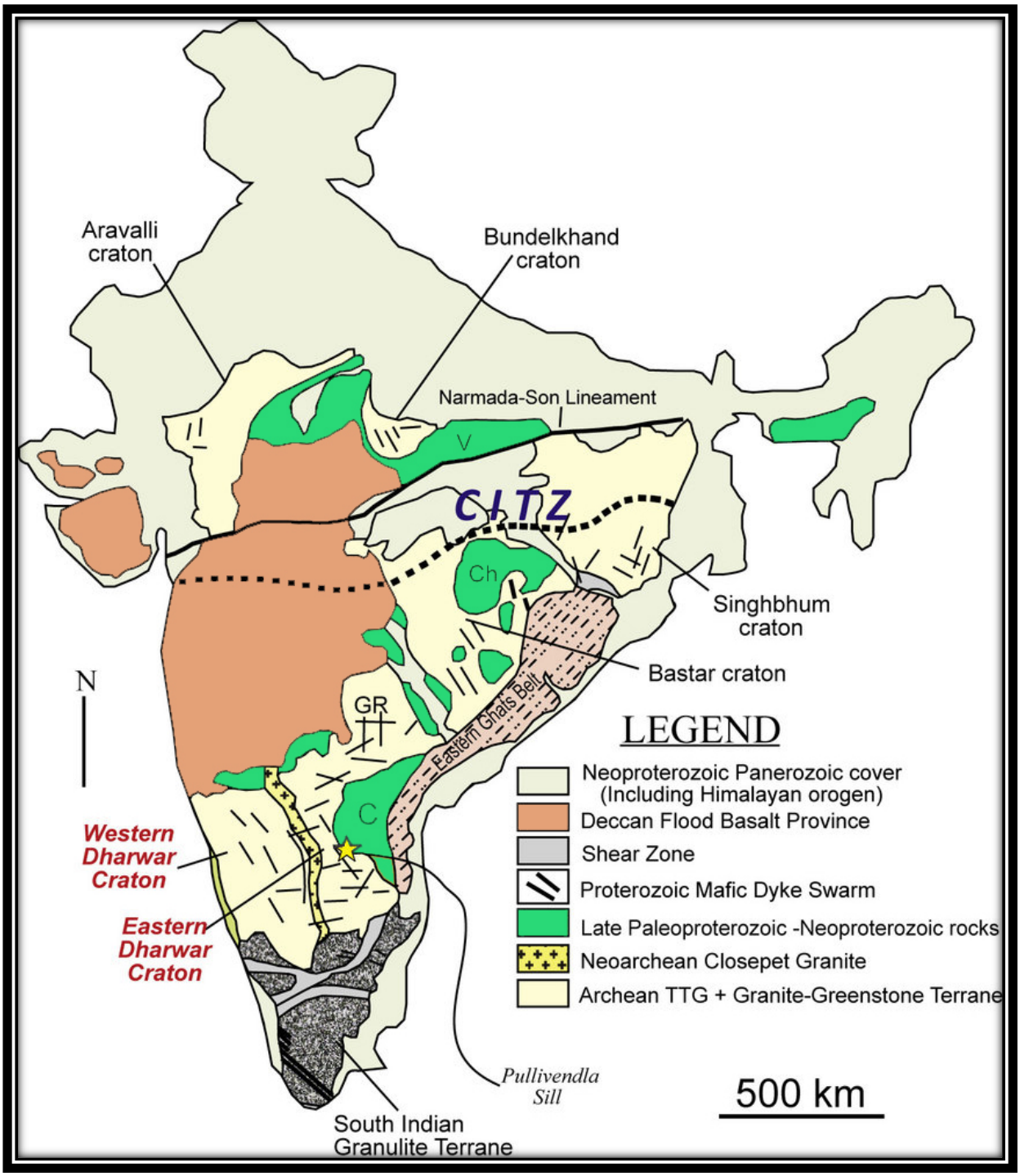


**Fig. 1.2** Generalized geological map of Peninsular India showing the major cratons and various dyke swarms including those cratons (modified after **Meert et al., 2011**). CITZ- Central Indian tectonic zone, NS- Narmada-Son lineament, GR- Godavari rift, C- Cuddapah Basin, V- Vindhyan Basin, Ch- Chattisgarh Basin

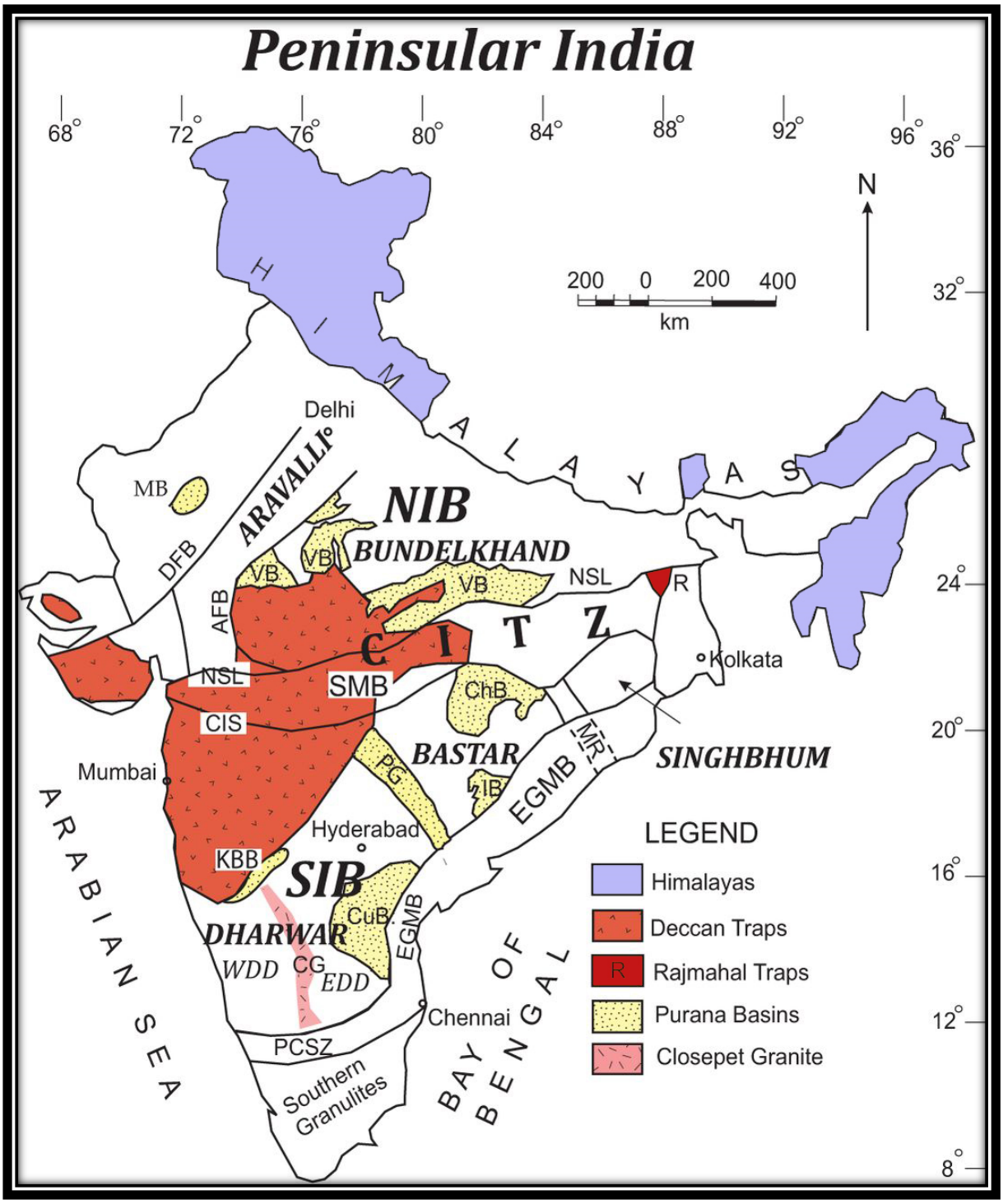


**Fig. 1.3** Generalized tectonic map of the Indian subcontinent including Purana basins, cratonic regions and fold belts (modified after **Meert and Pandit, 2015**). VB- Vindhyan Basin, PG- Prahnita-Godavari Basin, ChB- Chhattisgarh Basin, CuB-Cuddapah Basin, KBB- Kaladgi-Bhima Basin, MB- Marwar Basin, IB- Indravati Basin, EDD- Eastern Dharwar Crtaton, WDD- Western Dharwar Craton, MR- Mahandi Rift, R- Rajmahal trap, CG- Closeper Granite, SIB- South Indian Block, NIB- North Indian Block, AFB- Aravalli Fold Belt, DFB- Delhi Fold Belt, EGMB- Eastern Ghat Mobile Belt, SMB- Satpura Mobile Belt, NSL- Normada-Son lineament, CIS- Central Indian Suture, PCSZ- Palghat-Cauvery Shear Zone

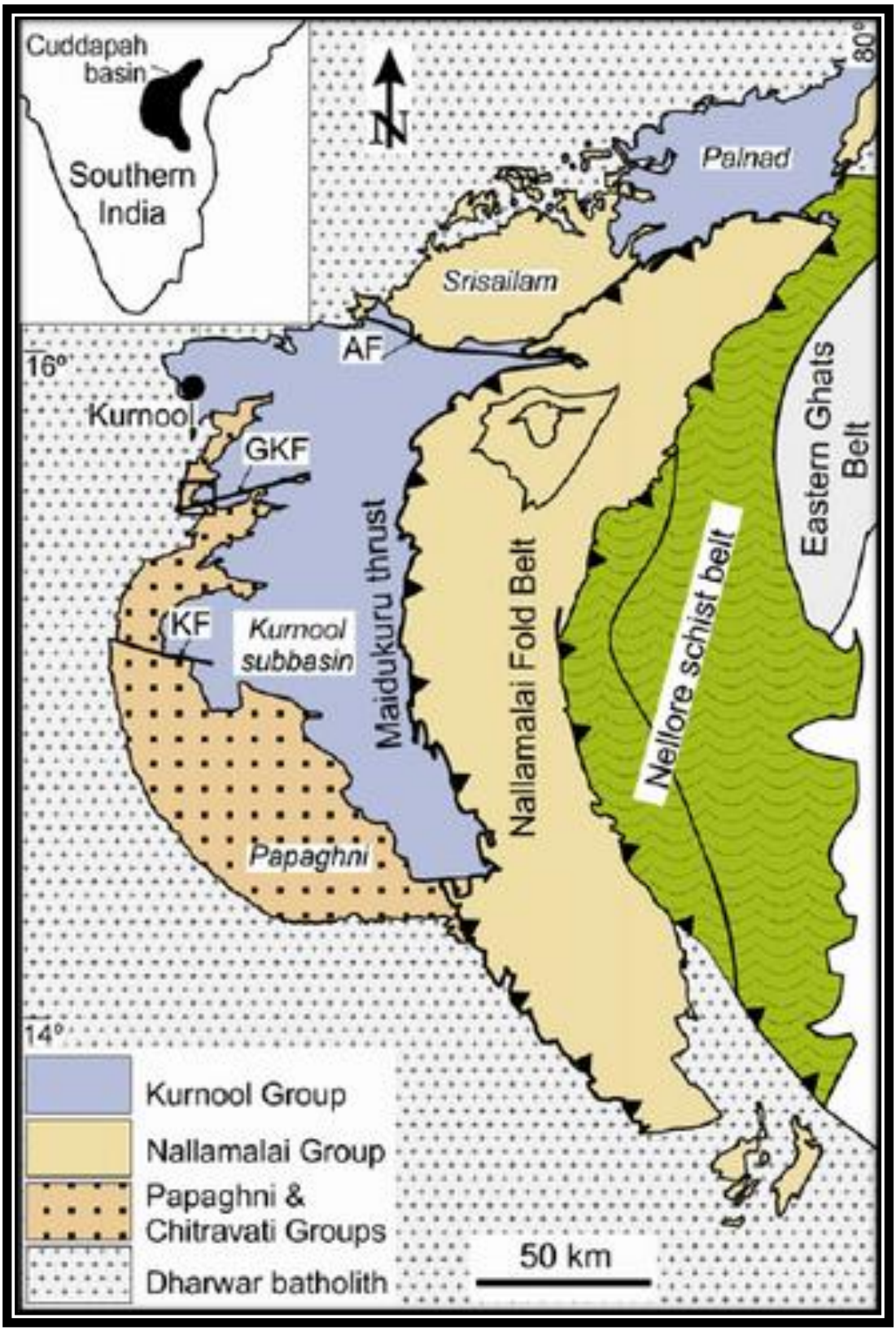


**Fig. 1.4** Simplified geological map of the Cuddapah Basin (modified after **Saha and Tripathy, 2012**). Western margin of the basin is convex and developed over the Eastern Dharwar, whereas the eastern margin is concave and has a contact with Nellore schist belt and Eastern Ghat Belt

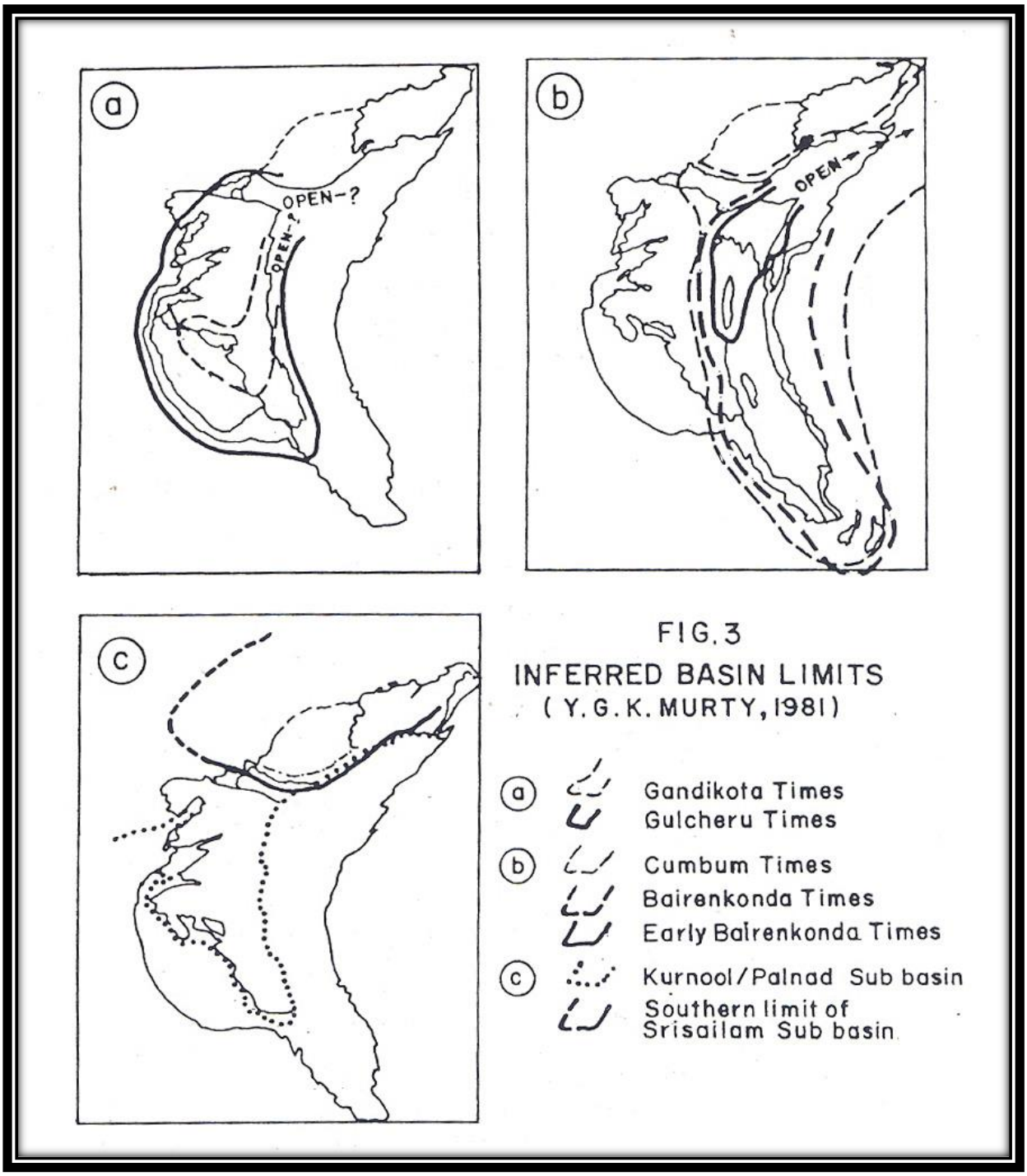


**Fig. 1.5** Inferred Cuddapah Basin Limits. The great similarities for the crescent shaped boundaries of all the Formations of Cuddapah Basin have resulted from a land-locked condition of the basdin with a probable connection to the open sea in the North East (after **Murthy, 1981**)

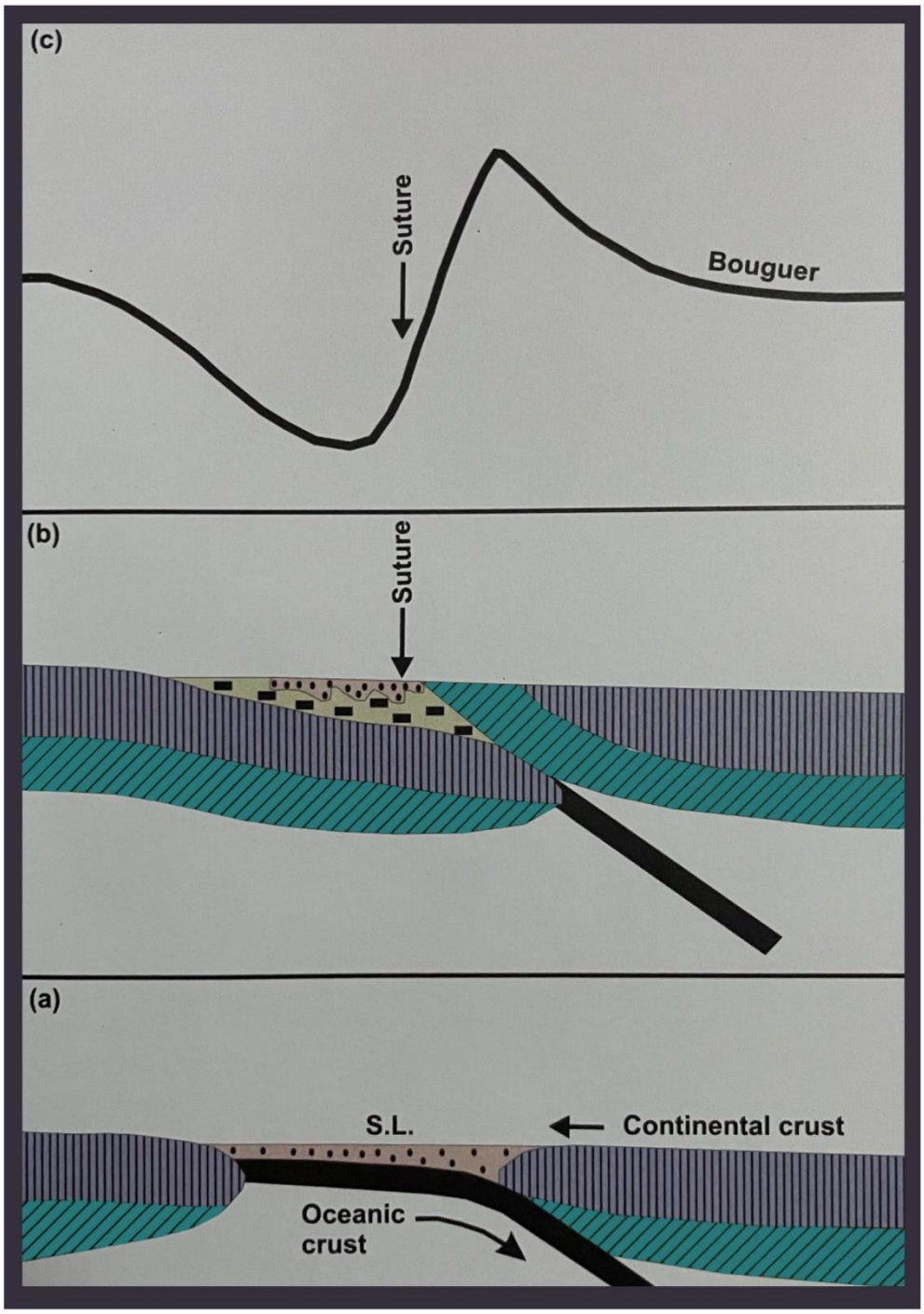


**Fig. 1.6** (a) Impending collision between two continents; (b) Postulated geometry produced by collision; and (c) Theoretical Bouguer anomaly calculated for such crustal suture (modified after **Singh and Mishra, 2002**)

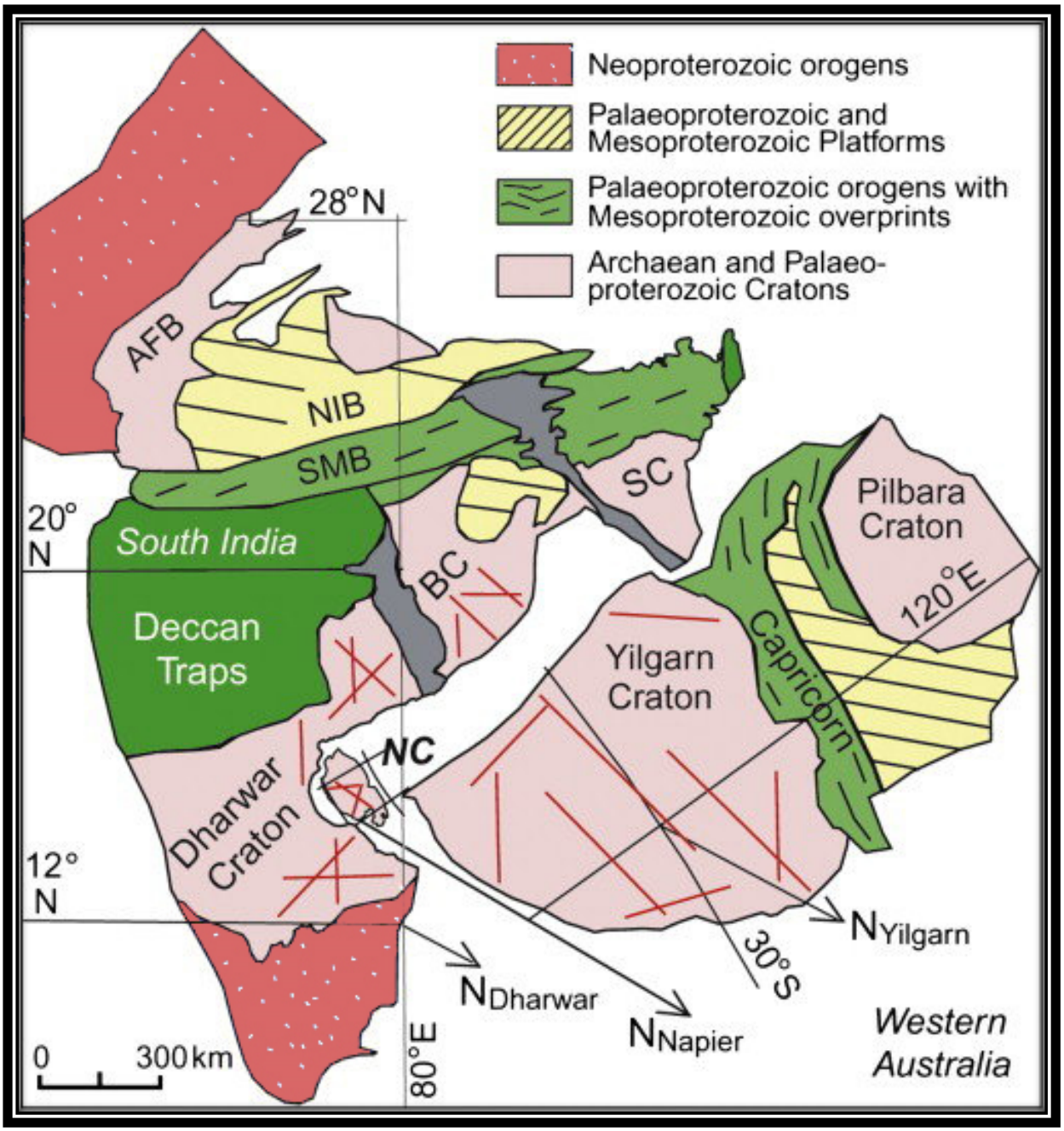


**Fig. 1.7** Configuration of an Archaean-Palaeoproterozoic supercontinent "SIWA", with the Napier Complex located at the position of the Cuddapah Basin of India and Yilgarn craton at the eastern coast of India. Representative basic dykes of the Napier Complex, South India (SI), and the Western Australia (WA) are shown by red color. Arrows marked as $N_{yilarn}$, $N_{Napier}$ and $N_{dharwar}$ are north directions for ~2400 Ma for the Yilgarn craton, the Napier complex and the Dharwar craton, respectively (modified after **Mohanty, 2011**)

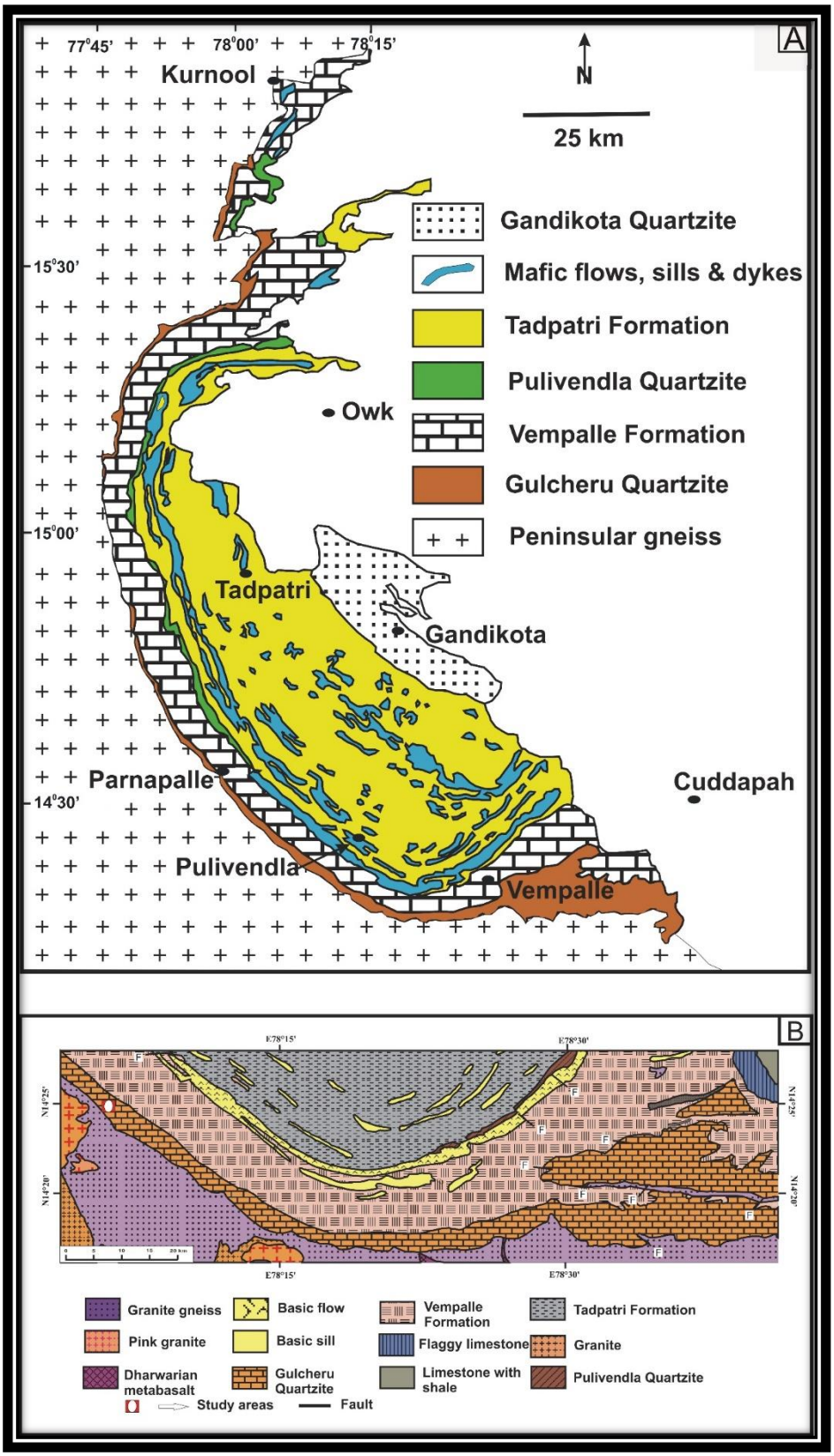


**Fig. 1.8** Geological maps of the study area (a) Geological map of western Cuddapah showing the lower Cuddapah rock groups (after **Nagaraja Rao et al. 1987**). (b) Detail of the south-western Cuddapah Basin showing locations of the measured sections investigated in this study

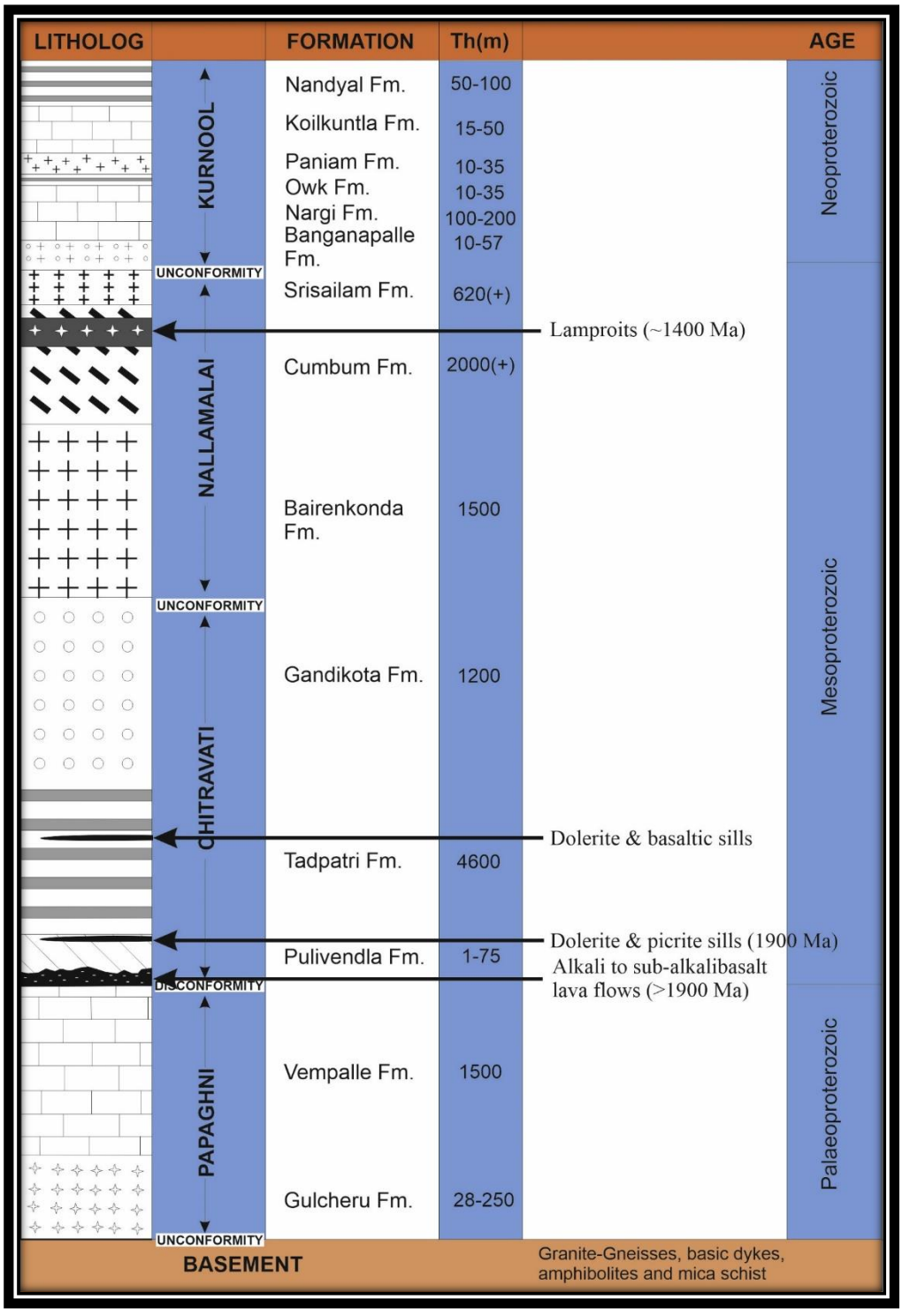


**Table 1.1** Lithological succession of Cuddapah Sedimentary Basin (after **Anand et al., 2003**)

# CHAPTER 2

# GEOLOGICAL SETTINGS AND STRATIGRAPHY

## 2.1 REGIONAL GEOLOGY AND STRATIGRAPHY:

**King (1872)** proposed a four-fold classification of the Cuddapah Basin lithostratigraphy. There are two broadly classified litho-units as older Kadapah (Cuddapah) and younger Karnul (Kurnool) Formation. Each of the formation sub-divided into four sub-groups viz. the Kadapah Formation consists of Paupugnee (Papaghni) beds, Cheyair beds, Nullamullay (Nallamalai) beds, kistnah (Kistna) beds **(Table 1.1)**, and Karnul Formation consists with Banaganpilly unit, Jummulmudgoo unit, Paneum unit, Khoond-air unit. The stratigraphy was further revised by **Narayanaswami (1966)**, who proposed a five-fold classification. **Narayanaswami (1966)** proposed an additional Cheyar Group, which includes the Nagari Quartzite and Pullampet Formation, appears conformably above the Chitravati Group and is unconformably separated from the Bairenkonda Quartzite beneath it. After that, several workers attempt to reconstruct the stratigraphy of the Cuddapah Basin like **Meijerink et al. (1984); Nagaraja Rao et al. (1987); Ramakrishnan and Vaidyanadhan (2008); Saha and Tripathy (2012)**. Lithostratigraphy (four-fold classification) proposed by **Ramam and Murthy (1997)** is followed in this thesis **(Table 2.2)**.

Sedimentation in the Cuddapah Basin took place in a series of successively evolved, spatially distributed but interconnected subbsins viz. Papaghni, Nallamalai, Srisailam and Kurnool-Palnad **(Fig. 2.1; Table 2.2; Murthy 1981)**. These mainly consist of argillaceous and arenaceous sediments with relatively less amount of calcareous sediments **(Nagaraja Rao et al., 1987, Kale et al., 2020)**. The Papaghni Group consists of the basal Gulcheru Quartzite and the upper Vempalle Formation. The basal Gulcheru Formation considered as the oldest formation within Cuddapah Basin which unconformably overlies the Archean Tonalite-Trondhjemite-Granodiorite (TTG), and greenstones of Eastern Dharwar Craton (EDC). The Gulcheru Formation is dominantly composed of basal conglomertate followed by quartzite and sand-mud heterolithic units **(Nagaraja Rao et al., 1987; Patranabis-Deb et al., 2012;**

**Chakrabarti et al., 2015)**. The upper part of the Papaghni Group is represented by Vempalle Formation which gradationally overlies the Gulcheru Formation **(Fig 2.1)**. The Vempalle Formation, which is the lower most carbonate-dominant unit in the Cuddapah Basin, is made up of stromatolitic dolomite, calcareous shale, chert, and quartzite overlain by basic flows **(Nagaraja Rao et al., 1987; Patranabis-Deb et al., 2012; Chakrabarti et al., 2015).** The Vempalle Formation is conformably overlain by the Pulivendla Quartzite of the Chitravati Group, which is dominantly made of pebbly sandstone and conglomerate. The Pullivendla Formation grades upward into Tadpatri Formation, which is principally dominated by argillaceous unit with less amount of dolomite and quartzite. Dolomite units are often found in association with stromatolites. The Gandikota Quartzite overlies the Tadpatri Formation with a conformable and gradational contact. The sequence consists of shale, quartzite (glauconite-bearing) and alternate sequence of quartzite and shale. The Nallamalai Group occupying a larger area rests unconformably over the Chitravati Group. It is well developed in the eastern part of the Cuddapah basin. The discordant relationship between the Chitravati Group and the Nallamalai Group, however, may be explained as being due to a thrust contact **(Saha et al., 2010; Patranabis-Deb et al., 2012)** and hence, the Nallamalai Group may be allochthonus in origin **(Saha and Tripathy, 2012)**. And lower part of Nallamalai Group is represented by Bairenkonda Quartzite, is highly folded in the Nallamalai hills. This is basically an arenaceous unit and in most of the area it is represented by quartzite alone. Few intercalations of shale observed in between the quartzite unit. The succeeding Cumbum Formation of Nallamalai Group is mainly composed of shale with intercalations of quartzite and dolomite at various stratigraphic levels **(Nagaraja Rao et al., 1987)**. Further the Srisailam Formation is mainly composed of well-sorted, medium-grained, subarkose to quartz arenite that occasionally contains ferruginous material and glauconite (**Patranabis-Deb et al., 2012)**.

The Kurnool Group, which is 500 metres thick, is unconformably overlain by the Cuddapah Supergroup. The Kurnool and Palnad subbasin is composed of oligomictic conglomerate (with dominance of subrounded pebbles of chert, jasper), quartzite, barites, black shales, and ferruginous shales. Between the northern Srisailam sub-basin and the southern Papaghni sub-basin, the Kurnool subbasin is located in the west-central region of the Cuddapah basin. The north-eastern portion of the crescent-shaped Cuddapah basin is made up of the Palnad subbasin. The lower most part of the Kurnool Group is known as Banganapalle Quartzite, which is composed of conglomerate, coarse-grained dark red, grey or brown sandstone with occasional silicified stromatolitic limestone clasts **(Patranabis-Deb et al., 2012)**. The succeeding Nagari Formation overlies the Banganapalle Quartzite with a gradational contact, mainly consists of limestones which are dominantly micritic in nature. The Narji Formation also contains glauconite sandstone and a smaller proportion of calcareous shale **(Patranabis-Deb et al., 2012)**. The Owk Formation has a transitional contact with the Narji Formation and is primarily made of shale with welded tuff and volcano-clastic sandstone at various stratigraphic levels. The Owk Formation has a transitional contact with the Narji Formation and is primarily composed of shale with welded tuff and volcano-clastic sandstone at various stratigraphic levels **(Patranabis-Deb et al., 2012)**. The Paniam formation, which primarily consists of well- sorted quartz arenite, follows the Owk Formation with a sharp contact in between **(Nagaraja Rao et al., 1987; Patranabis-Deb et al., 2012)**. Gradually rising above the Paniam formation, the limestone-dominant Koilkuntala formation is made up primarily of micrite and marls chacterize limestone **(Patranabis-Deb et al., 2012)**. The Nandyal Formation, which is primarily made up of laminated shale and shaly limestone, is the topmost component of the Kurnool Group **(Nagaraja Rao et al., 1987; Patranabis-Deb et al., 2012)**.

## 2.2 GEOLOGY AND STRATIGRAPHIC SEQUENCE OF THE STUDY AREA:

The Gulcheru Formation of Papaghni Group is well exposed in the south western part of the Cuddapah Basin, and unconformably overlies the Archean Tonalite-Trondhjemite-Granodiorite (TTG), and greenstones of Eastern Dharwar Craton (EDC). Thickness of the Gulcheru Formation is ~28-250 m **(Anand et al., 2003)**. The study area from Kanampalle in the North West (NW) to Pendllimari in the South East (SE) via Gandi in the central part in the Vempalle is distinctly represented by the thick deposition of basal conglomerate and quartzite with minor occurrence of siltstone and shale. In the lower most part conglomerate and breccia alternates with coarse grained sandstone. Gradually the coarser sands replaced by the finer sandstone in the middle part of the succession. In the upper part sandstone alternate with mudstone represents heterolithic unit. The detailed stratigraphic sequence of the study area has been described in the **Table 2.2**. The detailed lithostratigrphic sequence has also been described in the chapter 3.

## 2.3 IGNEOUS ACTIVITY:

Dolerite, picrite, and gabbro sills, basaltic flows, ignimbrites, and ash-fall tuffs are the main igneous suites associated to the Vempalle and Tadpatri Formation in the western part of the basin. Whereas, dolerite sills, kimberlite dikes, and syenite stocks are discovered in the eastern part of the basin **(Nagaraja Rao et al., 1987)**. Within Cuddapah Supergroup six stages of igneous activity are identified by **Nagaraja Rao et al. (1987)** are as following:

2.3.1 Subaerial eruption of basic lava flows immediately following the deposition of the Vempalle Formation characterises the earliest stage of igneous activity in the Cuddapah Basin

2. Volcanic activity, which results in the development of fine-grained basic rocks and tuffs within the Tadpatri Formation, is the second stage of igneous activity.

3. Within the Vempalle and Tadpatri Formation sequence, the third stage is identified by the introduction of picritic and doleritic sills.

4. Volcanic activity in the Cumbum Formation that is enrichment in barium and iron oxide, is the fourth stage of igneous activity.

5. Alkaline and basic dykes intrusion into the Nallamalai Group of rocks represents the fifth stage.

6. Granitic rocks intrusion within the Nallamalai Group of rocks indicates the final stage.

The only stratigraphic unit with a series of lava flows is the Vempalle Formation **(Anand et al., 2003)**. Tholeiite, andesite, and spilite are the most prevalent volcanics in the Vempalle Formation, and they are all amygdaloidal at the top **(Nagaraja Rao et al., 1987)**. The Vempalle Formation's highest stratigraphic unit is overlain by the basic lava flow in the southern portion of the basin, specifically in and around Pulivendla, Vempalle, and Animala **(Fig 2.1)**. In the northern part of the basin, basaltic lavas are also visible over the Vempalle stromatolitic dolomites (in an around Malkapuram) **(Fig 2.1)**.

Numerous mafic-ultramafic sills are discovered at various stratigraphic levels of the Tadpatri formation. The Tadpatri Formation's lower portion contains the thickest sill bodies, while its top portion typically contains sill bodies that are rather thin. Sills are mafi-ultramafic in character, and the olivine-OPX-CPX-Plagioclase modal proportions range from 50:30:15:5 to 40:20:20:20 **(Anand et al., 2003)**. The quartzite unit of the Bairenkonda Formation frequently contains sill bodies of olivine dolerite **(Dutt, 1975; Nagaraja Rao et al., 1987)**. In

the Cumbum Formation, intrusive granite bodies, kimberlite, lamprophyre, and syenite are most frequently observed **(Leelanandam, 1980; Nagaraja Rao et al., 1987)**. Highly fractionated sub-alkaline tholeiite, produced in a within-plate environment by lithospheric extension probably from a prior subduction-enriched (metasomatized) spinel perididite by approximately 8% of partial melting, is the key factor to form mafic dyke and sills that intruded into the Cumbum Formation **(Das and Chakraborty, 2019)**.

## 2.4 MAFIC DYKE SWARMS AROUND THE CUDDAPAH BASIN:

Around the Cuddapah Basin in the Precambrian shield of Southern India, Proterozoic mafic dyke swarms of various trends and frequency are widely distributed **(Murthy et al., 1987; Mohanty, 2011; Fig. 2.2 and 2.3).** Dyke swarms (Bangalore swarm) occurring in the southern Cuddapah Basin are oriented ENE to ESE and are traversed by NNW-SSE and N-S dykes **(Murthy et al., 1987; Mohanty, 2011; Fig. 2.3).** The Hyderabad Swarm of mafic dykes, which are located in the northwest corner of Cuddapah Basin, exhibit ENE-WSW and WNW-ESE trends and are crossed by NNE-SSW to N-S dykes **(Murthy et al., 1987; Mohanty, 2011; Fig. 2.3)**. In the Western Dharwar Craton (WDC), another set of dyke swarms are widely distributed with the NNW-SSE and ENE-WSW sets. There have been at least five events of dyke emplacement recorded by **Murthy et al. (1987)**, viz. events (i) 2400-2200 Ma, (ii) 1900-1700 Ma, (iii) 1600-1400 Ma, (iv) 1400-1200 Ma and (v) younger than 475 Ma. The oldest Pre-Cuddapah mafic dyke swarms are composed primarily of tholeiitic rock and older than 1700 Ma. the remaining dyke swarms are mostly composed of tholeiitic and alkali in composition.

## 2.5 STRUCTURAL SETTINGS:

The sedimentary units of the Cuddapah and Kurnool Formation in the Cuddapah basin preserve a slight easterly dip throughout **(Fig.2.4)**. Although there is a lot of domal up-warp in the basin's centre, the eastern boundary is dominated by doubly-plunging structures, cross-culminations and depressions, and overturned isoclinal folding **(Nagaraja Rao et al., 1987)**. However, The western margin has remained comparatively undisturbed.

The strike of the rock units within the basin shows NNE-SSW strike trend in the north and swings through a N-S trend in the middle and NNW-SSE orientation in the south. The Rudravaram line divides the Cuddapah basin into two major structural parts **(Meijerink et al. 1984 and fig.2.5)**. The eastern half of this line is intensely deformed and lies specifically between the eastern thrust boundary of Cuddapah Basin and the Rudravaram Line in the east. The western sector of this line exhibits relatively mild deformation. This eastern sector is arcuate in shape and known as Nallamai Fold Belt (NFB) **(Narayanaswami, 1966; Fig. 2.4). Meijerink et al. (1984)** divided the NFB into four subparallel zones, from west to east, based on structural criteria. They are (i) monoclinal structures, (ii) low-amplitude, harmonic folds, (iii) disharmonic folds and (iv) tight, isoclinal folds.

The relatively undisturbed Papaghni Sub-basin is traversed by a variety of faults in the basin's western region, including the Gani-Kalva and Kona faults **(Narayanaswami, 1966; Tripathy and Saha, 2015; Fig. 2.5)**. These faults exhibit considerable strike-slip movements and are associated with granitoid intrusions and mineralization, which have produced anomalous structures like the "Kalva Wall" along the Kalva-Gani fault **(Tripathy and Saha, 2015)**.

Overall, the principal structural component of the Cuddapah basin is an asymmetric, N-plunging synclinorium composed of a highly folded, overturned, and thrusted eastern limb and

a gently dipping, practically non-folded western limb **(Narayanaswami, 1966)**. As the Cuddapah and Kurnool deposits came to an end or during some subsequent orogeny, vertical tectonism caused deep-seated faults to reactivate and leaving tectonic impressions in the form of domal up-warps in the middle of the Cuddapah Basin **(Kalia et al., 1979)**.

## 2.6 NALLAMALAI FOLD BELT:

The Nallamalai Fold Belt situated in proximity and west of the southern part of the Eastern Ghats belt (Krishna province), and is thrust over the lower Cuddapah sequences and the Kurnool Group of rocks **(Saha and Patranabis-Deb, 2014; Fig. 2.5).** The eastern margin of NFB again represents a major thrust front (Vellikonda thrust front) along which the Nellore schist belt (NSB) is juxtaposed against NFB **(Saha et al., 2010)**. Other than the Vellikonda thrust in the east and the Maidukuru thrust in the west, the NFB has smaller internal thrusts, bedding parallel detachments, and transverse faults. **(Fig. 11; Tripathy and Saha, 2015)**. In the north eastern part of NFB, three stages of deformation are – $D_1$, $D_2$, $D_3$. Among them $D_1$ and $D_2$ are associated to the thrusting of NFB and are considered to be occur prior ~1580 Ma **(Tripathy and Saha, 2015)**. Locally occurring $D_3$ type deformation exhibits a transverse link to the overall NFB trend **(Saha et al., 2010; Saha and Patranabis-Deb, 2014)**.

## 2.7 GEOCHRONOLOGICAL CONSTRAINTS ON STRATIGRAPHIC DEVELOPMENT:

A poorly defined Rb-Sr age of 1704±112 Ma **(Bhaskar Rao et al., 1993)** is provided by the Pullivendla sills intrusive into the base of the Tadpatri Formation (Chitravati Group, which overlies the Papaghni Group). Two samples from the same Pullivendla sill were tested for biotite and clinopyroxene, which produced ages of 1811 and 1831 Ma. These ages may be the absolute upper age limit for the sedimentation of the Papaghni and Chitravati groups, into

which it intrudes **(Murthy et al., 1987)**. The early phase of the Cuddapah Basin's expansion and volcanism are constrained to 1.9 Ga by $^{40}Ar/^{39}Ar$ laser-fusion data obtained on phlogopite mica from the same mafic-ultramafic sill complex **(Anand et al. 2003)**. On a comparable mafic sill from the Pullivendla region of the Cuddapah Supergroup, a high-precision U-Pb date of 1885±4 Ma was discovered **(French et al. 2008)**. The Pb/Pb age of 1756±29 Ma is interpreted as the time of uranium mineralization and as a minimum age for carbonate sedimentation and dolomitization. **Zachariah et al. (1999)** determined the Pb, Sr, and Nd isotopic compositions on uranium-mineralized and barren stromatolitic dolomite samples from the Vempalle and Tadpatri Formations. The Chelima Lamproite, dated at roughly 1400 Ma **(Chalapathi Rao et al. 1999)**, and 1573 Ma granite intrude the folded Nallamalai Group near its eastern boundary, according to **Crawford and Compston in 1969**.

The Cuddapah Supergroup's upper age limit has been fixed through this analysis. Therefore, it may be said that the Papaghni Group (Gulcheru Formation) is most likely between >1.8 and <-+2.1 Ga in age (age of pre-Cuddapah dyke swarms) **(Table 2.3)**.

# FIGURES AND TABLES

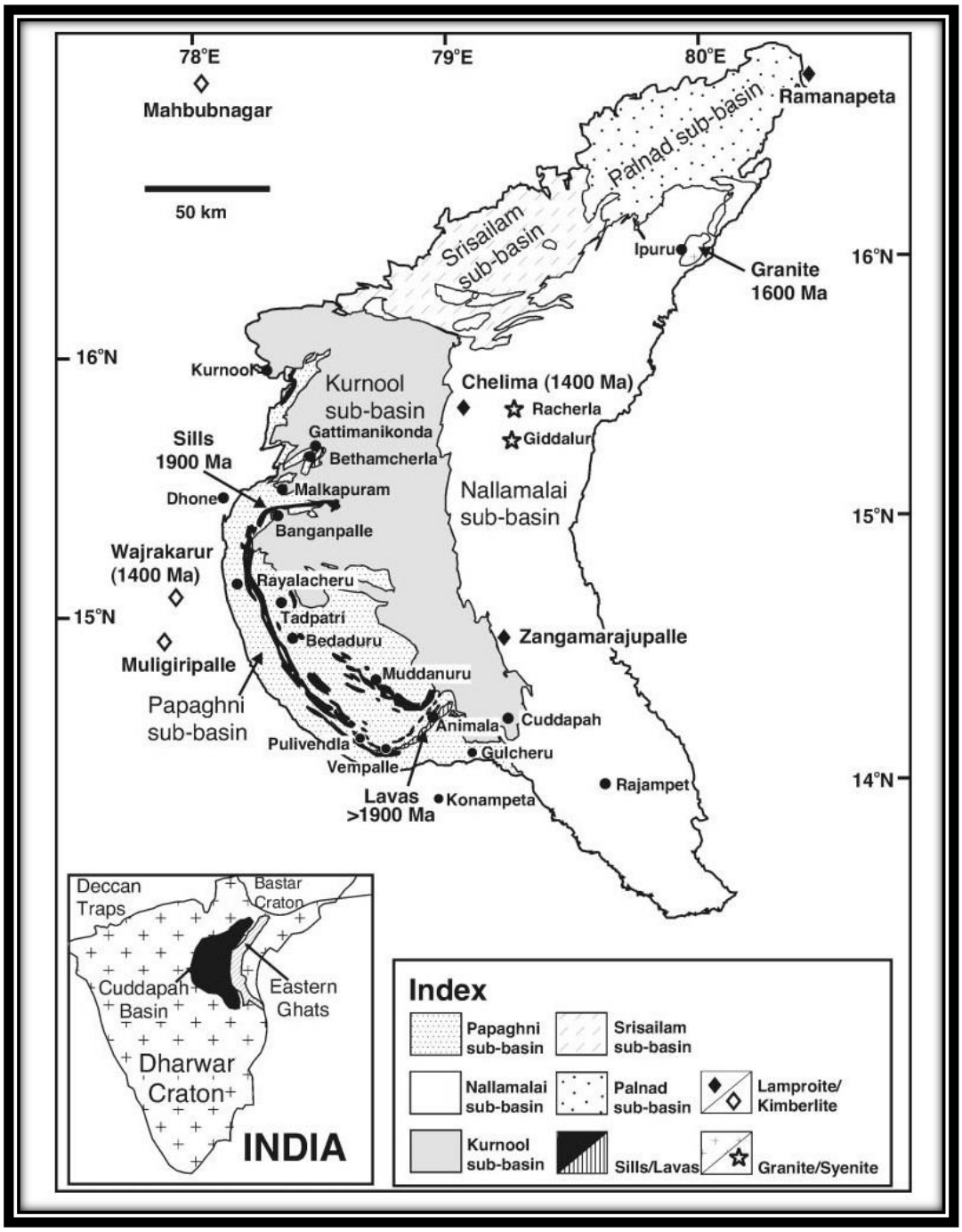


**Fig. 2.1** Geological map of the Cuddapah Basin (modified after **Nagaraja Rao and Ramalingaswamy, 1976**)

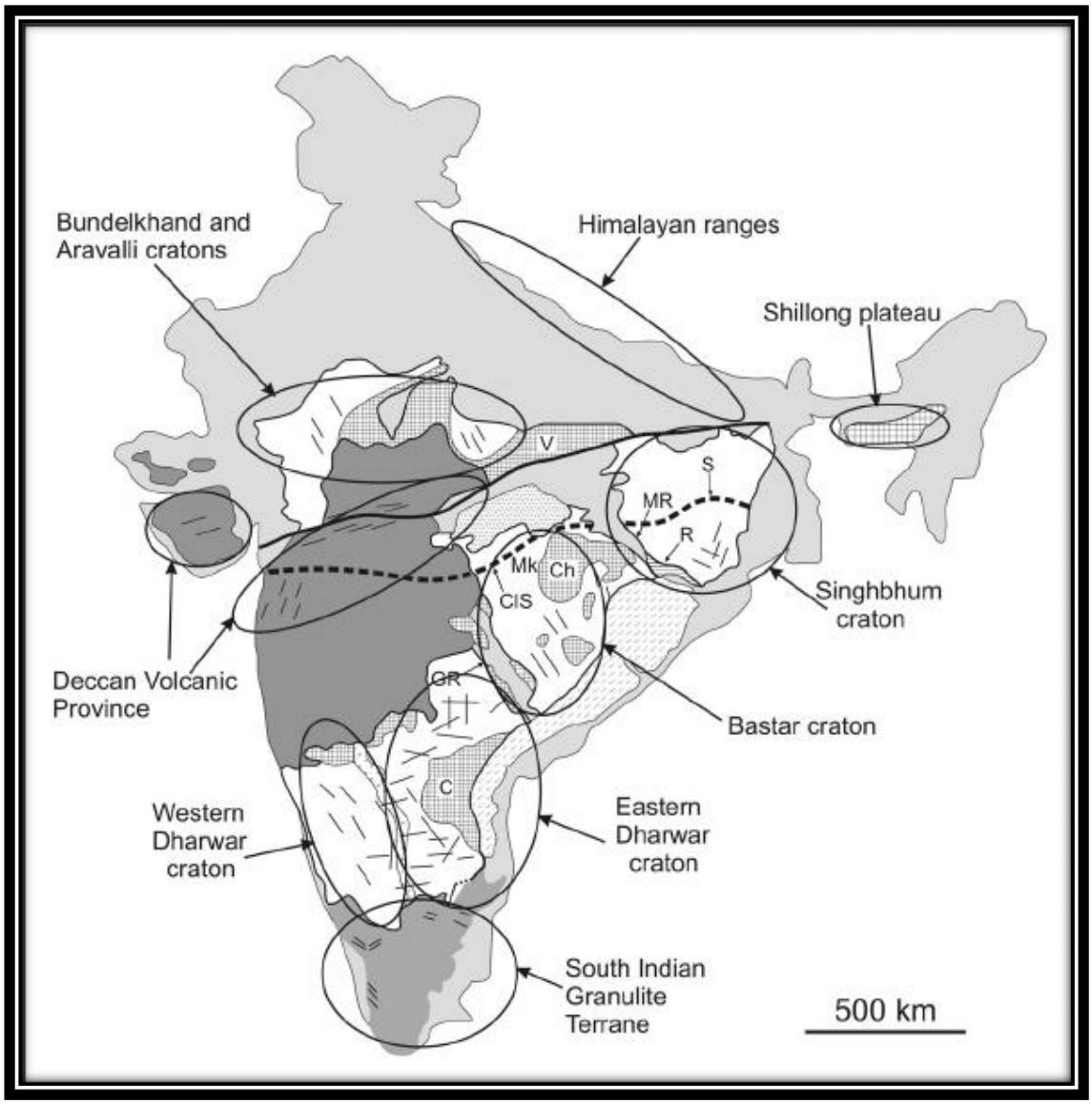


**Fig 2.2** Dykes/dyke swarms in different Archaean cratons, Deccan Volcanic Province and other regions (circled) of the Indian shield (modified after French et al., 2008). C, Cuddapah; Ch, Chattisgarth Basin; CIS, Central Indian Shear Zone; GR, Godavari Rift; M, Madras Block; Mk, Malanjkhand; MR, Mahanadi Rift; N, Nilgiri Block; NS, Narmada-Son Fault Zone; R, Rengali Province and Kerajang Shear Zone; S, Singhbhum Shear Zone; V, Vindhyan Basin **(Srivastava, 2006)**

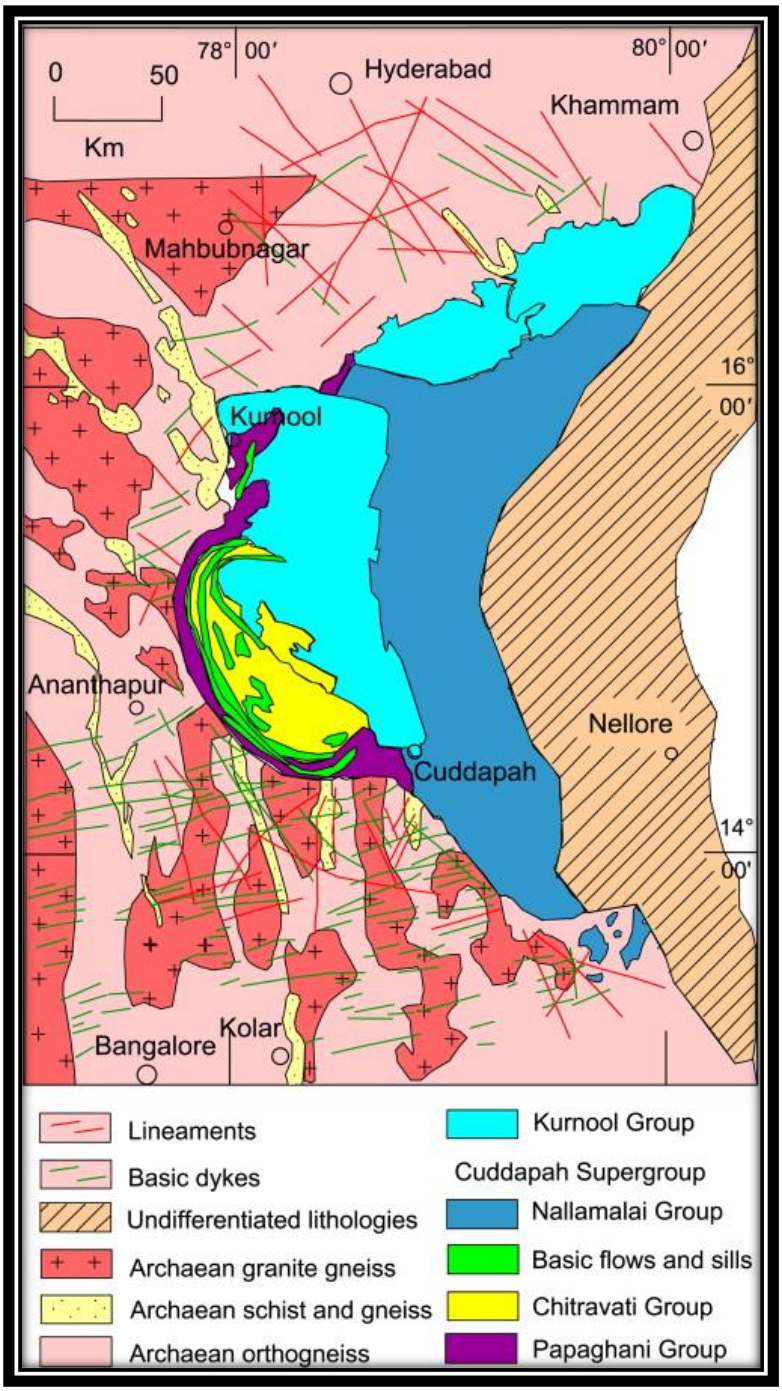


**Fig. 2.3** Detail geology of the Dharwar craton and the Cuddapah basin, showing truncation of mafic dykes and lineaments along the boundary of the Dharwar craton and the Cudapah basin (after **Mohanty, 2011**)

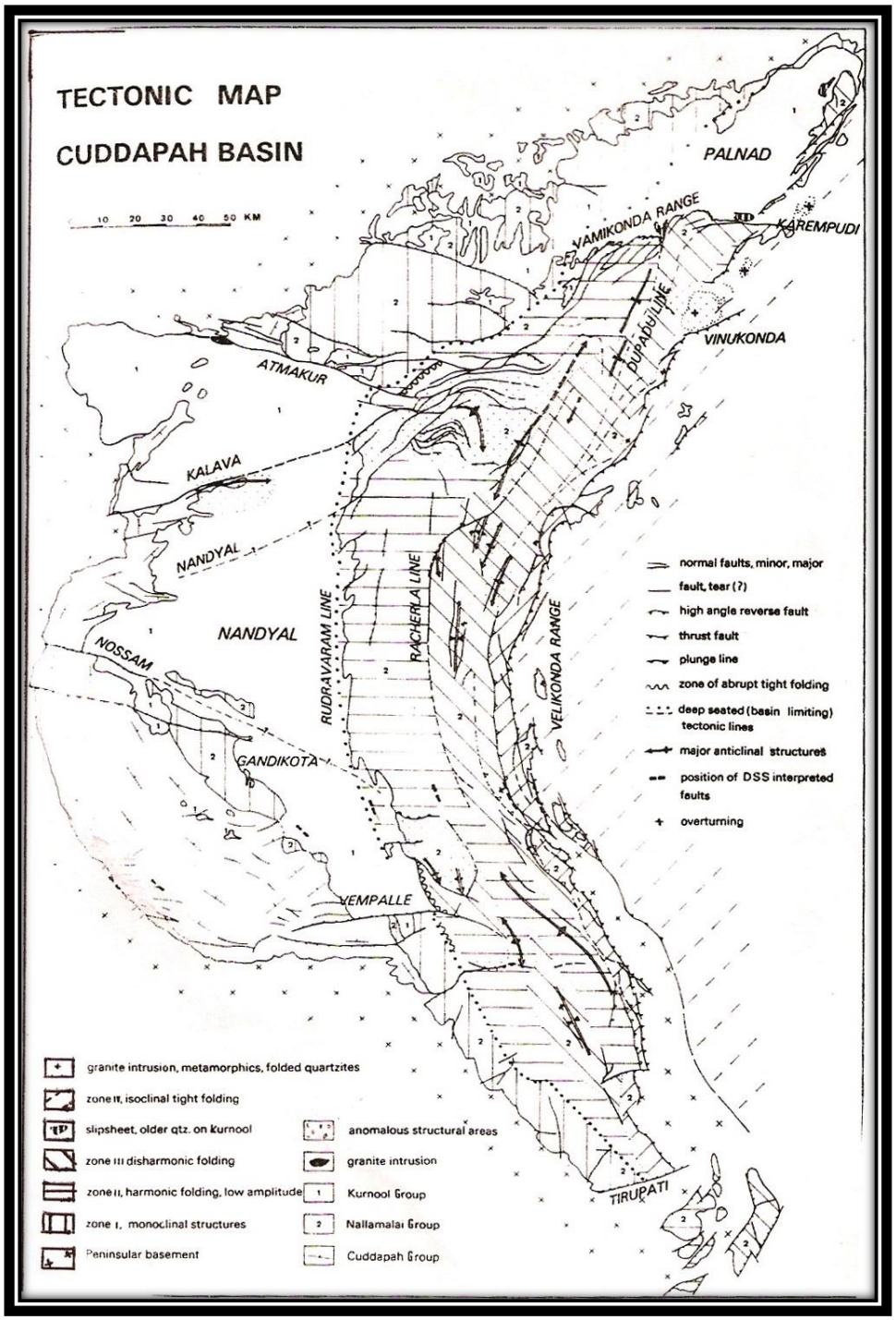


**Fig. 2.4** Tectonic map of Cuddapah Basin showing overall structural pattern on either side of Rudravaram line (after **Meijeink et al., 1984**)

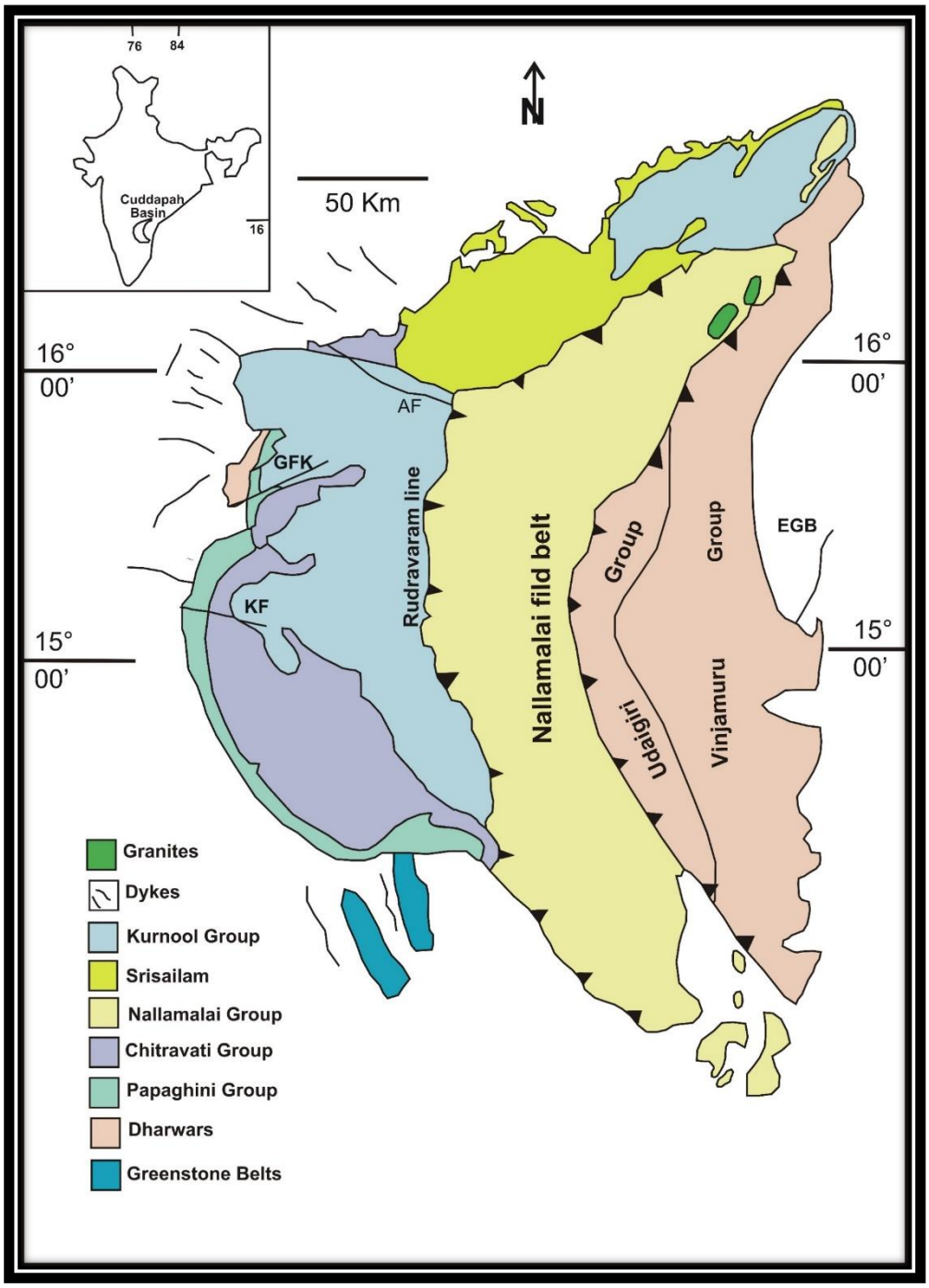


**Fig. 2.5** Simplified geological map of the Cuddapah Basin (modified after **Saha and Tripathy, 2012**). Western margin of the basin is convex and developed over the Eastern Dharwar, whereas the eastern margin is concave and has a contact with Nellore schist belt and Eastern Ghat Belt

| Formation | Bed | Unit |
|---|---|---|
| Kadapah | Kistnah | Sreeshalum Quartzite<br>Kolamnala Slates<br>Iralakonda Quartzite |
| | -------Unconformity------- | |
| | Nullamullay | Cumbum Slates<br>Byrenconda Quartzite |
| | Chey-air | Tadapurtee (Poolumpett) Slates with limestones<br>Poolavaindla or Naggery Quartzites |
| | Paupugnee | Vaimpully Slates and Limestones<br>Goolcheroo Quartzites |

**Table 2.1** Lithostratigraphic classification of Kadapah Formation (Cuddapah Supergroup) (Proposed by **King, 1872**)

| Group | | Formation | Lithology | Age |
|---|---|---|---|---|
| Kurnool | | Nandyal (50-100m) | Shale | Neoproterozoic |
| | | Koikuntala (15-50m) | Limestone | |
| | | Paniam (10-35m) | Quartzite | |
| | | Owk (10-15m) | Shale | |
| | | Narji (100-200m) | Limestone | |
| | | Banganapalli (10-15m) | Quartzite with Conglomerate | |
| -------Unconformity------ | | | | |
| Cuddapah Supergroup | | Srisailam (300m) | Quartzite | Mesoproterozoic |
| | -------Unconformity------ | | | |
| | Nallamalai | Cumbum (2000m) | Phyllite, Shale, Quartzite, Dolomite | |
| | | Bairenkonda (5500m) | Quartzite, | |
| | -------Unconformity------ | | | |
| | Chitravati | Gandikota (300m) | Quartzite, Shales | |
| | | Tadpatri (4600m) | Shale, Quartzite, dolomite | |
| | | Pulivendla (1-75m) | Conglomerate, Quartzite | |
| | -------Unconformity------ | | | |
| | Papaghni | Vempalle (1900m) | Dolomite, chert, Basic flows and Intrusive | Paleoproterozoic |
| | | Gulcheru (30-210m) | Conglomerate, quartzite and and shale | |
| -------Unconformity------ | | | | |
| Dharwar Craton | | | | Archean |

**Table 2.2** Stratigraphy of the Cuddapah Basin (Proposed by **Ramam and Murthy, 1997**)

| Group | Formation | Age (M.a.) | Dating Method | Comments | Reference |
|---|---|---|---|---|---|
| Srisailam Quartzite | | 1327±0.17 | Sm-Nd | Lambapur uraninite, primary crystallization age | Pandey et al., 2009 |
| | | 1787±22 | U-Pb | Quartz arenite | Collins et al., 2015 |
| -----Unconformity---- | | | | | |
| Nallamalai | Cumbum (Pullampet) | 1418±8 | Ar-Ar | Chelima lamproite trending NE-SW | Chalapathi Rao et al., 1999 |
| | | 1371±45 | K-Ar | Chelima lamproite trending NE-SW | Murthy et al., 1987 |
| | | 1615±25 | Rb-Sr | Vinukonda Granite | Gupta et al., 1984 |
| | Bairenkonda (Nagari) | | | Not reported | |
| -----Unconformity---- | | | | | |
| Chitravati | Gandikota | 1207±22 | U-Pb | Quartz arenite | Collins et al., 2015 |
| | Tadpatri | 809±29; 958±29 | K-Ar | Arc-concentric, mafic sill | Murthy et al., 1987 |
| | | 1756±29 | Pb-Pb | Uranium mineralized horizon | Zachariah et al., 1999 |
| | | 1672±38 | U-Pb | Zircon grains within stromatolites | Khelen et al., 2020 |
| | Pulivendla | 1817±24 | Rb-Sr | Mafic Sill | Bhaskar et al., 1995 |
| | | 1885.4±3.1 | U-Pb | Mafic Sill | French et al., 2008 |
| -----Unconformity---- | | | | | |
| Papaghni | Vempalle | 1550±147 | Rb-Sr | Mafic flow | Collerson & Sheraton, 1986 |
| | | 1879±5 | Ar-Ar | Mafic dyke | Murthy et al., 1987 |
| | | 1841±71 | K-Ar | Mafic dyke | Murthy et al., 1987 |
| | Gulcheru | 2490±19 | U-Pb | Polymict conglomerate | Collins et al., 2015 |

**Table 2.3** A brief summary on geochronological works from Cuddapah Supergroup

# CHAPTER 3

# FACIES ANALYSIS AND PETROGRAPHY

## 3.1 INTRODUCTION

An essential prerequisite to understand the modes of deposition in an ancient sedimentary basin is an organized classification of the rocks deposited therein. While the classification can be achieved in various ways, for a sedimentological investigation the primary choice would naturally be that, which would permit glimpses into the environment of deposition. A facies analysis dealing with the genetic aspects of co-existing rock bodies is very useful for the above-mentioned goal. Reconstruction of paleogeography and paleo-depositional milieu in terms of geochemistry as well as depositional processes requires thorough facies analysis for basin-fills. Hence, attempts have been made here to carry out the state-of-art facies analysis. The most important criteria for facies classification are the lithologies, overall geometries, internal structures and nature of bounding surfaces of the sedimentary bodies. Identification of sediment dispersal pattern and depositional agent along with some basic petrographic characters, like mineralogical and textural maturity, are also very much informative to delineate genetically different facies. The next step is to study their distribution in time and space along with the nature of contact among themselves. Facies association analysis can provide important information regarding the paleodepositional conditions.

## 3.2 SEDIMENTARY FACIES IN THE GULCHERU FORMATION

The Gulcheru Formation in the study area is represented by eleven facies as under **(Fig. 3.1)**.

Facies A: Clast supported poorly sorted breccia facies

Facies B: Clast supported conglomerate facies

Facies C: Stacked couplets of clast supported conglomerate and sandstone facies

Facies D: Medium to coarse grained trough cross stratified sandstone facies

Facies E: Medium to coarse grained tabular cross bedded sandstone facies

Facies F: Fine to medium grained ripple laminated sandstone facies

Facies G: Fine to medium grained tabular cross bedded sandstone facies

Facies H: Fine to medium grained massive sandstone with coarse basal lag facies

Facies I: Fine grained planar laminated sandstone facies

Facies J: Fine to Medium grained trough cross stratified sandstone facies

Facies K: Rhythmite facies

## Facies A: Clast supported poorly sorted breccia –

This facies is narrow and laterally discontinuous resting unconformably on the Archean basement **(Fig. 3.2)**, and attains maximum thickness of about 3.5m in the south-western part of the study area and gradually thins out northwards. This facies is characterized by angular cobbles (long axes ranges from 7.8cm to 15cm) to pebbles (long axes ranges from 0.8cm to 3.5cm) clasts cemented together in a coarse-grained sandy matrix. Randomly oriented clasts of granite and quartzite are the dominant clast fragments found in the framework. Megascopically the facies has greyish white in colour. The cement that binds the clasts in breccia is silica oxide with minor ferruginous clay. The upper boundary is truncated abruptly by coarse grained sandstone facies.

***Interpretation:*** Presence of bimodal clasts within coarse grained sandy matrix indicates that the deposition takes place in moderate to high energy environment. The bimodal size distribution of clasts seems to be generated due to the weathering product from different weathering site. The bed with dominance of tightly packed, poorly sorted and randomly oriented cobble to pebble sized clasts indicates short distance transport and fast sedimentation. This breccia is possibly the result of reworked sediments derived by subaerial cohesion less

debris flow with high grain/water ratio **(Mulder & Alexander 2001; Sohn et al. 2002; Dasgupta, 2005; Kim et al., 2018)**.

## Facies B: Clast supported conglomerate

This facies resting conformably on Facies D is characterized by well bedded clast supported conglomerate **(Fig. 3.3)**. The size of clasts varies from cobbles (long axes ranges from 6.5cm to 16cm) to pebbles (Long axes ranges from 0.6cm to 4.5cm). These framework grains are embedded in coarse grained sandy matrix. Mineralogically jasper, granite and quartzite are the dominant clast fragments found in the framework. Megascopically the facies has grayish white to pinkish red in colour. Clasts are moderately sorted, well rounded with disc shaped sphericity. The larger clasts dominate over the smaller one in the framework. Bedding plane is defined by the alignment of long axis of the clasts. The clasts occasionally show a(p)a(i) fabric with average clast inclination ~$20^0$ towards north. Overall, a fining upward succession is observed in this facies and this facies is overlain by medium to coarse grained trough cross stratified sandstone with gradational boundary contact.

***Interpretation:*** This clast supported conglomerate seems to be deposited by classical debris-flow **(Blair & McPherson, 1998)** in an alluvial fan depositional environment. The presence of large clasts in sandy matrix points to a flow with some cohesive strength **(Went, 2005)**. It is generally distributed near the mountain at the margin of the basin, and is a fan-shaped accumulation which is formed by coarse clasts derived from the weathered mountain after rolling down the slope break under gravity **(Moscariello, 2017)**. The fans were developed at the basin margin when the high energy ephemeral streams gushes into the basin. They carry the clasts (pebbles, cobbles and rarely boulders) along with substantial amount of finer fractions (granules, sands and silts) and dump them (debris flow) at the basin margin. Flat clast

supported conglomerate suggest the presence of periodic high-energy events, and are interpreted as evidence for the sedimentation influenced by gravity flow originated in the provenance highland near the basin margin and the finer sediments are deposited when the flow strength is slackened **(Basu et al., 2007)**.

## Facies C: Stacked couplets of clast supported conglomerate and sandstone

This facies overlies the framework supported conglomerate facies with gradational boundary contact and characterized by alternate repetition of matrix supported conglomerate and layers of quartzite **(Fig. 3.4)**. Conglomerate is characterized by 40-45% clasts (long axes ranges from 0.2cm to 18cm) content as frame work with composition of jasper, granite and quartzite and rest part occupied by the coarse-grained sandy matrix **(Fig. 3.5)**. Clasts are bimodal, sub angular to sub rounded and occasionally showing a(p)a(i) fabric with average clast inclination ~$15^0$ to $20^0$ towards north. The Pebbly stratified matrix supported conglomerate alternating with gritty to coarse graded sandy layer formed couplet facies. Each couplet is almost 0.5 to 1 m thick. The number of couplets varies from 2-3 over the entire study area. The total thickness of this couplet unit varies from 2m to 3m. The size range of the clasts decreases with respect to the underlying unit. The facies changes to trough cross stratified facies as sandstone with an erosional boundary in between.

***Interpretation:*** This facies seems to be formed under periodic high energy to medium flow energy condition. Occasionally the hyper concentrated flood flows are triggered through erosional incision **(Sohn et al., 1999)** during downslope movement over previously deposited unconsolidated coarse sandstone and the flows were transformed into cohesionless debris flows.

## Facies D: Medium to coarse grained trough cross stratified sandstone facies

This facies is characterized by compound trough cross-stratified medium to coarse grained ill-sorted sandstone bodies, with frequent oversized clasts **(Fig. 3.6)**. These bodies are broadly lenticular in flow perpendicular direction with planar base and convex upward top. Such bodies, initiated with large trough sets are followed upward by smaller ones **(Fig. 3.7)**. Smaller sets are found to be encased within the larger foresets in longitudinal section. The large cross-strata dip at low angle, usually less than $10^0$ and both the large and small cross strata are oriented in the same direction which is along $280^0$. Trough cross strata on the top of the bedding plane also indicate the paleocurrent direction towards NE **(Fig. 3.8)**. Rarely smaller foresets showing opposite dip direction to larger foresets have been identified also. Coexistence of two contrasting dimensions of troughs makes the set thickness range wide from 6cm to 83cm and bimodal. The oversized pebbles wherever present, generally defining the foreset bases are generally well rounded and range in length up to 1.2cm. Some facies units have also preferred pebble concentration on their tops in form of a laterally impersistent thin sheet overlying a planar erosion surface. Petrographically this sandstone is quartz arenite with about 90% quartz, 2-3% feldspar and 1-2% rock fragments, composed mainly of chert and quartzite **(Fig. 3.9)**. The matrix content is very low (about 7-8%), with a few pseudomatrix, formed by crashed feldspar grains. Scarce presence of quartz cement has also been observed. The quartz grains are subangular to subrounded in nature with poor sorting; hence the rock can be said as texturally immature.

***Interpretation:*** Migration of large curve crested bedforms or bar along channel floor is indicated **(cf. Collinson and Thompson, 1989; Erriksson et al., 2006)**. Large scale trough cross-stratification characterizes the bar, whereas small troughs over it accounts for the

accretionary part of the bar **(Reesink et al., 2013; Almeida et al., 2013)**. The compound cross strata with both large and small ones oriented in the same direction signify migration of smaller bedforms across the crest and along the gentle downstream surface of the large bedforms. Such phenomenon is known as downcurrent accretion. The other case on the other hand, suggests that the climb took place on stoss of large bedforms. Such upcurrent accretion on the bars suggests relatively rapid rate of sedimentation. The pebble sheets on top of the sets are a possible product of high shear flow before emergence of the bedform, winnowing out the finer fractions. Confinement of the facies to the basal part of division indicates higher depositional slope or in other words, higher flow velocities at the onset of deposition of the division **(Morris et al., 2014)**.

## Facies E: Medium to coarse grained tabular cross bedded sandstone facies –

This facies is characterized by strongly lenticular bodies of tabular cross-stratified medium to coarse sand-sized moderately-sorted sandstone, without any oversized clasts **(Fig. 3.10)**. Two varieties are found within this facies. One subgroup shows foreset dip conformable with the general palaeocurrent direction. This facies is found on top of master erosion surfaces, and associated with facies D laterally as well as vertically. The other subfacies is found to be associated with facies C, although rarely, recycling on it. Such bodies show planar sharp base with convex –up top with a maximum 20cm preserved thickness. The Coset of tabular cross-stratification varies from 1-4.2cm due to erosional bounding surfaces. Foresets dip directions make low angle with the overall paleoflow direction, as inferred from the troughs of other facies. Occasionally low amplitude long crested ripples present on the top surface of this facies **(Fig. 3.11)**. These inclined bedforms dip up to $18^0$ and are oriented perpendicular to paleo-flow. They are interpreted to be the accretionary deposits of a meandering deep water channel system **(Fig. 3.12 and Fig.3.13; Abreu et al., 2003)**. Petrographically this facies is arkosic

sandstone with medium to coarse sand grain-size and moderate sorting **(Fig. 3.14)**. This facies does not contain any oversized clasts.

***Interpretation:*** This facies make up a very minor proportion of the total succession. Subfacies with conformable paleocurrent direction accounts for transverse bars, moving along the channel floor towards the initial stage of channel filling **(Reading, 1996; Labourdette and Jones, 2007)**. The reclining nature of the other subfacies along with its strongly lenticular geometry and different paleocurrent directionpoints to its origin probably by the collapse of sandy material from the top of the bar bedform along the flanks **(Bose et al., 2008)**.

## Facies F: Fine to medium grained ripple laminated sandstone facies-

This facies is characterized by ripple laminated fine to medium grained moderately sorted, sub-rounded sandstone bodies with broadly lenticular geometry **(Fig. 3. 15)**. This facies overlies facies D, but not always and hence constitute a minor portion of the total succession. This facies is characterized by ripple lamination (high Ripple Index) with reverse grading within the foreset, sometimes showing ripple climb **(Fig. 3. 16)**. The individual set thickness varies in cm scale. On the bedding surface preserved ripples with average height 0.8cm and maximum ~1.2cm having straight or broadly sinuous crests have been found with coarsest grain fraction concentration in the crest area **(Fig 3.17)**. Petrographically this facies is quartz arenite showing subangular to subrounded grains size and moderate sorting **(Fig. 3.18)**.

***Interpretation:*** The presences of ripple laminated unit on top of the channel bedforms clearly indicate its lower flow regime origin **(Fielding, 2006)**. As the water depth decreases along with the water velocity larger dunes, previously moving on the channel floor are replaced by the

smaller scale ripples and hence such facies can be produced in the penultimate stage of a channel fill **(Cala et al., 2020)**.

## Facies G: Fine to medium grained tabular cross bedded sandstone facies –

This facies is characterized by tabular cross-stratified bodies of fine to medium sand-sized poorly sorted, subrounded to rounded sandstone **(Fig. 3.19)**. This facies is restricted within the topmost channel belt only overlying facies F. The cross-stratification is characterized by inverse grading within foreset laminae **(Fig. 3.20)**. This facies show sharp and planar lower contact as well as upper contact. The maximum measured thickness of this facies is about 5m. Occasionally, isolated low-amplitude ripple-forms are present on the bedding plane. Petrographically this facies is characterized by high matrix (clayey matrix) content and more than 80% quartz grains **(Fig. 3.21)**; hence it is arkosic sandstone in nature. Sorting is moderate with subrounded fine sand-sized grains. Moderate amount of silt sized material concentration has been found along the foreset boundaries.

***Interpretation:*** The tabular nature of the cross-stratified foresets along with concentration of silt sized material along the foresets clearly suggests deposition under lower flow regime condition. Reverse grading within foreset laminae suggest rapid sedimentation from accelerating heavily sediment-laden wind **(cf. Reineck and Singh, 1980; Collinson and Thompson, 1982)**. Isolated low amplitude ripples indicate liquefaction and adhesion of wind-blown sand **(cf. Collinson and Thompson, 1982)**.

## Facies H: Fine to medium grained massive sandstone with coarse basal lag facies –

This thick sandstone horizon shows a laterally persistent massive sandstone body **(Fig. 3.22)**. This facies comprises mainly sub-angular to sub-rounded, well sorted sanstone. No sedimentary structure observed in this facies. Fine to medium sand, often separated by lags of pea sized pebbles **(Fig. 3.23)**. Some high index ripples present on top of the bedding plane. Petrographically this facies is characterized by low matrix content and more than 96% quartz grains; hence it is quartz arenite in nature **(Fig. 3.24)**. Moderate amount of silt sized material concentration has been found along the sandstone boundaries.

***Interpretation:*** Sedimentation obviously took place in high to low flow regime with reference to the sediment grain size. Sedimentation took place as a result of saltation and accretion of sand from gently decelerating wind **(Fryberger et al., 1979; Kocurek and Nielson, 1986)**.

## Facies I: Fine grained plane laminated sandstone facies -

This facies is characterized by plane laminated fine to medium grained sandstone bodies with laterally impersistent to broadly tabular geometry **(Fig. 3.25)**. Two different subfacies can be proposed between this facies on the basis of their association and grain-size. The organization of fine to medium sand and silt grains into multiple layers represent the sedimentary structure called pin-stripe lamination **(Fig. 3.26)**. The layers of medium to coarse sand that interfinger with grainfall and wind ripple laminae. These distinct sedimentary structures variably referred to as grainflow **(Fig.3.27; Kocurek and Dott, 1981; Kocurek, 1996)**, This facies constitutes a comparatively smaller proportion of the total succession. This facies comprises of fine sand. The sorting varies from moderate to good. The sand grains are sub-rounded to rounded. The

framework grains consist of about 95% quartz, besides; a few feldspar and rock fragment grains are also present. Petrographically the sandstone is quartz arenite **(Fig. 3.28)**.

***Interpretation***: The presence of repetitive inverse-graded pin-stripe laminae with interbedded grainflow laminae and grainfall laminae are the product of wind activity **(Hunter, 1977a, 1981; Kocurek and Dott, 1981; Fryberger and Schenk, 1988; Kocurek, 1996)**. The coarser grained counterpart is a likely product of rising water stage and the finer grained counterparts is attributable to falling water stage. The common occurrence of granule-ripple deposits in this architectural element indicates the variable strength of the wind and a generally low availability of sand **(Basilici et al., 2020)**.

## Facies J: Fine to Medium grained trough cross stratified sandstone facies -

This facies is characterized by trough cross-stratified sandstone bodies, otherwise almost same as the previous facies, except for the geometry and internal structures **(Fig 3.29)**. These bodies show lenticular geometry in flow perpendicular direction with concave-upward erosional bases and relatively flat tops. Internally this facies is characterized by cosets of troughs, about 28 cm thick on average. Trough sets present in this facies is comparatively smaller in size. Generally, each body initiates with larger sets with gradual decrease in set thickness upward. The cross bedding in which foresets in successive sets are directed in opposite directions representing herringbone cross strata **(Fig. 3.30)**. Rarely a massive part overlies the erosional bottom surface followed by the larger trough sets. Pebbles define the foreset bases and generally smaller than those of facies D. Trough cross-strata orientation elicits bimodal paleocurrent direction. Petrographically this facies is similar to that of facies D,

with a slight reduction of grain size. Fine sand-sized grains are subrounded to rounded with moderate sorting, implying a comparatively larger transportation **(Fig. 3.31)**.

***Interpretation:*** The facies manifests dune migration presumably along the channels. Smaller cross-set thickness and comparatively finer grain size of this facies, with respect to facies D, in close association, signify dune migration under relatively lower flow shear. Common in-channel upward decrease in trough cross-set thickness without accompanying grain-size reduction within the sandstone bodies record gradual decline in the flow regime **(Harms et al., 1975)**, probably in rising water stage. Thus this facies represent the channel forms. Herrinbone cross strata records bidirectional flow, commonly observed in tidal-flat depositional environment **(Flemming, 2012; Bradley et al., 2018)**

## Facies K: Rhythmite facies-

This facies is characterized by very fine red coloured thin layers of shale **(Fig. 3.32)**. This facies is restricted only in the younger part of the Gulcheru succession of this section. Geometry of the mud bed defines sheet like in exposure scale but laterally discontinuous. The rock surface displaying well-developed polygonal oscillation crack **(Fig. 3.33)** present on the top surface of the mud layer. Alternate layers of sand and mud shows sand wave deposits with bundles of foresets separated by mudstone drapes **(Fig. 3.34)**. Petrographically this facies represents alternate layers of shale with siltstone layer **(Fig. 3.35)**. In some places mica and ferruginous material also present.

***Interpretation:*** During low wave condition, tides take a leading role in deposition, producing thin alternations of sand and mud laminae **(Daidu, 2013)**. A grouping pair of sand-dominated layers and mud-dominated layers is the product of seasonal alternations of wave **(Daidu, 2013)**.

### Cyclicity analysis of fine sand mud alteration within rhythmite facies:

Alternate layers of sand and mud shows sand wave deposits with bundles of foresets separated by mudstone drapes. Each laminae's thickness is determined by measuring it perpendicular to the foresets' dip along a horizontal axis connecting the top and lower boundary surfaces. The relative thickness of each laminae is determined in the field, and the Origin software has been used to plot the laminae numbers (x-axis) versus the succeeding laminae thickness (y-axis) **(Fig. 3.36)**. To further understand the nature of laterally accreted alternate thick-thin laminae, five-point smoothing is used. The smoothing procedure uses the Fast Fourier Transform (FFT) filtering method, and as per standard, laminae thickness is taken into account while computing smoothing. The thick-thin laminae alternations in **Fig. 3.36**, red colour curve is the result of smoothing, and the entire sequence in the foresets is referred to as tidal bundles.

## 3.3 FACIES ASSOCIATION

The array of facies as recorded in these sections can be grouped into four broad genetically related associations that represent alluvial fan, fluvial, aeolian and tidal flat palaeoenvironments.

### 3.3.1 ALLUVIAL FAN FACIES ASSOCIATION (FA-I)

This facies association mainly present at the marginal part of the basin. Alluvial fan facies association comprises Facies A, B and C. Facies A occurs as a narrow and laterally discontinuous bodies over basement granite gneiss. It is overlain by lensoidal bodies of Facies B with a sharp contact. In some places Facies A replaces Facies B directly rests over the basement granite gneiss. Further Facies B is overlain by Facies C. From mutual relationship and spatial distribution facies association I is interpreted as alluvial fan **(cf. Blair and**

**McPherson, 1994a and references therein)**. Whereas Facies A of this association represents proximal fan cohesionless debris flow, facies B and C represent proximal to middle fan hyperconcentrated flood flow deposits **(Köykkä, 2010 and references therein)**.

### 3.3.2 FLUVIAL FACIES ASSOCIATION (FA-II)

This facies association present in the lower part of the Gulcheru Formation is composed of channelized or lenticular medium to coarse grained sandstone with thin mudstone interlayers. The channelized sandstone is characterized by normally graded trough, ripple laminated and tabular cross stratification. Facies association II is comprised of Facies D, E and F, originated after the deposition of Facies association I. Facies D and E occur as alternating unit of conformable larger dimension, whereas Facies F occurs as isolated bodies of smaller dimension. Facies D and E are deposited as longitudinal and transverse bars respectively, depending on the discharge level. Depending on the mutual relation and spatial distribution facies association II is interpreted as ephemeral stream **(cf. Olsen, 1987; Dam, G. and Andreasen, 1990)**.

### 3.3.3 AEOLIAN FACIES ASSOCIATION (FA-III)

This facies association mainly comprises fine to medium grained sandstone and siltstone, of which grains are moderately to well sorted and subangular to rounded in shape. These sandstones are arranged into tabular and planar cross bedded set up. Facies association III comprises Facies G, H and I. Facies G and H occur as tabular bodies while I occur as sheet like sandstone bodies. In transverse section facies G is characterized by sharp bounding surface and always overlies the master erosion surfaces. FA-III seems to be represented by different depositional bedforms of an aeolian regime. Facies G and H represent rapid sedimentation from

decelerating heavily sediment-laden wind **(cf. Reineck and Singh, 1980; Collinson and Thompson, 1982)**. Facies I represent the migration of aeolian dune **(Kocurek and Dott, 1981)**.

### 3.3.4 TIDAL FLAT FACIES ASSOCIATION (FA-IV)

This facies association mainly restricted in the upper part of the Gulcheru Formation is composed of fine to medium grained trough cross stratified sandstone and thick layer of alternate sand and mud. Facies association III comprises Facies J and K. The major portion of the upper most part of the succession is made up of Facies J and K, along with minor proportion of Facies F. All these facies are found to be distributed among all the channel belts, although in upper two belts facies K dominate over facies I. Facies K is restricted only within topmost channel belt. FA-III represents different depositional bedform of a tidal flat regime **(cf. Proske et al., 2008; MacNaughton et al., 2018)**.

## 3.4 DEPOSITIONAL ENVIRONMENT

The Gulcheru sedimentation in the study area starts with deposition of breccias and conglomerate (Facies association 1) indicating the deposition has taken place in high energy environment. The bimodal size distribution indicates co-sedimentation of bedload and suspended load in fluctuating energy regime. Availability of abundant loose detritus produces high grain/water ratio in the flow originated initially. Consequently, proximal fan cohesionless debris flow deposits and middle fan hyperconcentrated flood flow deposits mainly occur at the base of the sedimentary succession near the basin margin **(Sohn, 1999)**. Features like coarser grain-size, poor sorting and subangular grains within the succession clearly point towards its alluvial fan origin. Occurrence of hyperconcentrated deposits directly above the debris flow deposits bear the evidence of erosional incision during downslope movement over previously deposited unconsolidated coarser sediments **(Eyal et al., 2019; Zhao et al., 2022)**. The

ungraded clast supported conglomerate with scoured base exemplifies the flow transformation from hypercontrated flood flow to cohesionless debris flow.

As a whole presence of medium to coarse grained trough cross-stratification within the total successions clearly indicates the deposits as a fluid gravity flow-product, where traction current is the sediment-transporting agent **(Miall, 1992)**. This very coarse grained multistoried tabular sandstone bodies, along with their poor sorting and subarkosic nature, can easily be identified as fluvial channel-fill sandstone **(Miall, 1996; Collinson, 1996; Eriksson et al., 1998)**. The mineralogical as well as textural immaturity of the sandstone reflects relatively poor efficiency of the depositional agent. Presence of oversized clasts, along the set or even foreset boundaries, points to the presence of erosion. The pebbles almost certainly are moved as rolling or sliding load and thus are better rounded for being subjected to greater abrasion during transport. Presence of over-sized clasts are also pointed towards the unsteadiness of the flow quite clearly, where the over-sized clasts are incorporated possibly by spurts of eddies. Common in-channel upward decrease in trough cross-set thickness without accompanying grain-size reduction within the sandstone bodies record gradual decline in the flow regime **(Harms et al., 1975; Went and McMahon, 2018)**, probably in rising water stage. Overall fining upward trend, as found in this area, is the result of fluvial aggradation, as described as general characteristic of fluvial sedimentation **(Catuneanu, 2006; Yuanfu et al., 2020)**. Channel pattern exert the most immediate control on fluvial architecture. Tectonics and climate, two extrabasinal factors, are the prime factors controlling the fluvial stratigraphic architecture and sea level change becomes important in relative proximity to the standing body of water in which the river debouches. The effect of climatic variations can produce large scale changes, in scales of different valley fills, but intra valley variations within a limited exposure can only be accounted for tectonic as well as base level fluctuations **(Gemignani et al., 2022)**.

The presence of an Aeolian system during the Gulcheru sedimentation is unequivocally settled by the presence of wind ripple migrated climbing translatent strata, pin-stripe lamination, high-index granule ripples, sand sheet deposits, grain-flow cross-strata and grain-fall laminae and massive sand bodies with bimodal fabric. The presence of well-rounded and well sorted sand grains is also typical example of aeolian deposits **(Bookfield, 2011)**. Dunes without slipface **(Kocurek and Dott, 1981)** or very small dunes (<1m; **Hunter, 1977a**) are characterized by wind ripple migrated climbing translatent strata. Occurence of translatent strata most significantly between Kanampalli (78˚05'25.18" E, 14˚25'13.60"N) to Gandi (14°18´25.34″ N, 78°28´ 36.52″ E) area indicates the predominance of small dunes without slipface. Amongst the Aeolian bedforms, translatent strata and sand sheet facies dominate the west, while massive beds and dunes with well-developed slipfaces dominate to the east. Extreme textural maturity of the sediments attests to protracted aeolian abrasion **(Pettijohn et al., 1972)** or multicyclic history **(Suttner et al., 1981)**. Lack of quartz grains with abraded overgrowth indicates reworking of loose detritus in the aeolian domain. Noticeable mineralogical maturity of the sediments is also indicative of aeolian abrasion **(Harald and Andrei, 2021)**.

Cyclical tidal rhythmites are probably of tide origin. Because of the availability of coarse to fine sediment sequence and landward decreasing of the total hydrodynamic energy, surface sediment usually fines landward from the fluvial to tidal flat except for a few transgressive tidal flats **(Petti et al., 2019)**. Therefore, a prograding tidal flat will build up an upward fining succession with well-developed herringbone cross strata, and well-developed mud cracks. The spectrum of open coast depositional settings is also displaying the change from muddy tidal flats of tide dominance with wave influence to beaches of wave dominance with tide influence **(Daidu, 2013)**.

## 3.5 CONCLUSION

1. Facies analysis of the Gulcheru Formation provide important information about sedimentation of the Cuddapah Basin during Paleoproterozoic time.
2. Sedimentation of Gulcheru Formation, well exposed in an around Kanampalle, Gandi and Pendllimarri area belongs north-western sector of the Cuddapah Basin, is represented by three litho-sections with a thick succession of Conglomerate, Quartzite and shale.
3. On the basis of facies associations and sedimentary structures, it is clear that the Gulcheru Formation in the study area is deposited in an alluvial fan, fluvial and tidal flat environmental condition with strong influence of wind activity.

# FIGURES AND TABLES

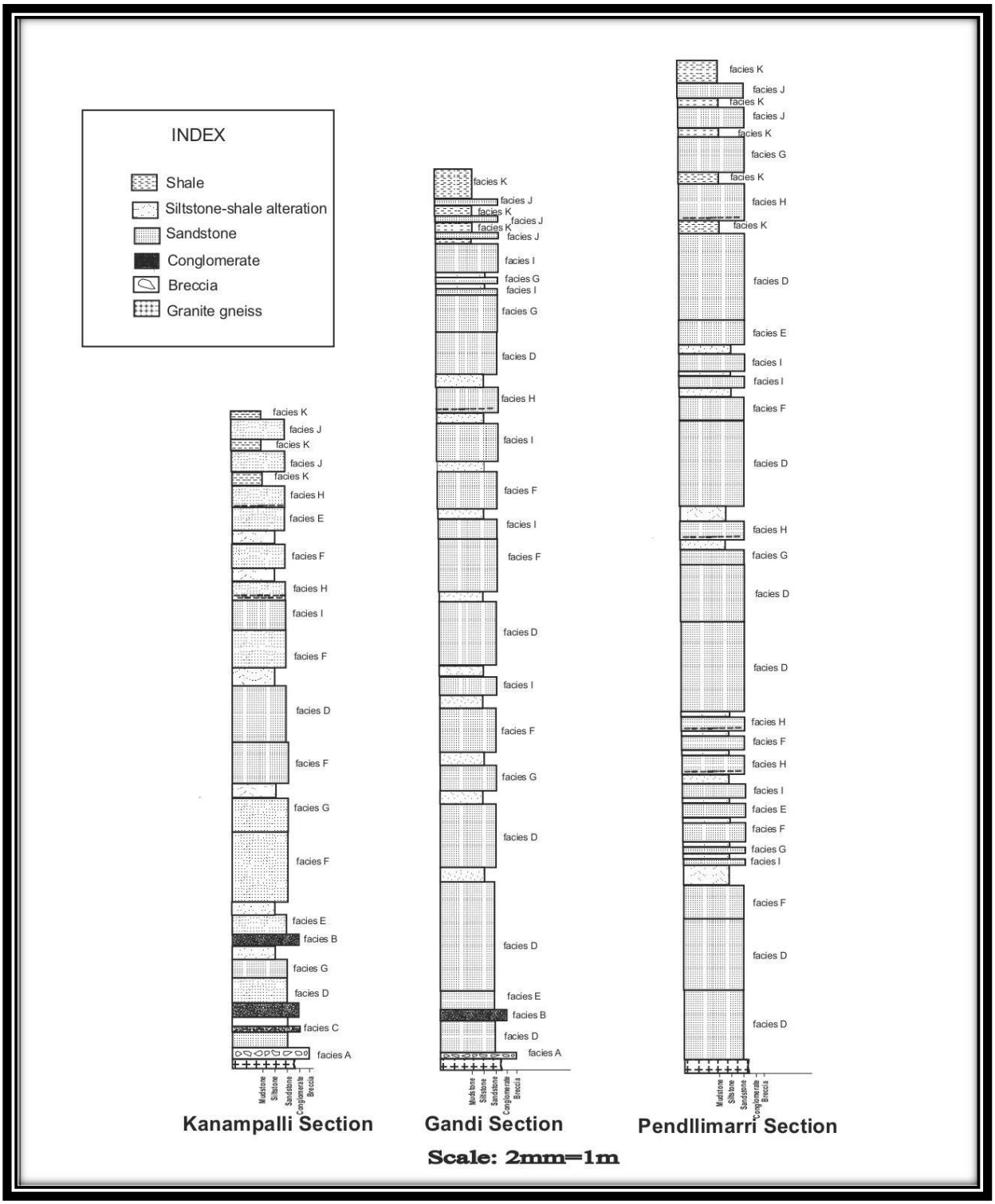


**Fig 3.1** Litho-logs of the measured sections from the Gulcheru Formation, Cuddapah Basin, India

**Fig. 3.2** Field photograph of sandy matrix-supported poorly sorted breccia from Kanampalle (lat-14˚25’13.22” N, long-78˚05’25.4” E) section, Gulcheru Formation, Cuddapah Basin, India indicating angular clasts are embedded in sandy matrix and showing poor sorting

**Fig. 3.3** Field photograph of clast supported conglomerate from Kanampalle (lat-14˚25’13.18” N, long-78˚05’24.2” E) section, Gulcheru Formation, Cuddapah Basin, India showinging subrounded clasts embedded in coarse grained sandy matrix

**Fig. 3.4** Stacked couplets of pebbly to granular conglomerate and very coarse to medium grained sandstone in facies C from Gandi (lat-14˚18’25.28” N, long-78˚28’36.42” E) section, Gulcheru Formation, Cuddapah Basin, India indicating alteration of thick layer of coarse to medium grained sandstone with thin layers of conglomerate form couplets

**Fig. 3.5** Close up view of matrix supported conglomerate in the couplet facies from Gandi section, Gulcheru Formation, Cuddapah Basin, India showing poorly sorted subrounded clasts embedded in sandy matrix

**Fig. 3.6** Trough cross stratified sandstone facies in the lower part of the Gulcheru Formation from the Kanampalle (14˚25'13.60" N, 78˚05'25.18" E) section, Gulcheru Formation, Cuddapah Basin, India showing thelarge and small cross strata oriented in same direction

**Fig. 3.7** Trough cross stratified sandstone facies in the lower part of the Gulcheru Formation from the Kanampalle (14˚25'13.60" N, 78˚05'25.18" E) section, Gulcheru Formation, Cuddapah Basin, India showing thesand bodies with large trough sets are followed upward by smaller ones

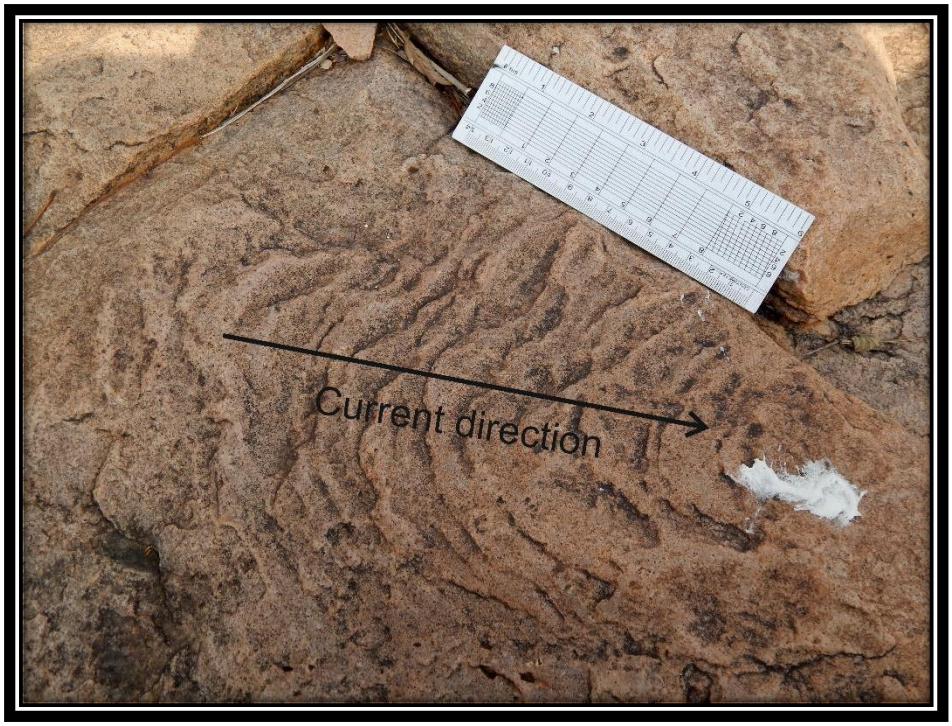


**Fig. 3.8** Top surface view of the trough cross stratified sandstone facies from Pendllimari (14˚24'55.2" N, 78˚36'43" E) section, Gulcheru Formation, Cuddapah Basin, India representing trough cross set on the top of the bedding plane showing paleocurrent direction

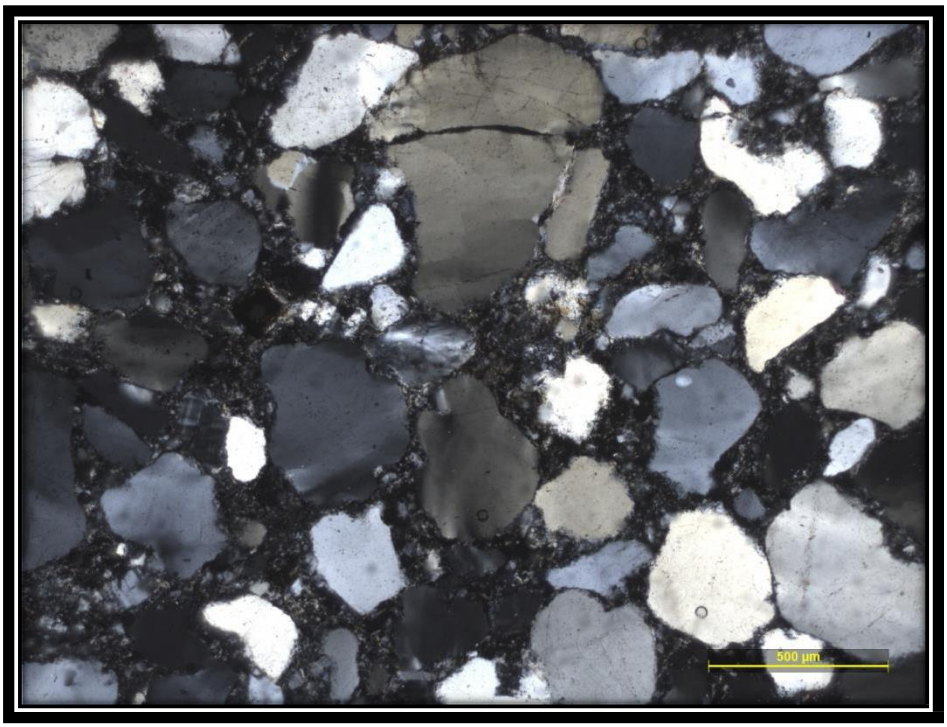


**Fig 3.9** Photomicrograph of trough cross stratified coarse-grained sandstone from Pendllimari section, Gulcheru Formation, Cuddapah Basin, India indicating quartz arenite with low matrix content and few pseudomatrix formed by crashed feldspar grains

**Fig. 3.10** Tabular cross stratified sandstone facies in the lower part of the Gulcheru Formation from Kanampalle section, Gulcheru Formation, Cuddapah Basin, India representing the foreset dip directions makes low angle and inclined bedforms oriented perpendicular to paleo-flow

**Fig. 3.11** Top surface view of the tabular cross stratified sandstone facies from Pendllimari section, Gulcheru Formation, Cuddapah Basin, India representing low amplitude current ripple on the top of bedding plane

**Fig. 3. 12** Tabular cross stratified sandstone from Pendllimari (14˚24'55.2" N, 78˚36'43" E) section, Gulcheru Formation, Cuddapah Basin, India indicating lateral accretion in the sand body

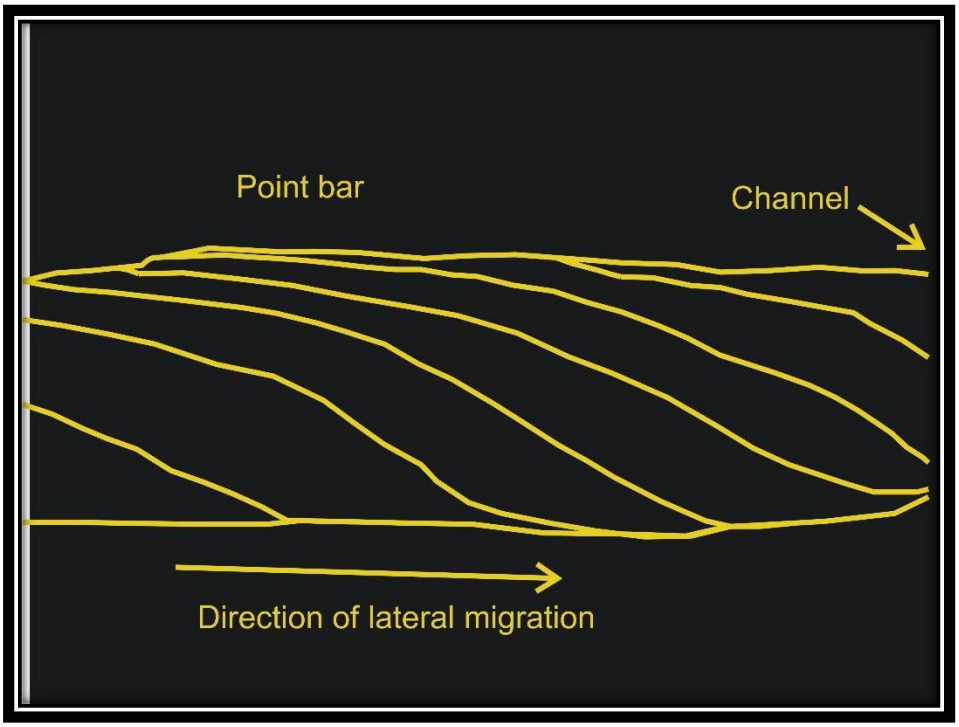


**Fig. 3.13** Sketch of Fig 3.12 showing the accretion surfaces would be formed by relatively continuous lateral sweep of channel bends by systematic erosion of the outer banks and deposition along inner banks

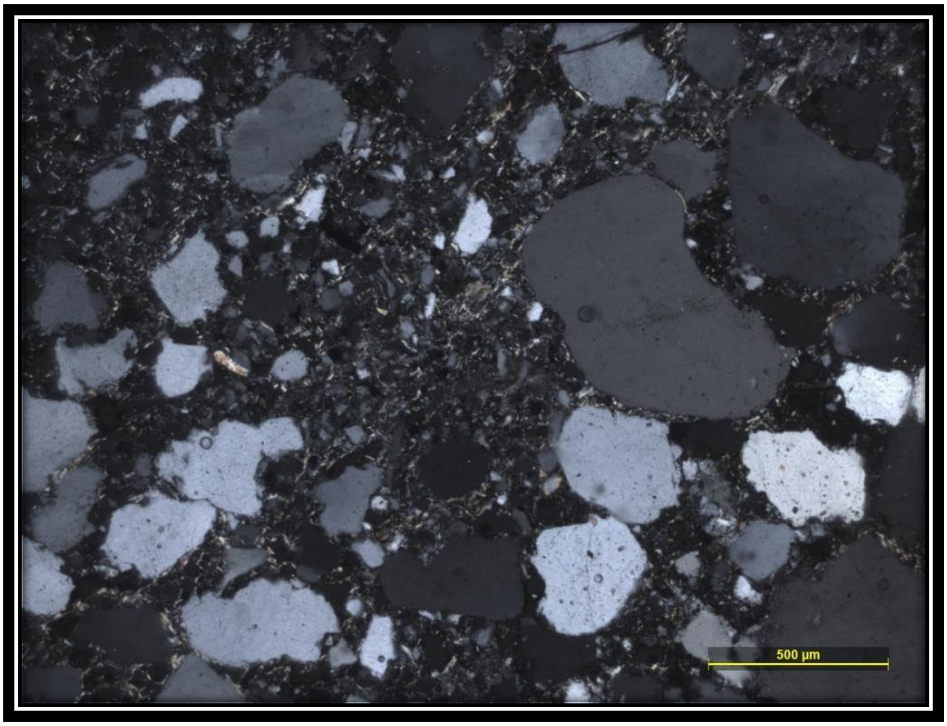


**Fig. 3.14** Microscopic view of coarse grained tabular cross stratified sandstone facies from Pendllimari (14˚24'55.2" N, 78˚36'43" E) section, Gulcheru Formation, Cuddapah Basin, India indicating arkosic sandstone with high clayey content and moderate to poor sorting

**Fig. 3.15** Medium grained sandstone in the ripple laminated sandstone facies from Kanampalli (14˚25’13.44" N, 78˚05’25.06" E) section, Gulcheru Formation, Cuddapah Basin, India showing lenticular geometry. Note the dimension of the geometry of the sand body decreases upward

**Fig 3.16** Ripple laminated sandstone facies from Kanampalli (14˚25’13.44" N, 78˚05’25.06" E) section, Gulcheru Formation, Cuddapah Basin, India representing solitary set of climbing ripple

**Fig. 3.17** High index ripple on the top surface of ripple laminated sandstone facies. Note the coarsest grain fraction concentrated in the crest

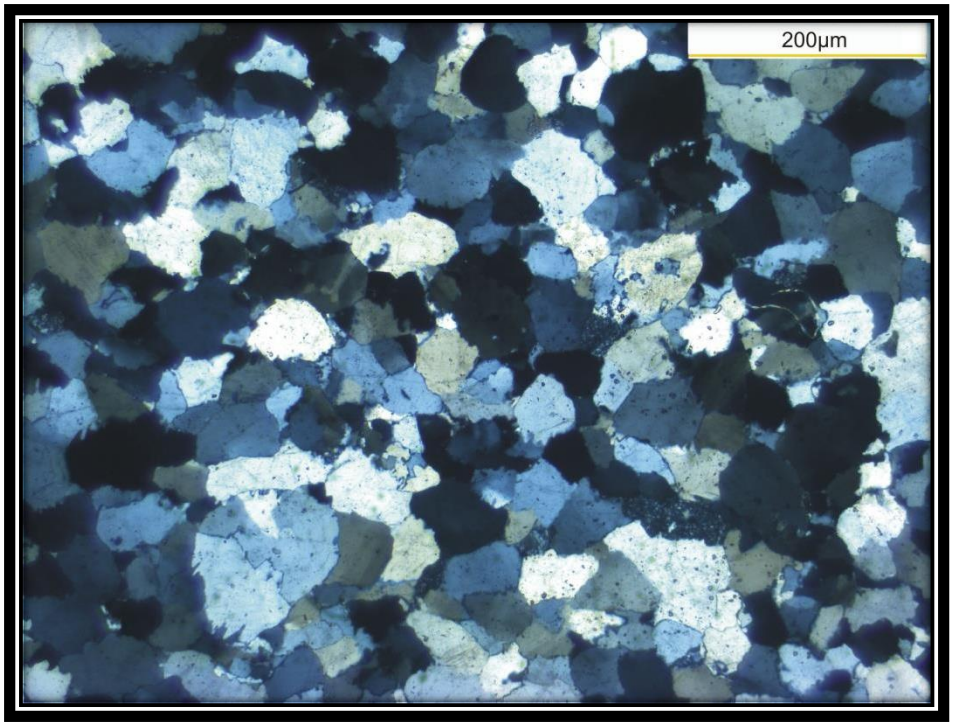


**Fig. 3.18** Photomicrograph of medium grained ripple laminated sandstone facies from Gandi (14°18´25.34" N, 78°28´ 36.52" E) section, Gulcheru Formation, Cuddapah Basin, India representing moderately sorted quartz arenite with subangular to subrounded grains

**Fig 3.19** Tabular cross stratified sandstone facies from Gandi (14°18´25.34" N, 78°28´ 36.52" E) section, Gulcheru Formation, Cuddapah Basin, India representing planar and sharp upper as well as lower bounding surface

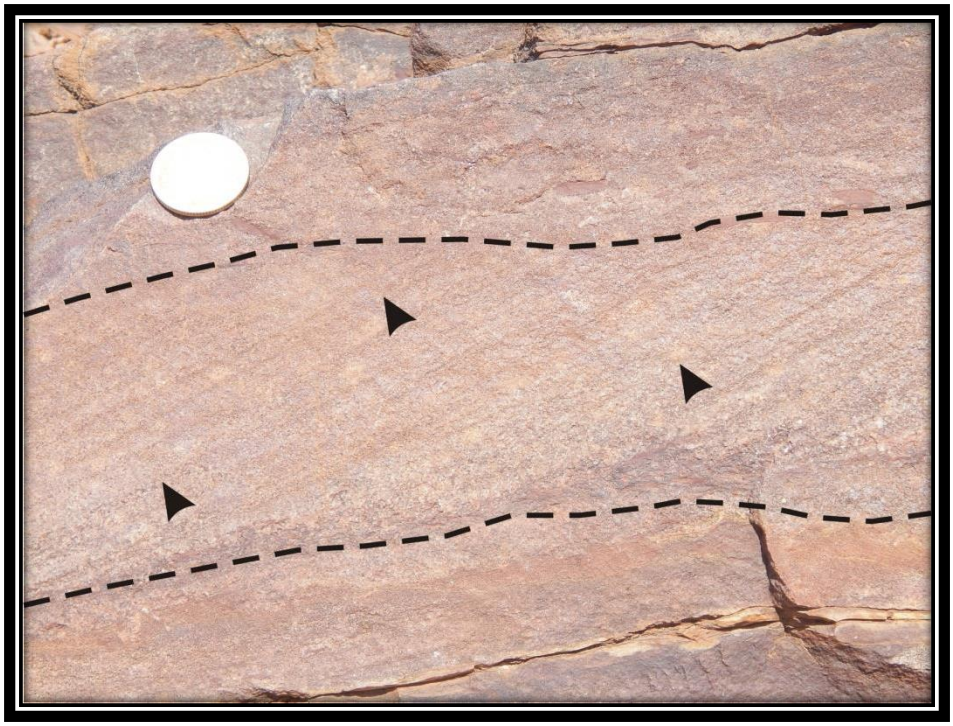

**Fig. 3.20** Close up view of facies G showing the nature of cross-stratification and inverse grading (arrow) with in foreset laminae

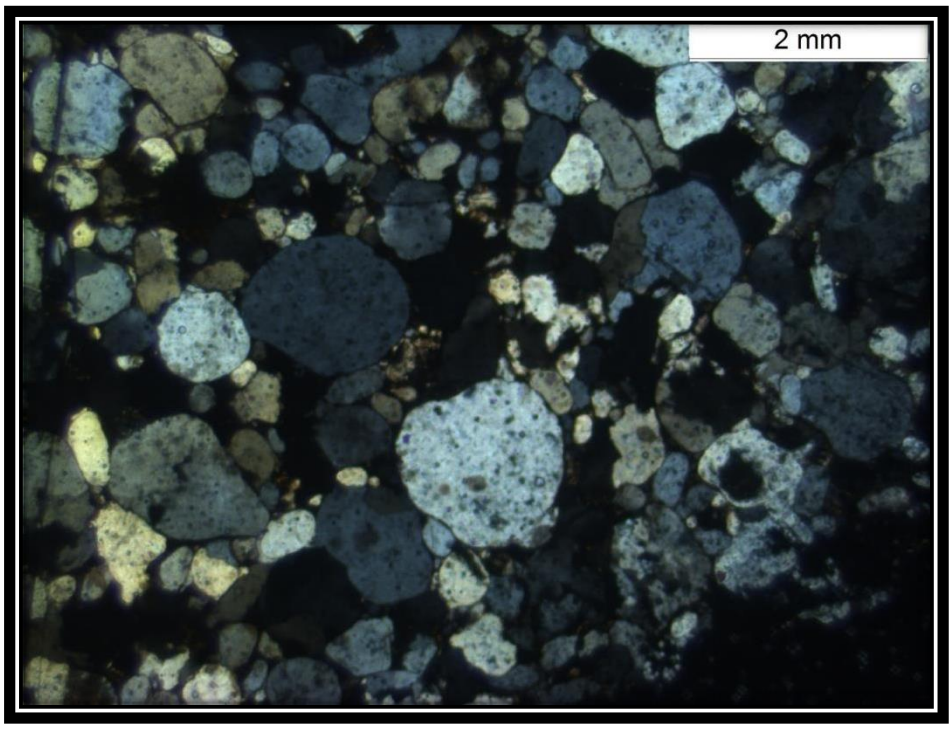


**Fig. 3.21** Microscopic view of fine to medium grained tabular cross stratified sandstone facies showing bimodal grain size distribution in matured sandstone is indicative of aeolian transportation of sand

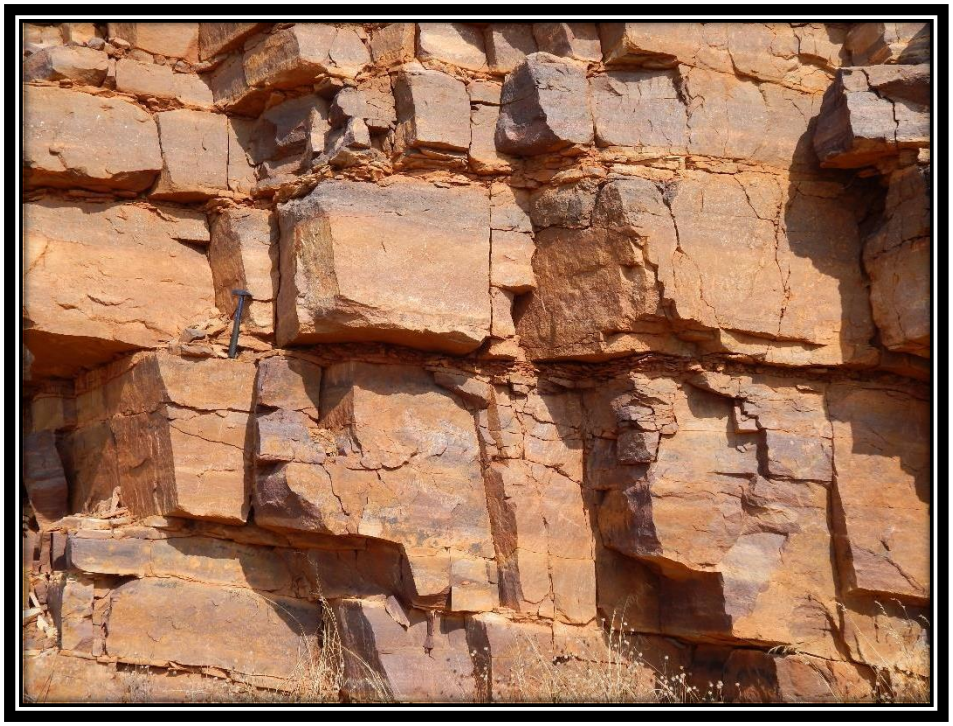

**Fig 3.22** Field photograph of sand sheet deposits in the facies H from Kanampalli (14˚25'13.60" N, 78˚05'25.18" E) section, Gulcheru Formation, Cuddapah Basin, India indicating thick layer of massive sand. Note the presence of pea-size pebble lags at the base of each channel

**Fig. 3.23** Close up view of pea sized pebbles near the lower part of the massive sandstone facies H

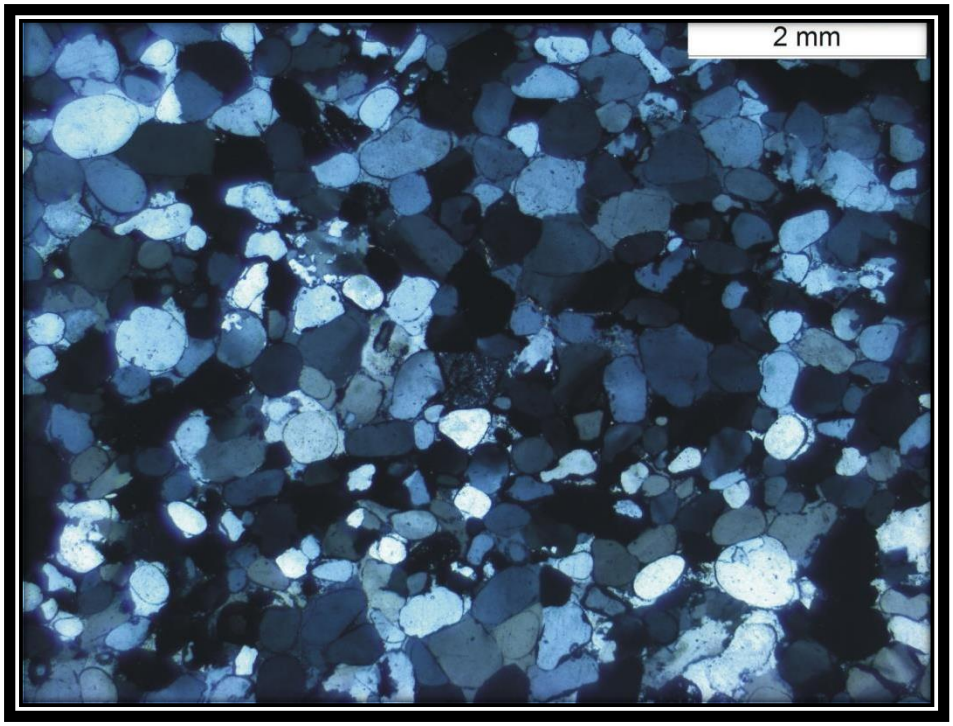


**Fig. 24** Microscopic view of fine to medium grained massive sandstone facies from Kanampalli (14˚25'13.60" N, 78˚05'25.18" E) section, Gulcheru Formation, Cuddapah Basin, India showing subrounded to rounded grain size distribution in matured sandstone is indicative of aeolian transportation of sand

**Fig. 3.25** Field photograph of planar laminated sandstone facies present in the upper part of the succession from Pendllimari (14˚24’54.2" N, 78˚36'43" E) section, Gulcheru Formation, Cuddapah Basin, India showing tabular geometry

**Fig. 3.26** Field photograpgh of fine-grained plane laminated sandstone facies from Pendllimari (14˚24'55.2" N, 78˚36'43" E) section. Each lamina comprises quartz-silt (dark coloured part) and fine to medium quartz-sand (light coloured), followed by wind-ripple migrated climbing translatent strata

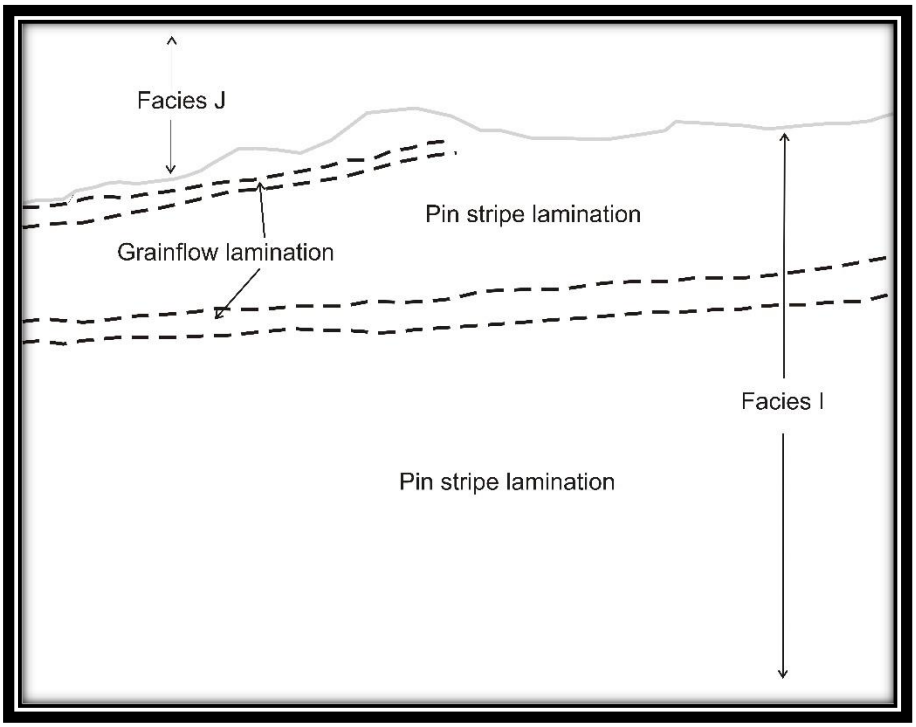


**Fig. 3.27** Sketch of Fig. 3.26, reflecting the multiple cycles of grain-flow lamination and pin-stripe lamination, of which grain-flow laminations are laterally discontinuous

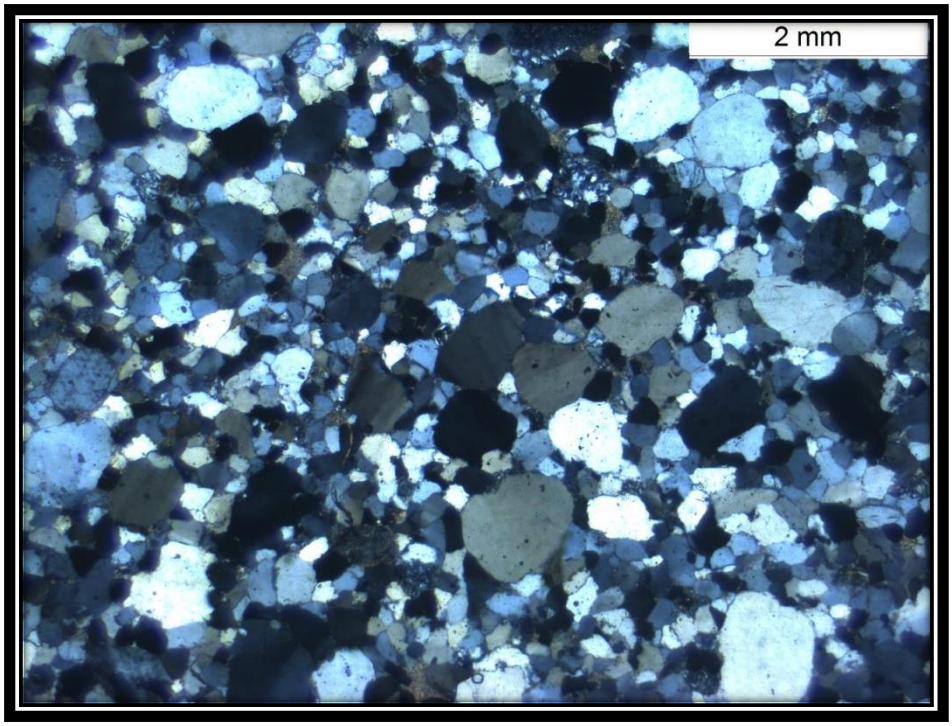


**Fig. 3.28** Photo micrograph of planar laminated sandstone facies I. Roundness of the sand grains suggests prevalence of a variable wind regime

**Fig. 3.29** Fine to medium grained trough cross stratified sandstone facies from Pendllimari (14˚24'55.2" N, 78˚36’23" E) section, Gulcheru Formation, Cuddapah Basin, India presenting small scale trough cross stratified sandstone alternating with fine mudstone

**Facies 3.30** Herringbone cross strata present in the trough cross stratified sandstone facies from Pendllimari (14˚24'55.2" N, 78˚36'43" E) section, Gulcheru Formation, Cuddapah Basin, India indicating a bidirectionalpaleo-flow

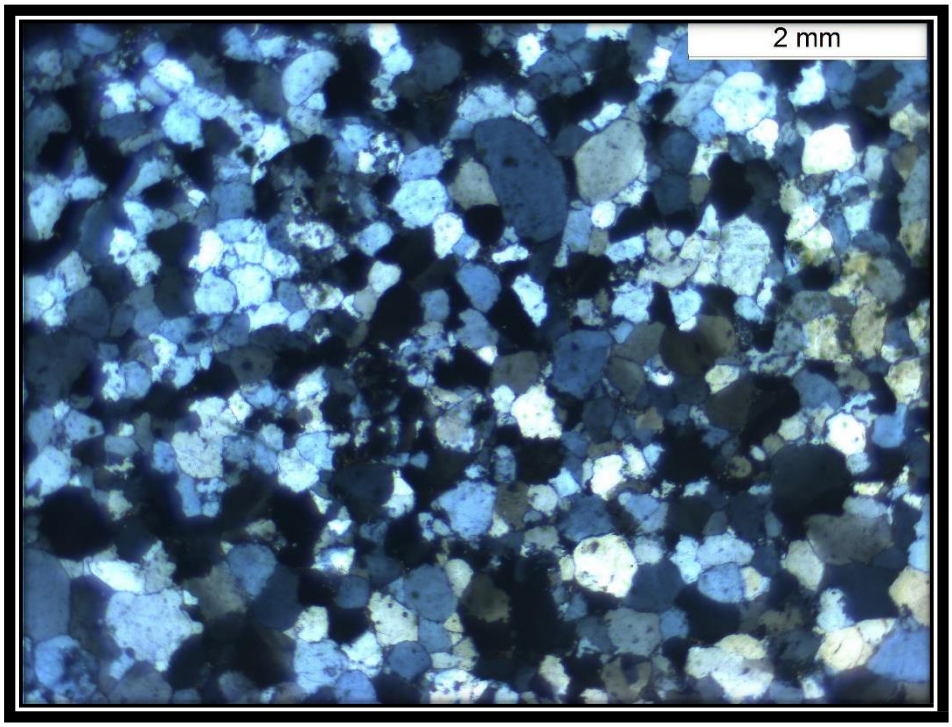


**Fig. 3.31** Microscopic view of fine to medium grained trough cross stratified sandstone facies representing quartz arenite. Fine sand sized grains are subrounded to rounded and moderate sorting

**Fig. 3.32** Alteration of sandstone and shale representing rhythmite facies from Pendllimari (14˚24’54.58" N, 78˚36'43" E) section, Gulcheru Formation, Cuddapah Basin, India indicating shallow water shelfal flow regime. Note the deformation features in the mud layer

**Fig. 3.33** Top view of the rhythmite facies from Gandi (14°18´25.34″ N, 78°28´ 36.52″ E) section, Gulcheru Formation, Cuddapah Basin, India representing mudcracks

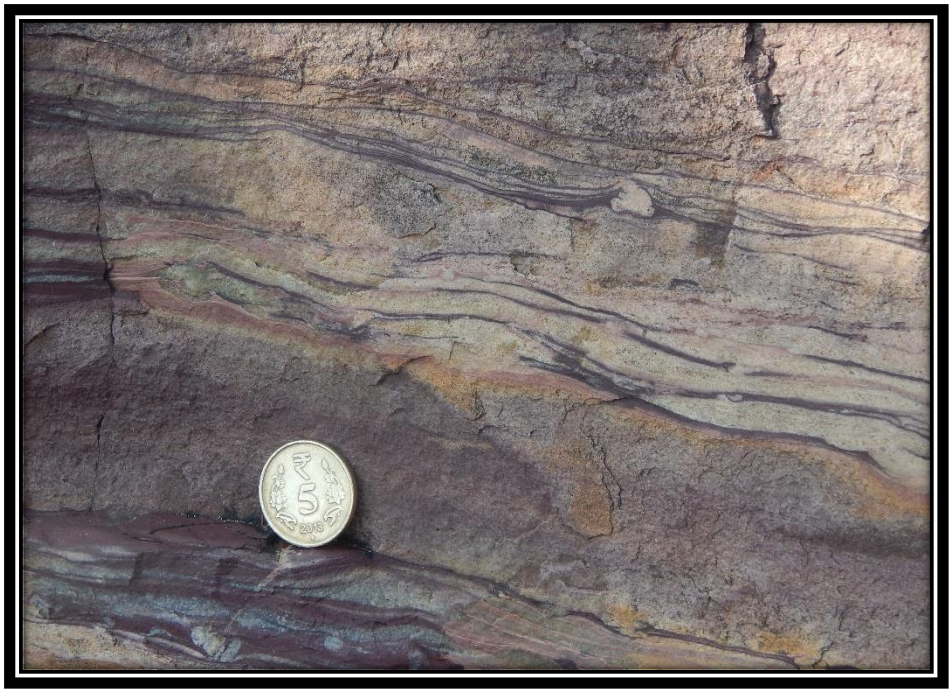

**Fig. 3.34** Tidal deposit in Facies K showing bundles of foresets separated by mudstone drapes (Double). Note the thickening and thinning of foreset bundles


**Fig. 3.35** Microscopic view of rhythmite facies showing graded clay layers with some lenticular silt layer

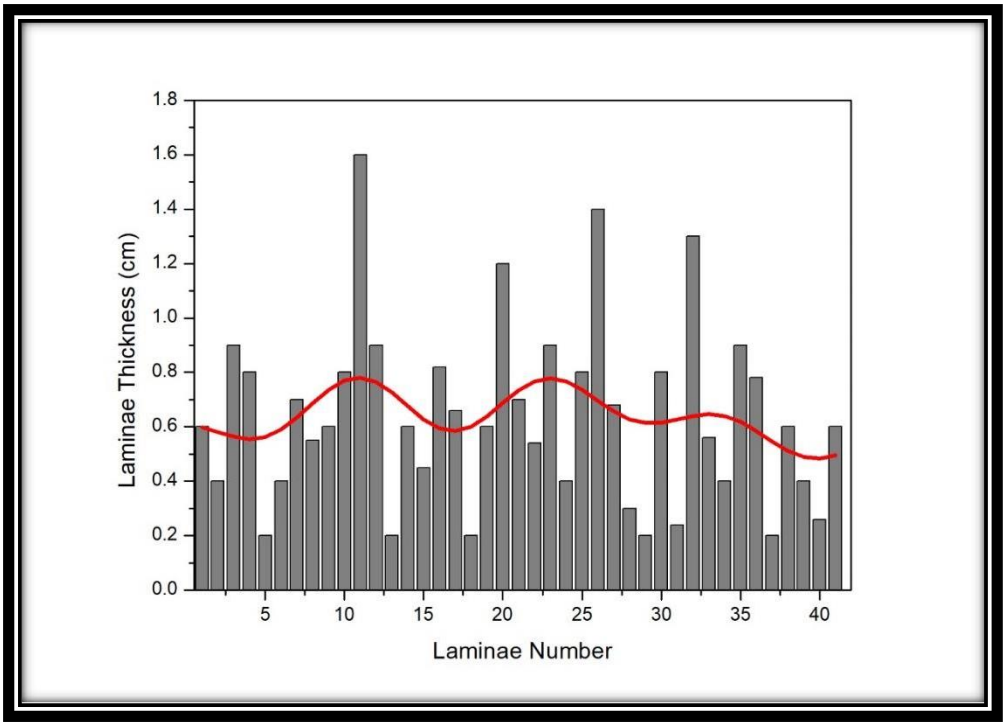


**Fig. 3.36** Analysis of thick-thin foreset laminae showing thickness variations in successive foresets

# CHAPTER 4

# PALAEOCURRENT ANALYSIS

## 4.1 INTRODUCTION

A palaeoflow indication, which is another name for a palaeocurrent indicator, provides proof of the flow direction at the time the sediment was deposited. Paleogeographic reconstructions are created using palaeoflow data along with facies analysis and provenance research. The investigation of sedimentary deposits that came before it demonstrates that these features can be utilised to identify depositional processes. They can show the trend of sand bodies as well as the direction of paleocurrent flow, paleo-slope, and paleogeography. By using the clinometer, this discipline, known as paleocurrent analysis, is a crucial component of facies study in both surface and subsurface studies. Paleocurrent analysis can be used to a variety of sedimentary structures. Some structures just produce a sensation of the direction of the current, whereas others produce both sense and direction. Groove marks, channels, washouts, and splitting lineation are examples of the first group. The cross-lamination, cross-bedding, slump folds, flute markings, and asymmetric ripple profiles are examples of the second category. Care must be taken when measuring the orientation of sedimentary structures. For regional paleocurrent mapping, an area sample grid of some form is ideal. This ideal strategy is frequently constrained in practise by access, exposure, and time restrictions. The azimuth and dip of planar structures that require rectification, as well as the alignment of the structures, will be noted. Only the azimuth needs to be documented for planar and linear structures in outcrops with little tectonic dip. At the same time, it is important to pay attention to the structure's size, kind, and lithology. We should measure foreset dip directions from cross-bedding in plan view. Only in extreme cases should dip directions seen in vertical sections be reported. Cross-beds do not usually drop directly downcurrent, which is the cause of this. Foresets are deposited perpendicular to or oblique to current flow in troughs and laterally infilled channels. The structural organisation of the foresets can be inferred from looking at cross-bedding in plan view. Only an apparent dip may typically be documented when cross-bedding is measured from

vertical facies. If there is extensive jointing, this may deviate greatly from the true dip direction. However, as foresets seem horizontal when seen normal to their dip direction, the discrepancy would not be too incorrect. Using a rose diagram, directional data, such as palaeocurrent data, is graphically summarised. The technique of palaeo-current analysis can provide clue to the four aspects of basin development **(Vakalas et al. 2018; Miall, 2000)**.

a) The direction of local or regional palaeoslope, which reflects tectonic-subsidence patterns
b) The direction of sediment supply
c) The geometry and trend of lithologic units
d) The depositional environment

with a view to take care of the aforementioned aspects of palaeocurrent analysis, the study areas of the Gulcheru Formation rocks of the Cuddapah Basin are undertaken.

## 4.2 TYPES OF PALAEOCURRENT INDICATORS

The dip direction of cross-bed foresets; the asymmetry and orientation of the crests of current ripples and the orientation of flute casts, groove casts and current lineation are all examples of directional data that can be obtained from sedimentary structures. How they yield current directions are explained below.

a) The inclination of foreset directions of ripple marks (particularly current ripple) and cross-bedding (particularly planar cross-bedding) is determined in the field with a brunton compass by taking measurements from as many different outcrops and individual beds as possible as practicable. Generally, the inclination of foreset directions is downcurrent. However, **Smith and Bretherton (1972)** demonstrated that planar crossbed sets in rivers commonly advance obliquely to the flow directions. **Hunter (1981)** showed large eolian

dunes commonly advanced oblique to the prevailing wind direction. In case of trough crossbeds the analysts must observe the orientation of the acute bisectrix of the trough.

b) Channels and scours which may indicate the major erosive currents are usually too large to be preserved in the outcrops **(Hubbard et al. 2014)**.

c) Parting lineation, visible on bedding-plane exposures indicates orientation but not direction of flow because of the ambiguity between two equally possible readings at $180^0$ to each other.

d) Imbrication of platy clasts, stacking up in a shingled pattern, with their flattest surface dipping upstream and resting on the next clast downstream provide palaeocurrent information and also depositional mechanism of conglomerate. Interpretation of clast fabrics in subaqueous poorly-sorted conglomerate (diamictites) will lead to the delineation of depositional mechanism, such as debris flow, ice rain-out and glacial lodgement, as well as provide palaeocurrent information **(Eyles et al., 1987)**.

e) Sole markings which are best seen on the underside of bedding surfaces are also used for palaeocurrent analysis. Tool markings yield information on orientation but not direction like parting lineation and flute marks are longitudinallu asymmetric with their deepest ends lying upstream. Slump structures generated on depositional slopes contain recumbent folds that may be aligned parallel to strike and therefore are good palaeoslope indicators.

## 4.3 DATA COLLECTION AND PROCESSING

In the 3 selected seectors viz. Kanampalle area, Gandi area and Pendllimari area where good exposures of Gulcheru Formation rocks of Papaghni Group are found, palaeocurrent data based on inclination of foreset direction of planar cross stratification in the sandstone, the direction of acute bisectrix of troughs in the sandstone, the direction of imbrication of clasts in the conglomerate have been collected. The following information has been included in course of collection of palaeocurrent data.

a) Location and precise position in a stratigraphic section
b) Structural type
c) Indicated current direction
d) Scale of structure
e) Local structural dip

It should be noted that foreset-dip orientation of cross-bedding is significantly affected by structural dip and should be corrected whereever the structural dip exceeds $10^0$ by using a stereogram to reorient directional data collected from field (cf. **Collinson and Thompson, 1989, p. 200**). But as the dip of the rock body in the study area is $<10^0$ (nearly horizontal) the orientation data are used intact without any correction using stereogram.

When the direction of the acute bisectrix of troughs or inclination of foreset of the planar cross-bedding are noted in the field, 3-D exposures are always preferred to measure the true direction.

25 readings per sample station is commonly regarded as the minimum necessary for statistically significant small samples **(Miall, 2000)**. Several hundred or a few thousand readings may be necessary for a thorough analysis of a complete basin. As, the concern of the present work is particularly concentrated only one stratigraphic unit of the Cuddapah basin, 30-

35 readings per sector has been collected and analysed.

It is also to be noted that a very cautious approach has been undertaken in course of collection of palaeocurrent data about the delineation of a particular bedding plane or particular unit spreading across the aforesaid sectors, i.e palaeocurrent data have been collected for a particular unit spreading across the different sectors of the study area so that the interpretation of palaeocurrent data is exclusively of the unit itself.

A variety of statistical data-reduction and data-display techniques is available for palaeocurrent work. Here, the most common approach is followed i,e to group data into subsets according to stratigraphic or areal distribution criteria, display them visually in current rose diagrams, and calculate mean and standard deviation (or variation).

## 4.4 ENVIRONMENT AND PALAEOSLOPE INTERPRETATIONS

Palaeocurrent distributions are commonly categorized as unimodal, bimodal, trimodal or polymodal. Each reflects a particular style of current dispersion.

Although fluvial deposits typically yield unimodal palaeocurrent pattern on an outcrop scale, on a larger scale they may exhibite very complex pattern. Bimodal, trimodal or polymodal distributions may result in the tide swept offshore bar **(Klein, 1970)**. However, time-velocity asymmetry of tidal currents can result in local concentration of currents so that they are locally unimodally ebb-or flood-dominated. So, in outcrop it is sometimes very difficult to delineate tidal facies from fluvial facies **(Davis and Dalrymple, 2012)**.

The asymmetric ripple in the facies E (Medium to coarse grained tabular cross bedded sandstone facies) in the Kanampalle area (mean direction $242^0$, **Fig. 4.1**) indicate development of consistent NE ward tidal/longshore current in the nearshore zone it is likely to be resolution of longshore current and asymmetry of orbital velocity **(Bose et al. 1988)**. However, the palaeocurrent pattern deducted from direction of the troughs is bimodal indicating tidal

influence (**Fig. 4.2**). In the Pendllimari area, the mean resultant palaeocurrent pattern (mean direction $20^0$, **Fig. 4.3**) clearly indicates transportation of sand towards onshore indicating the dominance of flood-tide over ebb-tide. However, direction of trough axis in the sandstones from Kanampalle area is towards onshore (mean direction $84^0$, **Fig. 4.4**) indicating the reworking of sand by incoming waves and tides. The overall bipolarity in palaeocurrent patterns in the Gandi area (Sandstone facies association) might have been contributed, to a certain extent by the tidal action **(Fig. 4.5 and Fig. 4.6).** From aeolian cross-bedding data from the fine to medium grained tabular cross strata facies, Kanampalle area dominant palaeocurrents are toward the SW **(Fig. 4.7)** and Pendllimari area toward the NE **(Fig. 4.8)**. Both the palaeocurrent data shows polymodal current direction.

One of the important characteristics of the overall palaeocurrent pattern of the Gulcheru Formation in the study area is the presence of one dominant flow direction somewhat perperdicular to the basin margin. Another noteworthy feature is the presence of bimodality of palaeocurrent pattern which clearly indicates the presence of tides in a very low gradient beach-shoreface region. The Gulcheru sea must have a great width but a very low gradient as indicated by the absence of any evidence for the generation of shelf turbidity currents **(Hobday and Morton, 1984)**.

# FIGURES AND TABLES

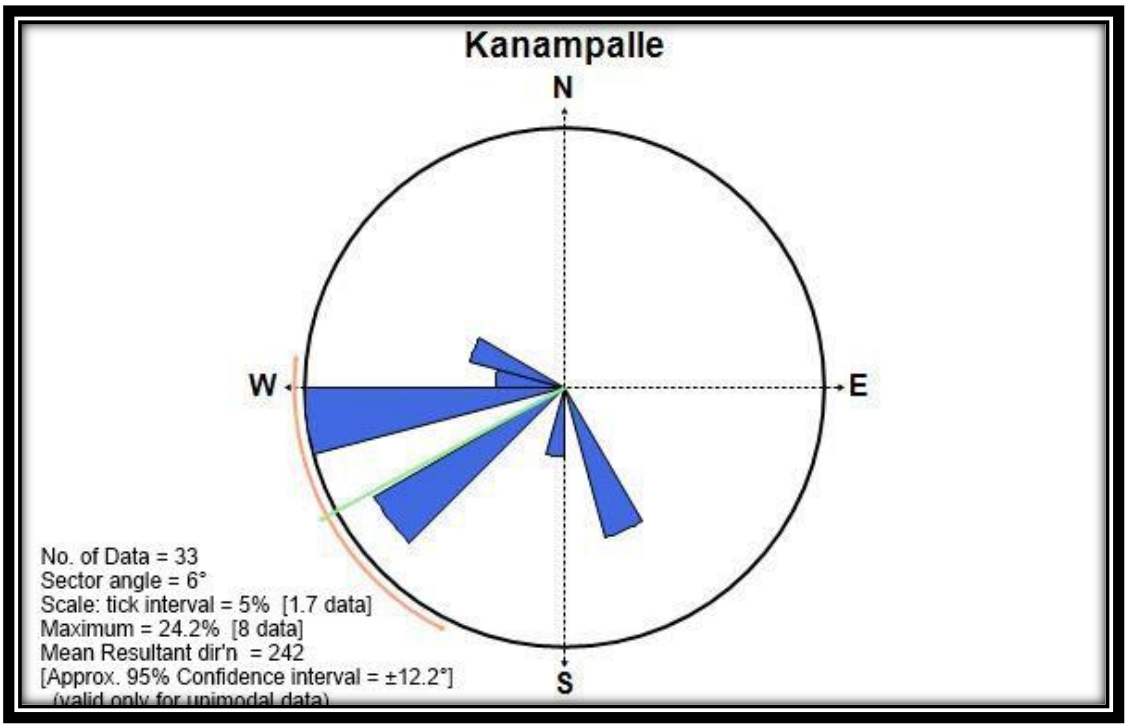


**Fig 4.1** Palaeocurrent analysis from current ripples of Kanampalle area (78˚05'25.18" E, 14˚25'13.60"N)

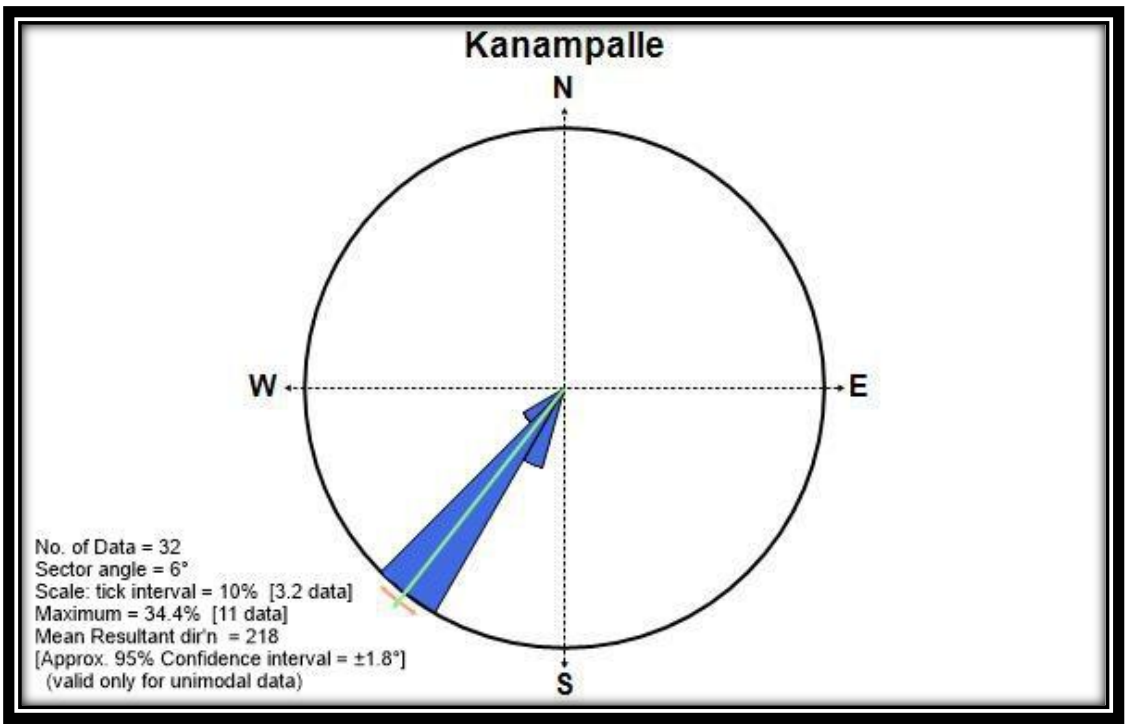


**Fig 4.2** Palaeocurrent analysis from trough axis of Kanampalle area (78˚05'25.18" E, 14˚25’13.40"N)

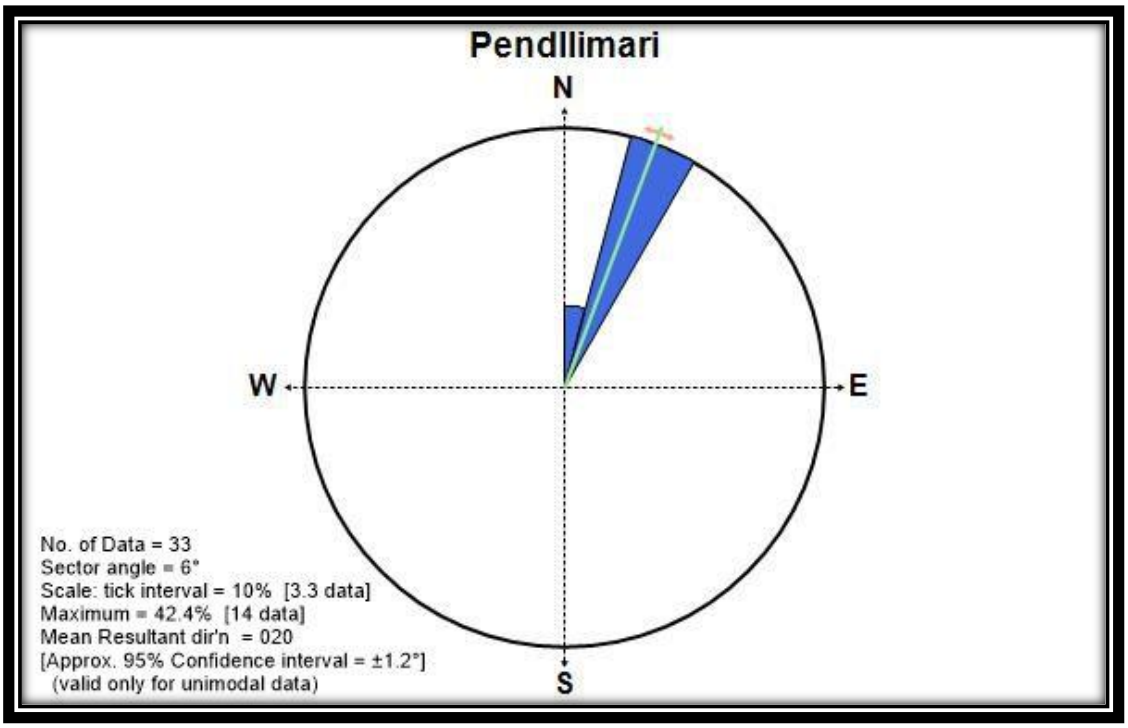


**Fig 4.3** Palaeocurrent analysis from current ripple of Pendllimari area (78˚36'43" E, 14˚24’55.1"N)

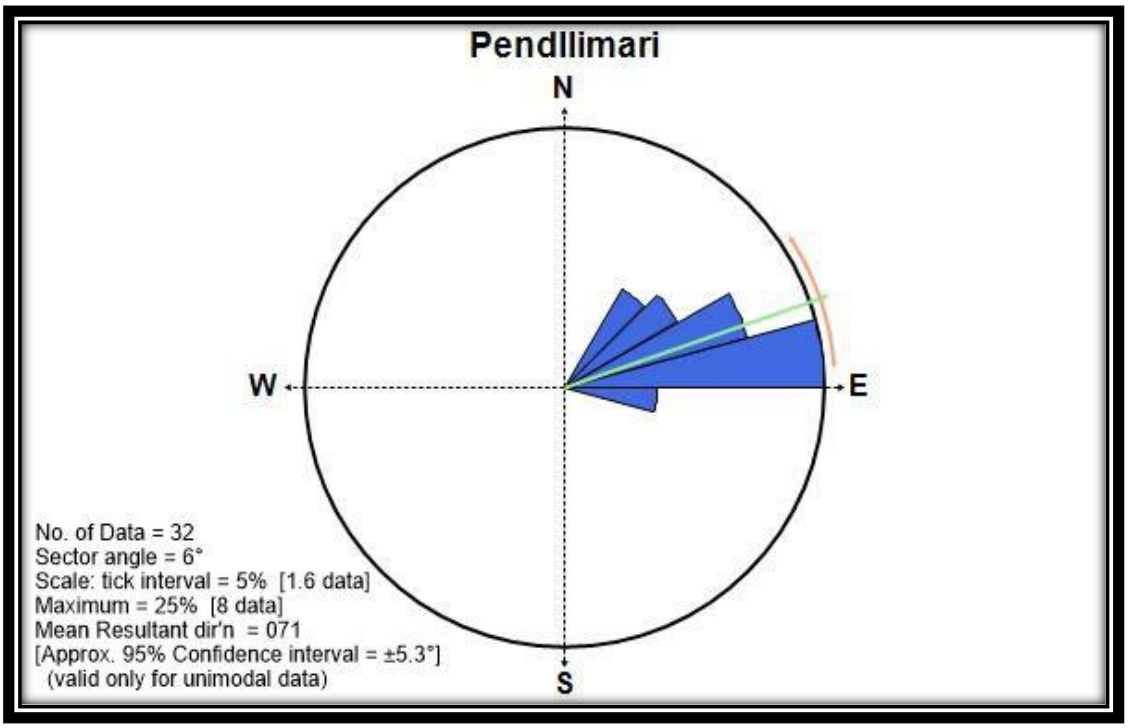


**Fig 4.4** Palaeocurrent analysis from trough axis of Pendllimari area (78˚36'43" E, 14˚24’54.2"N)

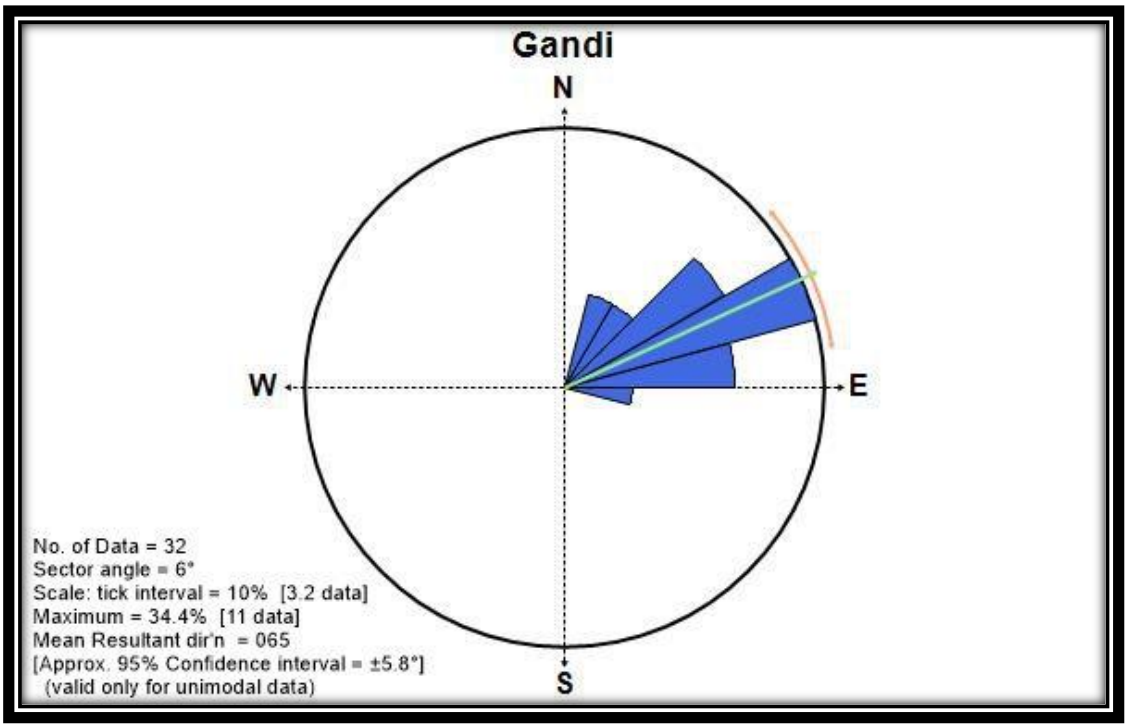


**Fig 4.5** Palaeocurrent analysis from current ripple of Gandi area (14°18´25.34″ N, 78°28´ 36.52″ E)

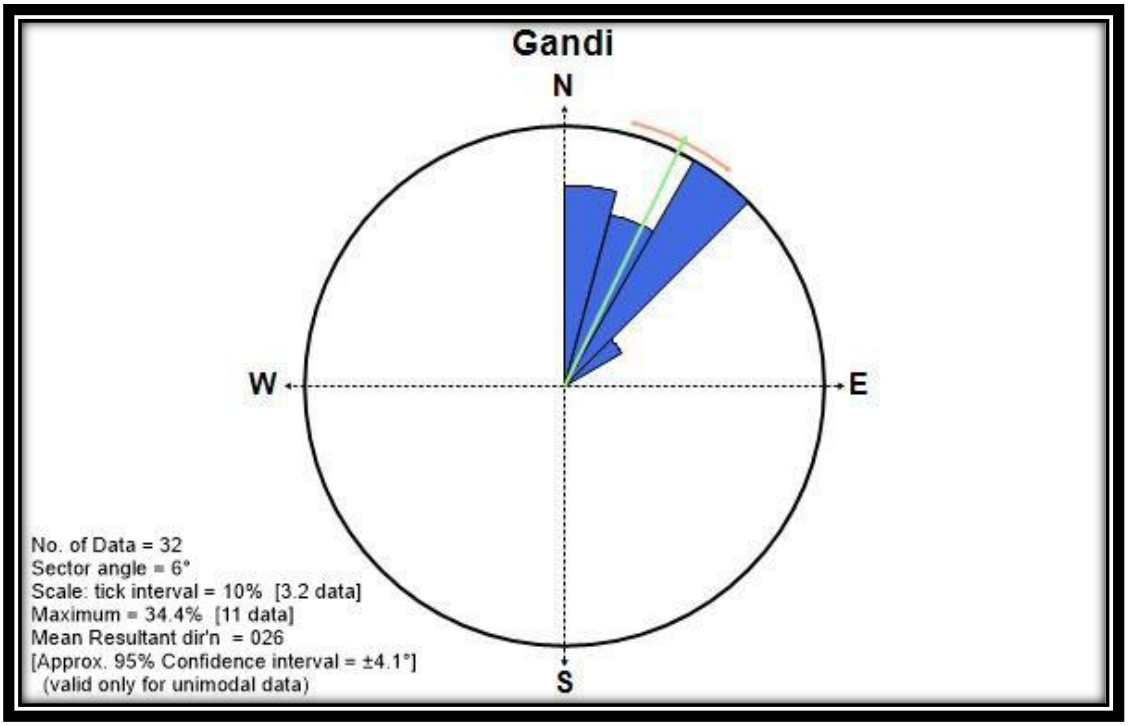


**Fig 4.6** Palaeocurrent analysis from trough axis of Gandi area (14°18´25.34″ N, 78°28´ 36.52″ E)

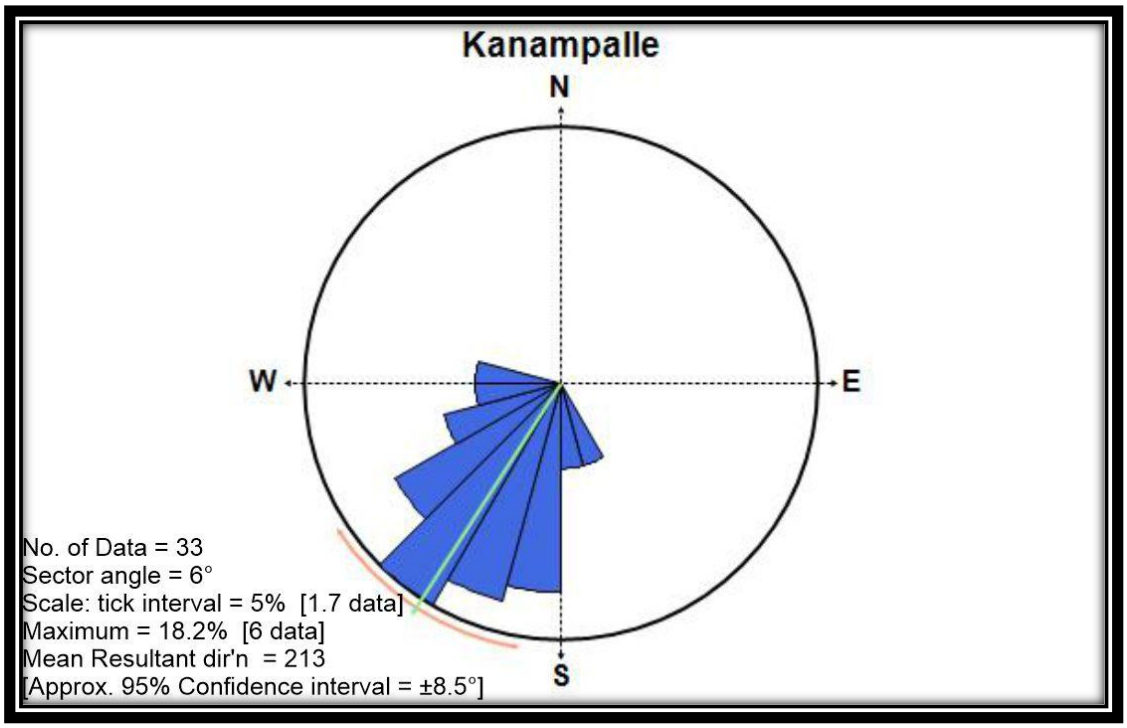


**Fig 4.7** Palaeocurrent analysis from aeolian cross bedding of Kanampalle area (78˚05'25.18" E, 14˚25'13.60"N)

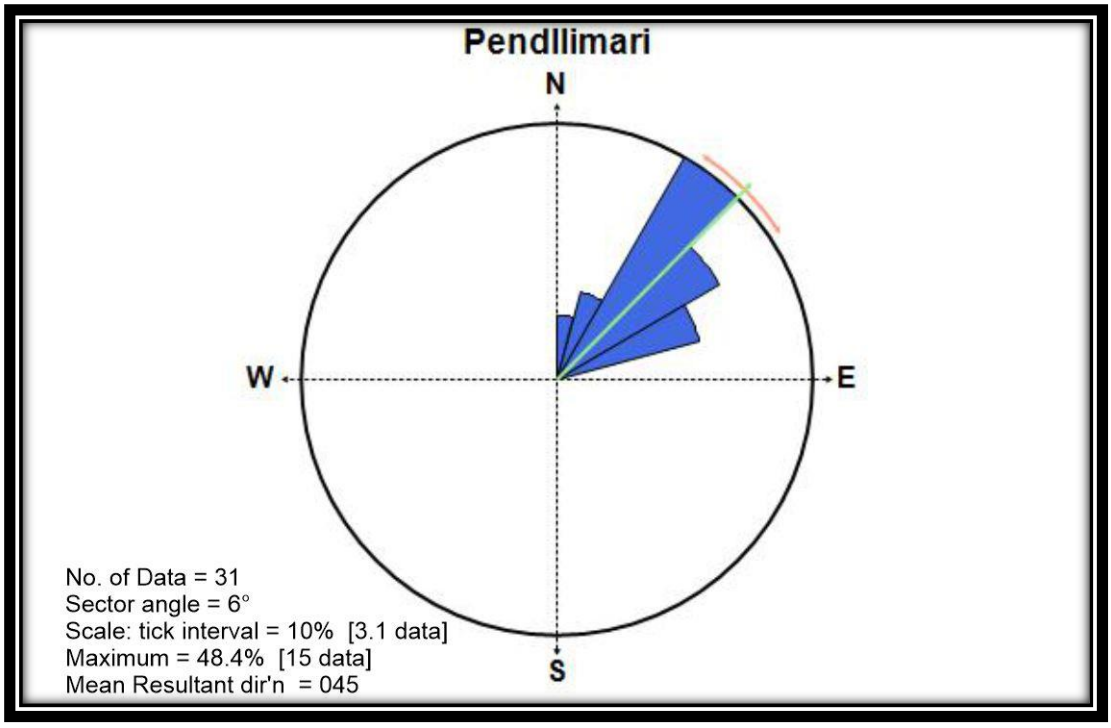


**Fig 4.8** Palaeocurrent analysis from aeolian cross bedding of Pendllimari area (78˚36'43" E, 14˚24’54.2"N)

# CHAPTER 5

# PETROGRAPHY AND GEOCHEMISTRY

## 5.1 INTRODUCTION

Geochemical investigation of the clastic sedimentary rocks gives us valuable information about weathering history, provenance, tectonic setting and depositional environment **(Armstrong-Altrin et al., 2004, 2015; Cullers and Padkovyrov, 2000; Mir, 2015; Nagarajan et al., 2007; Nesbitt et al., 1997)**. In geochemical provenance studies, fine grained sedimentary rocks like shales are viewed as the most valuable rock due to their homogeneity before deposition, post-depositional impermeability and higher concentration of minor components **(Baiyegunhi et al., 2017; Braccialli et al., 2007; Condie, 1993; McLennan et al., 1993)**. Not only provenance study, additionally paleoredox conditions can be recognized through these geochemical data of the clastic rocks **(Mir, 2015; Nararajan et al., 2007; Tobia and Mustafa, 2016)**. Trace elements such as La, Y, Sc, Cr, Th, Zr, Hf, Nb and rare earth elements (REE) are thought to be useful indicators of provenance, geological processes and tectonic setting due to their relatively low mobility and insolubility during sedimentary processes **(Armstrong-Altrin et al., 2014; Bhatia and Crook, 1986; Condie, 1993; Song et al., 2017; Taylor et al., 1985)**. Trace elemental concentration of V, Cr, Ni, Co, U and Th gives a vital information about the paleoredox conditions **(Bennett and Canfield, 2020)**. So, the **detailed geochemistry** has significant implications for the study about the **paleo-geology of Cuddapah Basin**, especially **provenance, paleoweathering and paleo-environment study of Gulcheru Formation**.

## 5.2 MATERIALS AND METHODS

Kanampalle stratigraphic section (Lat-14°25´13.60´´, Long-78°05´25.18´´) (Gulcheru Formation) records the preservation of various types of shale, sandstone and conglomerate. Fresh representative samples were carefully collected from the middle and upper part (7m interval) of this section for petrographic and geochemical study. After careful

observation under microscope, twelve samples of shale were selected for geochemical analysis.

The major elements concentration was acquired by Bruker model S4 Pioneer sequential wavelength-dispersive X-ray fluorescence (XRF) spectrometer. Rare earth element (REE) and trace elements were analysed by high resolution inductively coupled plasma mass spectrometer (HR-ICPMS) in which GSR-5was utilized as the standard. The analytical precision for major oxides by XRF is estimated to be better than 8%. Minor and rare earth element analysis with international standard GSR-5 indicated an analytical precision generally better than 6% for all elements.

Chemical Index of Alteration **(CIA; Nesbitt & Young, 1984)** is important to decide the level of weathering of the source rock. This index estimates the degree of change from feldspar to aluminous weathering items. The CIA estimates are resolved utilizing atomic extent from the equation:

$$CIA= [Al_2O_3/ (Al_2O_3+ Cao^*+Na_2O+K_2O)]*100$$

Where $CaO^*$ represents the CaO in silicates only.

Weathering impacts also can be assessed by the molecular proportions of the oxides components, utilizing the equation **(based on Harnois, 1988)**:

Chemical Index of Weathering (CIW) = $[Al_2O_3/(Al_2O_3+CaO^*+Na_2O)]*100$

Where $CaO^*$ is the CaO residing only in the silicate fraction.

Plagioclase Index of Alteration (PIA) reflects weathering of plagioclase feldspars and is characterized by the condition

$$PIA=[(Al_2O_3-K_2O)/(Al_2O_3+Cao^*+Na_2O-K_2O)]*100$$

Where all components are in molecular proportions and CaO* represents CaO in silicate fractions.

The Index of compositional variability **(ICV; Cox et al., 1995)** is the indicator of original composition and compositional maturity in clastic sedimentary rock.

$ICV = [(CaO+K_2O+Na_2O+Fe_2O_3^{(t)}+MgO+MnO+TiO_2)/Al_2O_3]$,

$Fe_2O_3^{(t)}$ indicates total iron and CaO includes all sources of Ca.

## 5.3 RESULTS AND DISCUSSION

### 5.3.1 PETROGRAPHY

Lithologically, the Gulcheru Formation consists of 3 units from bottom to top, Conglomerate, Quartzite and Shale. The lower part is represented by conglomerate with widespread quartzite, the middle part of the succession is dominated by sandstone, shale within band of siltstone. And the upper part siliceous mudstone gradually converted to carbonate mudstone. And upper part, siliceous mudstone is gradually converted to carbonate mudstone. Overall shale layers alternate with sandstone and siltstone bands with occasional ferruginous banding **(Fig. 5.1- 5.12)** and locally vertical fault plane is also found in some samples under microscope. The detailed petrography is described in **Table 5.1**.

### 5.3.2 MAJOR ELEMENT CONCENTRATIONS

The geochemical analysis of 12 shale samples from Kanampalle section indicate that, the $SiO_2$ content varies from 50.2 to 67.58 wt% and $Al_2O_3$ content from 8.51 to 22.64wt% **(Table 5.2)**. All the major oxides compared with the Post Archean Australian Shale (PAAS) **(Amajor, 1987; Taylor & McLennan, 1985)** shows more or less similar ratio except MgO enrichment and $Na_2O$ depletion.

Binary variation diagrams of $SiO_2$ *versus* $TiO_2$, $Al_2O_3$, $Na_2O$ and $K_2O$ **(Fig. 5.13A, B, G and H respectively)** and $Al_2O_3$ v*ersus* $TiO_2$, $Fe_2O_3$, $Na_2O$, $K_2O$ **(Fig. 5.14A,**

**B, F and G respectively)** shows similar linear trends. However, $Fe_2O_3$, MnO, MgO, CaO and $P_2O_5$ **(Fig. 5.13C, D, E, F and I, respectively)** and MnO, MgO, CaO and $P_2O_5$ **(Fig. 5.14C, D, E and H, respectively)** display negative linear trend with $SiO_2$ and $Al_2O_3$, respectively. Values of A $SiO_2$ /$Al_2O_3$ ratios ≥ 5 represent mature chemical components of rock **(Roser et al. 1986, 1988)**. The $SiO_2$ /$Al_2O_3$ proportions of Gulcheru shale are moderate (2.42-6.17, average=4.39), indicating mature chemical components **(Hossain et al., 2014)**. The bivariate diagram Log ($SiO_2$/$Al_2O_3$) *versus* Log ($Fe_2O_3$/$K_2O_3$) **(Fig. 5.15; Herron, 1988)** shows all samples representing the shale and greywacke composition.

The ternary diagram $Fe_2O_3$-$K_2O$-$Al_2O_3$ **(Fig. 5.16)** shows that all shale samples are plotted near the $Al_2O_3$ apex, which indicates the dominance of $Al_2O_3$ in the parent body. The information from $K_2O$/$Al_2O_3$ proportion suggests clay minerals (0.0-0.3) and feldspar (0.3-0.6) enrichment in the source rock. Gulcheru shales $K_2O$/$Al_2O_3$ ratio ranges from 0.31to 0.59 and these values are strong indicator of feldspar dominance in the parent rock.

The CIA calculated for the analysed shales have values ranging between 62.48 and 73.37 (average 68.14). The CIW value of the Gulcheru shale samples ranges from 97.33 to 98.94 (average 98.06). Gulcheru Formation clastic sediments shows PIA values with ranges from 93.26 to 96.86 (average 95.18). The ICV value of Gulcheru Formation Shales varies from 0.75 to 3.12 (average 1.57).

### 5.3.3 TRACE ELEMENT CONCENTRATIONS

The trace elements were normalised with PAAS values (Bhatia and Crook 1986; Taylor and McLennan 1995) and show depletion of Cs, Pb, Sr, V, Y, Zr, Nb and Th, and enrichment of Ba, Rb, Cr and U **(Fig. 5.17)**. The elements with strong field strength, such as Hf-Zr element pair does not alter after weathering due to the immobility and insolubility nature

**(Long et al., 2012)**. The high field strength elements, as Hf-Zr element pair does not differentiated during the weathering process due to their immobility and insolubility nature **(Long et al., 2012)**. Zr/Hf ratio of the Gulcheru shale samples varies from 32.82 to 35.68 with an average 33.83 **(Table 5.3)**, which is similar to the Zr/Hf ratio **(33, Crichton & Condie, 1993; Taylor & McLennan, 1985)** of upper continental crust (UCC).

The presence of Sr precipitation in the open marine basin or saline lake indicates high solubility of $SrSO_4$. So, generally the proportion of Sr/Ba steadily increases from the coast to the centre of the lake/seal. The Sr/Ba ratio suggests the salinity of the water, and Sr/Ba ratios < 0.6, 0.6-1.0, and >1.0 are indicative of fresh water, brackish water, and saline water, respectively **(Deng, 1993; Liu, 2007)**. The values of the Sr/Ba ratio of the Gulcheru shale vary from 0.24 to 0.78, which demonstrate the impact of marine transgression restriction with fresh water dominance **(Kuscu et al., 2016)**.

The concentrations of Ba range between 467 ppm to 4923 ppm and shows positive correlation with $K_2O$ **(Table 5.2)**. These Ba concentrations can be treated as a proxy of detrital flux **(Liguori et al., 2016)**. Gulcheru shale samples show overall enrichment in Ba. The Gulcheru shale samples are depleted in $Na_2O$, Rb and Sr and generally mildly enriched in $K_2O$ relative to the modelled mixture **(Fig. 5.18)**, which indicates intense weathering and little Na-K metasomatism **(Wang and Zhou, 2013)**.

### 5.3.4 RARE EARTH ELEMENT CONCENTRATIONS

REE concentrations of the Gulcheru Shales show range between 82.99-158.71ppm with an average 112.04ppm. The concentration of the light earth elements (LREEs=La+Ce+Pr+Nd) is higher than that of the heavy earth elements (HREEs= Ho+Er+Tm+Yb+Lu) and middle earth elements (MREEs= Sm+Eu+Gd+Tb+Dy). The average of 12 samples of the REE, LREE, MREE and HREE values are 112.04, 98.76, 9.29 and 3.99

ppm individually **(Table 5.4)**. All the samples demonstrate negative Eu anomaly. The chondrite normalized REE plot **(Fig. 5.19)** of Gulcheru shale samples show moderately inclined LREE (La-Nd part) and nearly flat HREE (Ho-Lu part) pattern with negative Eu anomaly **(Fig. 5.19)**. Similarly, Granodiorite and Tonalite shows similar chondrite normalized REE and LEE pattern **(Fig. 5.20)**. The Gulcheru shales have similar values of $La_N/Yb_N$ (~18.30), $La_N/Sm_N$ (~9.07), $Ce_N/Yb_N$ (~31.34) and Eu/Eu*(~0.73) as compared to PAAS values (Taylor and McLennan, 1985), and depleted value of $Gd_N/Yb_N$ (~2.60).

### 5.3.5 EFFECTSOF WEATHERING, SORTING AND RECYCLING

The degree of weathering of the source rock depends on the factors such as paleo-climate and properties of the source rocks. The quantitative evaluation of weathering level of source area recorded in sediments can be determined by the CIA **(Nesbitt & Young, 1982)**, PIA **(Fedo et al., 1995)**, ICV **(Cox et al., 1995)** and CIW **(Harnois, 1988)**.

The CIA values **(Fig. 5.21)** for the analysed shales have values ranging from 61to 73. The CIA values of the analyzed rocks indicate moderate chemical weathering in the source area **(Khan et al., 2019)**. The high PIA value represents 100 (Kaolinite, gibbsite) denote intense weathering whereas value of 50 suggests unweathered plagioclase. Gulcheru Formation clastic sediments show PIA values ranging from 93. to 94, which indicate intense weathering of the source rock.

The ICV values are indicator of the original composition of the source rock. ICV values of Gulcheru Formation shales vary from 0.68 to 3.12. Lower values of ICV indicate abundance in less weathered detrital minerals. These materials were probably derived from the source area with high relief **(Armstrong-Altrin et al., 2012, 2017; Cox et al., 1995)**. On the other hand, higher values indicate enrichment of pyroxene and

feldspar (non clayey minerals) in the source rock **(Depetris et al., 2014; Pasquini et al., 2017)**.

The CIW show values of 80 for un-weathered potassic granite and near to 100 value for clay minerals such as Kaolinite, illite and Gibbsite. The CIW **(Fig. 5.22)** value of the Gulcheru shale samples ranges from 95.25 to 98.52 (average 97.20), which indicate an intense weathering of the source rock.

The $Al_2O_3$- (CaO*+$Na_2O$)-$K_2O$ (A-CN-K) ternary diagram **(Nesbitt and Young, 1984)** is an imperative outline that is utilized to demonstrate the weathering attributes of clastic sedimentary rocks. The best possible weathering trend in A-CN-K diagram is indicated by the parallel line to A-CN side. For these Gulcheru Formation shale samples, weathering trend starts from granite **(Fig. 5.21)** and from the further weathering continue, the direction advances close to the illite composition **(Fedo et al., 1995)**. Gulcheru shale samples mainly fall on the $Al_2O_3$-$K_2O$ connection line, which is related to illite composition, demonstrating an intense degree of weathering of the source rock **(Hessler & Lowe, 2006)**. Since the pattern of the data does not end on the CN-K line of the A-CN-K diagram where normal ground water composition lies, this allows us infer that the K - metasomatism shows a critical influence on the formation of the Gulcheru meta-sedimentary rocks **(Li et al., 2007; McLennan et al., 1993)**. Gulcheru shales plot near to A-K line **(Fig. 5.21)** with critically high $K_2O$ content; it is a strong indicator of late potassium metasomatism **(Li et al., 2015)**.

Gulcheru Formation has been affected by low grade (green schist facies) and low-grade deformation. The coherent behaviour of U and Th metamorphism is manifested in the rocks by Th/U ratio ranges between 1.44 to 4.28, which is essentially lower than the upper amphibolite facies rocks. This shows that there is no preferential leaching of U during metamorphic dehydration processes **(Camire et al., 1993; Li et al., 2008)**. The possible alteration effects of metamorphism and deformation can further be elucidated

from the Harker variation diagrams **(Fig. 5.13)** where $SiO_2$ is compatible and positively correlated with $Al_2O_3$, $TiO_2$, $Na_2O$ and $K_2O$ and negatively correlated with MnO, $Fe_2O_3$, CaO, MgO and $P_2O_5$. The low value of $SiO_2$ however might be ascribed to chemical destruction under oxidising states of the source area.

Bivariate plot Th/Sc vs Zr/Sc **(Fig. 5.22)** can measure the amount of sedimentary process of sorting and recycling **(McLennan et al., 1993)**. Thorium is enriched in silicic rocks rather than basic rocks whereas Scandium shows more enrichment in basic rocks rather than silicic rocks. The ratio Th/Sc does not vary significantly during sedimentary recycling processes **(Cullers, 1995)**. But, the Zr/Sc proportion will increase gradually during the sediment recycling. So, the values of Zr/Sc are useful indicator of zircon enrichment **(McLennan, 1989)**. The Gulcheru Formation clastic sedimentary rocks show variable Th/Sc (0.37-1.06) and Zr/Sc (3.00-10.46) ratio **(Table 5.3)**. Despite the fact that these rocks have distinctive Th/Sc and Zr/Sc values, they show a solid positive relationship in the Th/Sc-Zr/Sc diagram **(Fig. 5.22)**. This indicates geochemical variation dominated by the composition of the source materials but not sediment recycling **(Li et al., 2015; Cullers, 1995)**.

### 5.3.6 PROVENANCE

Geochemical data of clastic sediments is an important tool to characterize the source rock **(Cullers, 2000; Mongelli et al., 1996)**. Chondrite normalized REE pattern of the Gulcheru shale shows similar pattern to granodiorite **(Jayananda et al., 2000)** and tonalite **(Allen, 1985)** of the Eastern Dharwar Craton **(Fig. 5.21)**. So, it indicates that Gulcheru shale samples should be derived from mixing of granodiorite and tonalite. As the basement of Cuddapah Group of rocks is the Eastern Dharwar Craton, granodiorite

and tonalite of the Eastern Dharwar Craton are possibly considered to be the parent rocks of the Gulcheru Formation **(Mitra et al., 2017)**.

The $SiO_2/Al_2O_3$ ratios a significant tool for indicating the maturity of the sediments **(Roser et al., 1996)**. Gulcheru Formation clastic sedimentary rocks show $SiO_2/Al_2O_3$ ratio ranging between 2.14 to 6.17 (average 4.39), which indicates the presence of mature sediments and quartz enrichment in the source rock **(K, 2017)**.

The ratio of $Al_2O_3/TiO_2$ in clastic sediments is generally utilized to depict the character of provenance **(Hayashi et al., 1997; Sun et al., 2013)**. The $Al_2O_3/TiO_2$ ratios varies from mafic (3-8), intermediate (8-21) to felsic (21-70) igneous rocks **(Sun et al., 2013; Hayashi et al., 1997)**. In Gulcheru shale samples, $Al_2O_3/TiO_2$ ratio **(Fig. 5.23)** varies between 22.32 and 33.72 (average of 26.33). In the binary diagram $Al_2O_3$*versus* $TiO_2$ **(Amajor 1987)** for Gulcheru shale samples **(Fig. 5.23)** are represents the granite field and indicates a felsic source rock for these sediments. Taking into account that $Al_2O_3$ residing in feldspars and $TiO_2$ in mafic minerals, the $Al_2O_3/TiO_2$ ratio of the Gulcheru shales indicates lower $TiO_2$ values than the PAAS **(Taylor & McLennan, 1985)**. This fact strongly indicates the presence of felsic material in the source rock. Gulcheru clastic sediments present high $K_2O/Na_2O$ ratio values (22.90-108.83), which suggests enrichment of feldspar, illite and mica in the source rock **(Crook, 1974)**.

The ternary diagram $K_2O$-$Fe_2O_3$-$Al_2O_3$ **(Fig. 5.16)** shows all the shale samples plotted near the $Al_2O_3$ apex, which indicates enrichment of $Al_2O_3$ in the parent rock **(Wronkiewicz & Condie, 1987)**. The $K_2O/Al_2O_3$ proportions of shale samples are useful to understand the original composition of the source rock. The $K_2O/Al_2O_3$ ratio of Gulcheru shale ranges from 0.31 to 0.53 (average 0.39). These proportions indicate the feldspar dominance in the parent body. Additionally, $TiO_2$/Ni bivariate diagram **(Fig. 5.24; Floyd et al., 1989)**, also indicates

that Gulcheru clastic sediments are mainly derived from felsic source rocks. Zr *versus* $TiO_2$ bivariate plot **(Fig. 5.25)** also demonstrates the felsic source of the Gulcheru sediments.

Chromium and Ni concentrations in siliciclastic rocks are important for the investigation of provenance. In Gulcheru clastic sediments, Cr/Ni ratio varies from 1.9 to 3.5. These values also indicate the felsic provenance of the Gulcheru shales. The triangular plot of $K_2O$-$Fe_2O_3$-$Al_2O_3$ **(Fig. 5.16)** of Gulcheru shales suggests derivation from felsic rocks of granite composition.

The REE and Eu anomaly is also a very important tool for delineation of parent rock **(Tapia-Fernandez et al., 2017)**. The Gulcheru clastic sediments show high LREE/HREE values (average 24.74) **(Table 5.3)** and negative Eu anomaly pointing towards felsic source for the sediments.

### 5.3.7 TECTONIC SETTING

Elemental geochemistry of the clastic sediments gives imperative data about structural setting of the parent rock **(Armstrong-Altrin et al., 2005, 2017; Bhatia, 1983; Ramakrishnan & Vaidyanadhan, 2008)**. The discrimination plot of La-Th-Sc and Th-Sc-Zr/10 shows that all of the Gulcheru Formation clastic sediments fall within the continental Island Arcs field **(Fig. 5.26 and 5.27)**. The sedimentary rock deposited on this continental arc setting is characterised by high LREE/HREE with negative Eu anomaly on chondrite normalized plots. These results are very well correlated with modern geological interpretations about the amalgamation of Columbia Supercontinent (~2Ga), which clearly states that Papaghni back arc extensional basin (Gulcheru Formation) was formed due to the subduction of oceanic crust underneath the Dharwar Craton **(Absar et al., 2016)**.

### 5.3.8 PALEO-ENVIRONMENT AND PALEO-CLIMATE

The redox conditions of clastic sediment formation are analysed with the help of some geochemical parameters. Some redox sensitive metals, such as U,Th,V,Ni,Cu,Zn and Cr in clastic sediments gives powerful information about paleoredox condition **(Madhavaraju & Ramasamy, 1999)**. Element proportions, for example, U/Th, Cu/Zn, Ni/Co and V/Cr, have been utilized to assess paleoredox condition **(Tribovillard et al., 2006)**.

Low U content is an indicator of sediments deposited in oxidising environment, whereas high concentration of U implies the deposition in oxygen minimum zone **(Armstrong-Altrin et al., 2015a; Ramos-Vazquez et al., 2017)**. So low U concentrations (average 3.59ppm) of the Gulcheru clastic sediment indicate an oxidizing depositional environment. As weathering increases, U is generally lost due to oxidization.

In addition, low U/Th values (<1.25) demonstrate oxidising depositional environment and high U/Th values (>1.25) indicate suboxic to anoxic environmental condition **(Nath et al., 1997)**. The Gulcheru shale samples have U/Th values lower than 1.25 (ranging from 0.22 to 0.69), which indicate oxic depositional conditions **(Jones & Manning, 1994)**. The values of the ratio Cu/Zn also demonstrate depositional conditions of clastic sediment **(Pandey et al., 2019)**. For clastic sediments high Cu/Zn ratios suggest reducing environment and low Cu/Zn ratios indicate oxidising environment **(Hallberg, 1976)**. In Gulcheru Formation shales the Cu/Zn ratios vary from 0.51 to 1.15 (average 0.74). These values indicate oxic condition during deposition. But wide ranges of this ratio indicate the change in bottom water conditions from oxic to sub-oxidising depositional environment **(Mitra et al., 2017)**.

Major oxides also play an important role in paleo-environmental studies (srivastava & Singh, 2018). The $SiO_2$ *versus* ($Al_2O_3$+$Na_2O$+$K_2O$) diagram **(Fig. 5.28; Suttner & Dutta,**

**1986)** of the Gulcheru shale samples indicates a semi-arid to arid domain suggesting their depositional climatic condition.

According to **Jones et al., (1994)**, values of the Ni/Co ratio < 5 represent oxic condition, 5-7 dyoxic condition and > 7 are associated with anoxic to suboxic environmental condition. In Gulcheru shale samples, Ni/Co ratios vary from 1.4 to 4.5, which suggest an oxic depositional condition. In addition, these authors suggested that V/Cr ratios: > 4.25 imply suboxic to anoxic environment; between 2.00-4.25 are related to dyoxic condition and; < 2.00 indicate oxic environments. The V/Cr values of Gulcheru shale samples ranging from 0.67 to 1.64 (average 0.9) show oxic condition during deposition. So,V/Cr *vesus* Ni/Co ratio **(Fig. 5.29)** of Gulcheru shale samples suggest an oxic environment and the Ni/Co *versus* V/(V+Ni) ratio **(Fig. 5.30)** suggests an oxic to slightly anoxic depositional condition for Gulcheru clastic sediments.

# FIGURES AND TABLES

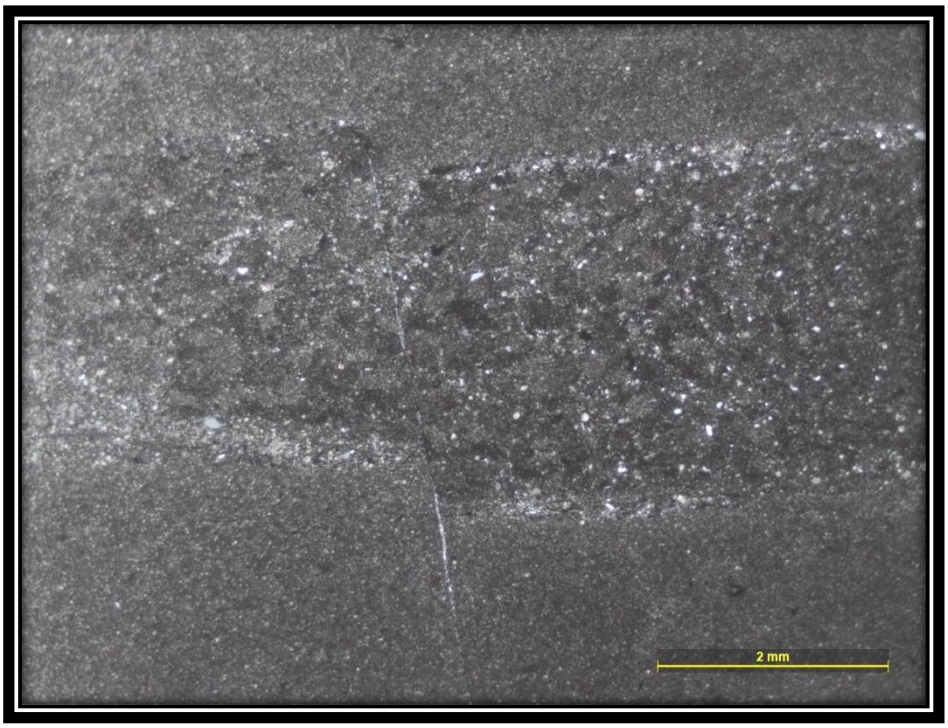


**Fig. 5.1** KM-1 Sample: Thick Siltstone layer bonded in between shale layer with a vertical fault plane

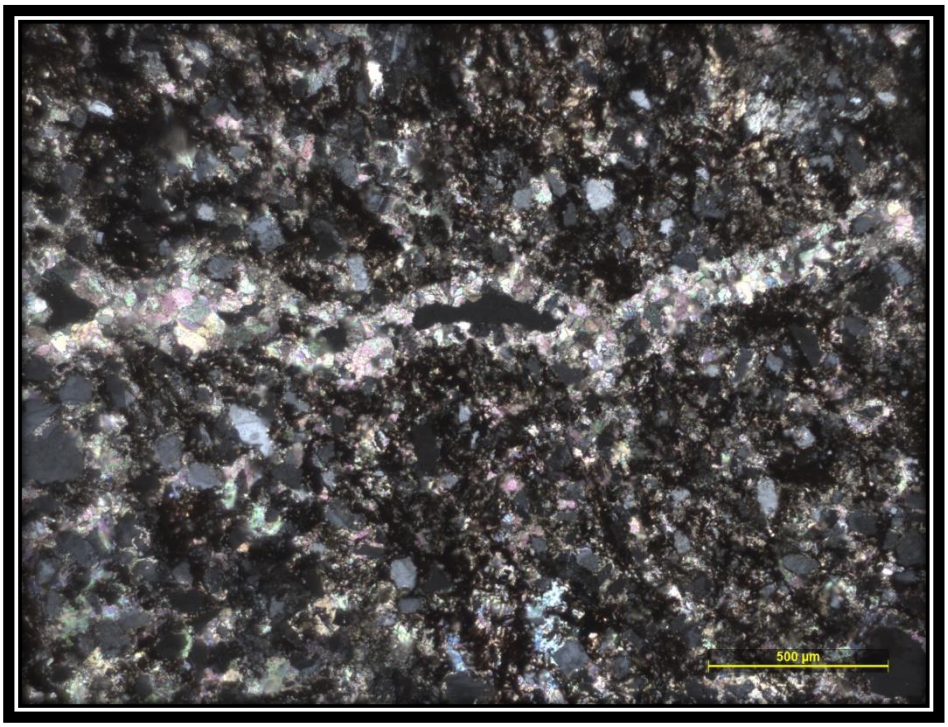


**Fig. 5.2** M-1 sample: Dominance of clay minerals with very few mica and ferruginous materials

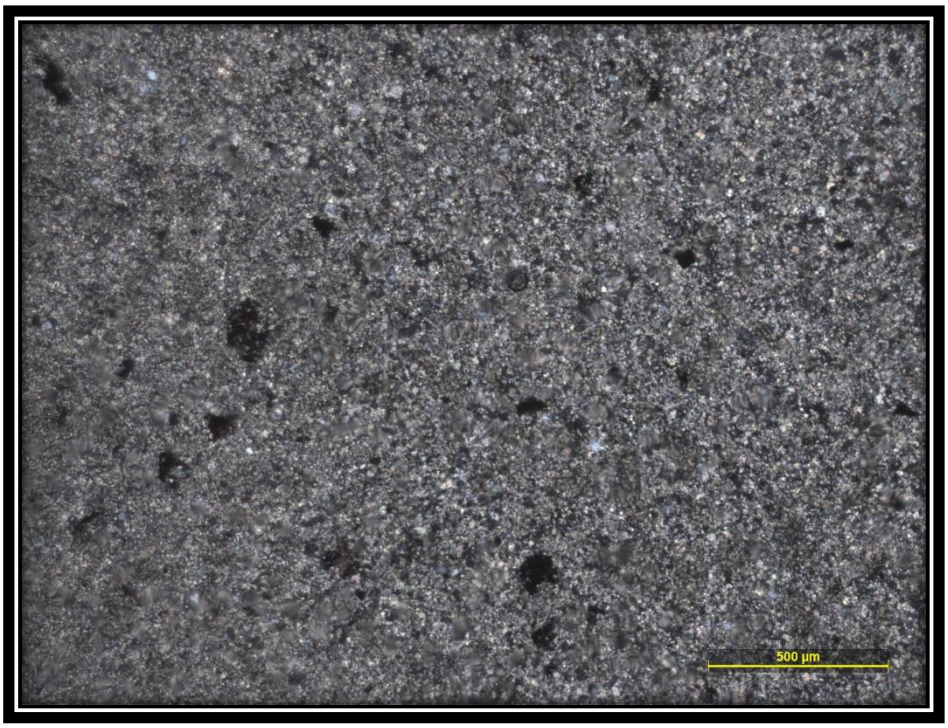


**Fig. 5.3** M-2 sample: Sample id dominated by siltstone with some mica and plagioclase feldspar

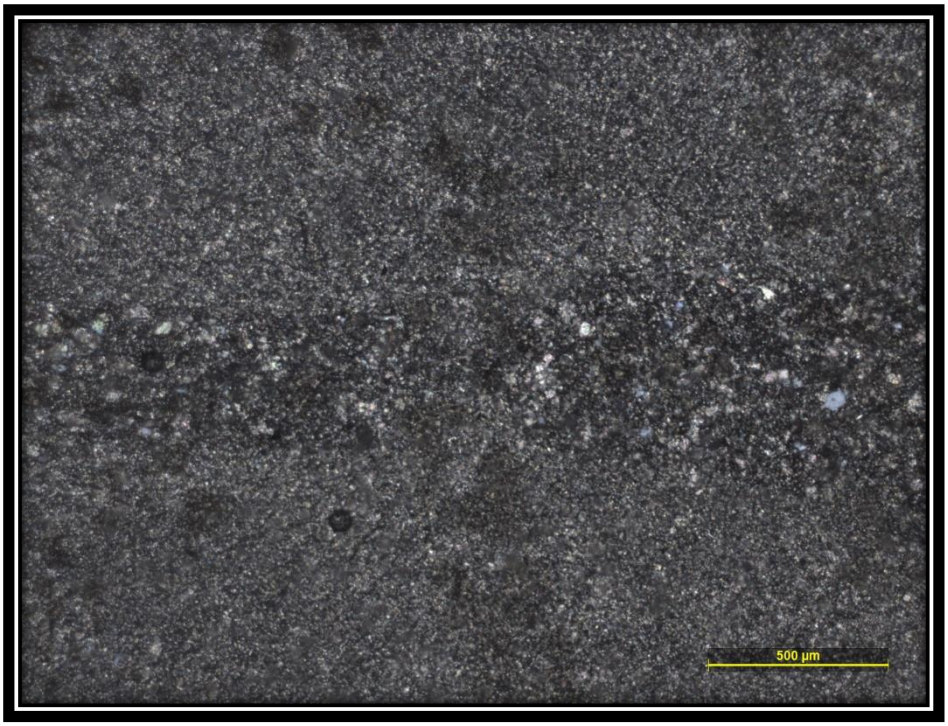


**Fig. 5.4** M-3 Sample: Thin siltstone laminae within the shale showing sharp boundary contact in between them

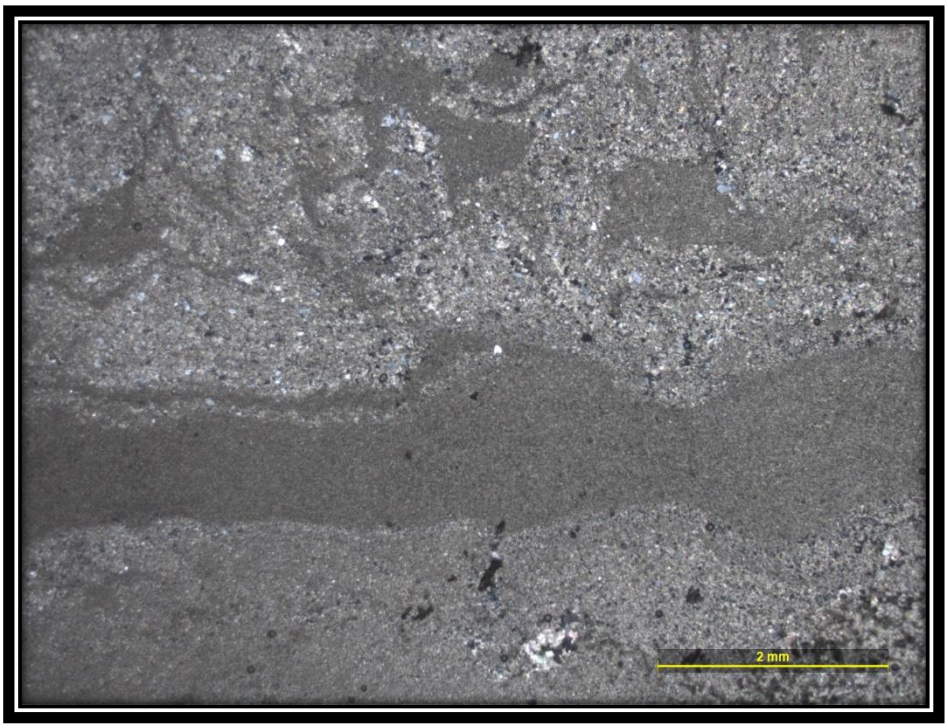


**Fig. 5.5** KU-2 Sample: Graded silt and shale couplet with wavy crinkly laminae of shale

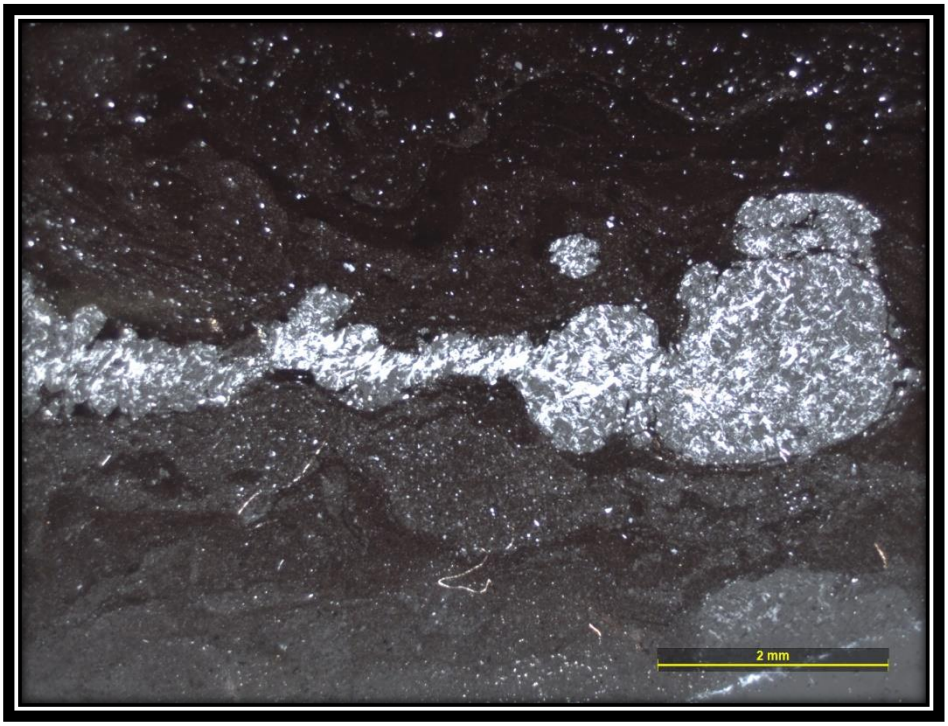


**Fig. 5.6** KU-3 Sample: Dark grey coloured very fine silt partially weathered with development of ferruginous layers

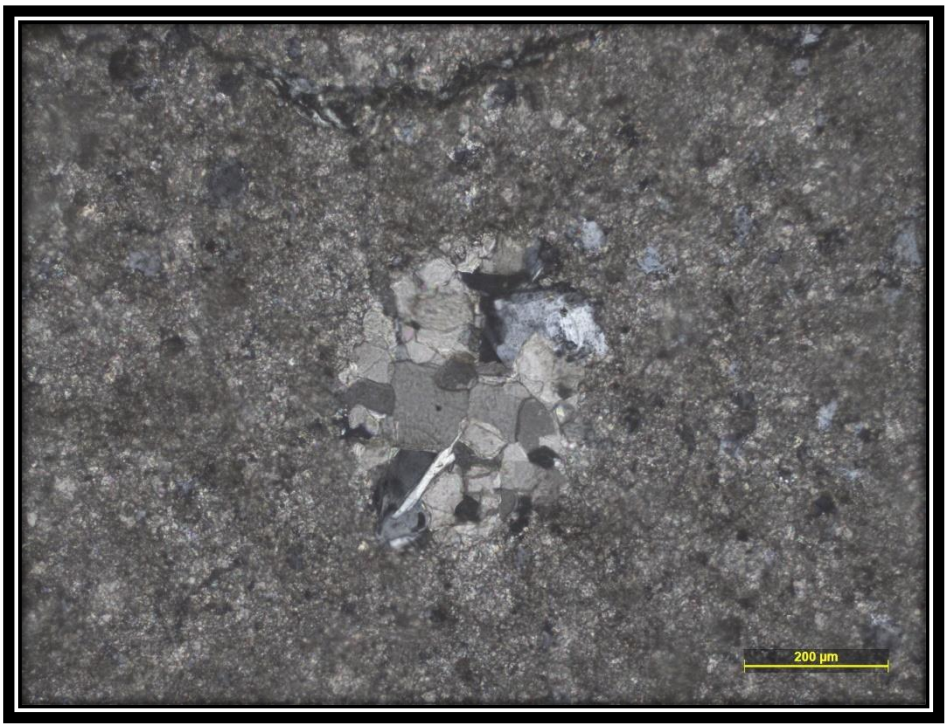


**Fig. 5.7** KU-4 sample: Thick layer of shale with clustering of quartz grains in the middle

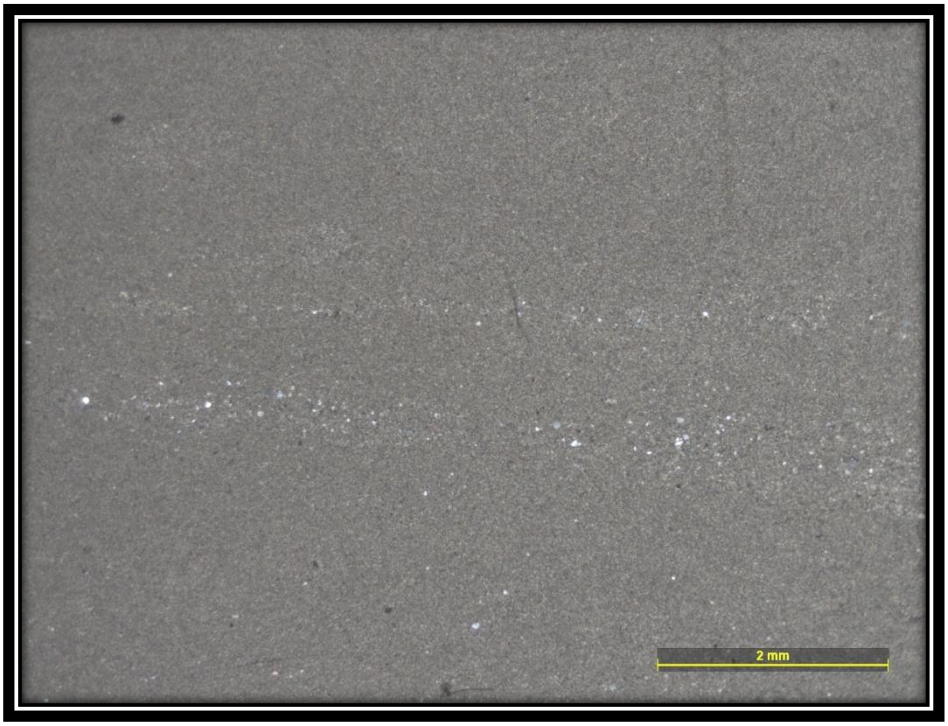


**Fig. 5.8** KU-5 sample: Thick layer of massive shale with horizontal thin coarse laminae

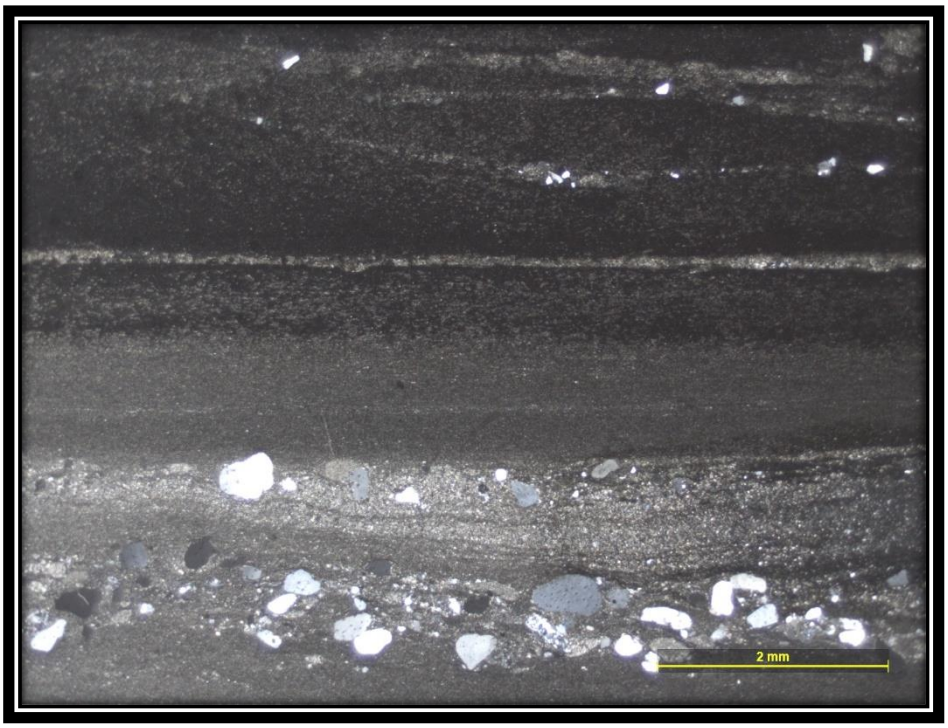


**Fig. 5.9** M-4 sample: Micaceous and arenaceous shale alternating with very fine-grained quartz layer. Fine grained sandstone channels interbedded with in the mudstone layers

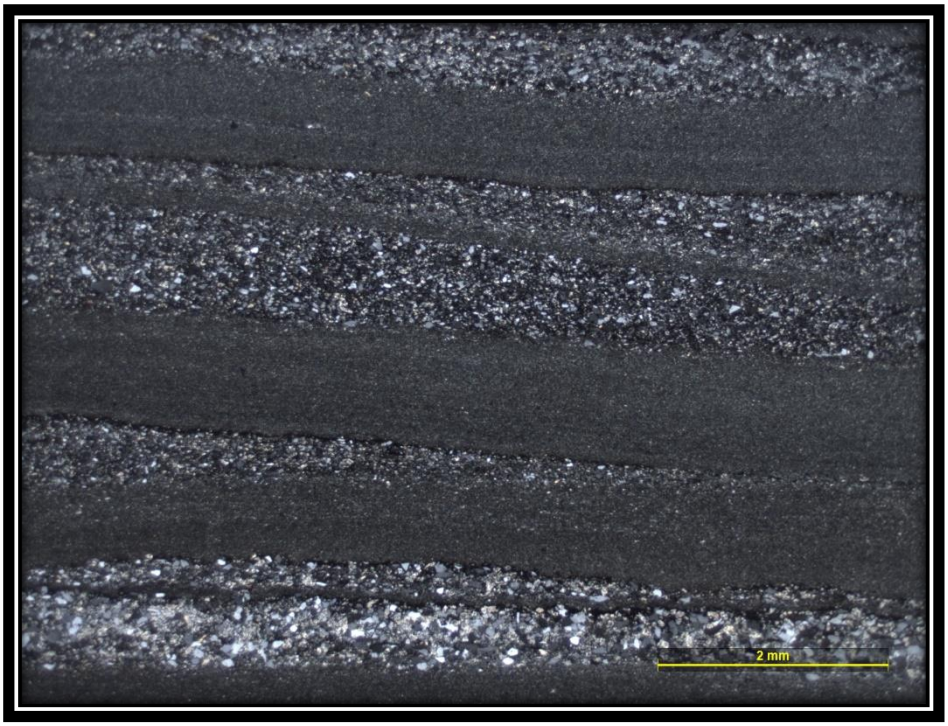


**Fig. 5.10** KU-7 sample: Shale forms thin laminations alternating with very fine sized sands and thereby forms a grain size banding in the rock

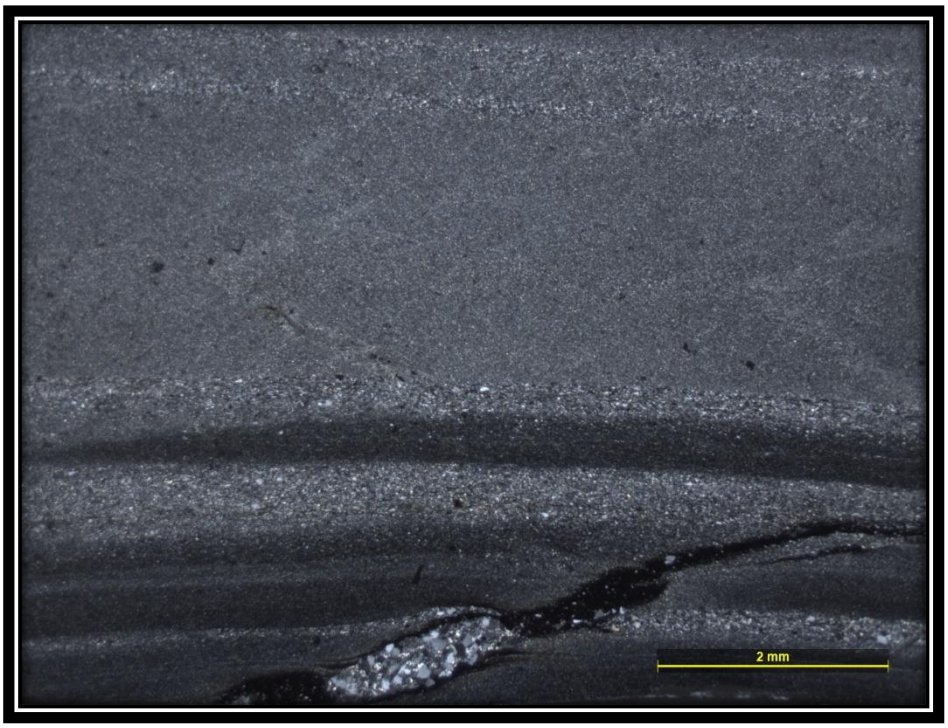


**Fig. 5.11** M-5 sample: Dominated by shale with few thin layers of siltstone. The siltstone laminae are wavy in nature

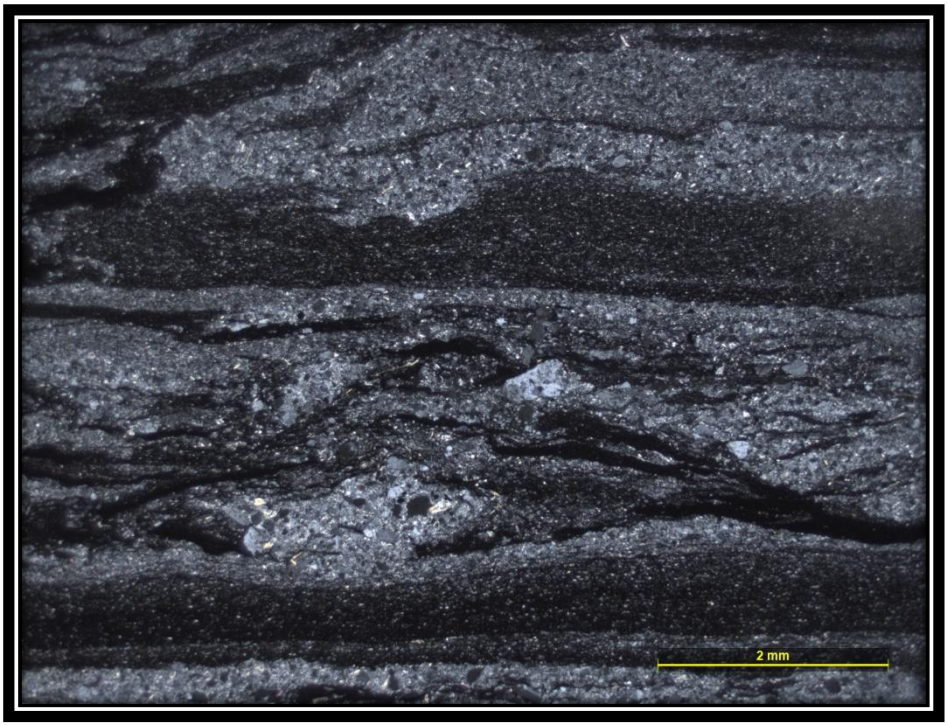


**Fig. 5.12** KU-10 sample: Graded shale and siltstone couplets with some folded ferruginous layers

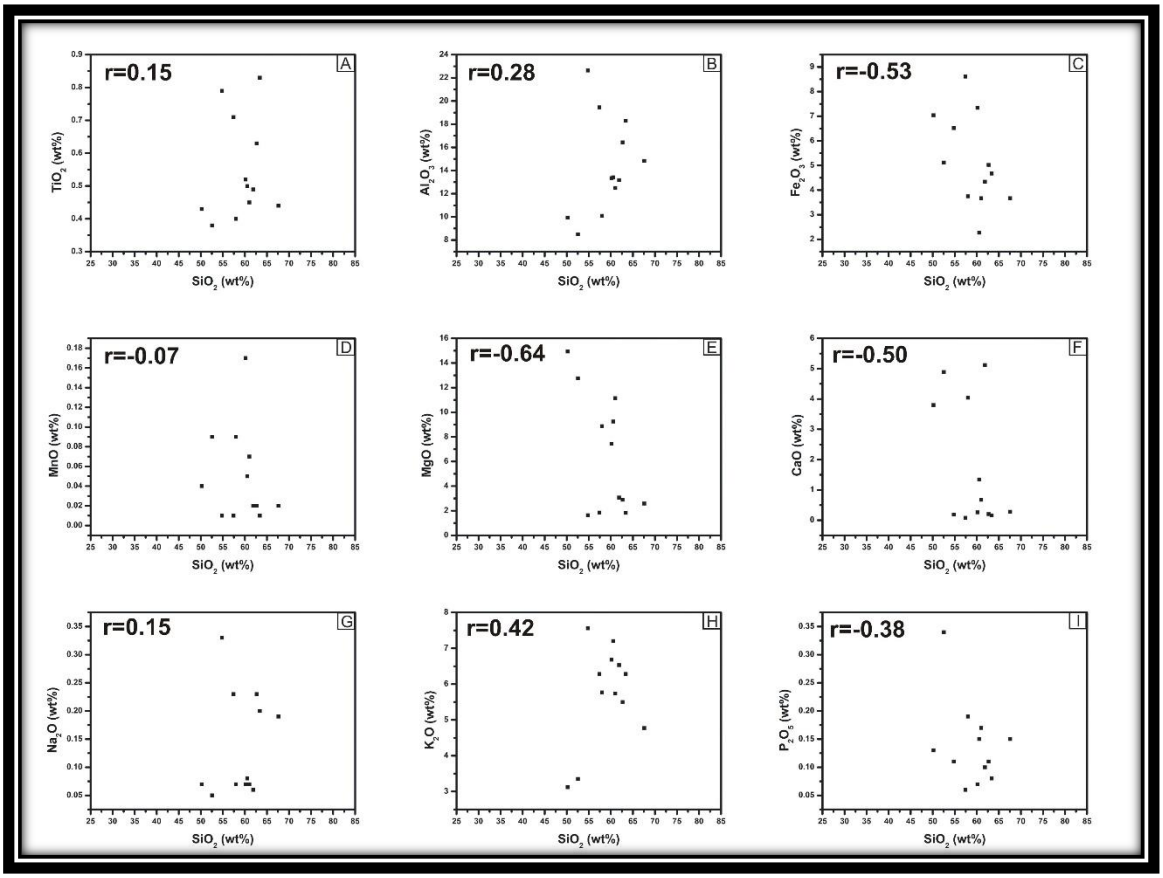


**Fig. 5.14** Binary plots of the Gulcheru siliciclastic rocks *versus* $SiO_2$

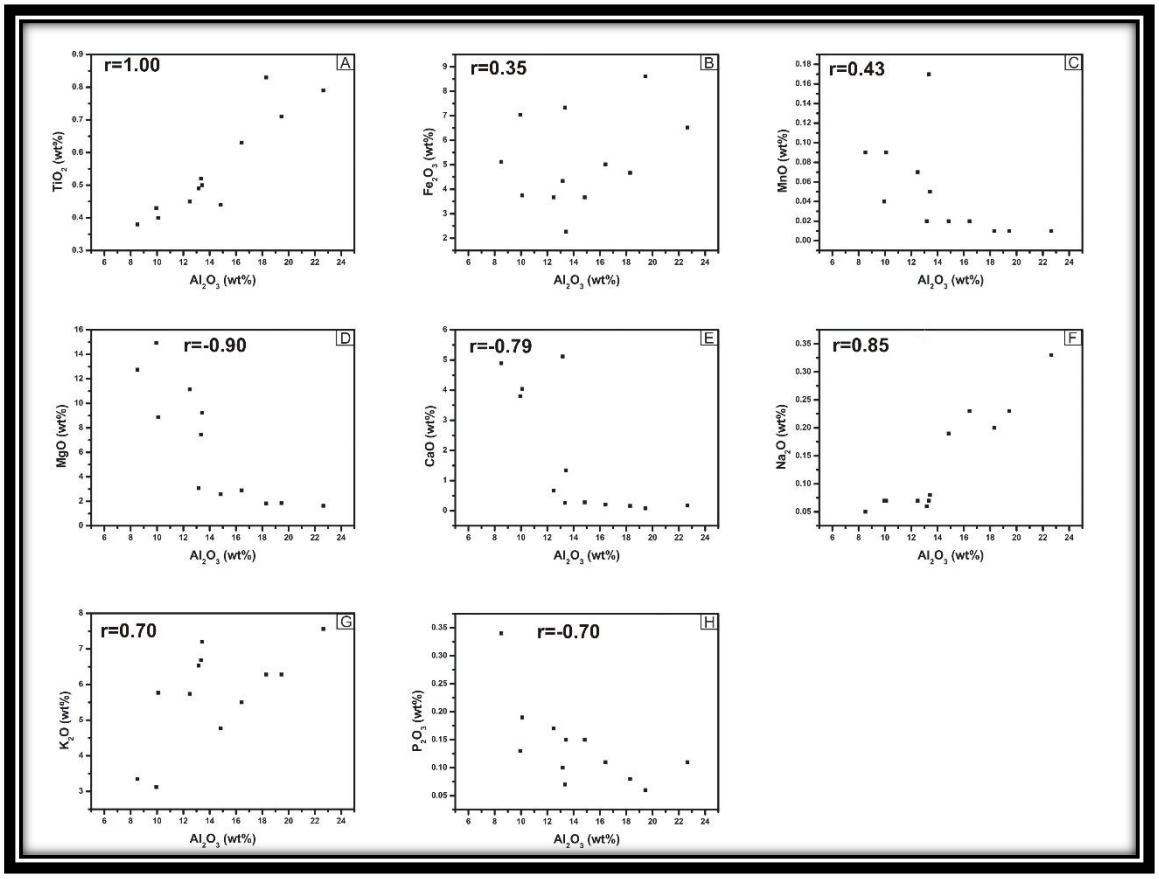


**Fig. 5.14** Binary plots of the Gulcheru siliciclastic rocks *versus* $AlO_2$

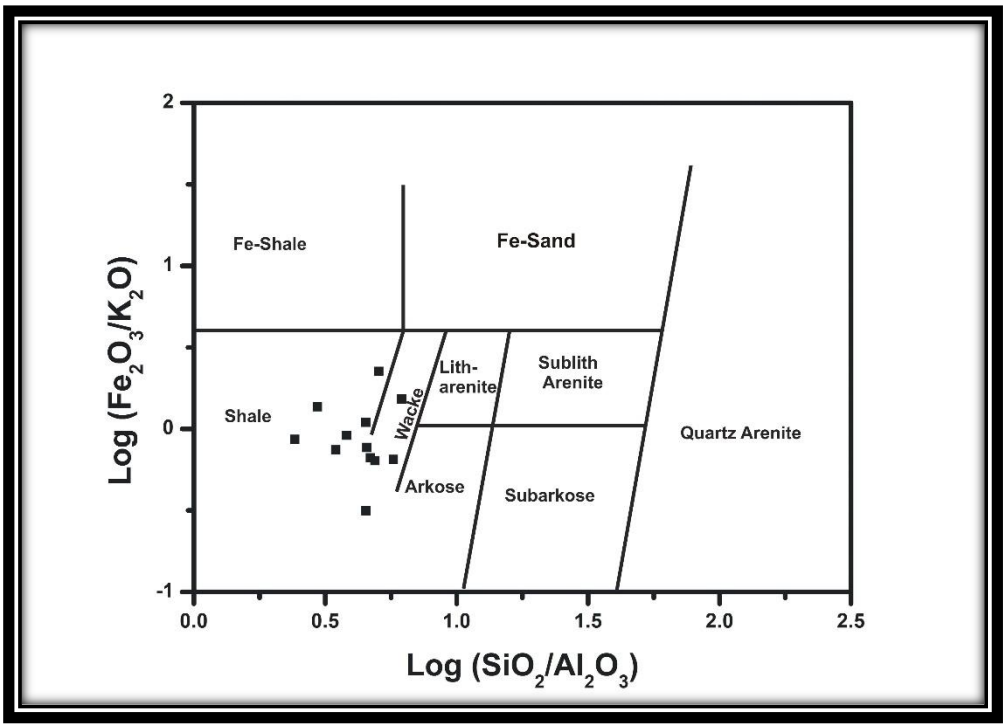


**Fig. 5.15** Binary diagram: Log ($Fe_2O_3/K_2O$) *versus* Log ($SiO_2/Al_2O_3$) diagram of **Herron (1988)**

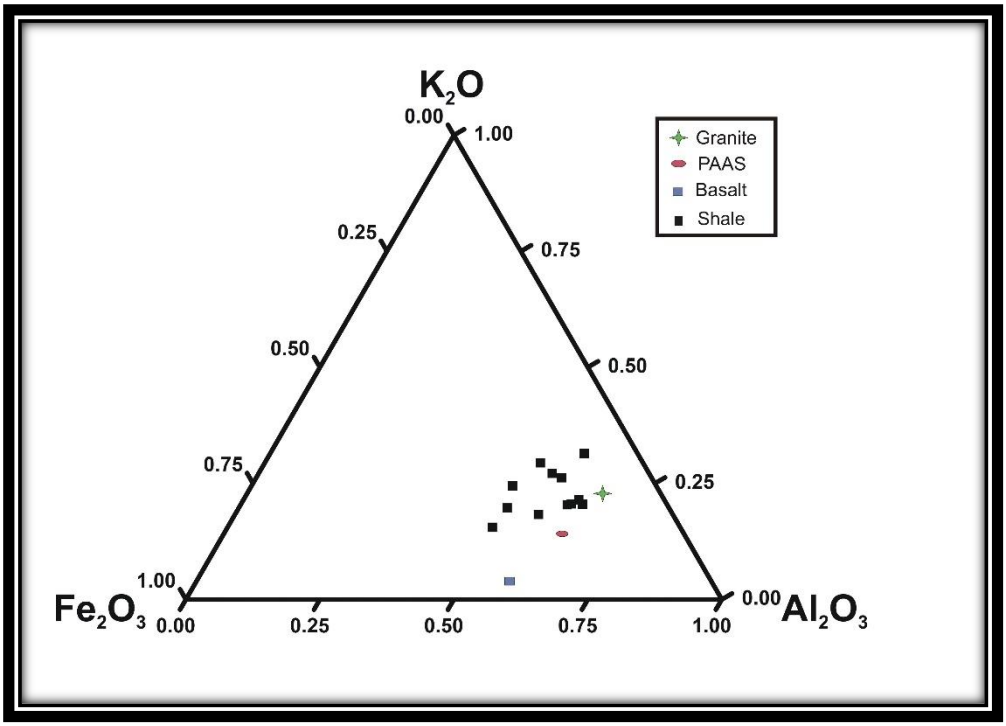


**Fig. 5.16** Major element distribution in the Gulcheru shales in $K_2O$-$Fe_2O_3$-$Al_2O_3$ ternary diagram. Granite, basalt and PAAS are defined from Condie, (1993) and Taylor and McLennan, (1985) respectively

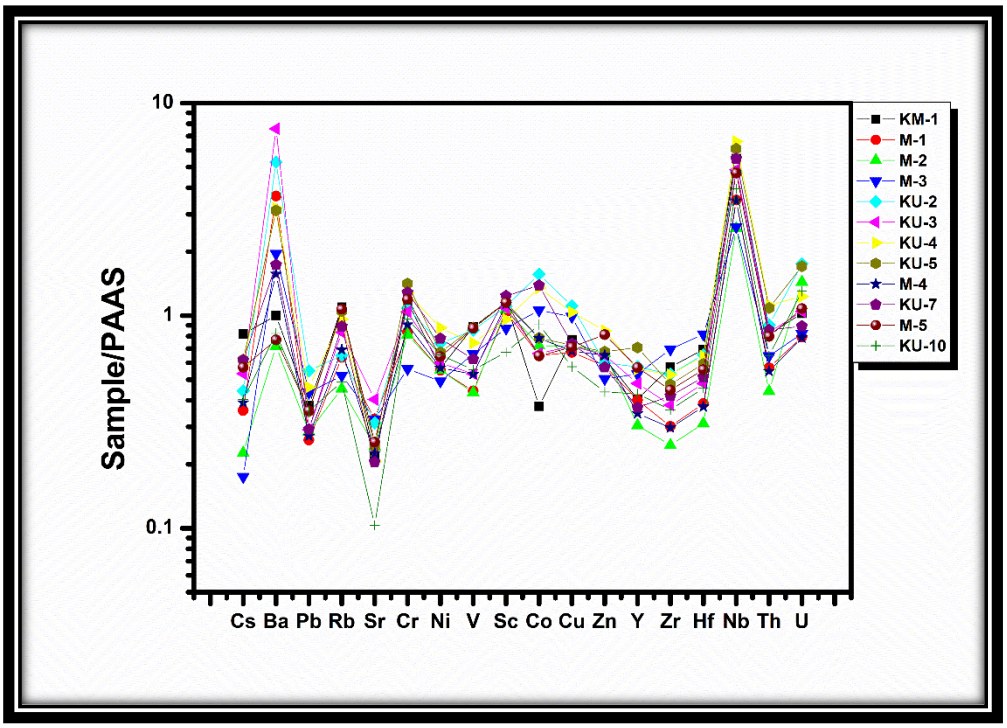


**Fig. 5.17 PAAS** normalized trace element pattern distribution

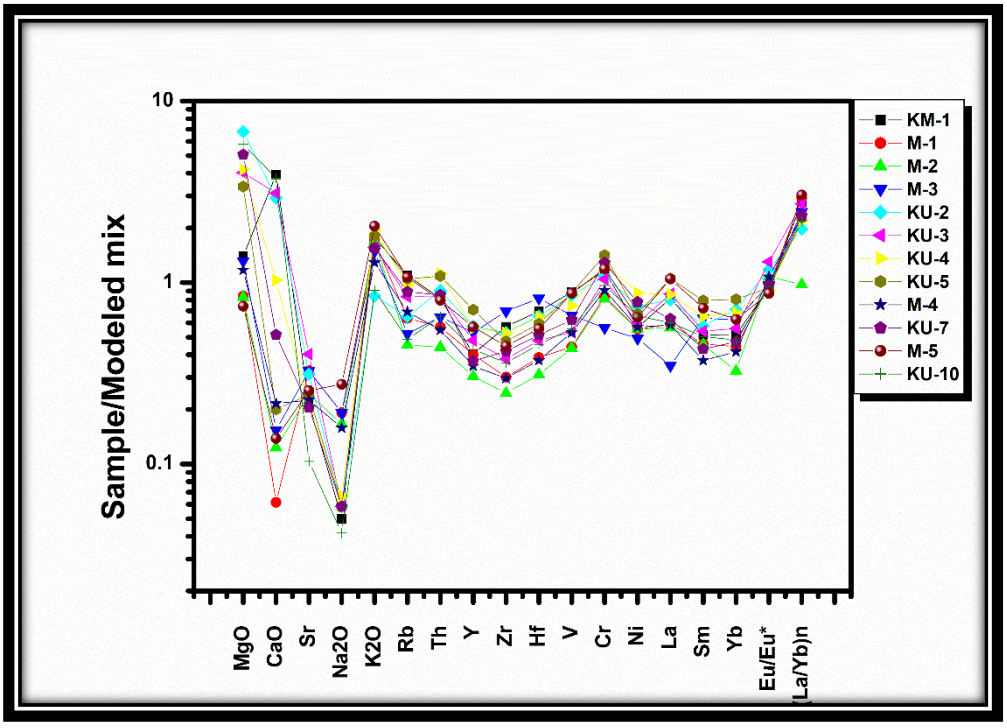


**Fig. 5.18** Major and trace elements normalized to modelling mix results **(Wang & Zhou, 2013)**

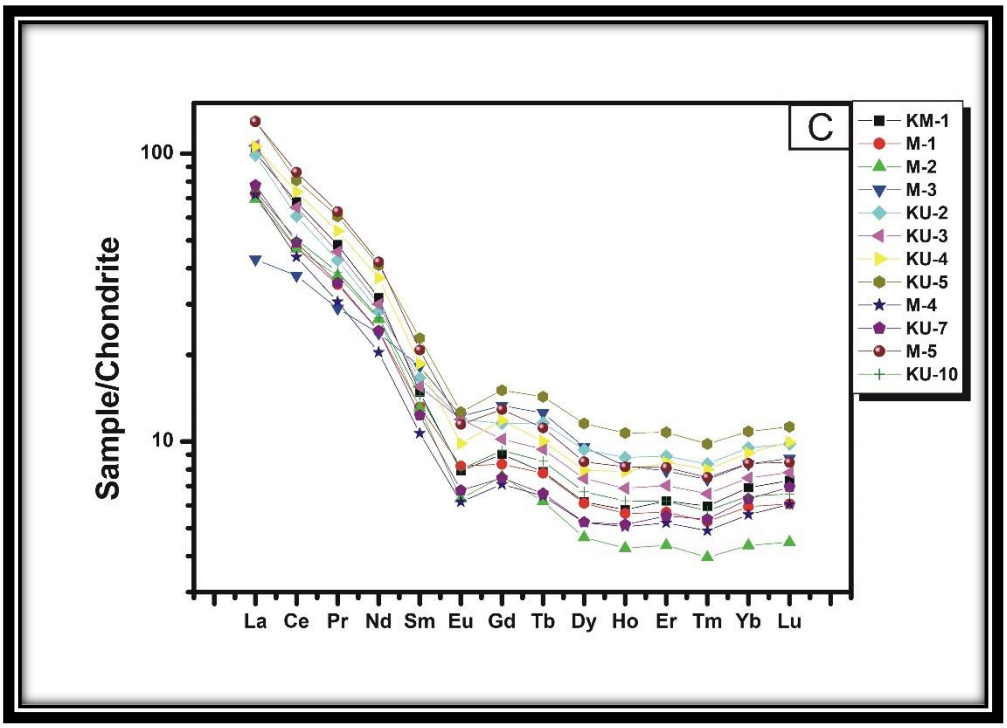


**Fig. 5.19** Chondrite normalized REE elements pattern distribution in Gulcheru shale samples. PAAS and Chondrite normalized values are defined from **Taylor & McLennan, (1985)**

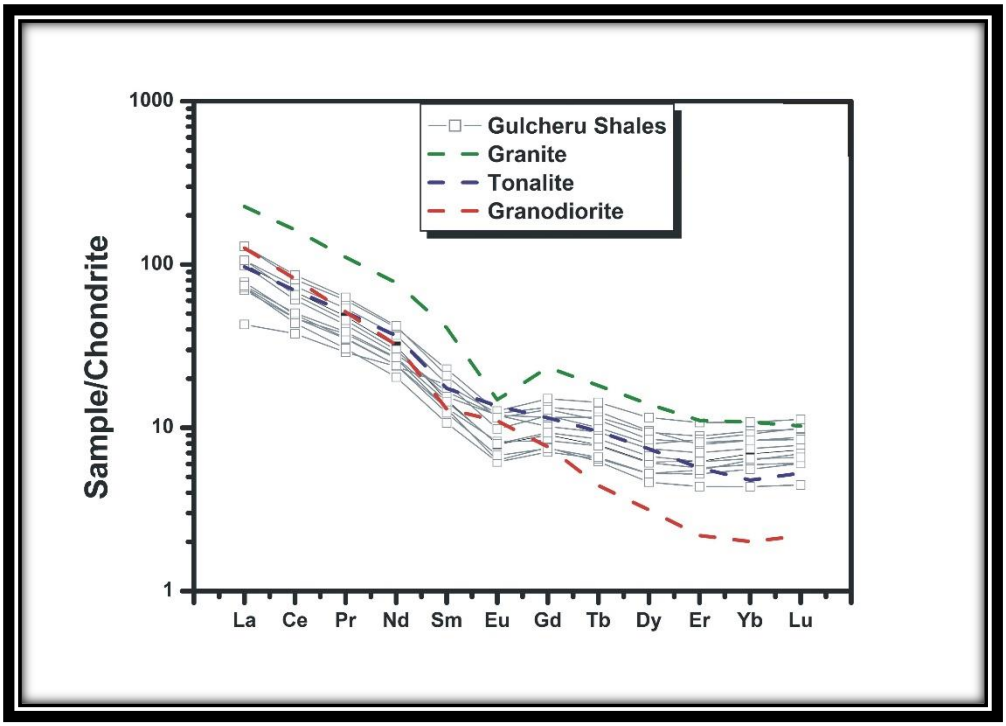


**Fig. 5.20** Chondrite-normalized REE pattern of potential source rocks (Granodiorite and tonalite) of Eastern Dharwar Craton with Gulcheru Formation shales

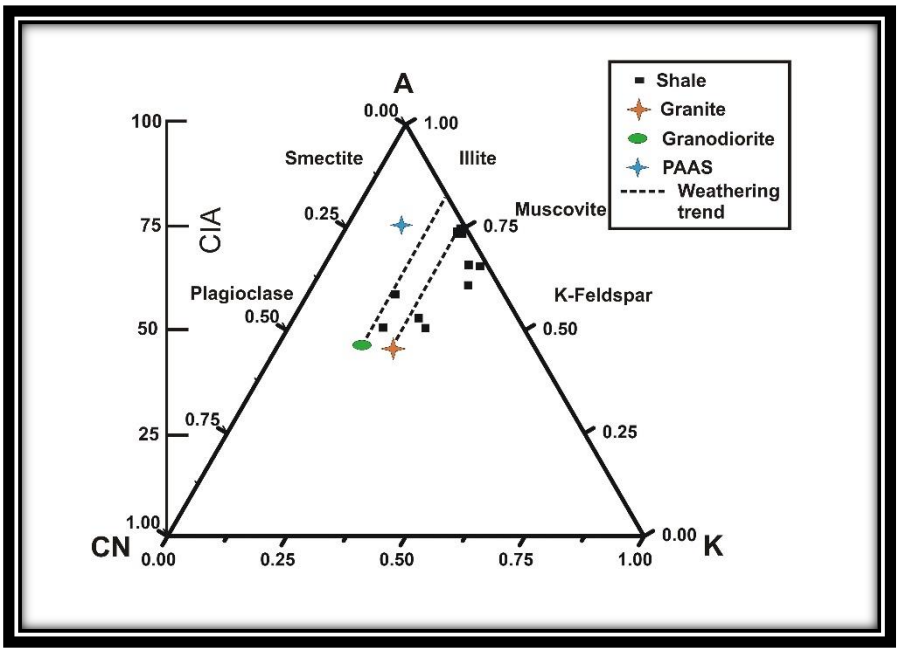


**Fig. 5.21** Major element compositions of Gulcheru shale samples in molecular proportion triangular diagram of $Al_2O_3$-($Na_2O_3$+CaO*)-$K_2O$ with the Chemical Index of Alteration (CIA) and Chemical Index of Weathering (CIW) scales shows the idealized weathering trend (after **Fedo et al., 1995**)

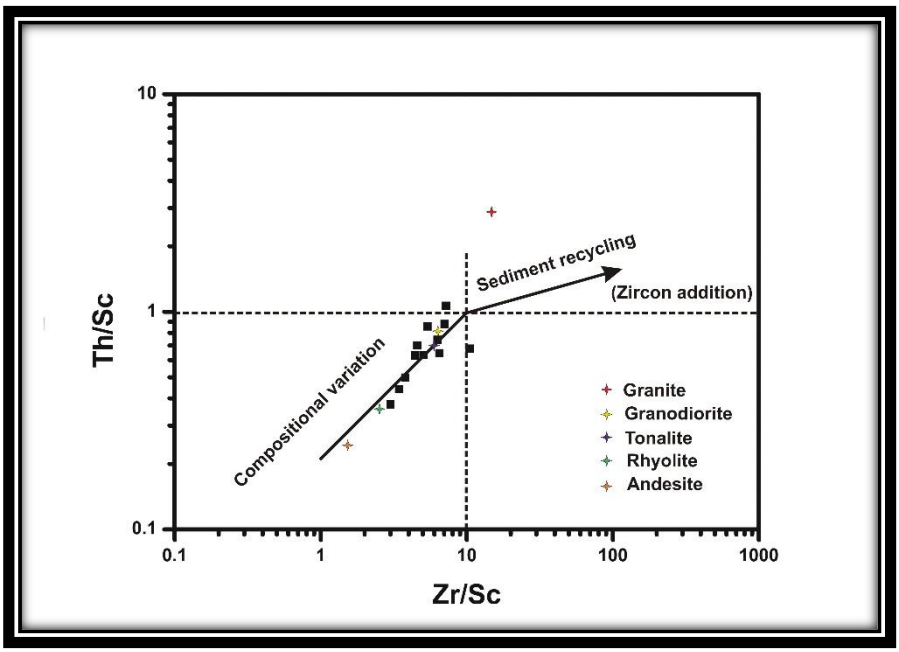


**Fig. 5.22** Th/Sc *versus* Zn/Th plot (after McLennan et al., 1993) showing sedimentary sorting for Gulcheru Formation sedimentary rocks. The data on average rock compositions (granodiorite, tonalite, rhyolite, and andesite) are defined from **Condie, (1993)**

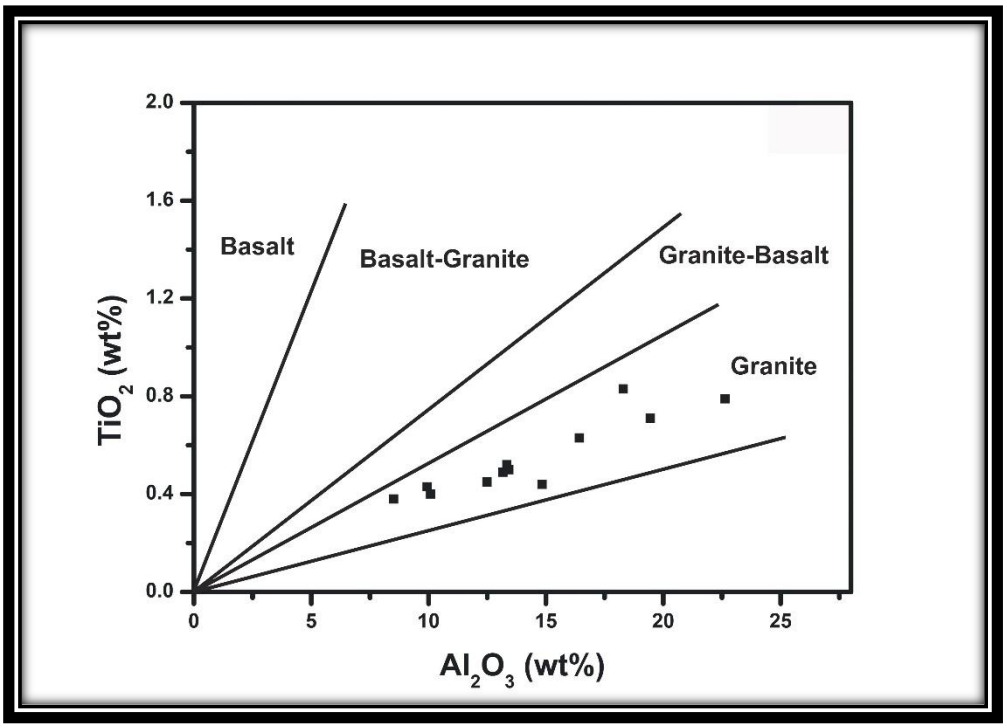


**Fig. 5.23** Scatter plots of A. $Al_2O_3$ *versus* $TiO_2$ for linear provenance indicators for shale samples from Gulcheru Formation

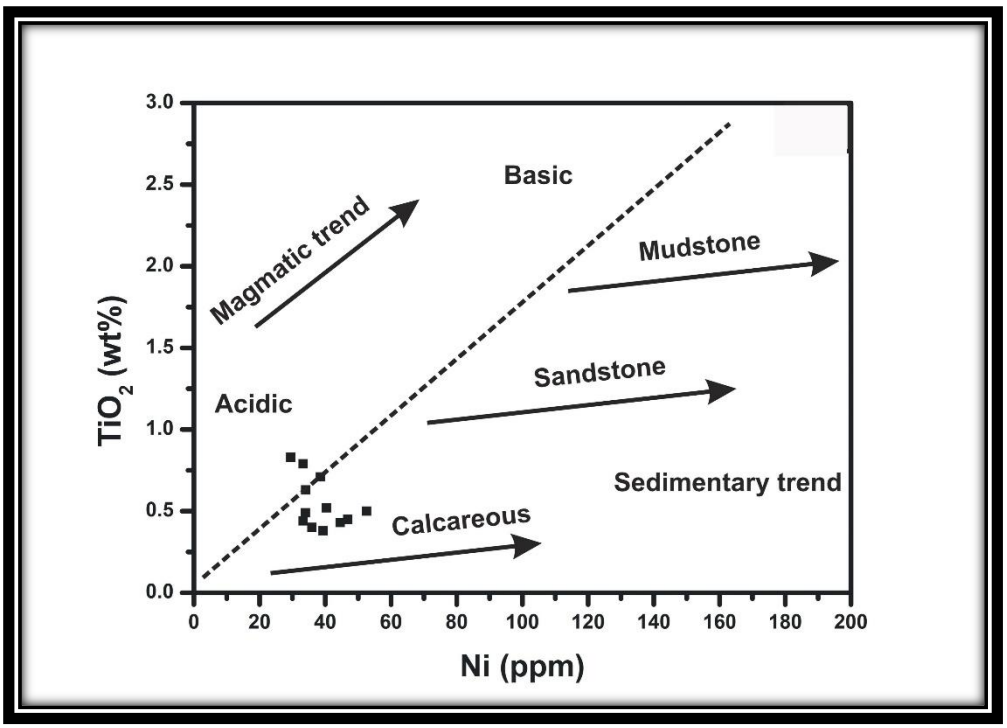


**Fig. 5.24** Scatter plots of Ni *versus* $TiO_2$ for linear provenance indicators for shale samples from Gulcheru Formation

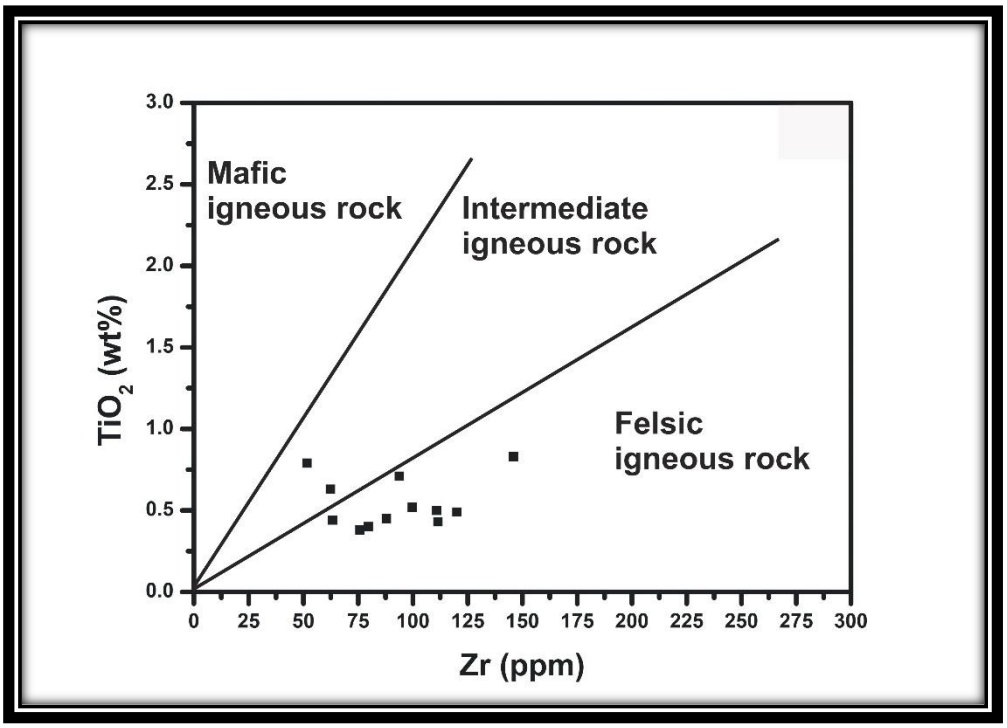


**Fig. 5.25** Zr *versus* $TiO_2$for linear provenance indicators for shale samples from Gulcheru Formation

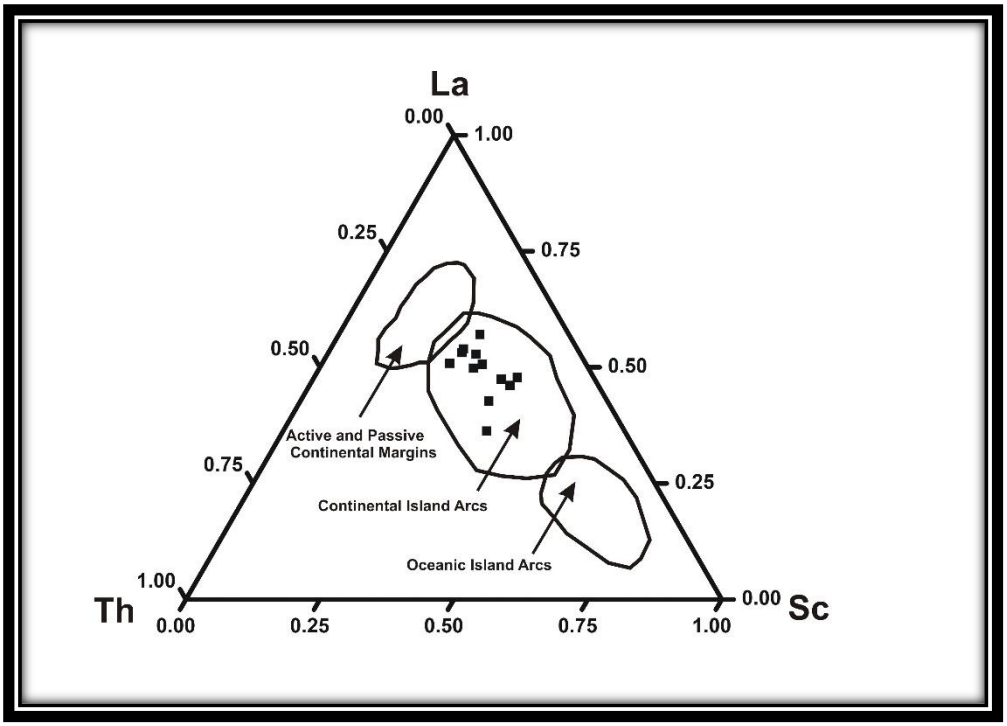


**Fig. 5.26** Discrimination plots A. La-Th-Sc and for tectonic settings **(Bhatia & Crook, 1986)** for siliciclastic sediments of Gulcheru Formation

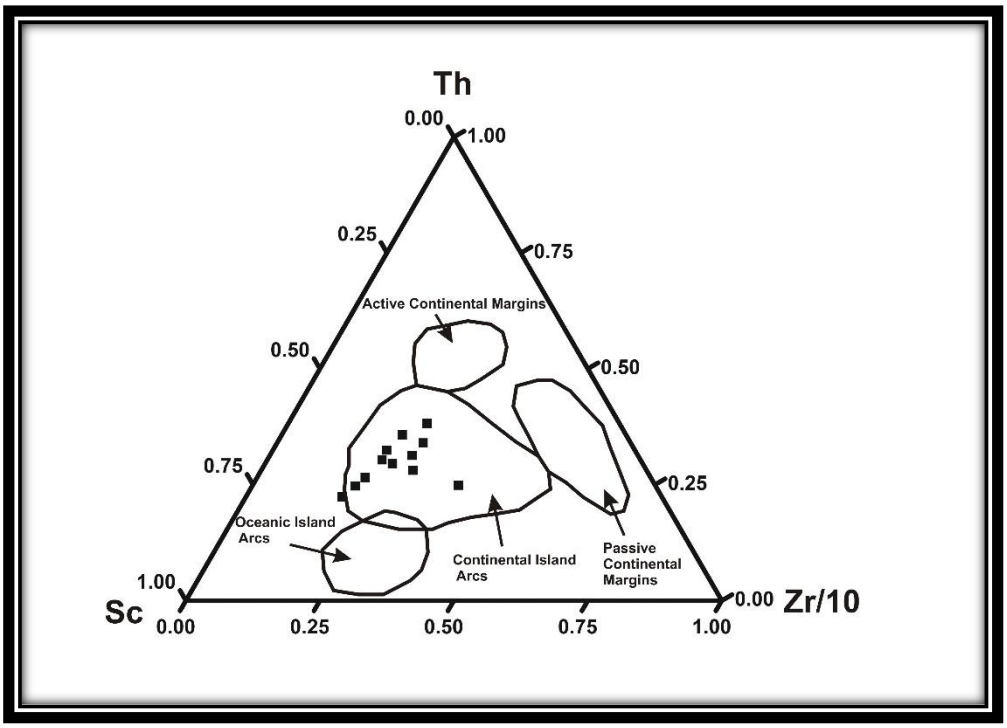


**Fig. 5.27** Discrimination plots A. La-Th-Sc and B. Th-Sc-Zr/10 for tectonic settings (**Bhatia & Crook, 1986**) for siliciclastic sediments of Gulcheru Formation

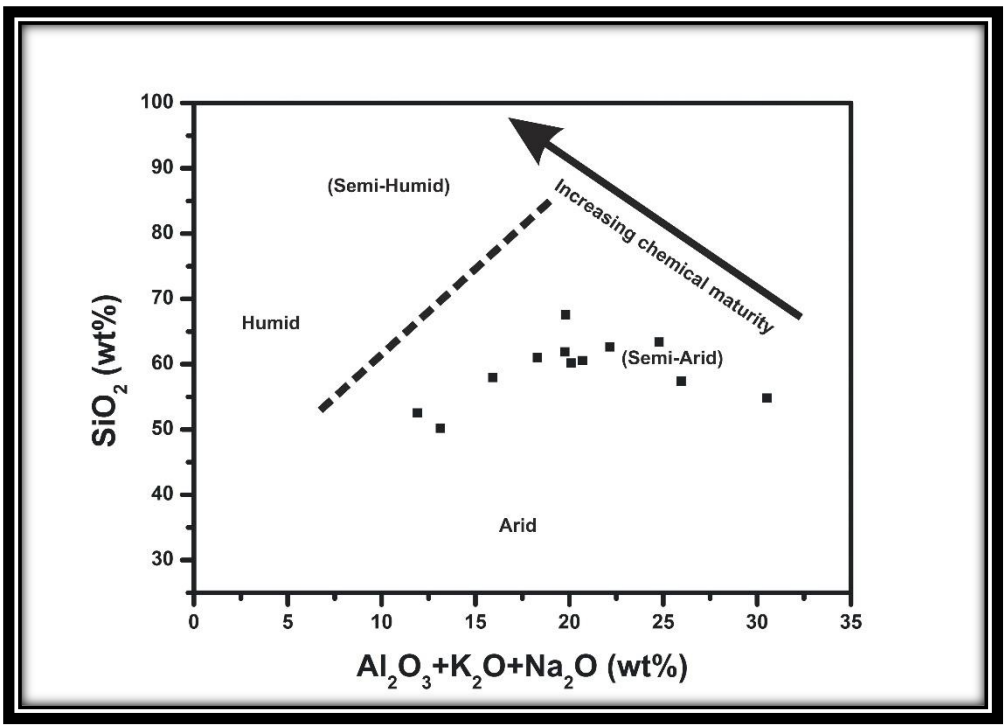


**Fig 5.28** Paleo-environment of Gulcheru shales. Bivariate plot of $SiO_2$*versus* ($Al_2O_3$+$K_2O$+$Na_2O$) to discriminate paleo-climatic condition of the Gulcheru sediments (**after Suttner & Dutta, 1986**)

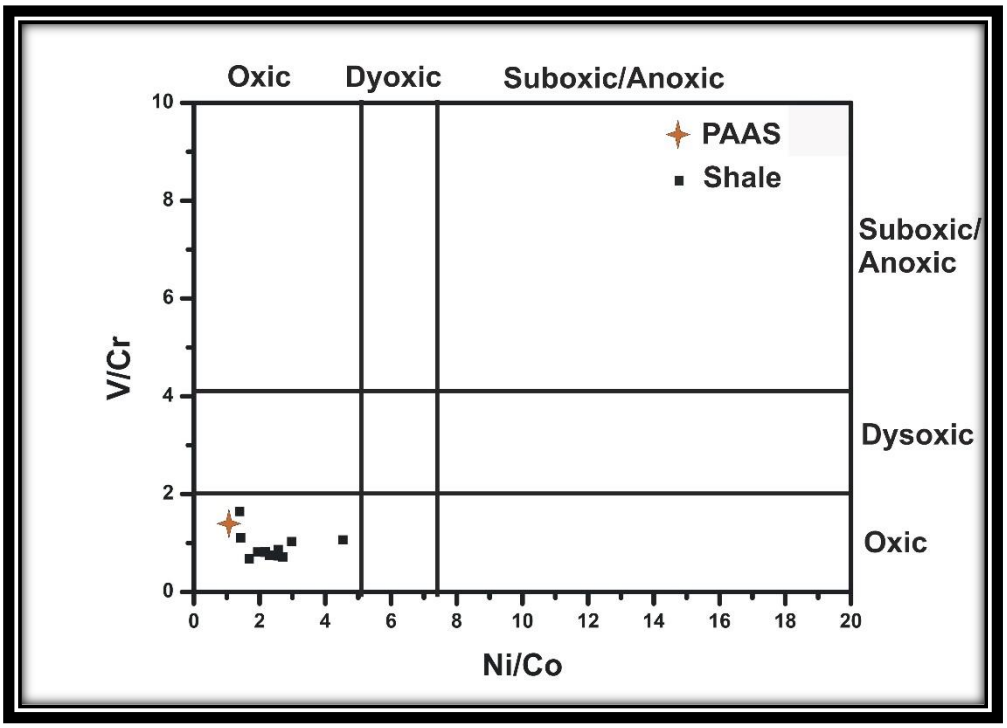


**Fig. 5.29** Paleo-environment of Gulcheru shales. Binary plot of Ni/Co *versus* V/Cr indicates oxic condition during deposition

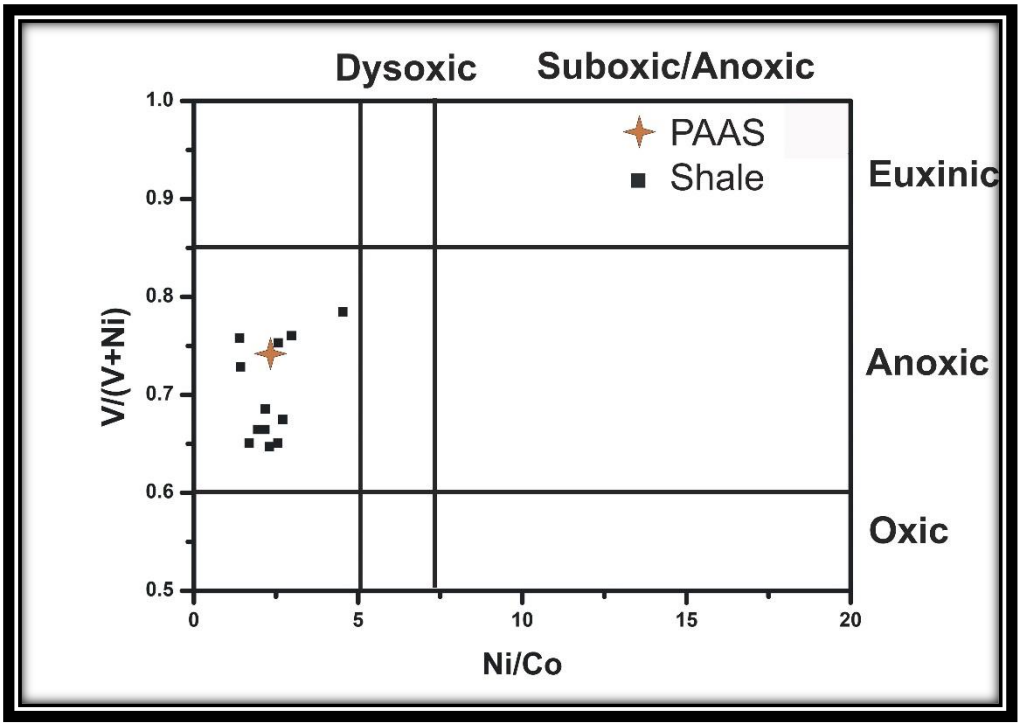


**Fig. 5.30** Paleo-environment of Gulcheru shales. Binary plot of Ni/Co *versus* V/(V+Ni) indicates oxic to anoxic condition during deposition

| Sample no | Rock type | Petrographic Description | Figure no |
|---|---|---|---|
| KM-1 | Alteration of Shale and siltstone | Shale sample from lower middle part of the section is interbedded with in a thin band siltstone and a thick layer of sandstone. This is a fine grained dark grey to black coloured quartzo-feldspathic rock which is highly silicified and often traversed by 3-5mm thick quartz veins. Microscopically this shale sample is dominated by shale with thick siltstone layer bounded in between shale layer with a vertical fault plane. | 4.1 |
| M-1 | Shale with alternate sandstone layer | The shale sample characterized by reddish brown colour alternating with buff coloured siltstone. The rock is partially weathered and ferrugination occur along the fracture planes. Overall, the slide shows the dominance of clay minerals with very few mica and ferruginous materials. Compaction deformation is minimal, as evidenced by common undeformed micas. | 4.2 |
| M-2 | Shale | Sample represents greyish black shale with few patches of mica . Principal constituent minerals are very fine-grained clay with profuse mica. Under the microscope, sample is dominated by siltstone with some mica and plagioclase feldspar. | 4.3 |
| M-3 | Shale with feruugiginous bands | Sample represents greyish shale with thin siltstone laminae. This is a fine grained grey coloured rock composed of alternation of 2-3 mm. thick layers of very fine grained quartzo-feldspathic mineral and also evidenced from the development of ferruginous film along fracture planes. Microscopically this sample shows dominance of clay minerals, quartz, muscovite, and biotite. | 4.4 |

**Table 5.1** Petrographic description of the selected shale samples from Gulcheru Formation

| Sample no | Rock type | Petrographic Description | Figure no |
|---|---|---|---|
| KU-2 | Shale with distorted ferruginous laminae | Sample characterized by dark grey to brown coloured shale with distorted ferruginous laminae. The siltstone, muscovite and boitite constitute thick bands alternating with clay mineral rich light-coloured bands. Under the microscope, this shale sample is dominated by graded silt and shale couplet with wavy crinkly laminae of shale. | 4.5 |
| KU-3 | Shale and siltstone alteration | Sample represents a dirty grey coloured very fine grained one, partially weathered with development of ferruginous layers along the fracture surfaces. Microscopically this sample is dominated by graded silt and shale couplet with wavy crinkly laminae of siltstone. | 4.6 |
| KU-4 | Massive Shale with few larger clasts | Sample characterized by red coloured thick layer of massive shale. Microscopically this sample shows a layer of shale with a clustering of quartz in the middle. | 4.7 |
| KU-5 | Massive Shale | Sample also characterized by red coloured thick layer of massive shale. Microscopically this sample shows a thick layer of massive shale. | 4.8 |

**Table 5.1** Petrographic description of the selected shale samples from Gulcheru Formation

| Sample no | Rock type | Petrographic Description | Figure no |
|---|---|---|---|
| M-4 | Shale alteration with sandstone | This shale sample is characterized by reddish brown shale with thin alternate layers of siltstone. This is a fine-grained rock composed principally of micaceous and arenaceous shale, alternating with very fine-grained quartz layer. Both quartz and shale bands are oriented in a preferred direction but it is often discontinuous in nature. Microscopically this sample shows normal grading of siltstone and shale. Fine grained sandstone channels interbedded within the mudstone layers. | 4.9 |
| KU-7 | Shale and siltstone alteration | Sample characterized by greyish shale with thin layers of siltstone alternating with shale. The shale forms thin laminations alternating with fine and very fine sized sands and thereby forms a grain size banding in the rock. Microscopically this sample shows Graded Silt/Clay couplets with some lenticular silt layer. | 4.10 |
| M-5 | Massive shale with few alterations of siltstone | Sample characterized by dark grey shale with thin layers of siltstone alternating with shale in the bottom part. Some larger size clast presents in lower part with overall fining upward sequence. | 4.11 |
| KU-10 | Shale | Sample characterized by greyish shale with thin layers of siltstone alternating with shale. Microscopically this sample shows Graded Silt/Clay couplets with some alternating silt layer in the lower part. | 4.12 |

**Table 5.1** Petrographic description of the selected shale samples from Gulcheru Formation

| | KM-1 | M - 1 | M - 2 | M - 3 | KU-2 | KU-3 | KU-4 | KU-5 | M - 4 | KU-7 | M - 5 | KU-10 | PAAS (Taylor and McLennan 1985; McLennan 2001) |
|---|---|---|---|---|---|---|---|---|---|---|---|---|---|
| **$SiO_2$** | 61.88 | 57.42 | 63.39 | 62.66 | 50.2 | 57.97 | 60.55 | 60.17 | 67.58 | 61.01 | 54.8 | 52.54 | 62.80 |
| **$TiO_2$** | 0.49 | 0.71 | 0.83 | 0.63 | 0.43 | 0.4 | 0.5 | 0.52 | 0.44 | 0.45 | 0.79 | 0.38 | 1.00 |
| **$Al_2O_3$** | 13.17 | 19.45 | 18.3 | 16.43 | 9.94 | 10.09 | 13.42 | 13.34 | 14.84 | 12.49 | 22.64 | 8.51 | 18.90 |
| **MnO** | 0.02 | 0.01 | 0.01 | 0.02 | 0.04 | 0.09 | 0.05 | 0.17 | 0.02 | 0.07 | 0.01 | 0.09 | 0.11 |
| **$Fe_2O_3$** | 4.34 | 8.61 | 4.67 | 5.02 | 7.04 | 3.75 | 2.27 | 7.34 | 3.67 | 3.67 | 6.52 | 5.12 | 6.50 |
| **CaO** | 5.12 | 0.08 | 0.16 | 0.2 | 3.8 | 4.04 | 1.34 | 0.26 | 0.28 | 0.67 | 0.18 | 4.89 | 1.3 |
| **MgO** | 3.07 | 1.85 | 1.83 | 2.89 | 14.93 | 8.87 | 9.24 | 7.44 | 2.58 | 11.14 | 1.63 | 12.75 | 2.20 |
| **$Na_2O$** | 0.06 | 0.23 | 0.2 | 0.23 | 0.07 | 0.07 | 0.08 | 0.07 | 0.19 | 0.07 | 0.33 | 0.05 | 1.20 |
| **$K_2O$** | 6.53 | 6.28 | 6.28 | 5.5 | 3.12 | 5.77 | 7.2 | 6.68 | 4.77 | 5.74 | 7.56 | 3.35 | 3.70 |
| **$P_2O_5$** | 0.1 | 0.06 | 0.08 | 0.11 | 0.13 | 0.19 | 0.15 | 0.07 | 0.15 | 0.17 | 0.11 | 0.34 | 0.16 |
| **LOI** | 4.64 | 5.14 | 3.48 | 5.66 | 9.79 | 8.39 | 4.29 | 3.08 | 5.12 | 3.76 | 4.85 | 11.27 | |
| **Total** | **99.41** | **99.84** | **99.23** | **99.3** | **99.47** | **99.63** | **99.06** | **99.12** | **99.64** | **99.24** | **99.42** | **99.28** | |

**Table 5.2** Major elements (%) concentration for shales of the Gulcheru Formation, Cuddapah Basin with average composition of PAAS **(Taylor and McLennan 1985)**

| | KM-1 | M-1 | M-2 | M-3 | KU-2 | KU-3 | KU-4 | KU-5 | M-4 | KU-7 | M-5 | KU-10 | PAAS (Taylor and McLennan 1985) |
|---|---|---|---|---|---|---|---|---|---|---|---|---|---|
| **Sc** | 18.50 | 18.43 | 13.94 | 18.13 | 17.70 | 17.38 | 15.36 | 18.51 | 16.69 | 19.81 | 17.15 | 10.76 | 16 |
| **V** | 123.85 | 122.21 | 92.39 | 74.22 | 119.58 | 74.60 | 104.20 | 122.96 | 61.90 | 87.27 | 60.94 | 77.89 | 150 |
| **Cr** | 116.36 | 118.99 | 56.22 | 90.69 | 108.25 | 104.27 | 127.78 | 141.60 | 83.74 | 128.44 | 81.35 | 96.34 | 110 |
| **Co** | 7.49 | 12.93 | 21.20 | 15.65 | 31.31 | 13.28 | 27.04 | 15.70 | 12.98 | 27.77 | 14.45 | 18.14 | 23 |
| **Ni** | 33.98 | 38.51 | 29.50 | 34.06 | 44.54 | 35.94 | 52.58 | 40.34 | 33.23 | 46.85 | 33.23 | 39.31 | 55 |
| **Cu** | 38.60 | 35.58 | 49.47 | 34.08 | 55.59 | 36.04 | 51.92 | 36.31 | 33.58 | 36.89 | 35.94 | 28.77 | 50 |
| **Zn** | 53.45 | 69.22 | 42.94 | 55.22 | 50.94 | 55.46 | 72.24 | 57.56 | 49.34 | 48.66 | 56.56 | 37.21 | 85 |
| **Ga** | 15.32 | 18.24 | 8.49 | 11.42 | 20.32 | 12.14 | 18.46 | 17.72 | 9.62 | 17.46 | 9.12 | 13.13 | 17.5 |
| **Rb** | 175.29 | 171.42 | 83.59 | 110.40 | 104.03 | 133.69 | 153.81 | 167.89 | 101.74 | 142.40 | 72.45 | 78.07 | 160 |
| **Sr** | 43.57 | 50.80 | 65.22 | 45.02 | 62.56 | 80.69 | 41.20 | 48.21 | 65.45 | 40.95 | 48.53 | 20.67 | 200 |
| **Y** | 10.94 | 15.37 | 14.31 | 9.35 | 15.51 | 12.96 | 15.11 | 19.12 | 10.83 | 9.99 | 8.22 | 11.57 | 27 |

**Table 5.3** Trace element (ppm) concentration for shales of the Gulcheru Formation, Cuddapah Basin with average composition of PAAS **(Taylor and McLennan 1985)**

| | KM-1 | M-1 | M-2 | M-3 | KU-2 | KU-3 | KU-4 | KU-5 | M-4 | KU-7 | M-5 | KU-10 | PAAS (Taylor and McLennan 1985) |
|---|---|---|---|---|---|---|---|---|---|---|---|---|---|
| **Zr** | **120.08** | **93.82** | **145.91** | **62.36** | **111.42** | **79.64** | **110.85** | **99.76** | **63.32** | **87.88** | **51.61** | **75.76** | **210** |
| **Nb** | **10.43** | **8.89** | **4.98** | **6.60** | **9.04** | **9.22** | **12.53** | **11.59** | **6.65** | **10.40** | **4.89** | **7.53** | **19** |
| **Cs** | **4.91** | **3.43** | **1.05** | **2.34** | **2.66** | **3.20** | **3.56** | **3.72** | **2.15** | **3.70** | **1.36** | **2.42** | **15** |
| **Ba** | **651.78** | **499.98** | **1271.09** | **1018.80** | **3430.09** | **4922.53** | **2084.29** | **2031.82** | **2376.85** | **1127.72** | **466.58** | **536.10** | **650** |
| **Hf** | **3.47** | **2.78** | **4.09** | **1.86** | **3.27** | **2.40** | **3.23** | **2.97** | **1.93** | **2.57** | **1.56** | **2.28** | **5** |
| **Ta** | **0.97** | **0.85** | **0.54** | **0.65** | **0.96** | **0.93** | **1.18** | **1.09** | **0.66** | **0.98** | **0.52** | **0.77** | **1.28** |
| **Pb** | **7.54** | **7.14** | **8.70** | **5.43** | **11.01** | **5.81** | **9.21** | **7.09** | **5.20** | **5.83** | **5.69** | **7.11** | **20** |
| **Th** | **11.93** | **11.65** | **9.44** | **8.00** | **13.16** | **12.18** | **16.35** | **15.84** | **8.31** | **12.47** | **6.44** | **9.46** | **14.60** |
| **U** | **3.18** | **3.35** | **2.55** | **2.44** | **5.44** | **3.24** | **3.81** | **5.29** | **2.46** | **2.77** | **4.46** | **4.04** | **3.1** |
| **CIA** | **64.44** | **72.02** | **71.30** | **71.00** | **73.37** | **60.90** | **62.48** | **64.13** | **71.94** | **65.96** | **70.95** | **69.18** | **70.38** |
| **CIW** | **98.52** | **96.25** | **96.57** | **95.59** | **97.73** | **97.76** | **98.07** | **98.3** | **95.95** | **98.18** | **95.42** | **98.1** | **82.72** |

**Table 5.3** Trace element (ppm) concentration for shales of the Gulcheru Formation, Cuddapah Basin with average composition of PAAS **(Taylor and McLennan 1985)**

| | KM-1 | M-1 | M-2 | M-3 | KU-2 | KU-3 | KU-4 | KU-5 | M-4 | KU-7 | M-5 | KU-10 | PAAS (Taylor and McLennan 1985) |
|---|---|---|---|---|---|---|---|---|---|---|---|---|---|
| **PIA** | **96.86** | **94.35** | **94.68** | **93.26** | **96.6** | **94.34** | **95.53** | **96.36** | **93.93** | **96.46** | **93.01** | **96.74** | **79.05** |
| **ICV** | **1.49** | **0.91** | **0.75** | **0.88** | **2.96** | **2.27** | **1.54** | **1.68** | **0.80** | **1.74** | **0.75** | **3.12** | **0.88** |
| **$K_2O/Al_2O_3$** | **0.49** | **0.49** | **0.33** | **0.33** | **0.31** | **0.31** | **0.53** | **0.53** | **0.32** | **0.59** | **0.33** | **0.36** | **0.20** |
| **$Al_2O_3/TiO_2$** | **26.87** | **27.39** | **22.32** | **26.07** | **23.11** | **25.22** | **26.84** | **25.65** | **33.72** | **27.75** | **28.65** | **22.39** | **19.09** |
| **La/Sc** | **1.68** | **2.17** | **0.95** | **1.23** | **1.72** | **1.90** | **2.13** | **2.17** | **1.35** | **1.21** | **1.25** | **2.13** | **2.39** |
| **Th/Sc** | **0.64** | **0.63** | **0.67** | **0.44** | **0.74** | **0.70** | **1.06** | **0.85** | **0.49** | **0.62** | **0.37** | **0.87** | **0.91** |
| **Co/Th** | **0.62** | **1.10** | **2.24** | **1.95** | **2.37** | **1.09** | **1.65** | **0.99** | **1.56** | **2.22** | **2.24** | **1.91** | **1.58** |
| **Th/U** | **3.75** | **3.48** | **3.70** | **3.27** | **2.42** | **3.75** | **4.28** | **2.99** | **3.37** | **4.50** | **1.44** | **2.33** | **4.76** |
| **Cu/Zn** | **0.72** | **0.51** | **1.15** | **0.61** | **1.09** | **0.64** | **0.71** | **0.63** | **0.68** | **0.75** | **0.63** | **0.77** | **0.59** |
| **Ni/Co** | **4.53** | **2.97** | **1.39** | **2.17** | **1.42** | **2.70** | **1.94** | **2.56** | **2.56** | **1.68** | **2.29** | **2.16** | **2.39** |
| **V/Cr** | **1.06** | **1.02** | **1.64** | **0.81** | **1.10** | **0.71** | **0.81** | **0.86** | **0.73** | **0.67** | **0.74** | **0.80** | **1.36** |

**Table 5.3** Trace element (ppm) concentration for shales of the Gulcheru Formation, Cuddapah Basin with average composition of PAAS **(Taylor and McLennan 1985)**

| | KM-1 | M-1 | M-2 | M-3 | KU-2 | KU-3 | KU-4 | KU-5 | M-4 | KU7 | M-5 | KU10 | PAAS (Taylor and McLennan 1985; McLennan 2001) |
|---|---|---|---|---|---|---|---|---|---|---|---|---|---|
| **La** | **31.20** | **40.01** | **13.30** | **22.31** | **30.60** | **33.05** | **32.82** | **40.22** | **22.54** | **24.09** | **21.58** | **22.97** | **38.00** |
| **Ce** | **54.94** | **69.69** | **30.44** | **35.35** | **49.01** | **52.59** | **59.52** | **65.34** | **38.03** | **39.76** | **37.82** | **40.69** | **79.60** |
| **Pr** | **5.89** | **7.68** | **3.54** | **3.73** | **5.21** | **5.57** | **6.57** | **7.39** | **4.28** | **4.34** | **4.59** | **4.73** | **8.83** |
| **Nd** | **18.93** | **25.25** | **14.26** | **12.24** | **17.04** | **18.01** | **22.17** | **24.61** | **14.52** | **14.54** | **15.97** | **16.17** | **33.90** |
| **Sm** | **2.89** | **4.05** | **3.56** | **2.08** | **3.24** | **3.02** | **3.63** | **4.46** | **2.57** | **2.41** | **2.55** | **2.82** | **5.55** |
| **Eu** | **0.58** | **0.84** | **0.90** | **0.45** | **0.88** | **0.88** | **0.72** | **0.93** | **0.60** | **0.50** | **0.46** | **0.59** | **1.08** |
| **Gd** | **2.34** | **3.35** | **3.45** | **1.84** | **3.00** | **2.64** | **3.07** | **3.90** | **2.16** | **1.93** | **1.96** | **2.41** | **4.66** |
| **Tb** | **0.37** | **0.53** | **0.60** | **0.31** | **0.55** | **0.45** | **0.48** | **0.68** | **0.37** | **0.31** | **0.29** | **0.41** | **0.77** |

**Table 5.4** REE concentration (ppm) for shales of the Gulcheru Formation, Cuddapah Basin with average composition of PAAS **(Taylor and McLennan 1985)**

| | KM-1 | M-1 | M-2 | M-3 | KU-2 | KU-3 | KU-4 | KU-5 | M-4 | KU7 | M-5 | KU10 | PAAS (Taylor and McLennan 1985; McLennan 2001) |
|---|---|---|---|---|---|---|---|---|---|---|---|---|---|
| **Dy** | 1.99 | 2.74 | 3.08 | 1.69 | 3.02 | 2.40 | 2.56 | 3.72 | 1.96 | 1.69 | 1.49 | 2.15 | 4.48 |
| **Ho** | 0.42 | 0.59 | 0.59 | 0.36 | 0.63 | 0.49 | 0.56 | 0.77 | 0.40 | 0.37 | 0.31 | 0.45 | 0.99 |
| **Er** | 1.31 | 1.71 | 1.66 | 1.10 | 1.87 | 1.48 | 1.78 | 2.26 | 1.19 | 1.16 | 0.92 | 1.30 | 2.85 |
| **Tm** | 0.19 | 0.24 | 0.24 | 0.16 | 0.27 | 0.21 | 0.26 | 0.32 | 0.17 | 0.17 | 0.13 | 0.19 | 0.41 |
| **Yb** | 1.45 | 1.75 | 1.75 | 1.16 | 1.99 | 1.56 | 1.91 | 2.27 | 1.24 | 1.32 | 0.91 | 1.35 | 2.82 |
| **Lu** | 0.24 | 0.27 | 0.28 | 0.19 | 0.32 | 0.25 | 0.32 | 0.36 | 0.20 | 0.22 | 0.14 | 0.21 | 0.43 |
| **∑REE** | 122.71 | 158.71 | 77.64 | 82.99 | 117.61 | 122.59 | 136.37 | 157.23 | 90.25 | 92.81 | 89.12 | 96.45 | 184.37 |

**Table 5.4** REE concentration (ppm) for shales of the Gulcheru Formation, Cuddapah Basin with average composition of PAAS (**Taylor and McLennan 1985)**

# CHAPTER 6

# INTEGRATION

## 6.1 INTRODUCTION

Integration of the data as presented in the preceding chapters is crucial for understanding the evolution of the Proterozoic Papaghni sub-basin of the Cuddapah basin during the deposition of the basal Gulcheru Formation sediments that were deposited unconformably on Archean basement rocks. Now we want to synthesize all the clues/features as represented so far with a view to address our last objective of this study, i.e., to better understand in respect of the evolution of Papaghni sub-basin during the deposition of Gulcheru Formation in the Palaeoproterozoic time.,

## 6.2 CLUES FROM FACIES ANALYSIS AND PETROGRAPHY

The Paleoproterozoic Gulcheru Formation as exposed in the Pendllimari, Gandi, and Kanampalle regions of the Cuddapah Basin mostly consists of four facies associations representing (a) alluvial fan, (b) fluvial, (c) aeolian and (d) tidal flat environment.

Taking into account the characteristics of the various sedimentary facies and their distribution in the lower Gulcheru Formation as well as the temporal control over a number of depositional systems **(cf. Eriksson and Simpson, 1998; Simpson et al., 2004)**, it is assumed that an alluvial fan regime initiated by hyperconcentrated flood flow and cohesionless debris flow is the major depositional regime during the early phase of the Gulcheru Sedimentation. Features like very coarser grain-size, poor sorting and subangular grains within the succession pointed clearly towards its alluvial fan origin. Occurrence of randomly distributed (ungraded) clasts in unsorted sandy matrix and multiple trough cross stratified depositional couplets organized into an overall fining upward unit clearly indicate fluctuation in water table with high grain/water ratio.

The signatures of aeolian depositional regime is also found. Massive amounts of supermature quartzose debris are produced as a result of the provenance's extensive weathering in a warm, semiarid climate. However, the formation of a thermally induced sink is necessary before these super mature sediments could be formed and preserved **(Chatterjee and Bhattacharji, 2001; Mall et al., 2008)**. The aeolian sediments begin to accumulate there when the initial sink is formed. The presence of wind-ripple migrated climbing translatent strata, pin-stripe lamination, high-index granule ripples, sand sheet deposits, grain-flow cross-strata, grainfall laminae, and massive sand bodies with bimodal fabric conclusively demonstrate the existence of an aeolian regime during the initial phase of sedimentation. A variety of aeolian bedforms are created depending on the particle size, moisture availability, water table height, wind strength, and availability of sediments.

Along with that, the surroundings of Papaghni subbasin is also evolved to an ephemeral fluvial system. However, only during and soon after a sudden rainstorm does sediment transfer in the newly formed fluvial system which is a typical characteristic of warm and arid to semiarid climate. Channel pattern exert the most immediate control on fluvial architecture. Tectonics and climate, two extrabasinal factors, are the prime factors controlling the fluvial stratigraphic architecture and sea level change becomes important in relative proximity to the standing body of water in which the river debouches. The effect of climatic variations can produce large scale changes, in scales of different valley fills, but intravalley variations within a limited exposure can only be accounted for tectonic as well as base level fluctuations **(Capra et al., 2013)**. The presence of high percentage of oversized clasts along with coarse grain-size within the lowest channel belt implies erosion quite clearly, which follows basin upliftment **(Javanbakht et al., 2022)**.

Cyclical rhythmites generally formed in tidal set-up. Because of the availability of coarse to fine sediment sequence and landward decreasing of the total hydrodynamic energy, surface

sediment usually fines landward from the fluvial to tidal flat except for a few transgressive tidal flats.

## 6.3 CLUES FROM GEOCHEMICAL ANALYSIS AND PETROGRAPHY

The geochemical analysis of Gulcheru shales gives significant information about (a) source rock including paleo-environment condition, (b) tectonic setting during deposition of sediments and (c) condition of deposition of the sediments. The ternary diagram $Fe_2O_3$-$K_2O$-$Al_2O_3$ demonstrates that all of the shale samples are drawn close to the $Al_2O_3$ apex, demonstrating $Al_2O_3$'s dominance in the parent body. Strong evidence of feldspar dominance in the source rock is shown by the $K_2O/Al_2O_3$ ratio. The Gulcheru shale's Sr/Ba ratio show how fresh water dominance and marine transgression restriction interact. These Ba concentrations can be used as a stand-in for detrital flow. Samples of Gulcheru shale have a general enrichment in Ba. The Gulcheru shale samples are depleted in $Na_2O$, Rb, and Sr and often modestly enriched in $K_2O$ relative to the predicted combination, which indicates extensive weathering and little Na-K metasomatism. The moderately sloped LREE (La-Nd portion) and almost flat HREE (Ho-Lu part) patterns with a negative Eu anomaly can be seen on the chondrite normalised REE plot of Gulcheru shale samples. The CIA values for the examined shales show that the source region has experienced only modest chemical weathering. The PIA values show that the source rock has undergone severe weathering. The Gulcheru Formation shales' wide range of ICV values point to an abundance of less weathered detrital minerals. The lower values suggest that these items were likely sourced from a high relief area because of their origin. Higher levels, on the other hand, show concentration of feldspar and pyroxene (non-clayey minerals) in the parent rock. The Gulcheru shale samples' CIW values show that the source rock underwent severe weathering. For these Gulcheru Formation shale samples, the best

weathering trend shown in the A-CN-K diagram begins with granite and moves closer to the composition of illite as further weathering occurs. The composition of Gulcheru shale samples is related to illite, indicating a severe degree of weathering of the source rock. Exceptionally high $K_2O$ content in Gulcheru shales is a reliable sign of late potassium metasomatism. The Th/Sc and Zr/Sc values in the Gulcheru shale samples are unique, and they exhibit a strong positive connection in the Th/Sc-Zr/Sc diagram, which suggests that the composition of the source materials dominates geochemical variation rather than sediment recycling. The presence of mature sediments and quartz enrichment in the source rock is indicated by the $SiO_2/Al_2O_3$ ratio of the clastic sedimentary rocks of the Gulcheru Formation. For the Gulcheru shale samples, the binary diagram $Al_2O_3$versus $TiO_2$ reflects the granite field and denotes a felsic source rock for these sediments. High $K_2O/Na_2O$ ratios in the clastic deposits of Gulcheru indicate feldspar, illite, and mica enrichment in the source rock. The $SiO_2$, $Al_2O_3$, $Na_2O$ and $K_2O$ raio of the Gulcheru shale samples and super mature quartz arenite indicates a semi-arid to arid domain suggesting their aeolian depositional climatic condition. The concentrations of $K_2O$, $Al_2O_3$, $Fe_2O_3$, $TiO_2$, Ni, and Zr in shale samples show that the Gulcheru sediments came from a felsic source. The Gulcheru Formation's clastic deposits are all contained within the continental Island Arcs field, according to the discrimination plot of La-Th-Sc and Th-Sc-Zr/10. The ratios of some elements, such as U/Th, Cu/Zn, Ni/Co, and V/Cr, point to an oxidising depositional environment during the evolution of Gulcheru Formation.

## 6.4 CLUES FROM PALAEOCURRENT ANALYSIS

The constant NE direction of the palaeocurrent in the fluvial facies association **(Fig. 5.3, Fig. 5.4, Fig. 5.5, Fig. 5.6)** indicates the incoming of sea-water towards the Dharwar craton from NE. the bimodal direction of troughs of sandstone from fluvial and tidal flat facies association **(Fig. 5.4, Fig. 5.6)** indicates the action of tides in the coastal region. The paleocurrent direction of the sandstone association also confirms the dominance of flood-tide in the Kanampalle region and the dominance of ebb-tide in the Gandi region.

## 6.5 DISCUSSION

### 6.5.1 EVOLUTION OF PAPAGHNI SUB-BASIN DURING THE DEPOSITION OF THE GULCHERU FORMATION LITHOLOGY:

Four stages of evolution are represented by the several fining upward stacking pattern of the Gulcheru Formation in the study area. The alluvial fan facies association clearly shows spatial and vertical variations that point to an abundance of loose debris created by subaerial debris flow with high grain/water ratio. Therefore, the base of the sedimentary succession close to the basin boundary represented by proximal fan cohesionless debris flow deposits and middle fan hyper concentrated flood flow deposits. Further deposits from the distal fan sheetflood were deposited inside the basin.

The fluvio-aeolian deposits in the lower Gulcheru Formation show that the Cuddapah Basin region and beyond experienced semiarid and warm paleoclimatic conditions during the Palaeoproterozoic period. Super mature quartzose aeolian deposits were able to form because of the warm palaeoclimatic conditions. Extreme textural maturity of the sediments indicates multi-cyclic history or prolonged aeolian abrasion **(Pettijohn et al. 1975; Suttner et al., 1986)**. Aeolian abrasion is also shown by the sediment's mineralogical maturity.

Due to sand deposition from ephemeral channel sandstone, the slope of the area in the upper part of the Gulcheru Formation further decreased, which facilitated the deposition of rhythmites facies association in the distal portion of the sea. Thus, after the early Proterozoic period, a fining upward succession occurs as a result of the recession of the fluvial front and concurrent marine transgression, demonstrating a change towards higher aggradation rates linked to an increase in the available accommodation space **(Marriott, 1999)**.

### 6.5.2 COMPARISON OF GULCHERU FORMATION WITH OTHER COEVAL SUCCESSIONS

The Paleoproterozoic Gulcheru Formation is strikingly similar to those reported from near coeval strata like the Berwar Formation(2-1.4Ga) of the Bijawar Basin, Par Formation (2.1-1.8Ga) of the Gwalior Basin, Beasley River Quartzite Formation (2.4 Ga) of lower Wyloo Group, Ashburton Basin, Western Australia, Karutola Formation (Palaeoproterozoic?) in India, Makgabeng Formation(1.9-1.7Ga) in South Africa, Magondi Supergroup (2.1Ga) in Zimbabwe, Maguse Member of Kinga Formation (2.45-2.1Ga) in Canada etc. The Berwar Formation of the Bijawar Basin records a succession of conglomerate, Quartzite, slate, and carbonate and seems to be deposited in slightly reducing sedimentary environment at suitable Eh and pH in shallow marine alkaline conditions (Dar et al., 2014). The Par Formation of the Gwalior Basin records a succession of conglomerate, granular/pebbly sandstone, siltstone, and mudstone and seems to be deposited in alluvial fan and braided fluvial environmental condition (Chakraborty and Paul, 2014). Beasley River Quartzite Formation of lower Wyloo Group, Ashburton Basin records a succession of conglomerate, sandstone, siltstone and mudstone and seems to be deposited in the result of basin subsidence during the onset of rifting. Such subsidence may occur in intracontinental or continental margin rifts, or back-arc, or transtensional settings within an orogen (Majumder and Martin, 2013).The

Karutola Formation in India records a succession of sandstone and mudstone and seems to be deposited inaeolian and tidal flat depositional environment with hot and humid climatic condition **(Chakraborty and Sensarma, 2008)**. The Makgabeng Formation in South Africa records a succession of fine to medium grained sandstone and mudstone and seems to be deposited inplaya, saline lake and saline pan deposits of aeolian depositional environment with possible climatic amelioration and saline pan expansion **(Callaghan et al., 1991)**. The Magondi Supergroup in Zimbabwe records a succession of sandstones, shales, carbonates and evaporite minerals and seems to be deposited in alluvial fan, fluvial, aeolian and playa depositional environment **(Master, 1991)**. The Maguse Member of Kinga Formation in Canada records a succession of quartz pebble conglomerate, granule stone, sandstone and mudstone and seems to be deposited in fluvio-aeolian depositional environment **(Aspler & Chiarenzelli, 1997)**.

The presence of fluvial deposits within the aeolian sediments signifies the role of ephemeral streams during sedimentation and thus indicates warm and semiarid palaeo-climatic condition, that is identified globally during Paleoproterozoic time. Therefore, the depositional environment of the Gulcheru Formation compared with age-equivalent formations within India as well as in global, points to similar type of depositional environment during Paleoproterozoic time.

### 6.5.3 GULCHERU SEDIMENTATION AND SUPERCONTINENT ASSEMBLY/BREAK-UP

There is rising evidence for two supercontinent assembly and break-up events throughout the Proterozoic, the Columbia and the Rodinia, despite the lack of data, notably for the early Proterozoic. Thus, it would seem that the oldest unconformity-bound sequence in the Cuddapah Basin represents a stage of sea level rise before the assembly of the Columbia/Nuna

**(Santosh, 2010)**. The existence of conglomerate, arkose, and the mafic dykes that invaded the lower portion of the succession serve as proof of the extension and rifting event. The occurrence of an underplated layer below the southwestern region of the Cuddapah Basin as thick as 15-20 Km has made the crust thicker (40-44 Km) compared to 33-36 Km in the surrounding parts of EDC **(Gupta and Rai, 2005; Rai et al., 2003)** upon which Cuddapah Basin sits. Such extensive underplating and crustal thickening would indicate the possibility of direct asthenospheric interaction with the base of the crust **(Mall, D.M. et al., 2008)**. Such accretionis quite common below intraplate hot spots, active and passive volcanic areas, as well as rift zones all over the world. Examples include: western margin and Rajmahal traps, India (**Singh and Mall, 1998; Mall et al., 1999; Singh et al., 2004)**, Costa Rican Isthmus, Caribbean Plateau **(Sallares et al., 2001)**, basin and Range province of northwestern Nevada, USA **(Catchings and Mooney, 1991)**, Lofoten volcanic margin, northern Norway **(Mjelde et al. 1996)**, Kenya Rift **(Green et al. 1991)** and many passive volcanic margins **(White and McKenzie, 1989)**. This extensional event might be the beginning of Columbia's breakup and the separation of the South Indian and North China cratons **(cf. Ravikant, 2010)**.

The global cycle of amalgamation of the Nuna (Columbia) Craton is marked in the EDC by the cessation of sediments in the Papaghni sub-basin of the Cuddapah Basin and the tectonism of the Vinjamuru block in the Nellore Schist Belt (NSB) **(Kale et al., 2020)**. The development of the Papaghni sub-basin coincides with the William's Lunar torque intensity peak at 2000 Ma, that affect the outer part of the earth; the stagey's galactic astronomical cycle -1945Ma; Indian suryasiddhanta cycle, 1972-1956 Ma **(Babu, 2001)**. The Indian plate $40^0$ N in the 2000-1900 Ma period **(Radhakrishna and Joseph, 1996)**.

## 6.6 CONCLUSION

1. Palaeoproterozoic sedimentation Gulcheru Initial formation took place in the aeolian domain in a warm, semi-arid climate.
2. Fluvial input from ephemeral streams that occasionally formed after rainstorms frequently disrupted the aeolian regime for a short time.
3. Channel sandstone or coarse load braided channel deposits inside the basin and alluvial fan deposits at the basin's base along its margin are signs of transient fluvial activity.
4. A fining upward succession in the upper part of the succession occurs as a result of the recession of the fluvial front and concurrent marine transgression, demonstrating a change towards higher aggradation rates linked to an increase in the available accommodation space
5. The Gulcheru Formation rocks were deposited prior to the amalgamation of the Supercontinent Columbia.
6. The discrimination plot La-Th-Sc and Th-Sc-Zr/10 suggest that the Gulcheru Formation rocks were deposited in continental Island arc setting.
7. The $Al_2O_3$ versus $TiO_2$ plot, Ni versus $TiO_2$ plot, Zr versus $TiO_2$ plot, REE pattern and elemental ratio of La,Th,Sc and Co calculated from geochemical data indicates that the Gulcheru clastic sediments are derived from mixed source rocks of granite, granodiorite and tonalite of Eastern Dharwar Craton (EDC).
8. Some redox sensitive metal (U,Th,V,Co and Cr) ratios indicate that the Gulcheru clastic sediments were deposited under oxic environmental condition. But wide ranges of Cu/Zn ratios suggest change in depositional setup due to sea level fluctuation in Post Archean time.
9. $SiO_2$ versus ($Al_2O_3$+$K_2O$+$Na_2O$) ratio indicate an arid to semi-arid environment during deposition of Gulcheru Formation rocks.

10. The constant NE direction of the palaeocurrent in the fluvial facies association indicates the incoming of sea-water towards the Dharwar craton from NE.

In summary, the following pictures **(Fig. 6.1 and Fig. 6.2)** may emerge from our studies on facies, geochemistry and palaeocurrent analysis of Gulcheru Formation clastic sediments. The Gulcheru clastic sediments are deposited in fluvio-aeolian environmental condition with alluvial fan in the lower part and tidal-flat in the upper region. The clastic sediments having been eroded from mixed source rocks of granite, granodiorite and tonalite (felsic igneous rocks) of Eastern Dharwar Craton (EDC) of southern India during late Paleoproterozoic time, are deposited in alluvial-fan, fluvial, aeolian and low-gradient tidal-flat environment under continental island arc setting in semi-arid climatic set-up during the process of amalgamation of supercontinent Columbia. This back-arc extensional basin **(cf. Absar et al. 2016)** seems to be formed due to the subduction of oeanic crust underneath the Dharwar Craton. The sediments are deposited mostly in an oxic environment under arid to semi-arid condition. The depositional set-up changes occasionally with fluctuation of sea-level during the post Archean time. Thus, the initiation of the epicratonic Cuddapah Basin as marked by the Gulcheru Formation lithology in the Eastern Dharwar Craton due to rifting of eroded Archaean Crust in an extensional set-up and subsequent transgressive encroachment of the contemporary sea onto the Archaean Crust **(Singh, 1980; Radhakrishna, 1987; Jayaprakash, 2007)** indicates the interaction of tectonism and sedimentation during Palaeo-Mesoproterozoic times on the Eastern Ghat Craton **(Khan et al., 2020)**.

# FIGURES AND TABLES

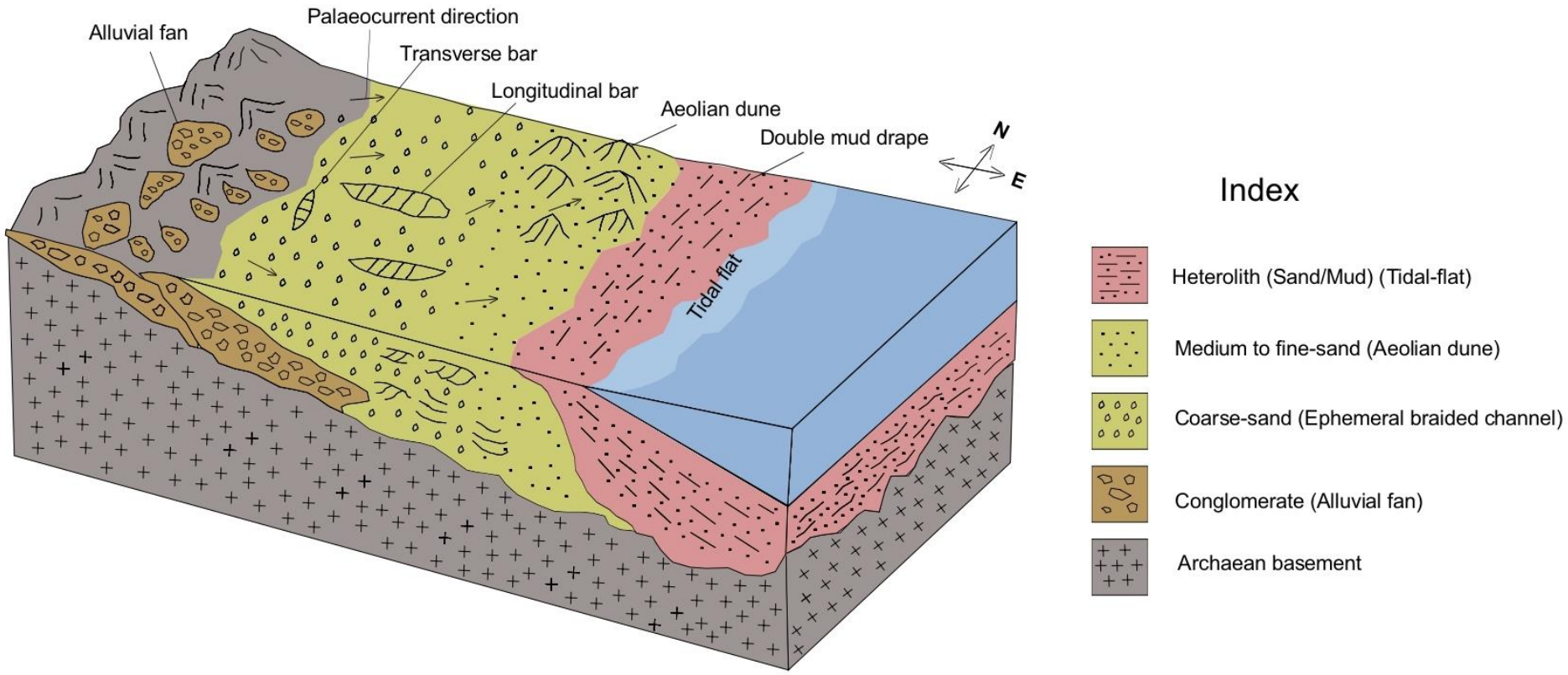


**Fig 6.1** Inferred depositional model and resulting facies distribution of the Gulcheru Formation lithology in the study areas. The arrows on the block indicate flow vector from the palaeocurrent analysis

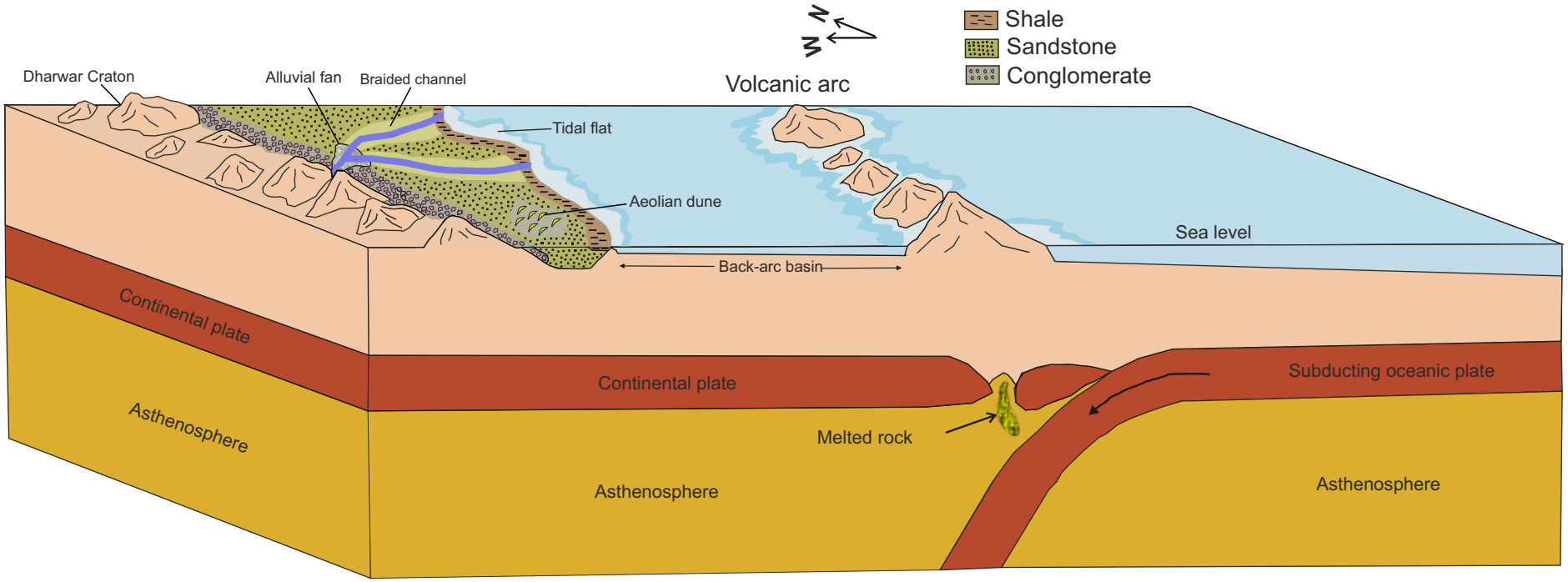


**Fig 6.3** Cartoon diagram of inferred tectonic setting and depositional environment of Gulcheru Formation rocks, Cuddapah Basin, India

# BIBLIOGRAPHY

**REFERENCES:**

**Abreu, V., Sullivan, M., Pirmez, C., Mohrig, D. (2003).** Lateral accretion packages (LAPs): an important reservoir element in deep water sinuous channels. , 20(6-8), 0–648. doi:10.1016/j.marpetgeo.2003.08.003

**Absar, N., Nizamudheen, B. M., Augustine, S., Managave, S., Balakrishnan, S. (2016).** C, O, Sr And Nd isotope systematics of carbonates of Papaghni sub-basin, Andhra Pradesh, India: Implications for genesis of carbonate-hosted stratiform uranium mineralisation and geodynamic evolution of the Cuddapah basin. Lithos 263, 88–100 (in this issue).

**Allen, P. (1985).** The geochemistry of the Amphibolite-Granulite facies transition in Central South India (Ph.D. thesis). New Mexico Institute of Mining and Technology, Socorro, New Mexico, USA.

**Almeida M.E., Macambira M.J.B., Santos J.O.S., Nascimento R.S.C., Paquette J.L. (2013).** Evolução crustal do noroeste do Cráton Amazônico (Amazonas, Brasil) baseada em dados de campo, geoquímicos egeocronológicos. In: Simpósio de Geologia da Amazônia, 13, 201-204.

**Amajor, L. C. (1987).** Major and trace element geochemistry of Albian and Turonianshales from the Southern Benue trough, Nigeria. Jour. African Earth Sci., v.6, pp.633-641.

**Anand, M., Gibson, S. A., Subbarao, K. V., Kelley, S. P., Dickin, A. P. (2003).** Early proterozoic melt generation processes beneath the intra cratonic Cuddapah basin, Southern India. J Petrol 44:2139–2171.

**Anderson, Don L. (1982).** Rise of deep diapirs; Reply. Geology, 10, 561-562.

**Armstrong-Altrin, J. S., Verma, S. P., Madhavaraju, J., Ramaswami, S. (2004)**. Geochemistry of sandstones from the Upper Miocene Kudankulam Formation, Southern

India:Implications for provenance, weathering and tectonic setting:Jour. Sedimentary Res., v.74(2), pp.285-297.

**Armstrong-Altrin, J. S., Verma, S. P. (2005).** Critical evaluation of six tectonic setting discrimination diagrams using geochemical data of Neogene sediments from known tectonic setting. Sediment Geol 177:115-129.

**Armstrong-Altrin, J. S., Lee, Y. I., Kasper-Zubillaga, J. J., Carranza-Edwards, A., Garcia, D., Eby, N., Balaram, V., Cruz-Ortiz, N. L. (2012).** Geochemistry of beach sands along the western Gulf of Mexico, Mexico: implication for provenance. Chemie der Erde-Geochemistry 72:345–362.

**Armstrong-Altrin, J. S., Machain-Castillo, M. L., Rosales-Hoz, L., Carranza-Edwards, A., Sanchez-Cabeza, J.A., Ruíz-Fernández, A. C. (2015a).** Provenance and depositional history of continental slope sediments in the Southwestern Gulf of Mexico unraveled by geochemical analysis.Cont Shelf Res 95:15–26.

**Armstrong-Altrin, J. S., Lee, Y.I., Kasper-Zubillaga, J. J., Trejo-Ramirez, E. (2017).** Mineralogy and Geochemistry of sands along the Manzanillo and El Carrizal beach areas, Southern Maxico: Implications for palaeoweathering, provenance and tectonic setting. Geol J 52(4):559-582.

**Aspler; L.B., Chiarenzelli, J.R. (1997).** Initiation of ~2.45-2.1 Ga intracratonic basin sedimentation of the Hurwitz Group, Keewatin Hinterland, Northwest territories, Canada. , 81(3-4), 0–297. doi:10.1016/s0301-9268(96)00038-1

**Babu, V.R.R.M., (2001).** Plate tectonic history of the Indian Plate Nellore-Khammam Schist Belt: Indian Acad. Geosciences, Hyderabad, 1839.

**Basu A. K. (2007).** Role of the Bundelkhand Granite Massif and theSon-Narmada megafault in Precambrian crustal evolution and tec-tonism in Central and Western India. Journal of the GeologicalSociety of India

**Basu, H., Sastry, R.S., Achar, K.K., Umamaheswar, K., Parihar, P. S. (2014).** Palaeoproterozoic fluvio-aeolian deposits from the lower Gulcheru Formation, Cuddapah Basin, India. Precambrian Research, 246(), 321–333. doi: 10.1016/j.precamres.2014.03.011

**Basu, A., Bickford, M. E. (2015).** An alternate perspective on the opening and closing of the intracratonic Purana basins in peninsular India. Journal of the Geological Society of India, 85(1), 5–25. doi:10.1007/s12594-015-0190-y

**Bhaskar Rao, Y.J., Pantulu, G.V.C., Damodar Reddy, V. and Gopalan, K. (1995).** Time of Early sedimentation and volcanism in the Proterozoic Cuddapah basin, south India: evidence from Rb-Sr age of Pulivendla mafic sill. Geol. SOC. India, Mem., No. 33, pp. 329-338.

**Bhattacharji, S., Singh, R.N. (1984).** Thermo-mechanical structure of the southern part of the Indian Shield and its relevance to Precambrian basin evolution. , 105(1-4), 103–120. doi:10.1016/0040-1951(84)90197-5

Bhattacharji, S. (1987). Lineaments and igneous episodes in the evolution of intracratonic Proterozoic basins on the Indian Shield. – (ed.) A K Saha, In: Geological evolution of Peninsular India – petrological and structural aspects. Recent Researches in Geology, 13-15

**Bhatia, M. R. (1983).** Plate tectonics and geochemical composition of sandstones. J. Geol 91:611-627.

**Bhatia, M. R., Crook, K. A. W. (1986).** Trace element characteristics of graywackes and tectonic setting discrimination of sedimentary basins. Contrib. Mineral. Petrol., v.92, pp.181-193.

**Blair, T.C., McPherson J.G. (1998).** Recent debris-flow processes and resultant form and facies of the Dolomite alluvial fan, Owens Valley, California. Journal of Sedimentary Research 68:800-818

**Blair T.C., McPherson J.G. (1994a)**. Alluvial fan processes and forms. In: Abrahams AD, Parsons A (eds.) Geomorphology of desert environments. Chapman Hall, London, pp. 354-402

**Bose, P.K., Ghosh, G., Shome, S., Bardhan, S. (1988).** Evidence of superimposition of storm waves on tidal currents in rocks from the Tithonian-Neocomian Umia Member, Kutch, India., 54(4), 321–329. doi:10.1016/0037-0738(88)90039-5

**Bose, P.K., Sarkar, S., Mukhopadhyay, S., Saha, B., Eriksson, P. (2008).** Precambrian basin-margin fan deposits: Mesoproterozoic Bagalkot Group, India. , 162(1-2), 0–. doi:10.1016/j.precamres.2007.07.022

**Bradley, K., Qin, Y., Carton, H., Hananto, N., Villanueva-Robles, F., Leclerc, F., Shengji, W., Tapponier, P., Sieh, K., Singh, S. (2019).** Stratigraphic control of frontal décollement level and structural vergence, and implications for tsunamigenic earthquake hazard in Sumatra, Indonesia. Geochemistry, Geophysics, Geosystems, (), 2018GC008025–. doi:10.1029/2018GC008025

**Callaghan, C.C., Eriksson, P.G., and Snyman, C.P., (1991).** The sedimentology of the Waterberg Group in the Transvaal, South Africa: An overview: Journal of African Earth Sciences, v. 13, p. 121- 139.

**Camire, M. E., Zhao, J., Violette, D. A. (1993).** In vitro binding of bile acids by extruded potato peels. Journal of Agricultural and Food Chemistry, 41, pp. 2391-2394.

**Capra, L., Bernal, J.P., Carrasco, G., Roverato, M. (2013).** Climatic fluctuations as a significant contributing factor for volcanic collapses. Evidence fromMexico during the Late Pleistocene. Global Planet. Change. 100, 194–203

**Catchings, R. D., Mooney, W. D. (1991).** Basin and range crustal and upper mantle structure, northwest to central Nevada. Journal of Geophysical Research, 96(B4), 6247–. doi:10.1029/91jb00194

**Chakrabarti, G., Shome, D. (2007).** Reworked diamictite accumulation as debris flow in aqueous medium- an example from late Palaeoproterozoic basal Gulcheru Formation, Cuddapah Basin, India. Himal. Geol.28, 87-98.

**Chakrabarti, G., Shome, D., Bauluz, B., Sinha, S. (2009).** Provenance and weatheringhistory of Mesoproterozoicclastic sedimentary rocks from the basal GulcheruFormation, Cuddapah basin, India. Geol. Soc. Ind. 74, 119–130.

**Chakrabarti, G., Shome, D. (2010).** Interaction of microbial communities with clastic sedimentation during Palaeoproterozoic time — An example from basal Gulcheru Formation, Cuddapah basin, India: Sed. Geol., v. 226, p. 22-28.

**Chakrabarti, G., Eriksson, P. G., & Shome, D. (2015).** Chapter 17 Sedimentation in the Papaghni Group of rocks in the Papaghni sub-basin of the Proterozoic Cuddapah Basin, India. Geological Society, London, Memoirs, 43(1), 255–267.

**Chakraborty, S., Ganguly, J. (1991)** Compositional Zoning and Cation Diffusion in Garnets. In Advances in Physical Geochemistry. Springer US. p.120-175. doi:10.1007/978-1-4613-9019-0_4

**Chakraborty, P.P., Paul, P. (2014).** Depositional character of a dry-climate alluvial fan system from Palaeoproterozoic rift setting using facies architecture and palaeohydraulics: Example from the Par Formation, Gwalior Group, central India. Journal of Asian Earth Sciences, 91(), 298–315. doi:10.1016/j.jseaes.2013.09.019

**Chakraborty, T., Sensarma, S. (2008).** Shallow marine and coastal eolian quartz arenites in the Neoarchean-Palaeoproterozoic Karutola Formation, Dongargarh Volcano-

sedimentary succession, central India. , 162(1-2), 0–
301. doi:10.1016/j.precamres.2007.07.024

**Chalapathi Rao, N.V., Miller, J.A., Gibson, S.A., Pyle, D.M. and Madhavan, V. (1999)**. Precise 40Ar/39Ar age determinations of the Kotakonda kimberlite and Chelima lamproite, India: implication for the mafic dyke swarm emplacement in the Eastern Dharwar craton. J. Geol. SOC. India, v. 53, pp. 425-432.

**Chaudhuri, A.K., Saha, D., Deb, G.K., Deb, SP., Mukherjee, M.K., Ghosh, G. (2002).** The Purana Basins of Southern Cratonic Province of India - A Case for Mesoproterozoic Fossil Rifts., 5(1), 23–33. doi:10.1016/s1342-937x (05)70884-4

**Chatterjee, N., Bhattacharji, S. (2001).** Petrology, geochemistry and tectonic settings of the mafic dikes and sills associated with the evolution of the Proterozoic Cuddapah Basin of south India. , 110(4), 433–453. doi:10.1007/bf02702905

**Chetty, T.R.K., Murthy, D.S.N. (1994).** Collision tectonics in the late Precambrian Eastern Ghats Mobile Belt: mesoscopic to satellite-scale structural observations. , 6(1), 72–81. doi:10.1111/j.1365-3121. 1994.tb00635.x

**Chetty, T. R. K. (2011).** Tectonics of proterozoic Cuddapah Basin, southern India: A conceptual model., 78(5), 446–456. doi:10.1007/s12594-011-0109-1

**Crichton, J. G., Condie, K. C. (1993).** Trace elements as source indicators in cratonic sediments: a case study from the Early Proterozoic Libby Creek Group, Southeastern Wyoming J. Geol., 101 (1993), pp. 319-332.

**Collins, Alan S.; Patranabis-Deb, Sarbani; Alexander, Emma; Bertram, Cari N.; Falster, Georgina M.; Gore, Ryan J.; Mackintosh, Julie; Dhang, Pratap C.; Saha, Dilip; Payne, Justin L.; Jourdan, Fred; Backé, Guillaume; Halverson, Galen P.; Wade, Benjamin P. (2015).** Detrital mineral age, radiogenic isotopic stratigraphy and

tectonic significance of the Cuddapah Basin, India. Gondwana Research, (), S1342937X14003189–. doi:10.1016/j.gr.2014.10.013

**Collinson, J.D. (1996)**. Alluvial Sediments. In: Reading, H.G., Ed., Sedimentary Environments: Processes, Facies and Stratigraphy, 3rd Edition, Blackwell Science, Oxford, 37-81.

**Coilinson, J. D., Thompson, D. B. (1982).** Sedimentary Structures. Allen and Unwin, London.

**Collinson, J.D., Thompson, D.B. (1989).** Sedimentary Structures. 2nd Edition, Chapmann & Hall, London, 207 p.

**Condie, K. C. (1993).** Chemical composition and evolution of the upper continental crust: Contrasting results from surface samples and shales. Chemical Geology, 104(1-4), 1–37.

**Conrad, J. E.; Hein, J. R.; Chaudhuri, A. K.; Patranabis-Deb, S.; Mukhopadhyay, J.; Deb, G. K.; Beukes, N. J. (2011).** Constraints on the development of Proterozoic basins in central India from 40Ar/39Ar analysis of authigenic glauconitic minerals. Geological Society of America Bulletin, 123(1-2), 158–167. doi:10.1130/b30083.1

**Cox, R., Lowe, D. R., Culleres, R. L. (1995).** The influence of sediment recycling and basement composition on evolution of mudrock chemistry in the SW rn United States. Geocchem Cosmochim Acta, v.59(14), pp.2919-2940.

**Crawford, A. R., Compston, W. (1969).** The age of the Vindhyan System of Peninsular India. Quarterly Journal of the Geological Society, 125(1-4), 351–371. doi:10.1144/gsjgs.125.1.0351

**Crook, K. A. W. (1974).** Lithogenesis and geotectonics: the significance of compositional variation in flyscharenites (greywackes). Soc. Econ. Paleontol.Mineral. Spec. Pub., 19, 304-310.

**Cullers, R. L. (1995).** The controls on major and trace element evolution of shales, siltstones, and sandstones of Ordovician to Tertiary age in the Wet Mountains region, Colorado, USA. Chemical Geol., v.123, pp.107-131.

**Cullers, R. L. (2000).** The geochemistry of shales, siltstones and sandstones of Pennsylvanian–Permian age, Colorado, USA: implications for provenance and metamorphic studies. Lithos 51:181–203.

**Dar, S.A., Khan, K.F., Khan, S.A. (2014).** Uranium (U) concentration and its genetic significance in the phosphorites of the Paleoproterozoic Bijawar Group of the Lalitpur district, Uttar Pradesh, India. Arab J Geosci 7, 2237–2248. https://doi-org.libproxy.viko.lt/10.1007/s12517-013-0903-8

**Daidu F.** (2013). Classifications, sedimentary features and facies associations of tidal f lats. Journal of Palaeogeography 2013, 2(1): 66-80

**Dam, G., Andreasen F. (1990).** High-energy ephemeral stream deltas; an example from the Upper Silurian Holmestrand Formation of the Oslo Region, Norway. , 66(3-4), 197–225. doi:10.1016/0037-0738(90)90060-7

**Das, S., Chakraborty, M. (2019).** Petrology and geochemistry of mafic dyke and sills in Cumbum Formation, of the Proterozoic Nallamalai fold belt, Rajampet area, Andhra Pradesh, India. Journal of Earth System Science, 128(5), 116–. doi:10.1007/s12040-019-1102-0

**Das, K., Yokoyama, K., Chakraborty, P.P., Sarkar, A., (2009).** Basal Tuffs and Contemporaneity of the Chattisgarh and Khariar Basins Based on New Dates and Geochemistry. The Journal of Geology, 117(1), 88–102. doi:10.1086/593323

**Dasgupta, P.K., De, S., De, S. (1990).** Facies variations and different stages of basin evolution in the Proterozoic Cuddapah basin, India. In: Abstract Volume of seminar on Evolution of Precambrian Crust in India'. Geological survey of India, 5-6.

**Dasgupta, P.K., Biswas, A., Mukherjee, R. (2005).** Cyclicity in Paleoproterozoic to Neoproterozoic Cuddapah Supergroup and its significance in basinal evolution. In: Mabesoone, J.M., Neuman, V.H. (Eds.), Cyclic Development of Sedimentary Basins. Elsevier, pp. 313-345.

**Davis, R.A., Dalrymple, R.W. (2012).** Principles of Tidal Sedimentology || Processes, Morphodynamics, and Facies of Tide-Dominated Estuaries. , 10.1007/978-94-007-0123-6(Chapter 5), 79–107. doi:10.1007/978-94-007-0123-6_5

**Deng, P. (1993).** The application of trace amount of elements in the exploration of oil and gas Petrol Explor.Dev. 20 27-32 (in Chinese with English abstract).

Depetris, P. J., Pasquini, A. I., Lecomte, K. L. (2014). Weathering and the riverine denudation of continents. Springer, Berlin 95.

**Dobmeier, C. J.; Raith, M. M. (2003).** Crustal architecture and evolution of the Eastern Ghats Belt and adjacent regions of India. Geological Society, London, Special Publications, 206(1), 145–168. doi:10.1144/GSL.SP.2003.206.01.09

**Drury, S. A. (1984).** A Proterozoic Intracratonic Basin, Dyke Swarms and Thermal evolution in Southern India. Journal of the Geological Society of India, 25(7), 437-444.

**Eriksson, P.G., Altermann, W. and Hartzer, F.J. (2006).** The Transvaal Supergroup and its precursors. In: M.R. Johnson, C.R. Anhaeusser and R.J. Thomas (Editors), The Geology of South Africa. Geol. Soc. S. Afr., Council for Geoscience, Pretoria, Johannesburg, 237-260.

**Eriksson, K.A., Simpson, E.L. (1998).** Controls on spatial and temporal distribution of Precambrian aeolianites: Sedimentary Geology, v. 120, p. 275-294.

**Eriksson, P.G., Merwe, R.V.D., Bumby, A.J. (1998).** The Palaeoproterozoic Woodlands Formation of eastern Botswana-northwestern South Africa: lithostratigraphy

and relationship with Transvaal Basin inversion structures., 27(3-4), 349
358. doi:10.1016/s0899-5362(98)00067-0

**Ernst, R.E., Bleeker, W., Söderlund, U., Kerr, A.C. (2013).** Large Igneous Provinces and Supercontinents: Toward completing the plate tectonic revolution. Lithos, 174, 1-14.

**Eyal, H., Dente, E., Haviv, I., Enzel, Y., Dunne, T., Lensky, N.G. (2019).** Fluvial incision and coarse gravel redistribution across the modern Dead Sea shelf as a result of base-level fall. Earth Surface Processes and Landforms, (), esp.4640–
. doi:10.1002/esp.4640

**Eyles, N.; Day, T. E.; Gavican, A. (1987).** Depositional controls on the magnetic characteristics of lodgement tills and other glacial diamict facies. Canadian Journal of Earth Sciences, 24(12), 2436–2458. doi:10.1139/e87-229

**Fedo, C. M., Nesbitt, H. W., Young, G. M. (1995).** Unraveling the effects of potassium metasomatism in sedimentary rocks and paleosols, with implications for paleoweathering conditions and provenance. Geology, 23, 921-924.

**Fielding, C.R. (2006).** Upper flow regime sheets, lenses and scour fills: Extending the range of architectural elements for fluvial sediment bodies. , 190(1-4), 227–
240. doi:10.1016/j.sedgeo.2006.05.009

**Flemming, B.W. (2012).** Principles of Tidal Sedimentology || Siliciclastic Back-Barrier Tidal Flats. , 10.1007/978-94-007-0123-6(Chapter 10), 231–267. doi:10.1007/978-94-007-0123-6_10

**Floyd, P. A., Winchester, J. A., Park, R. G. (1989).** Geochemistry and tectonic setting of Lewisian clastic metasediments from the Early Proterozoic Loch MareeGroup of Gairloch, NW Scotland. Precambrian Res.45:203–214.

**French, J.E., Heaman, L.M., Chacko, T., Srivastava, R.K. (2008).** 1891–1883  Ma Southern Bastar–Cuddapah mafic igneous events, India: A newly recognized large igneous province. , 160(3-4), 0– 322. doi: 10.1016/j.precamres.2007.08.005.

**Gemignani, L., Mittelbach, B.V., Simon, D., Rohrmann, A., Grund, M.U., Bernhardt, A., Hippe, K., Giese, J., Handy, M.R. (2022).** Response of Drainage Pattern and Basin Evolution to Tectonic and Climatic Changes Along the Dinarides-Hellenides Orogen. *Front. Earth Sci.* 10:821707. doi: 10.3389/feart.2022.821707

**Goswami, S., Dey, S., Zakaulla, S., Verma, M. B. (2020).** Active rifting and bimodal volcanism in Proterozoic Papaghni sub-basin, Cuddapah basin (Andhra Pradesh), India. Journal of Earth System Science, 129(1), 21–. doi:10.1007/s12040-019-1278-3

**Green, W., Achauer, U. & Meyer, R. (1991).** A three-dimensional seismic image of the crust and upper mantle beneath the Kenya rift. Nature 354, 199–203. https://doi.org/10.1038/354199a0

**Gupta, S. and Rai, S.S. (2005).** Structure and Evolution of south Indian crust using Teleseismic Waveform modelling, Himalayan Geology, v.26, pp.109–123.

**Gurnis, M. (1988).** Large-scale mantle convection and the aggregation and dispersal of supercontinents. Nature 332, 695–699. doi.org/10.1038/332695a0.

**Hallberg, R. O. (1976).** A geochemical method for investigation of paleo redox conditions in sediments: Ambio, Special Report 4, 139-147.

**Harms, J.C., Southard, J.B., Spearing, D.R., and Walker, R.G. (1975).** Depositional Environments as Interpreted from Primary Sedimentary Structures and Stratification Sequences. Society of Economic Paleontologists and Mineralogists, Short Course 2, 2nd edn, 1982.

**Harald, G.D., Andrei, B. (2022).** From the aeolian landform to the aeolian mineral deposit in the present and its use as an ore guide in the past. Constraints from mineralogy, chemistry and sediment petrography. Ore Geology Reviews.

**Harnois, L. (1988).** The CIW index: a news index of weathering. Sed. Geol. 55:319-322.

**Hayashi, K. I., Fujisawa, H., Holland, H. D., Ohmoto, H. (1997).** Geochemistry of ~1.9Ga sedimentary rocks from northeastern Labrador, Canada. Geochim Cosmochim Acta 61(19):4115-4137.

**Hartley, R.W., Allen, P.A. (1994).** Interior cratonic basins of Africa: relation to continental break-up and role of mantle convection., 6(2-3), 95–113. doi:10.1111/j.1365-2117. 1994.tb00078.x.

**Henderson, B., Collins, A.S., Payne, J.L., Forbes, C.J., Saha, D. (2014).** Geologically constraining India in Columbia: The age, isotopic provenance and geochemistry of the protoliths of the Ongole Domain, Southern Eastern Ghats, India. Gondwana Research, 26(3-4), 888–906. doi:10.1016/j.gr.2013.09.002

**Herron, M. M. (1988).** Geochemical classification of terrigenous sands and shales from core or log data. J Sediment Pet 58(5):820–829.

**Hessler, A. M., Lowe, D. M. (2006).** Weathering and sediment generation in the Archean: an integrated study of the evolution of siliciclastic sedimentary rocks of the 3.2 Ga Moodies Group, Barberton Greenstone Belt, South Africa. Precambrian Res 151:185–210.

**Hobday, D.K., Morton, R.A. (1984).** "Lower Cretaceous Shelf Storm Deposits, Northeast Texas", Siliciclastic Shelf Sediments, Roderick W. Tillman, Charles T. Siemers

**Hossain, I., Roy, K. K., Biswas, P. K., Alam, M., Moniruzzaman, M., & Deeba, F. (2014).** Geochemical characteristics of Holocene sediments from Chuadanga district,

Bangladesh: Implications for weathering, climate, redox conditions, provenance and tectonic setting. Chinese Journal of Geochemistry, 33(4), 336–350.

**Hou, G.T., Santosh, M., Qian, X.L., Lister, G.S., Li, J.H. (2008).** Configuration of the Late Paleoproterozoic supercontinent Columbia: Insights from radiating mafic dyke swarms. Gondwana Research, 14, 395-409.

**Huan, X., Xu, G., Zhang, Y., Sun, F., Xue, S. (2021).** Study on Thermo-Hydro-Mechanical Coupling and the Stability of a Geothermal Wellbore Structure. Energies, (), –. doi:10.3390/en14030649

**Hubbard, S.M., Covault, J.A., Fildani, A., Romans, B.W. (2014).** Sediment transfer and deposition in slope channels: Deciphering the record of enigmatic deep-sea processes from outcrop. Geological Society of America Bulletin, 126(5-6), 857–871. doi:10.1130/B30996.1

**Hunter, R.**E. (1981). Stratification styles in eolian sandstones: Pennsylvanian to Jurassic examples from the Western interior U.S.A.. in Ethridge, F.G., R.M., eds. Recent and ancient nonmarine depositional environments: models for exploration: SEPM Spl. Pub., 31, 315-329.

**Jain, S. C., Nair, K. K. K., Yedekar, D. B. (1995).** Tectonic evolution of the Son–Narmada–Tapti lineament zone; Project Crumansonata Spec. Publ. 10 333–371.

**Javanbakht, M., Beheshtipur, M.R. & Raftari Farimani, S. (2022).** Factors affecting average grain size changes in rivers of a catchment area (Ardak catchment area, northeast Iran). Arab J Geosci 15, 448. https://doi.org/10.1007/s12517-021-08512-2

**Jayananda, M., Moyen, J.F., Martin, H., Peucat, J.J., Auvray, B., Mahabaleswar, B. (2000).** Late Archaean (2550–2520 Ma) juvenile magmatism in the Eastern Dharwar

craton, southern India: constraints from geochronology, Nd–Sr isotopes and whole rock geochemistry., 99(3-4), 0–254. doi:10.1016/s0301-9268(99)00063-7

**Jayaprakash, A. V. (2007).** Puarana Basins of Karnataka. Geological Survey of India, Kolkata, Memoirs, 129.

**Jones, B., Manning, D. A. C. (1994).** Comparison of geochemical indices used for the interpretation of palaeoredox conditions in ancient mudstones: Chemical Geology, v. 111, no. 1-4, p. 111-129.

**Joy, S., Jelsma, H., Tappe, S., Armstrong, R. (2015).** SHRIMP U–Pb zircon provenance of the Sullavai Group of Pranhita–Godavari Basin and Bairenkonda Quartzite of Cuddapah Basin, with implications for the Southern Indian Proterozoic tectonic architecture. Journal of Asian Earth Sciences, (), S1367912015300432–. doi: 10.1016/j.jseaes.2015.07.023

**K, B. (2017).** Geochemical characteristics of sandstones from Cretaceous Garudamangalam area of Ariyalur, Tamilnadu, India: Implications of provenance and tectonic setting. Journal of Earth System Science, 126(3).

Kale, V.S., Patil-Pillai, S. (2022). Sediments from Purana basins, India: Where were they derived from? Geosystems and Geoenvironment.

**Kale, V.S., Phansalkar, V.G. (1991).** Purana basins of peninsular India: a review. Basin Research, 3, 1–36. doi:10.1111/j.1365-2117. 1991.tb00133.x.

**Kale, V.S. (2016).** Proterozoic Basins of Peninsular India: Status within the Global Proterozoic systems. Proceedings Indian National Science Academy, 82(3), 461-477.

**Kale, V. S., Saha, D., Patrabnis-Deb, S., Sesha Sai, V. V., Tripathy, V., Patil-Pillai, S. (2020).** "Cuddapah Basin, India: A collage of proterozoic subbasins and terranes". Journal Articles. 356. https://digitalcommons.isical.ac.in/journal-articles/356

**Kaila, K.L., Roy Chowdhury, K., Reddy, P.R., Krishna, V.G., Hari Narain, Subbotin, S.I., Sollogub, V.B., Chekunov, A.V., Kharetchko, G.E., Lazarenko, M.A. and Ilchenko, T.V., (1979).** Crustal structure along Kavali Udipi profile in the Indian peninsular shield from deep seismic sounding. J. Geol. Soc. India, 20, 307-333.

**Kalpana, G., Madhavi, T., Patil, DJ., Dayal, A.M., Raju, S.v. (2010).** Light gaseous hydrocarbon anomalies in the near surface soils of Proterozoic Cuddapah Basin: Implications for hydrocarbon prospects., 73(1-2), 161–170. doi: 10.1016/j.petrol.2010.05.017.

**Khan, T., Sarma, D. S., Somasekhar, V., Ramanaiah, S., & Reddy, N. R. (2019).** Geochemistry of the Palaeoproterozoic quartzites of Lower Cuddapah Supergroup, South India: Implications for the palaeoweathering, provenance, and crustal evolution. Geological Journal.

**Khan, T., Sarma, D.S., Khan, M.S. (2020).** Geochemical study of the Neoproterozoic clastic sedimentary rocks of the Khambal Formation (Sindreth Basin), Aravalli Craton, NW Indian Shield: Implications for paleoweathering, provenance, and geodynamic evolution. Geochemistry, (), 125596–. doi:10.1016/j.chemer.2019.125596

**Khelen, A. C.; Manikyamba, C.; Tang, Li; Santosh, M.; Subramanyam, K.S.V.; Singh, Th Dhanakumar (2020).** Detrital zircon U-Pb geochronology of stromatolitic carbonates from the greenstone belts of Dharwar Craton and Cuddapah basin of Peninsular India. Geoscience Frontiers, 11, 229-242, S167498711930088X–. doi: 10.1016/j.gsf.2019.04.010.

**Kim, S., De S. L., Hong, J.K., Cottlerle, D., Petronio, L., Colizza, E., Kim, Y.G., Kang, Seung-G., Kim, H. J., Kim, S., Wardell, N., Geletti, R., Bergamasco, A., McKay, R., Jin, Y. K., Kang, S.H. (2018).** Seismic stratigraphy of the Central Basin in northwestern Ross Sea slope and rise, Antarctica: Clues to the late Cenozoic ice-sheet

dynamics and bottom-current activity. Marine Geology, 395(), 363–379. doi:10.1016/j.margeo.2017.10.013

**King, (1872).** Cuddapah and Kurnool Formations in the Madras Presidency. Mem. Geological Survey of India, 8, 1-346.

**Klein, G.D. (1970).** Depositional and Dispersal Dynamics of Intertidal Sand Bars. SEPM Journal of Sedimentary Research, Vol. 40(), –. doi:10.1306/74D72144-2B21-11D7-8648000102C1865D

**Köykkä,J. (2010)**. Lithostratigraphy of the Mesoproterozoic Telemark supracrustal rocks, South Norway: revision of the sub-Heddersvatnet unconformity and geochemistryof basalts in the Heddersvatnet Formation. Norw. J. Geol. 90, 49 – 64

**Kumar, A., Parashuramulu, V., Nagaraju, E. (2015).** A 2082Ma radiating dyke swarm in the Eastern Dharwar Craton, southern India and its implications to Cuddapah basin formation. Precambrian Research, 266(), 490–505. doi: 10.1016/j.precamres.2015.05.039

**Kuscu, M., Ozsoy, R., Ozcelik, O., Altunsoy, M. (2016).** Trace and Rare Earth Element Geochemistry of Black Shales in Triassic Kasimlar Formation, Anamas-Akseki Platform, Western Taurids, Turkey.IOP conference series Earth and Environmental Sciences.

**Labourdette, R., and Jones, R.R., (2007).** Characterization of fluvial architectural elements using a three-dimensional outcrop dataset: Escanilla braided system - South-Central Pyrenees, Spain: Geosphere, v.3, p. 422–434.

**Leelanandam, C. (1980).** Some observations on the Alkaline provinces in Andhra Pradesh. Current Science, 50, 799-802.

**Li, Z. L., Yang, S. F., Chen, H. L., Langmuri, C. H., Yu, X., Lin, X. B. (2008).** Chronology and geochemistry of Taxinan basalts from the Tarim Basin: Evidence for

Permian plume magmatism. Acta Petrologica Sinica, 24, 959–970 (in Chinese with English abstract).

**Li, Q., Liu, S., Wang, Z., Chu, Z., Song,B., Wang, Y., Wang, T. (2007).** Contrasting provenance of Late Archean metasedimentary rocks from the Wutai Complex, North China Craton: detrtal zircon U-Pb, whole-rock Sm-Nd isotope, and geochemical data. Int. J Earth Sci (GeolRundsch) (2008) 97:443-458.

**Li, Z., Chen, B., Wei, C., Wang, C., Han, W. (2015).** Provenance and tectonic setting of the Pa;eoproterozoic metasedimentary rocks from the Liaohe Group, Jiao-Liao-Ji Belt, North China Craton: Insights from detrital zircon U-Pb geochronology, whole-rock Sm-Nd isotopes, and geochemistry. J of Asian Earth sciences 111(2015)711-732.

**Liguori, B. T. P., Almeida, M. G. D., & Rezende, C. E. D. (2016).** Barium and its Importance as an Indicator of (Paleo) Productivity. Anais Da Academia Brasileira de Ciências, 88(4), 2093–2103.

**Liu, J., Sitaram, A., Burd, C. G. (2007).** Regulation of copper-dependent endocytosis and vacuolar degradation of the yeast copper transporter, Ctr1p, by the Rsp5 ubiquitin ligase. Traffic 8(10):1375-84.

**Long, X. P., Yuan, C., Sun, M., Safonova, I., Xiao, W. J., Wang, Y. J. (2012).** Geochemistry and U–Pb detrital zircon dating of Paleozoic greywackes in Junggar, NW China: insights into subduction accretion processes in the southern Central Asian Orogenic Belt. Gondwana Res 21:637–653.

**MacNaughton, R.B., Hagadorn, J.W., Dott, R.H. (2018).** Cambrian wave-dominated tidal-flat deposits, central Wisconsin, USA. Sedimentology, (), –. doi:10.1111/sed.12546

**Madhavaraju, J., Ramasamy, S. (1999).** Rare earth elements in limestones of Kallankurichchi Formation of Ariyalur Group, Tiruchirapalli Cretaceous, Tamil Nadu. J GeolSoc India 54:291–301.

**Master, S., Bekker, A., Hofmann, A. (2010).** A review of the stratigraphy and geological setting of the Palaeoproterozoic Magondi Supergroup, Zimbabwe – Type locality for the Lomagundi carbon isotope excursion. , 182(4), 0–273. doi:10.1016/j.precamres.2010.08.013

**Mazumder, R., Van Kranendonk, M. J. (2013).** Palaeoproterozoic terrestrial sedimentation in the Beasley River Quartzite, lower Wyloo Group, Western Australia. Precambrian Research, 231(), 98–105. doi:10.1016/j.precamres.2013.03.018

**Malone, S.J., J.G. Meert, D.M. Banerjee, M.K. Pandit, E. Tamrat, G.D. Kamenov, V.R. Pradhan, V.R. and Sohl, L.E. (2008).** Paleomagnetism and detrital zircon geochronology of the Upper Vindhyan Sequence, Son Valley and Rajasthan, India: A ca. 1000 Ma closure age for the Purana Basins? *Precambrian Res.*, 164, 137-159, doi: 10.1016/j.precamres.2008.04.004.

**Marriott, S. (1999).** The use of models in the interpretation of the effects of base-levelchange on alluvial architecture, in Smith, N., and Rogers, J., eds., Fluvial Sedimentology VI, International Association of Sedimentology, Special Publication28, p. 271–281

**Matin, A. (2015).** Tectonics of the Cuddapah basin and a model of its evolution: A review; Geol. Soc. London Memoir 43(1) 231–254.

**McLennan, S. M. (1989).** Rare earth elements in sedimentary rocks: influence of provenance and sedimentary processes: Reviews in Mineralogy and Geochemistry, 24, 169-200.

**McLennan, S. M., Hemming, S., McDaniel, D. K., Hanson, G. N. (1993).** Geochemical approaches to sedimentation, provenance and tectonics. In: Johnson MJ, Basu A (eds) Processes controlling the composition of clastic sediments, vol 284. Geological society of America, Boulder, pp 21–40 (Special Paper).

**Meert, J.G., Pandit, M.K., Pradhan, D.R., Kamenov, G. (2011).** Preliminary report on the Paleomagnetism of 1.88 dykes from the Bastar and Dharwar cratons, Peninsular India. Gondwana Research 20, 335e343.

**Meert, J.G., Pandit, M.K. (2015).** The The Archaean and Proterozoic history of Peninsular India: tectonic framework for Precambrian sedimentary basins in India. In: Mazumder, R., Eriksson, P.G. (Eds.), Precambrian Basins of India: Stratigraphic and Tectonic Context, Geological Society of London Memoir, 43, 29–54.

**Meijerink, A. M. J., Rao, D. P., Rupke, J. (1984).** Stratigraphic and structural development of the Precambrian Cuddapah Basin, S.E. India. Precambrian Res., v.26, pp.57-104.

**Miall, A. D. (1996).** The Geology of Fluvial Deposits. Sedimentary Facies, Basin Analysis, and Petroleum Geology. xvi + 582 pp. Berlin, Heidelberg, New York, London, Paris, Tokyo, Hong Kong: Springer-Verlag. Price DM 118.00 Ös 861.40, SFr 113.50 (hard covers). ISBN 3 540 59186 9.

**Miall, A.D. (2000).** Principles of Sedimentary Basin Analysis. 3rd and Enlarged Edition, Springer-Verlag, Berlin, 616 p. http://dx.doi.org/10.1007/978-3-662-03999-1

**Mir, A. R. (2015).** Rare earth element geochemistry of Post- to Neoarchean shales from Singhbhum mobile belt, Eastern India: implications for tectonic setting and paleo-oxidation conditions. Chin J Geochem 34(3):401–409.

**Mishra, D.C. (2011).** Long hiatus in Proterozoic sedimentation in India: Vindhyan, Cuddapah and Pakhal Basins — A plate tectonic model. , 77(1), 17–25. doi:10.1007/s12594-011-0004-9

**Mitra, R.,Chakrabarti, G., Shome, D. (2017).** Geochemistry of Paleo-Mesoproterozoic Tadpatrishales, Cuddapah basin, India: implications on provenance, paleoweathering and paleoredox conditions. Acta Geochim (2017).

**Mjelde, R., Kodaira, S., Hassan, R.K., Goldschmidt-Rokita, A., Tomita, N., Sellevoll, M.A., Hirschleber, H.B., Shimamura, H., Wasaki, T., Kanazawa, T. (1996).** The continent/ocean transition of the Lofoten volcanic margin, N. Norway. , 22(3-4), 0–206. doi:10.1016/0264-3707(96)00016-6

**Mohanty, S. (2011).** Palaeoproterozoic assembly of the Napier Complex, Southern India and Western Australia: Implications for the evolution of the Cuddapah basin. , 20(2-3), 344–361. doi:10.1016/j.gr.2011.03.009

**Mongelli,G., Cullers, R. L., Muelheisen, S. (1996).** Geochemistry of Late Cretaceous-Oligocenic shales from the Varicolori Formation, southern Apennines, Italy: implications for mineralogical, grain-size control and provenance. Eur. J. Mineral., 8: p.733–754.

**Morris, E. A., Hodgson, D. M., Flint, S. S., Brunt, R. L., Butterworth, P. J., Verhaeghe, J. (2014).** Sedimentology, Stratigraphic Architecture, and Depositional Context of Submarine Frontal-Lobe Complexes. Journal of Sedimentary Research, 84(9), 763–780. doi:10.2110/jsr.2014.61

**Moscariello, A. (2017).** Alluvial fans and fluvial fans at the margins of continental sedimentary basins: geomorphic and sedimentological distinction for geo-energy exploration and development. Geological Society, London, Special Publications, (), SP440.11–. doi:10.1144/SP440.11

**Mukherjee, S., Goswami, S., Mukherjee, A. (2019).** Structures and Their Tectonic Implications of the Southern Part of Cuddapah Basin, Andhra Pradesh, India. Iranian Journal of Science and Technology, Transactions A: Science, (), –. doi:10.1007/s40995-018-0566-0.

**Mulder, T., Alexander, J. (2001).** The physical character of subaqueous sedimentary density flows and their deposits. , 48(2), 269–299. doi:10.1046/j.1365-3091.2001.00360.x

**Murthy, Y.G.K. (1981).** The Cuddapah basin: A review of Basin development and basement framework relations. Fourth Workshop on 'Status, Problems and Programmes in Cuddapah Basin', Institute of India Peninsular Geology, Hyderabad, 51-72.

**Murthy, Y. G. K., Babu Rao, V., Guptasarma, D., Rao, J. M., Rao, M. N., Bhattacharji, S. (1987).** Tectonic petrochemical and geophysical studies of mafic dike swarms around the (Eds.) Proterozoic Cuddapah Basin, south India, In: H.C. Halls & W.F. Fahrig Mafic Dykes Swarms, Geological Association of Canada Special Paper No. 34, pp. 303-316.

**Nagaraja Rao, B. K., Rajurkar, S. T., Ramalingaswami, G., Ravindra Babu, B. (1987).** Stratigraphy structure and evolution of cuddapah Basin. In: B.P. Radhakrishna (Ed.), Purana Basins of Peninsular India. Mem. Geol. Soc. India, no.6, pp.33-86.

**Nagarajan, R., Madhavaraju, J., Nagendra, R., Armstrong-Altrin, J. S., Moutte, J. (2007).** Geochemistry of Neoproterozoicshales of Rabanpalli formation, Bhima basin, Northern Karnataka, SouthernIndia: implications for provenance and paleo-redox conditions. Revista Mexicana de Ciencias Geológicas 24(2):150–160.

**Nagaraja Rao, B.K., Ramalingaswamy, G. (1976).** Some New Thoughts on the Stratigraphy of Cuddapah Supergroup. Seminar on Kaladgi-Badami, Bhima and Cuddapah Supergroup, pp. 17–20.

**Nagarajan, R., Roy, P. D., Jonathan, M. P., Lozano, R., Kessler, F. L., Prasanna, M. V. (2014).** Geochemistry of Neogene sedimentary rocks from Borneo basin, East Malaysia: paleo-weathering, provenance and tectonic setting. ChemErde 74:139–146.

**Narayanaswami, S. (1966).** Tectonics of the Cuddapah Basin. Journal of the Geological Society of India, 7, 33-50.

**Nath, B. N., Bau, M., RamalingeswaraRao, B., Rao, C. H. M. (1997).** Trace and rare earth elemental variation in Arabian Sea sediments through a transect across the oxygen minimum zone. Geochimica et Cosmochimica Acta, 61(12):2375–2388.

**Nesbitt, H. W., Young, G. M. (1982).** Early Proterozoic climates and plate motions inferred from major element chemistry of lutites. Nature, v.299, pp.715-717.

**Nesbitt, H. W., Young, G. M. (1984).** Prediction of some weathering trends of plutonic and volcanic rocks based on thermodynamic and kinetic considerations. Geochim Cosmochim Acta 48:1523–1534.

**Olsen, H. (1987).** Coarsening upward sequences - the products of laterally established river subsystems, M. Devonian, Hornelen Basin, Norway. Bull. geol. Soc. Denmark, Vol. 36, pp 203-219, Copenhagen December, 31st, 1987.

**Pandey, S., Parcha, S. K., & Srivastava, P. K. (2019).** Petrography and geochemistry of the Neoproterozoic sedimentary rocks from the Batal Formation of Spiti Basin: implication on provenance. Arabian Journal of Geosciences, 12(2).

**Pascoe F.H., (1973).** A manual of the Geology of India and Burma (3rd Edition). GoI., Geological Survey, 1-485.

**Pasquini, A. I., Campodonico, V. A., Rouzaut, S., Giampaoli, V. (2017).** Geochemistry of a soil catena developed from loess deposits in a semiarid environment, Sierra Chica de Córdoba, central Argentina. Geoderma 295:53–68.

**Patranabis-Deb, S., Bickford, M.E., Hill, B., Chaudhuri, A.K., Basu, A. (2007).** SHRIMP Ages of Zircon in the Uppermost Tuff in Chattisgarh Basin in Central India Require ~500-Ma Adjustment in Indian Proterozoic Stratigraphy. The Journal of Geology, 115(4), 407–415. doi:10.1086/518049

**Patranabis-Deb, S., Saha, D., Tripathy, V. (2012).** Basin stratigraphy, sealevel fluctuations and their global tectonic connections—evidencefrom the Proterozoic Cuddapah basin. Geol J 47:263–283.

**Petti, A.A., Williams, S.R., Miller, C.A., Fiddes, I.T., Srivatsan, S.N., Chen, D.Y., Fronick, C.C., Fulton, R.S., Church, D.M., Ley, T.J. (2019).** A general approach for detecting expressed mutations in AML cells using single cell RNA-sequencing. Nature Communications, 10(1), 3660–. doi:10.1038/s41467-019-11591-1

**Pettijohn, F.J. (1975)**. Sedimentary Rocks. 2nd Edition, Harper and Row Publishers, New York, 628 p.

**Proske, U., Hanebuth, T.J.J., Meggers, H., Leroy, S.A.G. (2008).** Tidal flat sedimentation during the last millennium in the northern area of Tidra Island, Banc d'Arguin, Mauritania. , 50(1), 37–48. doi:10.1016/j.jafrearsci.2007.09.002

**Radhakrishna, T., Joseph, M. (1996).** Proterozoic palaeomagnetism of the mafic dyke swarms in the high-grade region of southern India. , 76(1-2), 0–46. doi:10.1016/0301-9268(95)00022-4

**Radhakrishna, B.P. (1987).** "Purana Basins of Peninsular India (Middle to Late Proterozoic)," Memoirs of the Geological Survey of India, Vol. 66, pp. 1-518.

**Rai, S. S. Priestley, K., Suryaprakasam, K., Srinagesh, D., Gaur, V.K.,Du, Z. (2003).** Crustal shear velocity structure of the south Indian shield. Journal of Geophysical Research, 108(B2), 2088–. doi:10.1029/2002jb001776

**Ramakrishnan, M., Vaidyanadhan, R. (2008).** Geology of India, Volume 1. Geological

Society of India, Bangalore, 556.Determination of tectonic setting of sandstone-mudstone suites using $SiO_2$ content and $K_2O$-$Na_2O$ ratio.Journal of Geology; 94, 635-660.

**Ramos-Vázquez, M., Armstrong-Altrin, J. S., Rosales-Hoz, L., Machain- Castillo, M. L., Carranza-Edwards, A. (2017).** Geochemistry of deepsea sediments in two cores retrieved at the mouth of the Coatzacoalcos River delta, Western Gulf of Mexico, Mexico. Arab J Geosci 10(6):148.

**Rasmussen, B., Bose, P.K., Sarkar, S., Banerjee, S., Fletcher, I.R., McNaughton, N.J. (2002).** 1.6 Ga U-Pb zircon age for the Chorhat Sandstone, lower Vindhyan, India: Possible implications for early evolution of animals. *Geology*; 30 (2): 103–106. doi: https://doi.org/10.1130/0091-7613(2002)030<0103:GUPZAF>2.0.CO;2

**Ravikant, V. (2010).** Palaeoproterozoic (~1.9 Ga) extension and breakup along the eastern margin of the Eastern Dharwar Craton, SE India: New Sm–Nd isochron age constraints from anorogenic mafic magmatism in the Neoarchean Nellore greenstone belt. , 37(1), 0–81. doi:10.1016/j.jseaes.2009.07.008

**Ray, J.S., Martin, M.W., Veizer, J., Bowring, S.A. (2002).** U-Pb zircon dating and Sr isotope systematics of the Vindhyan Supergroup, India. Geology, 30, 131-134.

**Ray, J.S., Veizer, J., Davis, W.J. (2003).** C, O, Sr and Pb isotope systematics of carbonate sequences of the Vindhyan Supergroup, India: age, diagenesis, correlations and implications for global events., 121(1-2), 0–140. doi:10.1016/s0301-9268(02)00223-1

**Reading, H.G. (1996).** Sedimentary Environments: Processes, Facies and Stratigraphy. 3rd Edition, Blackwell, Oxford, 689 p.

**Reddy, V.P., Reddy, N.S., Prasad, C.V.R.K. (1990).** Quartzites of the Cuddapah Group and their environment of deposition. J. Geol. Soc. India, 35, 408-420.

**Reesink, A.J.H., Parsons, D., Ashworth, P., Hardy, R., Best, J., Unsworth, C., McLelland, S., Murphy, B. (2013).** The response and hysteresis of alluvial dunes under

transient flow conditions. Marine and River Dunes 2013, Conference Proceedings, pp. 215–220.

**Reineck, H.E. and Singh, I.B. (1980).** Depositional Sedimentary Environments. Springer-Verlag, New York, 549. https://doi.org/10.1007/978-3-642-81498-3

**Roser, B. P., Korsch, R. J. (1986).** Determination of tectonic setting of sandstone-mudstone suites using $SiO_2$ content and $K_2O/Na_2O$ ratio. J Geol 94(5):635–650.

**Roser, B. P., Korsch, R. J. (1988).** Provenance signature of sandstone-mudstone suite determined using discriminant function analysis of major-element data. Chem. Geol., v.67, pp.119-139.

**Roser, B. P., Cooper, R. A., Nathan, S., Tulloch, A. J. (1996).** Reconnaissance sandstone geochemistry, provenance and tectonic setting of the lower Paleozoicterranes of the West Coast and Nelson, New Zealand. New Zealand Journal of Geology and Geophysics 39:116.

**Saha. D., Chakraborti, S., Tripathy, V. (2010).** Intracontinental thrusts and inclined transpression along eastern margin of the East Dharwar craton, India. , 75(1), 323–337. doi:10.1007/s12594-010-0019-7

**Saha, D., Patranabis-Deb, S. (2014).** Proterozoic evolution of Eastern Dharwar and Bastar cratons, India – An overview of the intracratonic basins, craton margins and mobile belts. Journal of Asian Earth Sciences, 91(), 230–251. doi: 10.1016/j.jseaes.2013.09.020

**Saha, D., Tripathy, V. (2012).** Palaeoproterozoic sedimentation in the Cuddapah Basin, south India and regional tectonics – a review. In: Paleoproterozoic of India (Eds. Mazumder R and Saha D) Geologal Society, London SpPubl 365 159-182.

**Santosh, M. (2010).** A synopsis of recent conceptual models on supercontinent tectonics in relation to mantle dynamics, life evolution and surface environment. , 50(3-4), 0–133. doi:10.1016/j.jog.2010.04.002

**Sesha Sai, V.V., Tripathy, V., Bhattacharjee, S., Khanna, T.C. (2017).** Paleoproterozoic magmatism in the Cuddapah Bain, India. The Journal of Indian Geophysical Union, 21(6), 516-525.

**Sheppard, S., Rasmussen, B., Zi, J., Somasekhar, V., Srinivasa Sarma, D.; Ram Mohan, M., Krapež, B., Wilde, S. A.; McNaughton, N. J. (2017).** Sedimentation and magmatism in the Paleoproterozoic Cuddapah Basin, India: Consequences of lithospheric extension. Gondwana Research, (), S1342937X16303550–. doi:10.1016/j.gr.2017.04.024

**Mall, D. M.; Rao, V. K.; Reddy, P. R. (1999).** Deep sub-crustal features in the Bengal Basin: Seismic signatures for plume activity. Geophysical Research Letters, 26(16), 2545–2548. doi:10.1029/1999gl900552

**Mall, D.M., Pandey, O.P., Chandrakala, K., Reddy, P.R. (2008).** Imprints of a Proterozoic tectonothermal anomaly below the 1.1 Ga kimberlitic province of Southwest Cuddapah basin, Dharwar craton (Southern India). , 172(1), 422–438. doi:10.1111/j.1365-246x.2007.03623.x

**Sallarès, V., Dañobeitia, J.J., Flueh, E.R. (2001).** Lithospheric structure of the Costa Rican Isthmus: Effects of subduction zone magmatism on an oceanic plateau. Journal of Geophysical Research, 106(B1), 621–. doi:10.1029/2000jb900245

**Singh, P. (1980)**. Note on the Geology of the Subathu Group of the Nilkanth, Garhwal Himalaya. Geoscience Journal, 1, 81-83.

**Singh, A.P., Mall, D.M. (1998).** Crustal accretion beneath the Koyna coastal region (India) and Late Cretaceous geodynamics. , 290(3-4), 0–297. doi:10.1016/s0040-1951(98)00053-5

**Singh, A. P., Mishra, D. C. (2002).** Tectonosedimentary evolution of Cuddapah Basin & Eastern Ghat Mobile belt (India) as Proterozoic Collision: gravity, seismic & geo dynamic constrains. Journal of Geodynamics, 33, 249-267.

**Sloss, L. L. (1991).** The tectonic factor in sea level change: A countervailing view. Journal of Geophysical Research, 96(B4), 6609–. doi:10.1029/90jb00840

**Smith, N.D. (1972).** Some sedimentological aspects of planar cross-stratification in a sandy braided river. Jour. Sed. Petrol., 42, 624-634.

**Sohn, Y.K., Rhee, C.W., Kim, B.C. (1999).** Debris Flow and Hyperconcentrated Flood-Flow Deposits in an Alluvial Fan, Northwestern Part of the Cretaceous Yongdong Basin, Central Korea. The Journal of Geology, 107(1), 111–132. doi:10.1086/314334

**Son, M., Chong, H.-Y. & Kim, I.-S. (2002).** Geology and geological structures in the vicinities of the southern part of the Yonil Tectonic Line, SE Korea. Journal of Geological Society of Korea, 38, 175–197 [in Korean with English abstract].

**Srivastava, R.K. (2006).** Geochemistry and petrogenesis of Neoarchaean high-Mg low-Ti mafic igneous rocks in an intracratonic setting, Central India craton: Evidence for boninite magmatism. Geochemical Journal, 40(1), 15–31. doi:10.2343/geochemj.40.15 .

**Srivastava, V. K., & Singh, B. P. (2018).** Depositional environments and sources for the middle Eocene Fulra Limestone Formation, Kachchh Basin, western India: Evidences from facies analysis, mineralogy, and geochemistry. Geological Journal.

**Sun, L., Gui, H. & Chen, S. (2013).** Geochemistry of sandstones from the Neoproterozoic Jinshanzhai Formation in northern Anhui Province, China: Provenance, weathering and tectonic setting. Chin. J. Geochem. 32, 95–103.

**Suttner, L. J., Dutta, P. K. (1986).** Alluvial sandstones composition and paleoclimate, I, framework mineralogy, Jour. Sed. Petrology., 56: 329 – 345.

**Tapia-Fernandez, H. J., Armstrong-Altrin, J. S., Selvaraj, K. (2017).** Geochemistry and U–Pb geochronology of detrital zircons in the Brujas beach sands, Campeche, Southwestern Gulf of Mexico, Mexico. J S Am Earth Sci 76:346–361.

**Taylor, S. R., Mclennan, S. M. (1985).** The Continental Crust: Its Composition and Evolution. Blackwell, Oxford, 312p.

**Taylor, S. R., Mclennan, S. M. (1995).** The geochemical evolution of the continental crust, Rev. Geophys, 33, 241-265.

**Tribovillard, N., Algeo, T. J., Lyons, T., & Riboulleau, A. (2006).** Trace metals as paleoredox and paleoproductivity proxies: An update. Chemical Geology, 232(1-2), 12–32.

**Tripathy, V., Saha, D. (2015).** Inversion of calcite twin data, paleostress reconstruction and multiphase weak deformation in cratonic interior – Evidence from the Proterozoic Cuddapah basin, India. Journal of Structural Geology, 77(), 62–81. doi:10.1016/j.jsg.2015.05.009

**Vakalas, J., Ananiadis, G., Mpourlokas, J., Poulimenos, D., Getsos, K., Pantopoulos, G., Avramidis, P., Zelilidis, A., Kontopoulos, N. (2018).** Palaeocurrent directions as an indicator of Pindos foreland evolution (central and southern part), Western Greece. Bulletin of the Geological Society of Greece, 34(2)

**Vijaya Kumar, K., Leelanandam, C., (2008).** Evolution of the Eastern Ghats Belt., a plate tectonic prospective. Jour. Geol. India, 72, 720-749.

**Wang, W., Zhou, M. F. (2013).** Petrological and geochemical constraints on provenance, paleoweathering, and tectonic setting of the Neoproterozoic sedimentary basin in the

eastern Jiangnan orogen, south china. Journal of Sedimentary Research, 2013, v. 83, 974–993.

**Went D.J. (2005).** Pre-vegetation alluvial fan facies and processes: an example from the Cambro-Ordovician Rozel Conglomerate Formation, Jersey, Channel Islands. , 52(4), 693–713. doi:10.1111/j.1365-3091.2005.00716.x

**Went, D.J., McMahon, W.J. (2018).** Fluvial products and processes before the evolution of land plants: Evidence from the lower Cambrian Series Rouge, English Channel region. Sedimentology, 65(7), 2559–2594. doi:10.1111/sed.12478

**White, R., McKenzie, D. (1989).** Magmatism at rift zones: The generation of volcanic continental margins and flood basalts. Journal of Geophysical Research, 94(B6), 7685–. doi:10.1029/jb094ib06p07685

**Yuanfu Z., Xin D., Min W., Xinxin L. (2020).** The concept, characteristics and significance of fluvial fans, Petroleum Exploration and Development, Volume 47, Issue 5,

**Zachariah, J. K., Bhaskar Rao, Y. J., Srinivasan, R., Gopalon, K. (1999).** Pb, Sr, Nd isotope systematics of uranium mineralized stromatolitic dolomites from the Proterozoic CuddapahSupergroup, south India: Constraints on age and provenance, chem. Geol 162:49-64.

**Zhao, T., Zhou, G.G.D., Sun, Q. (2022).** Slope erosion induced by surges of debris flow: insights from field experiments. Landslides . https://doi.org/10.1007/s10346-022-01914-7

# PHOTO GALLERY

**Fig** Dark brown coloured coarse sand alternating with massive sand in the massive sandstone facies (Pendllimari section). Note the coarse sand bands are continuous and nearly straight

**Fig** Multi directional long crested wave ripples on the top of ripple laminated sandstone facies from Pendllimari section

**Fig** High index bifurcated current ripple in the tabular cross stratified sandstone facies from the Kanampalle section

**Fig** Microbially induced sedimentary structure in trough crodd stratified sandstone facies from Gandi section

**Fig** Coarse frained sandstone facies E graded upward into fine grained sandstone facies I in the Pendllimari section. The contact between these two facies is very sharp and straight

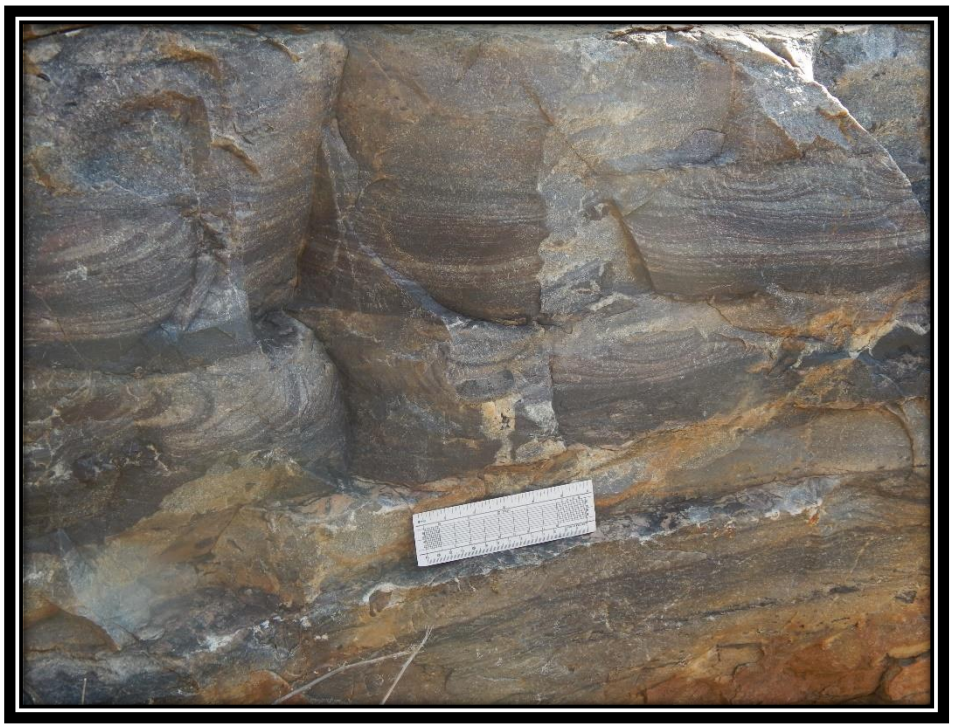

**Fig** Deformed trough cross stratification in the trough cross stratified sandstone facies Penddlimari section

**Fig** Desiccation crack on the top surface of the rhythmite facies from the Pendllimari section

**Fig** Conglomerate showing clast fragments of jasper, granite and quartzite in the framework (from Gandi section)

# SUPPLEMENTARY MATERIALS

# Supplementary Material: 1

Laminae numbers and the respective thickness of each laminae measured from medium to coarse grained sandstone facies. The data has been plotted in Origin software and figure has been given as Fig. 3.36 within the Chapter 3.

| Laminae Number | Laminae Thickness |
|---|---|
| 1 | 0.6 |
| 2 | 0.4 |
| 3 | 0.9 |
| 4 | 0.8 |
| 5 | 0.2 |
| 6 | 0.4 |
| 7 | 0.7 |
| 8 | 0.55 |
| 9 | 0.6 |
| 10 | 0.8 |
| 11 | 1.6 |
| 12 | 0.9 |
| 13 | 0.2 |
| 14 | 0.6 |
| 15 | 0.45 |
| 16 | 0.82 |
| 17 | 0.66 |
| 18 | 0.2 |
| 19 | 0.6 |
| 20 | 1.2 |
| 21 | 0.7 |
| 22 | 0.54 |
| 23 | 0.9 |
| 24 | 0.4 |
| 25 | 0.8 |
| 26 | 1.4 |
| 27 | 0.68 |
| 28 | 0.3 |
| 29 | 0.2 |
| 30 | 0.8 |
| 31 | 0.24 |
| 32 | 1.3 |
| 33 | 0.56 |
| 34 | 0.4 |
| 35 | 0.9 |
| 36 | 0.78 |
| 37 | 0.2 |
| 38 | 0.6 |
| 39 | 0.4 |
| 40 | 0.26 |
| 41 | 1.6 |

# Supplementary Material: 2

The SEM images of selected grains (Sandstone from Pendllimari area, 78˚36'43" E, 14˚24’54.2"N) was acquired at the Petrology Laboratory, Institute of Geophysics, Universidad Nacional Autónoma de México (UNAM), using a PHILLIPS XL-30 scanning electron microscope (SEM) equipped with EDAX spectrometer (EDS) system.

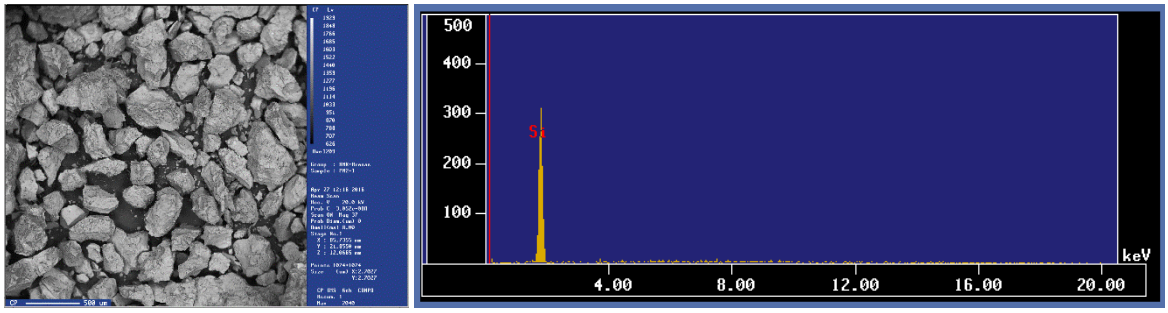


Sample: PM-2 Image of fine grained sandstone from trough cross stratified sandstone facies

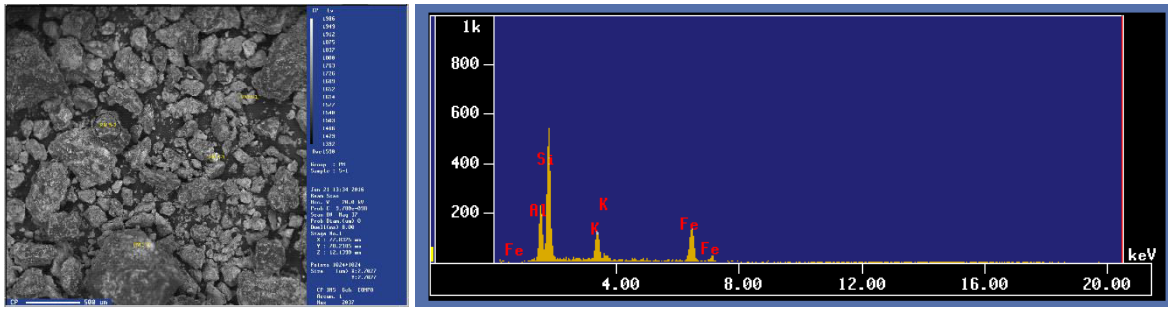


Sample: PM-5 Image of fine grained sandstone from tabular cross stratified sandstone facies

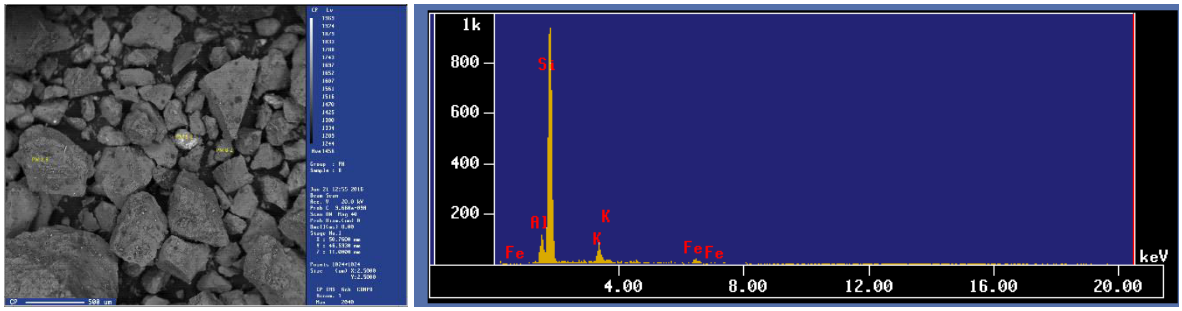


Sample: PM-8 Image of medium grained sandstone from tabular cross stratified sandstone facies

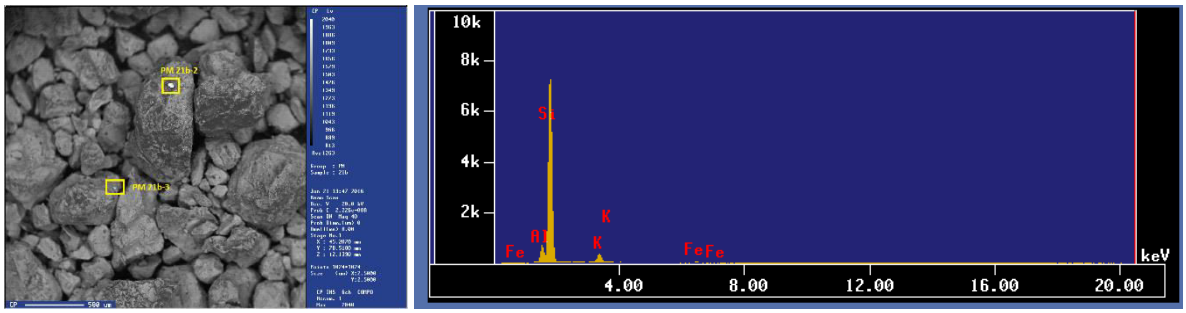


Sample: PM-12 Image of medium grained sandstone from plane laminated sandstone facies

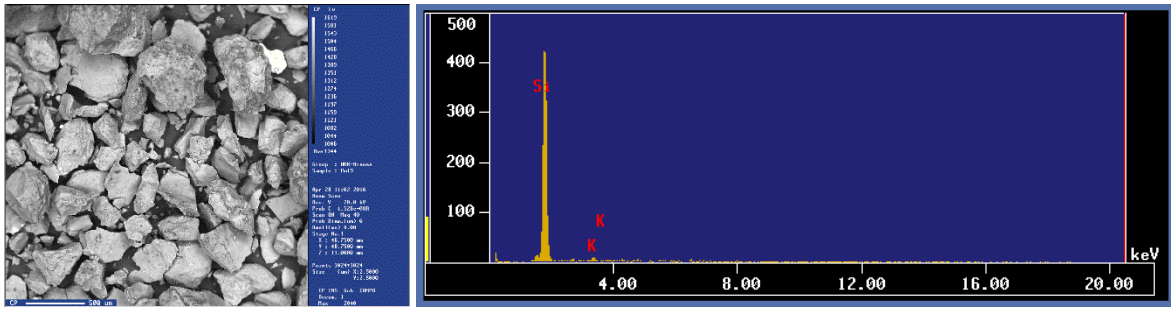


Sample: PM-19 Image of medium grained sandstone from ripple laminated sandstone facies

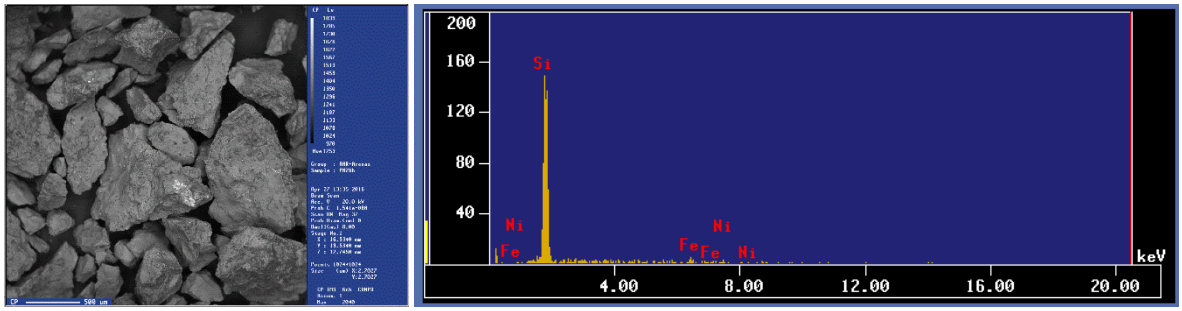


Sample: PM-25b Image of coarse grained sandstone from trough cross stratified sandstone facies

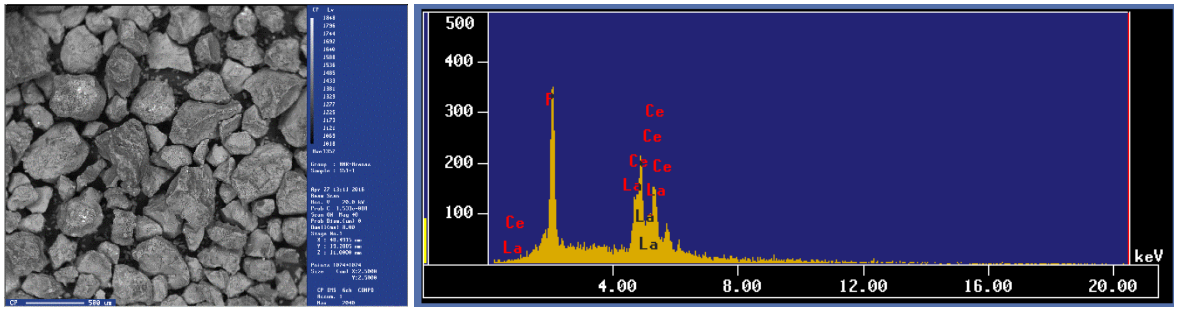


Sample: S-51 Image of medium grained sandstone from massive sandstone facies

# Supplementary Material: 3

Geochemical analysis of the Mud sample from Gandi section (14°18´25.34″ N, 78°28´ 36.52″ E) from Geological Survey of India, Kolkata.

| Sample No | Mud - 1 | Mud - 2 | Mud - 3 | Mud - 4 | Mud - 5 | Mud - 6 |
|---|---|---|---|---|---|---|
| SERIAL NO | 1 | 2 | 3 | 4 | 5 | 6 |
| $SiO_2$ (%) | 62.12 | 58.31 | 54.66 | 51.85 | 59.6 | 62.53 |
| $Al_2O_3$ (%) | 17.32 | 12.35 | 19.21 | 12.61 | 21.83 | 16.56 |
| $Fe_2O_3$ (%) | 6.41 | 4.65 | 4.52 | 2.68 | 5.59 | 7.83 |
| MnO (%) | 0.02 | 0.02 | 0.01 | 0.01 | 0.02 | 0.01 |
| $TiO_2$ (%) | 0.63 | 0.79 | 0.72 | 0.58 | 0.83 | 0.96 |
| CaO (%) | 0.09 | 0.14 | 0.19 | 0.21 | 0.16 | 0.22 |
| MgO (%) | 1.68 | 2.48 | 1.69 | 1.88 | 2.03 | 2.61 |
| $Na_2O$ (%) | 0.21 | 0.24 | 0.28 | 0.22 | 0.25 | 0.18 |
| $K_2O$ (%) | 5.16 | 7.02 | 6.34 | 3.88 | 6.39 | 4.18 |
| $P_2O_5$ (%) | 0.03 | 0.06 | 0.09 | 0.14 | 0.13 | 0.08 |
| Ba (ppm) | 893 | 2933 | 185 | 777 | 662 | 2599 |
| Ga (ppm) | 17 | 17 | 17 | 17 | 17 | 17 |
| Sc (ppm) | 16 | 7 | 14 | 10 | 15 | 10 |
| V (ppm) | 73 | 61 | 122 | 41 | 115 | 81 |
| Th (ppm) | 12 | 16 | 15 | 12 | 17 | 14 |
| U (ppm) | 7 | 4 | 6 | 5 | 8 | 4 |
| Ni (ppm) | 57 | 15 | 71 | 19 | 66 | 28 |
| Nb (ppm) | 41 | 32 | 32 | 9 | 41 | 28 |
| Co (ppm) | 10 | 9 | 15 | 10 | 4 | 12 |
| Cr (ppm) | 190 | 248 | 276 | 505 | 202 | 297 |
| Rb (ppm) | 160 | 143 | 182 | 111 | 209 | 139 |
| Sr (ppm) | 13 | 10 | 19 | 24 | 19 | 17 |
| Y (ppm) | 11 | 11 | 17 | 11 | 13 | 15 |
| Zr (ppm) | 108 | 203 | 200 | 192 | 188 | 286 |

# Supplementary Material: 4

Palaeocurrent data from current ripples of Kanampalle area (78˚05'25.18" E, 14˚25'13.60"N) representing rose diagram Fig 4.1 in the chapter 4.

| Number | Palaeocurrent Direction (in degree) |
|---|---|
| 1 | 270 |
| 2 | 265 |
| 3 | 265 |
| 4 | 268 |
| 5 | 270 |
| 6 | 265 |
| 7 | 264 |
| 8 | 258 |
| 9 | 264 |
| 10 | 262 |
| 11 | 261 |
| 12 | 259 |
| 13 | 260 |
| 14 | 258 |
| 15 | 272 |
| 16 | 230 |
| 17 | 232 |
| 18 | 233 |
| 19 | 234 |
| 20 | 233 |
| 21 | 234 |
| 22 | 235 |
| 23 | 236 |
| 24 | 230 |
| 25 | 231 |
| 26 | 290 |
| 27 | 288 |
| 28 | 160 |
| 29 | 162 |
| 30 | 165 |
| 31 | 163 |
| 32 | 162 |
| 33 | 194 |

# Supplementary Material: 5

Palaeocurrent data from trough axis of Kanampalle area (78˚05'25.18" E, 14˚25'13.40"N) representing rose diagram Fig 4.2 in the chapter 4.

| Number | Palaeocurrent Direction (in degree) |
|---|---|
| 1 | 220 |
| 2 | 218 |
| 3 | 215 |
| 4 | 216 |
| 5 | 208 |
| 6 | 220 |
| 7 | 211 |
| 8 | 212 |
| 9 | 209 |
| 10 | 222 |
| 11 | 224 |
| 12 | 225 |
| 13 | 224 |
| 14 | 216 |
| 15 | 214 |
| 16 | 212 |
| 17 | 217 |
| 18 | 218 |
| 19 | 215 |
| 20 | 216 |
| 21 | 214 |
| 22 | 222 |
| 23 | 223 |
| 24 | 224 |
| 25 | 225 |
| 26 | 226 |
| 27 | 221 |
| 28 | 218 |
| 29 | 219 |
| 30 | 208 |
| 31 | 222 |
| 32 | 225 |

# Supplementary Material: 6

Palaeocurrent data from current ripples of Pendllimari area (78˚36'43" E, 14˚24’55.1"N) representing rose diagram Fig 4.3 in the chapter 4.

| Number | Palaeocurrent Direction (in degree) |
|---|---|
| 1 | 20 |
| 2 | 22 |
| 3 | 22 |
| 4 | 21 |
| 5 | 24 |
| 6 | 25 |
| 7 | 26 |
| 8 | 22 |
| 9 | 24 |
| 10 | 18 |
| 11 | 17 |
| 12 | 18 |
| 13 | 19 |
| 14 | 18 |
| 15 | 18 |
| 16 | 19 |
| 17 | 21 |
| 18 | 20 |
| 19 | 21 |
| 20 | 26 |
| 21 | 25 |
| 22 | 24 |
| 23 | 17 |
| 24 | 16 |
| 25 | 15 |
| 26 | 16 |
| 27 | 14 |
| 28 | 15 |
| 29 | 16 |
| 30 | 18 |
| 31 | 24 |
| 32 | 26 |
| 33 | 25 |

# Supplementary Material: 7

Palaeocurrent data from trough axis of Pendllimari area (78˚36'43" E, 14˚24’54.2"N) representing rose diagram Fig 4.4 in the chapter 4.

| Number | Palaeocurrent Direction (in degree) |
|---|---|
| 1 | 80 |
| 2 | 82 |
| 3 | 84 |
| 4 | 85 |
| 5 | 86 |
| 6 | 78 |
| 7 | 76 |
| 8 | 79 |
| 9 | 81 |
| 10 | 82 |
| 11 | 86 |
| 12 | 85 |
| 13 | 88 |
| 14 | 82 |
| 15 | 84 |
| 16 | 60 |
| 17 | 61 |
| 18 | 62 |
| 19 | 64 |
| 20 | 61 |
| 21 | 62 |
| 22 | 64 |
| 23 | 62 |
| 24 | 61 |
| 25 | 55 |
| 26 | 54 |
| 27 | 92 |
| 28 | 96 |
| 29 | 42 |
| 30 | 43 |
| 31 | 48 |
| 32 | 44 |

# Supplementary Material: 8

Palaeocurrent data from current ripples of Gandi area (14°18´25.34″ N, 78°28´ 36.52″ E) representing rose diagram Fig 4.5 in the chapter 4.

| Number | Palaeocurrent Direction (in degree) |
|---|---|
| 1 | 70 |
| 2 | 72 |
| 3 | 68 |
| 4 | 72 |
| 5 | 74 |
| 6 | 75 |
| 7 | 71 |
| 8 | 76 |
| 9 | 71 |
| 10 | 68 |
| 11 | 69 |
| 12 | 66 |
| 13 | 68 |
| 14 | 68 |
| 15 | 69 |
| 16 | 55 |
| 17 | 54 |
| 18 | 56 |
| 19 | 55 |
| 20 | 54 |
| 21 | 55 |
| 22 | 58 |
| 23 | 36 |
| 24 | 24 |
| 25 | 28 |
| 26 | 32 |
| 27 | 94 |
| 28 | 88 |
| 29 | 82 |
| 30 | 86 |
| 31 | 85 |
| 32 | 85 |

# Supplementary Material: 9

Palaeocurrent data from trough axis of Gandi area (14°18´25.34″ N, 78°28´ 36.52″ E) representing rose diagram Fig 4.6 in the chapter 4.

| Number | Palaeocurrent Direction (in degree) |
|---|---|
| 1 | 70 |
| 2 | 72 |
| 3 | 68 |
| 4 | 72 |
| 5 | 74 |
| 6 | 75 |
| 7 | 71 |
| 8 | 76 |
| 9 | 71 |
| 10 | 68 |
| 11 | 69 |
| 12 | 66 |
| 13 | 68 |
| 14 | 68 |
| 15 | 69 |
| 16 | 55 |
| 17 | 54 |
| 18 | 56 |
| 19 | 55 |
| 20 | 54 |
| 21 | 55 |
| 22 | 58 |
| 23 | 36 |
| 24 | 24 |
| 25 | 28 |
| 26 | 32 |
| 27 | 94 |
| 28 | 88 |
| 29 | 82 |
| 30 | 86 |
| 31 | 85 |
| 32 | 85 |

# Supplementary Material: 10

Palaeocurrent data from aeolian cross bedding of Kanampalle area (14°18´25.34″ N, 78°28´ 36.52″ E) representing rose diagram Fig 4.7 in the chapter 4.

| Number | Palaeocurrent Direction (in degree) |
|---|---|
| 1 | 200 |
| 2 | 205 |
| 3 | 206 |
| 4 | 210 |
| 5 | 220 |
| 6 | 212 |
| 7 | 204 |
| 8 | 206 |
| 9 | 208 |
| 10 | 214 |
| 11 | 165 |
| 12 | 168 |
| 13 | 236 |
| 14 | 238 |
| 15 | 242 |
| 16 | 244 |
| 17 | 184 |
| 18 | 186 |
| 19 | 185 |
| 20 | 184 |
| 21 | 216 |
| 22 | 218 |
| 23 | 222 |
| 24 | 238 |
| 25 | 224 |
| 26 | 216 |
| 27 | 232 |
| 28 | 230 |
| 29 | 264 |
| 30 | 272 |
| 31 | 211 |
| 32 | 185 |
| 33 | 184 |

# Supplementary Material: 11

Palaeocurrent data from aeolian cross bedding of Pendllimari area (14°18´25.34″ N, 78°28´ 36.52″ E) representing rose diagram Fig 4.8 in the chapter 4.

| Number | Palaeocurrent Direction (in degree) |
|---|---|
| 1 | 46 |
| 2 | 48 |
| 3 | 40 |
| 4 | 38 |
| 5 | 45 |
| 6 | 44 |
| 7 | 46 |
| 8 | 48 |
| 9 | 24 |
| 10 | 26 |
| 11 | 12 |
| 12 | 61 |
| 13 | 66 |
| 14 | 67 |
| 15 | 69 |
| 16 | 70 |
| 17 | 45 |
| 18 | 46 |
| 19 | 48 |
| 20 | 44 |
| 21 | 39 |
| 22 | 38 |
| 23 | 45 |
| 24 | 48 |
| 25 | 45 |
| 26 | 40 |
| 27 | 44 |
| 28 | 46 |
| 29 | 38 |
| 30 | 37 |
| 31 | 35 |

# Supplementary Material: 12

Accepted abstract in National Seminar on Neo Multi-disciplinary studies on the Cuddapah Basin, Andhra Pradesh & Telangana, India (NMDSCB-2016)

## Fluvial to marine transition on a Paleoproterozoic siliciclastic shelf during post-plusme thermal relaxation, Gulcheru Quartzite, Cuddapah Basin, India.

Saurav Jana*, Suparna Bose, Rahul Mitra

*Department of Geological Sciences, Jadavpur University, Kolkata-700032, India.*

*Jana.geol@gmail.com

The Paleoproterozoic Gulcheru Quartzite (30-200m thick) of Papaghni Group overlying Archean basement rocks of Cuddapah Basin, India comprises of impersistent conglomerate, wide spread Quartzite with and shale with ferruginous interbeds from base to top. Facies defined in the Gulcheru Quartzite in and around Ambakapalle(Lat-14°25′13.60′′ , Long-78°05′25.18′′), Pendllimarri (Lat-14°24′55.2′′, Long-78°36′43′′) and Gandi (Lat-14°18′25.34′′, Long-78°28′36.52′′) consisting of Clast supported conglomerate facies, Couplet facies, coarse grained massive sandstone facies, medium to fine grained trough cross stratified facies, massive granule stone facies, medium to fine grained tabular cross bedded sandstone facies, Penecontemporaneous deformed sandstone facies, Fine grained parallel laminated sandstone facies, Fine to medium grained sandstone with thin basal lag facies, MISS bearing sandstone facies and Rhythmite facies are the dominant facies of this formation. The clast supported Conglomerates characterized by bimodal, moderately sorted, sub angular to sub rounded clasts as framework embedded in a coarse grained sandy matrix. Clast size in conglomerate ranges from cobble to pebble size. Mineralogically jasper, granite and quartzite are the dominant clast fragments present in the framework. The larger clasts dominate over the smaller one in the framework. Clastering of the clasts are well observed in some places. The clasts shows a(p)a(i) fabric with average clast inclination ~$20^0$ towards north. The sandstone units characterized by trough cross stratified, tabular cross stratified or parallel laminated units with coarse to fine in grain size. Alternate layers of sandstone occur as multistory sand body. General paleo-current data from older to younger part of the succession indicate a gradual shift in flow from NW to NE direction. Several flat topped long crested multi directional wave ripples, very few current and ladder back ripple and occasional herringbone cross strata defining fluvial activity in the region whereas adhesion ripple and pin stripe lamination in translatent climbing ripple sandstone indicate Aeolian signature. Shale units characterized by red coloured thin layers of shale with well developed polygonal oscillation cracks. Overall the formation shows a fining upward as well as thinning upward sequence. Thus the facies assemblage and lithological attributes indicates a fluvio-aeolian condition which are supposed to be deposited initially in an alluvial fan environment in front of a high energy coastline, which gradually evolved to shallow marine coastal milieu where shale is deposited.

**Keywords:** Gulcheru Formation, Palaeo- proterozoic, Fluvio-aeolian, Pin stripe lamination, post-plusme thermal relaxation , Cuddapah Basin

# PUBLICATIONS

Journal of Sedimentary Environments
https://doi.org/10.1007/s43217-021-00059-2

ORIGINAL ARTICLE

# Provenance, tectonic setting and depositional environment of the Paleo-proterozoic Gulcheru Formation, Cuddapah Basin, Southern India—clues

**Saurav Jana[1] · Gopal Chakrabarti[2] · Debasish Shome[1]**

Received: 16 January 2021 / Revised: 10 April 2021 / Accepted: 18 April 2021


**Abstract**
The Paleo-proterozoic Gulcheru Formation (30–200 m thick) of Papaghni Group overlying Archean basement rocks of Proterozoic Cuddapah Basin, India is composed of conglomerate at the bottom overlain by extensive quartzite with grey shales as interbeds. Major oxides, trace and rare earth element (REE) elemental abundance gives significant information about (a) source rock including paleo-environment condition, (b) tectonic setting during deposition of sediments and (c) condition of deposition of the sediments. The high Chemical Index of Weathering (CIW) [average 97], Plagioclase Index of Alteration (PIA) [average 95] values of the Gulcheru shales suggest strong chemical weathering processes of the source rock. The $Al_2O_3$/$TiO_2$, $TiO_2$/Ni ratio, LREE/HREE ratios with negative Eu anomaly and Cu/Zn, Ni/Co,U/Th and V/Cr ratio indicate a mixed felsic igneous provenance which seems to be derived from Dharwarian Granite Gneiss. The geochemical components of V, Cr, Ni, Co, U and Th strongly suggest that these clastic rocks are deposited in an oxic condition. The discrimination plot La-Th-Sc and Th-Sc-Zr/10 suggest that the Gulcheru clastic sediments were deposited in continental island arc setting during the process of amalgamation of supercontinent Columbia. This back-arc extensional basin was formed due to the subduction of the oceanic crust underneath the Dharwar Craton. These findings have significant implications for the study about the paleo-geology of Cuddapah Basin, especially paleo-climate of Gulcheru Formation in which there are limited previous work.

**Keywords** Sedimentary basin · Paleo-proterozoic · Sediment provenance · Elemental geochemistry · Shale · Chemical Index of Alteration

## 1 Introduction

The geochemistry of fine-grained sedimentary rock like shale gives imperative data on territorial provenance characterisation, tectonic settings, weathering condition and recycling history of the sediments (Armstrong-Altrin & Verma, 2005; Armstrong-Altrin et al., 2004; Cullers, 1995; Li et al., 2008). Not only that, elemental geochemistry of shale also plays a key role to explain the paleo-environment and paleo-climate (Mir, 2015; Nagarajan et al., 2007, 2014). The present investigation looks at the geochemistry of Paleoproterozoic Gulcheru Formation of the Proterozoic Cuddapah Basin based on shale samples collected from Kanampalle territory, Andhra Pradesh, India. The motivation behind this examination is to feature the paleo-weathering, tectonic setting leads to the delineation of source rocks, extent of weathering in the provenance and depositional setup in detail. These components are assessed utilizing elemental abundance, weathering indices and elemental ratio in contrast with Post-Archean Australian Shale (PAAS) as evaluated from the representative surface rocks.

Previous works on the Gulcheru Formation typically concentrate on sedimentological aspects with limited geochemistry of clastics (essentially sandstone and conglomerate) which broadly indicate the depositional environment, tectonic evolution of this Formation (Chakrabarti & Shome, 2007). The limited geochemistry as reported by Chakrabarti et al. (2009) indicates a heterogeneous source rock with felsic influence for the sediments of Gulcheru Formation. The

Communicated by M. V. Alves Martins

✉ Saurav Jana
jana.geol@gmail.com

[1] Department of Geological Sciences, Jadavpur University, Kolkata 700032, India

[2] Government of West Bengal, Kolkata 700091, India

Published online: 04 May 2021

authors cited above further depict the recycled nature of the sediments and a cold climatic condition during deposition. So detailed geochemistry of shale illuminate the information about source rock, tectonic setting and environment of deposition of the Paleo-Proterozoic Gulcheru Formation.

## 2 Geologic background

The crescent-shaped intracratonic Cuddapah Basin (Fig. 1) of peninsular Indian shield is the second largest (after Vindhyan Basin) Proterozoic sedimentary basin of India. The eastern margin of the basin shows a curvilinear thrusted contact with the Eastern Ghat Mobile belt. The west, south and northern part is surrounded by an Archean granitic and Gneissic terrain. This boundary of the basin represents a structurally undisturbed geological contact, characterized in the literature as Eparchean Unconformity (Pascoe, 1973).

The Papaghni, Chitravati and Nallamalai groups are the subgroups of the Cuddapah Supergroup and each group seperated by each other with regional unconformities (Table 1). The Papaghni Group rocks exposed in a very thin arcuate strip along the western and southern part of the basin (Fig. 2a). The Chitravati group rocks exposed in the western part of the basin (Fig. 2b).The Nallamalai Group rocks, which are highly disturbed, folded and faulted, occupy the

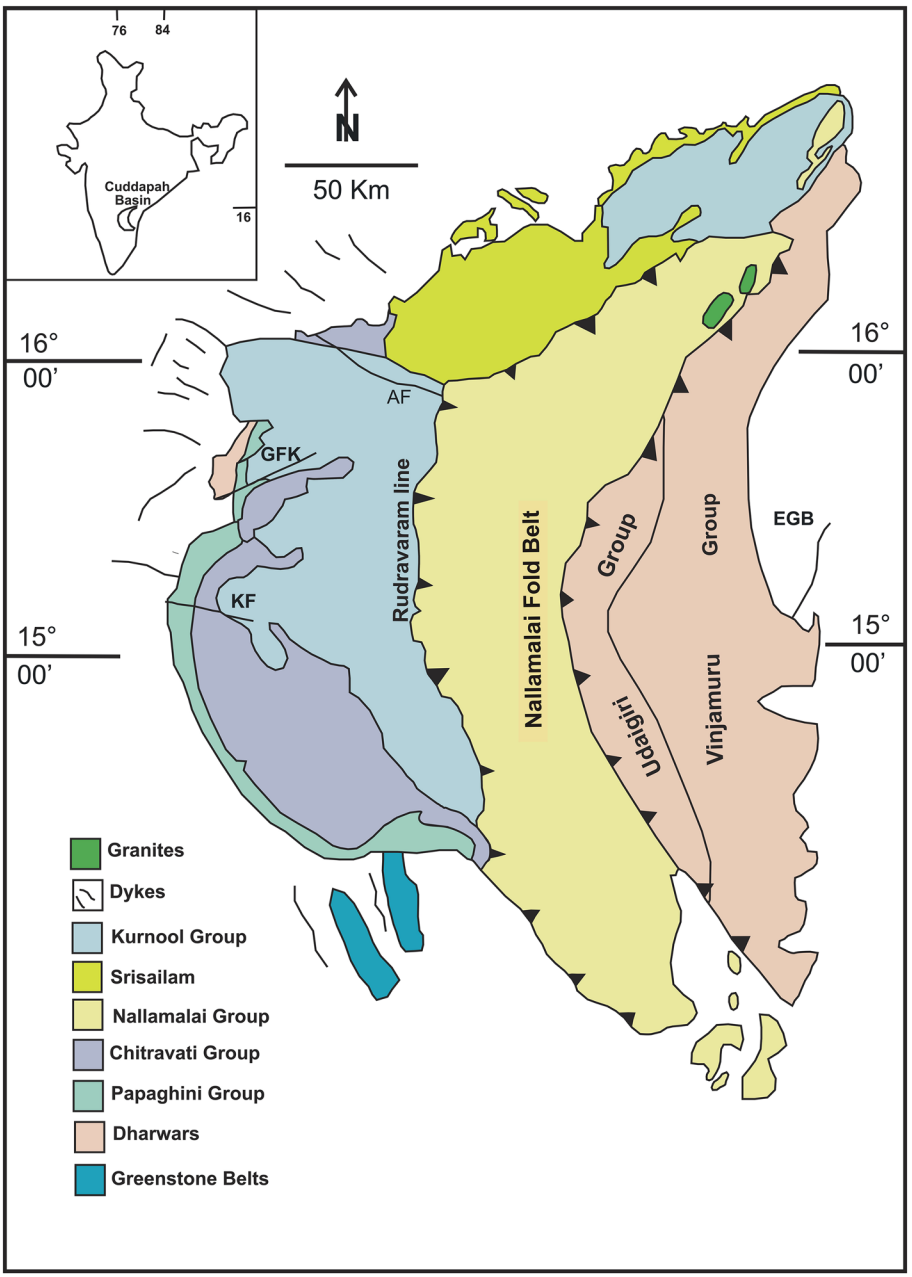


**Fig. 1** Geological map of the Cuddapah Basin (modified after Geological survey of India 1:2000000 map, 1988)

**Table 1** Stratigraphy of the Cuddapah Basin (after Ramam and Murthy, 1997)

| Group | Formation | Lithology | Age |
|---|---|---|---|
| Kurnool | Nandyal (50–100 m) | Shale | Neoproterozoic |
| | Koikuntala (15–50 m) | Limestone | |
| | Paniam (10–35 m) | Quartzite | |
| | Owk (10–15 m) | Shale | |
| | Narji (100–200 m) | Limestone | |
| | Banganapalli (10–15 m) | Quartzite with Conglomerate | |
| Cuddapah Supergroup | | | |
| | Unconformity | | |
| | Srisailam (300 m) | Quartzite | |
| | Unconformity | | |
| Nallamalai | Cumbum (2000 m) | Phyllite, Shale, Quartzite, Dolomite | Mesoproterozoic |
| | Bairenkonda (5500 m) | Quartzite, | |
| | Unconformity | | |
| Chitravati | Gandikota (300 m) | Quartzite, Shales | |
| | Tadpatri (4600 m) | Shale, Quartzite, dolomite | |
| | Pulivendla (1–75 m) | Conglomerate, Quartzite | |
| | Unconformity | | |
| Papaghni | Vempalle (1900 m) | Dolomite, chert, Basic flows and Intrusive | Paleoproterozoic |
| | Gulcheru (30–210 m) | Conglomerate, quartzite and and shale | |
| | Unconformity | | |
| Dharwar Craton | | | Archean |

eastern part of this basin (Fig. 2b). The central part of the basin is essentially occupied by the Kurnool Group of rocks (Fig. 1).

The Cuddapah Basin along with other basins of Peninsular India has been described as rift basin resulted from crustal doming, erosion and subsidence (Drury, 1984; Jain et al., 1995; Meijerinket al., 1984). On the basis of geophysical investigation Singh and Mishra, (2002) suggested that the Cuddapah Basin represents a peripheral foreland basin evolved through Proterozoic continent-continent collision of Indian Craton with Antartica block during the amalgamation of the supercontinent Columbia (1.9 Ga; Matin, 2015). Each of the three subgroups of the Cuddapah Basin begins with basal quartzite followed by finer shale upward representing prominent fining upward sequence, which indicate a shallow marine shelf depositional set-up (Patranabis-Deb et al., 2012).

## 3 Age

Magmatism associated with Papaghni group of rocks helps us to reconstruct the age of the Gulcheru Formation. Urenium mineralisation of the Vempalle formation shows 1756 ± 29 Ma age from Pb–Pb radiometric dating (Zachariah et al., 1999). Rb/Sr isochron age of clinopyroxene and biotite from an analogous sill, ranging from 1811 to 1831 Ma age, indicates that the intrusion probably going to be the late stage of sedimentation of the Papaghni and also the Chitravati groups (Murthy et al., 1987). K–Ar radiometric dating of mafic flow from upper Vempalle formation shows 1814 ± 71 Ma (Anand et al., 2003). So, with the combination of previous data we can conclude that the Gulcheru Formation was deposited within late Paleoproterozoic time.

## 4 Materials and methods

Kanampalle stratigraphic section (Lat-14° 25′ 13.60″, Long-78° 05′ 25.18″) (Gulcheru Formation) records the preservation of various types of shale, sandstone and conglomerate. Fresh representative samples were carefully collected from the middle and upper part (7 m interval) of this section for petrographic and geochemical study. After careful observation under microscope, twelve samples of shale were selected for geochemical analysis.

The major elements concentration was acquired by Bruker model S4 Pioneer sequential wavelength-dispersive X-ray fluorescence (XRF) spectrometer. Rare earth element (REE) and trace elements were analysed by a high resolution inductively coupled plasma mass spectrometer (HR-ICPMS) in which GSR-5 was utilized as the standard. The analytical precision for major oxides by XRF is estimated to be better than 8%. Minor and rare earth element analysis with

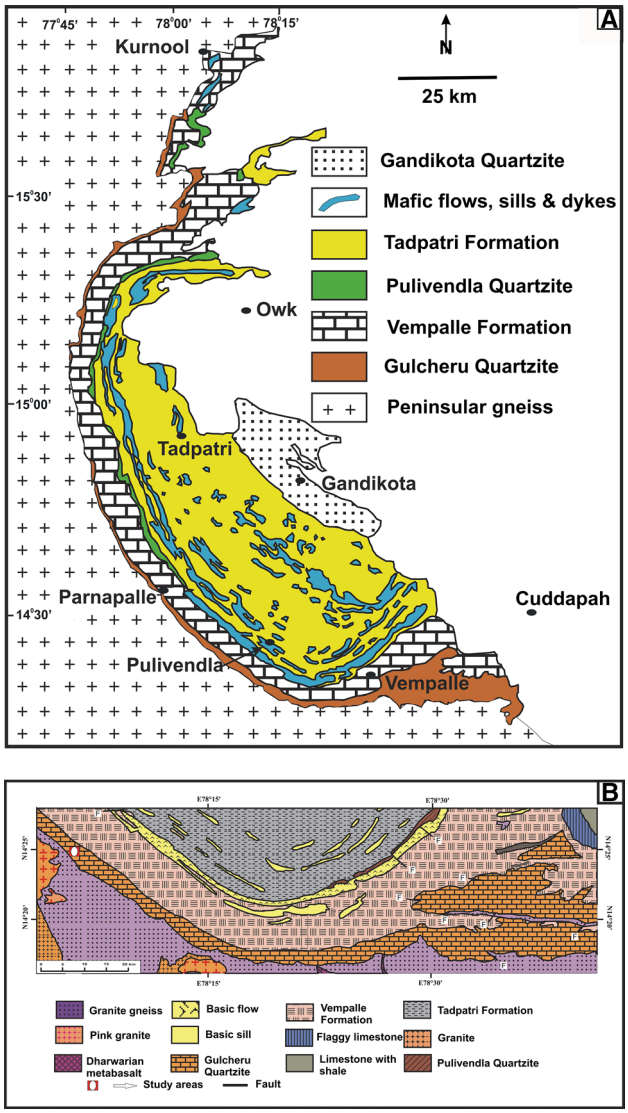


**Fig. 2** **a** Geological map of western Cuddapah basin showing the lower Cuddapah group of rocks (Saha & Tripathy, 2012); **b** Detailed geological map of the Cuddapah Supergroup showing Gulcheru Formation and the study area

international standard GSR-5 indicated an analytical precision generally better than 6% for all elements.

Chemical Index of Alteration (CIA; Nesbitt & Young, 1984) is important to decide the level of weathering of the source rock. This index estimates the degree of change from feldspar to aluminous weathering items. The CIA estimates are resolved utilizing atomic extent from the equation:

$$\mathrm{CIA} = \left[\mathrm{Al_2O_3}/\left(\mathrm{Al_2O_3} + \mathrm{CaO^*} + \mathrm{Na_2O} + \mathrm{K_2O}\right)\right] \times 100$$

where $\mathrm{CaO^*}$ represents the CaO in silicates only.

Weathering impacts also can be assessed by the molecular proportions of the oxides components, utilizing the equation (based on Harnois, 1988):

Chemical Index of Weathering(CIW)

$$= \left[\mathrm{Al_2O_3}/\left(\mathrm{Al_2O_3} + \mathrm{CaO^*} + \mathrm{Na_2O}\right)\right] \times 100$$

where $\mathrm{CaO^*}$ is the CaO residing only in the silicate fraction.

Plagioclase Index of Alteration (PIA) reflects weathering of plagioclase feldspars and is characterized by the condition

$$\mathrm{PIA} = \left[\left(\mathrm{Al_2O_3} - \mathrm{K_2O}\right)/\left(\mathrm{Al_2O_3} + \mathrm{Cao} * + \mathrm{Na_2O} - \mathrm{K_2O}\right)\right] \times 100$$

where all components are in molecular proportions and $\mathrm{CaO^*}$ represents CaO in silicate fractions.

The Index of compositional variability (ICV; Cox et al., 1995) is the indicator of original composition and compositional maturity in clastic sedimentary rock.

$$\mathrm{ICV} = \left[\left(\mathrm{CaO} + \mathrm{K_2O} + \mathrm{Na_2O} + \mathrm{Fe_2O_3^{(t)}} + \mathrm{MgO} + \mathrm{MnO} + \mathrm{TiO_2}\right)/\mathrm{Al_2O_3}\right],$$

$\mathrm{Fe_2O_3^{(t)}}$ indicates total iron and CaO includes all sources of Ca.

## 5 Results and discussion

### 5.1 Petrography

Lithologically, the Gulcheru Formation consists of three units from bottom to top, Conglomerate, Quartzite and Shale. The lower part is represented by conglomerate with widespread quartzite, the middle part of the succession is dominated by sandstone, shale within the band of siltstone. And the upper part siliceous mudstone gradually converted to carbonate mudstone. And the upper part, siliceous mudstone is gradually converted to carbonate mudstone. Overall shale layers alternate with sandstone and siltstone bands with occasional ferruginous banding (Fig. 3a–l) and locally vertical fault plane is also found in some samples under microscope. The detailed petrography is described in Table 2.

### 5.2 Major element concentrations

The geochemical analysis of 12 shale samples from Kanampalle section indicate that, the $\mathrm{SiO_2}$ content varies from 50.2 to 67.58 wt% and $\mathrm{Al_2O_3}$ content from 8.51 to 22.64 wt% (Table 3). All the major oxides compared with the Post Archean Australian Shale (PAAS) (Amajor, 1987; Taylor & McLennan, 1985) shows more or less similar ratio except MgO enrichment and $\mathrm{Na_2O}$ depletion.

Binary variation diagrams of $\mathrm{SiO_2}$ versus $\mathrm{TiO_2}$, $\mathrm{Al_2O_3}$, $\mathrm{Na_2O}$ and $\mathrm{K_2O}$ (Fig. 4a, b, g and h respectively) and $\mathrm{Al_2O_3}$ versus $\mathrm{TiO_2}$, $\mathrm{Fe_2O_3}$, $\mathrm{Na_2O}$, $\mathrm{K_2O}$ (Fig. 5a, b, f and g respectively) shows similar linear trends. However $\mathrm{Fe_2O_3}$, MnO, MgO, CaO and $\mathrm{P_2O_5}$ (Fig. 4c, d, e, f and i, respectively) and MnO, MgO, CaO and $\mathrm{P_2O_5}$ (Fig. 5c, d, e and

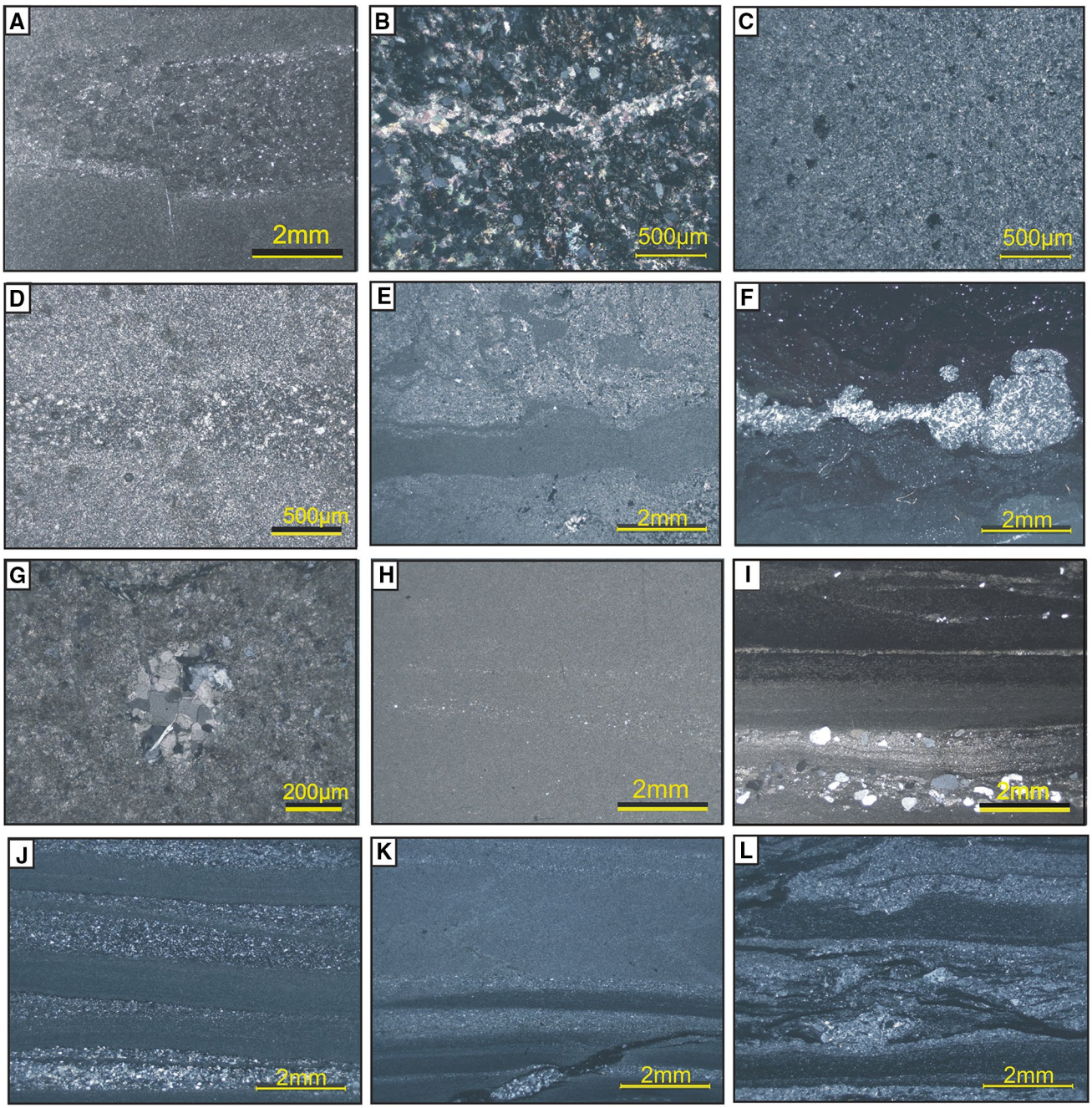


**Fig. 3** Microscopic features of the Gulcheru shale samples used for geochemical analysis. **a** KM-1 sample: dominated by shale with thick siltstone layer bounded in between shale layer with a vertical fault plane; **b** M-1 sample: dominated by clay minerals with mica and ferruginous materials; **c** M-2 sample: dominated by siltstone with some mica and plagioclase feldspar; **d** M-3 sample: thin siltstone laminae within the shale showing sharp boundary contact in between them; **e** KU-2 sample: graded silt and shale alternation showing folds; **f** KU-3 sample: graded silt and shale alternation showing folds; **g** KU-4 sample: thick layer of shale with clustering of quartz grains in the middle. **h** KU-5 sample: thick layer of massive shale; **i** M-4 sample: graded siltstone and shale with normal grading; **j** KU-7 sample: Graded Clay layers with some lenticular silt layer; **k** M-5 sample: dominated by shale with few thin layers of siltstone in the lower part; **l** KU-10 sample: graded shale and siltstone layer with some folded ferruginous layers

h, respectively) display a negative linear trend with $SiO_2$ and $Al_2O_3$, respectively. Values of A $SiO_2/Al_2O_3$ ratios ≥ 5 represent mature chemical components of rock (Roser & Korsch, 1986, 1988). The $SiO_2/Al_2O_3$ proportions of Gulcherushale are moderate (2.42–6.17, average = 4.39), indicating mature chemical components (Hossain et al., 2014). The bivariate diagram Log ($SiO_2/Al_2O_3$) versus

**Table 2** Petrographic description of the selected shale samples from Gulcheru Formation

| Sample no | Rock type | Petrographic description | Figure no |
|---|---|---|---|
| KM-1 | Alteration of Shale and siltstone | Shale sample from lower middle part of the section is interbedded with in a thin band siltstone and a thick layer of sandstone. This is a fine grained dark grey to black coloured quartzo-feldspathic rock which is highly silicified and often traversed by 3–5 mm thick quartz veins. Microscopically this shale sample is dominated by shale with thick siltstone layer bounded in between shale layer with a vertical fault plane | Fig. 4a |
| M-1 | Shale with alternate sandstone layer | The shale sample characterized by reddish brown colour alternating with buff coloured siltstone. The rock is partially weathered and ferrugination occur along the fracture planes. Overall the slide shows the dominance of clay minerals with very few mica and ferruginous materials. Compaction deformation is minimal, as evidenced by common undeformed micas | Fig. 4b |
| M-2 | Shale | Sample represents greyish black shale with few patches of mica. Principal constituent minerals are very fine grained clay with profuse mica. Under the microscope, sample is dominated by siltstone with some mica and plagioclase feldspar | Fig. 4c |
| M-3 | Shale with feruugiginous bands | Sample represents greyish shale with thin siltstone laminae. This is a fine grained grey coloured rock composed of alternation of 2–3 mm. thick layers of very fine grained quartzo-feldspathic mineral and also evidenced from the development of ferruginous film along fracture planes. Microscopically this sample shows dominance of clay minerals, quartz, muscovite, and biotite | Fig. 4d |
| KU-2 | Shale with distorted ferruginous laminae | Sample characterized by dark grey to brown coloured shale with distorted ferruginous laminae. The siltstone, muscovite and boitite constitute thick bands alternating with clay mineral rich light coloured bands. Under the microscope, this shale sample is dominated by graded silt and shale couplet with wavy crinkly laminae of shale | Fig. 4e |
| KU-3 | Shale and siltstone alteration | Sample represents a dirty grey coloured very fine grained one, partially weathered with development of ferruginous layers along the fracture surfaces. Microscopically this sample is dominated by graded silt and shale couplet with wavy crinkly laminae of siltstone | Fig. 4f |
| KU-4 | Massive Shale with few larger clasts | Sample characterized by red coloured thick layer of massive shale. Microscopically this sample shows a layer of shale with a clustering of quartz in the middle | Fig. 4g |
| KU-5 | Massive Shale | Sample also characterized by red coloured thick layer of massive shale. Microscopically this sample shows a thick layer of massive shale | Fig. 4h |
| M-4 | Shale alteration with sandstone | This shale sample is characterized by reddish brown shale with thin alternate layers of siltstone. This is a fine grained rock composed principally of micaceous and arenaceous shale, alternating with very fine grained quartz layer. Both quartz and shale bands are oriented in a preferred direction but it is often discontinuous in nature. Microscopically this sample shows normal grading of siltstone and shale. Fine grained sandstone channels interbedded within the mudstone layers | Fig. 4i |
| KU-7 | Shale and siltstone alteration | Sample characterized by greyish shale with thin layers of siltstone alternating with shale. The shale forms thin laminations alternating with fine and very fine sized sands and thereby forms a grain size banding in the rock. Microscopically this sample shows Graded Silt/Clay couplets with some lenticular silt layer | Fig. 4j |
| M-5 | Massive shale with few alteration of siltstone | Sample characterized by dark grey shale with thin layers of siltstone alternating with shale in the bottom part. Some larger size clast present in lower part with overall fining upward sequence | Fig. 4k |
| KU-10 | Shale | Sample characterized by greyish shale with thin layers of siltstone alternating with shale. Microscopically this sample shows Graded Silt/Clay couplets with some alternating silt layer in the lower part | Fig. 4l |

**Table 3** Major elements (%) concentration for shales of the Gulcheru Formation, Cuddapah Basin with average composition of PAAS (Taylor & McLennan, 1985)

| | KM-1 | M-1 | M-2 | M-3 | KU-2 | KU-3 | KU-4 | KU-5 | M-4 | KU-7 | M-5 | KU-10 | PAAS (Taylor & McLennan, 1985; McLennan, 2001) |
|---|---|---|---|---|---|---|---|---|---|---|---|---|---|
| $SiO_2$ | 61.88 | 57.42 | 63.39 | 62.66 | 50.2 | 57.97 | 60.55 | 60.17 | 67.58 | 61.01 | 54.8 | 52.54 | 62.80 |
| $TiO_2$ | 0.49 | 0.71 | 0.83 | 0.63 | 0.43 | 0.4 | 0.5 | 0.52 | 0.44 | 0.45 | 0.79 | 0.38 | 1.00 |
| $Al_2O_3$ | 13.17 | 19.45 | 18.3 | 16.43 | 9.94 | 10.09 | 13.42 | 13.34 | 14.84 | 12.49 | 22.64 | 8.51 | 18.90 |
| MnO | 0.02 | 0.01 | 0.01 | 0.02 | 0.04 | 0.09 | 0.05 | 0.17 | 0.02 | 0.07 | 0.01 | 0.09 | 0.11 |
| $Fe_2O_3$ | 4.34 | 8.61 | 4.67 | 5.02 | 7.04 | 3.75 | 2.27 | 7.34 | 3.67 | 3.67 | 6.52 | 5.12 | 6.50 |
| CaO | 5.12 | 0.08 | 0.16 | 0.2 | 3.8 | 4.04 | 1.34 | 0.26 | 0.28 | 0.67 | 0.18 | 4.89 | 1.3 |
| MgO | 3.07 | 1.85 | 1.83 | 2.89 | 14.93 | 8.87 | 9.24 | 7.44 | 2.58 | 11.14 | 1.63 | 12.75 | 2.20 |
| $Na_2O$ | 0.06 | 0.23 | 0.2 | 0.23 | 0.07 | 0.07 | 0.08 | 0.07 | 0.19 | 0.07 | 0.33 | 0.05 | 1.20 |
| $K_2O$ | 6.53 | 6.28 | 6.28 | 5.5 | 3.12 | 5.77 | 7.2 | 6.68 | 4.77 | 5.74 | 7.56 | 3.35 | 3.70 |
| $P_2O_5$ | 0.1 | 0.06 | 0.08 | 0.11 | 0.13 | 0.19 | 0.15 | 0.07 | 0.15 | 0.17 | 0.11 | 0.34 | 0.16 |
| LOI | 4.64 | 5.14 | 3.48 | 5.66 | 9.79 | 8.39 | 4.29 | 3.08 | 5.12 | 3.76 | 4.85 | 11.27 | |
| Total | 99.41 | 99.84 | 99.23 | 99.3 | 99.47 | 99.63 | 99.06 | 99.12 | 99.64 | 99.24 | 99.42 | 99.28 | |

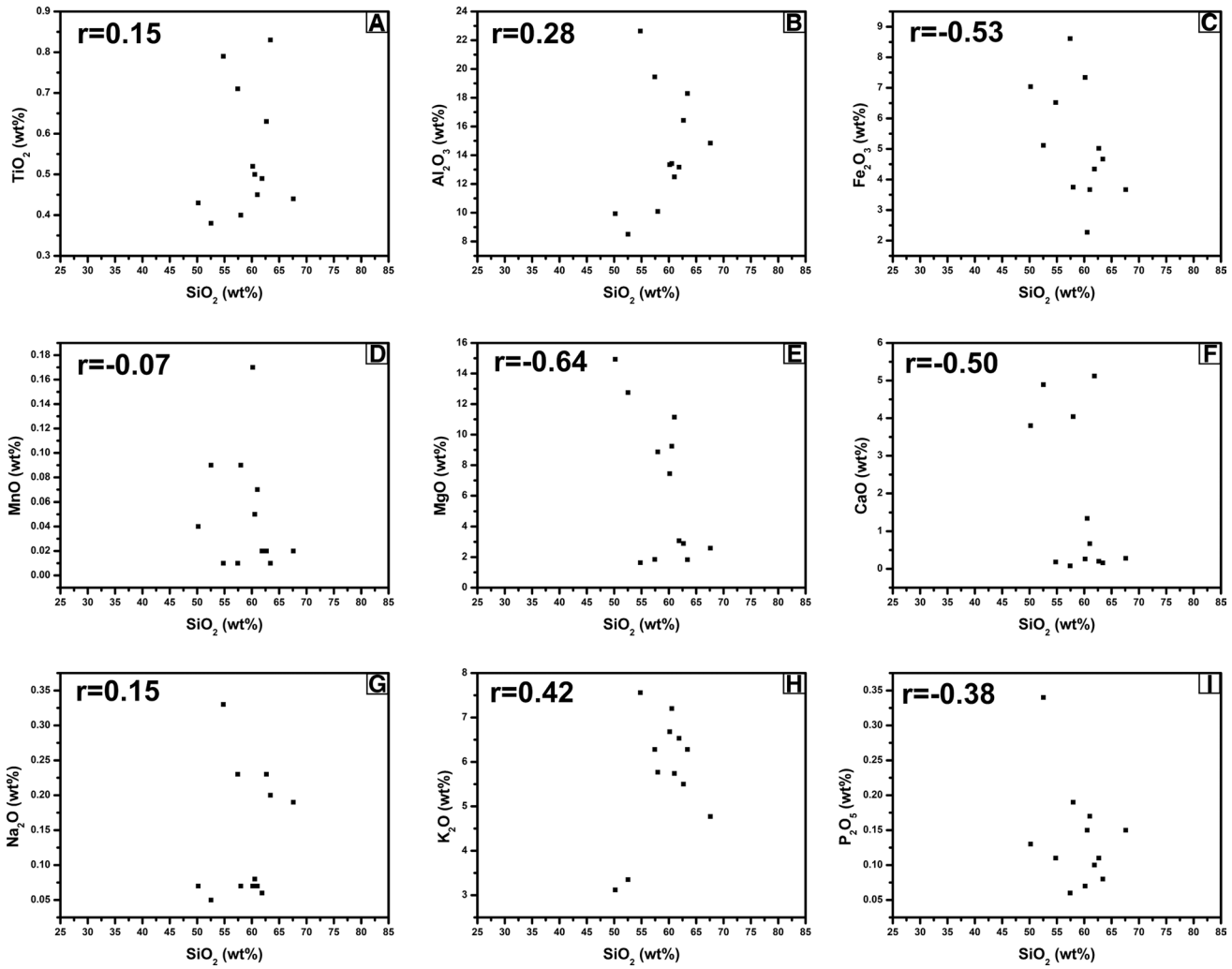


**Fig. 4** Binary plots of the Gulcheru siliciclastic rocks versus $SiO_2$

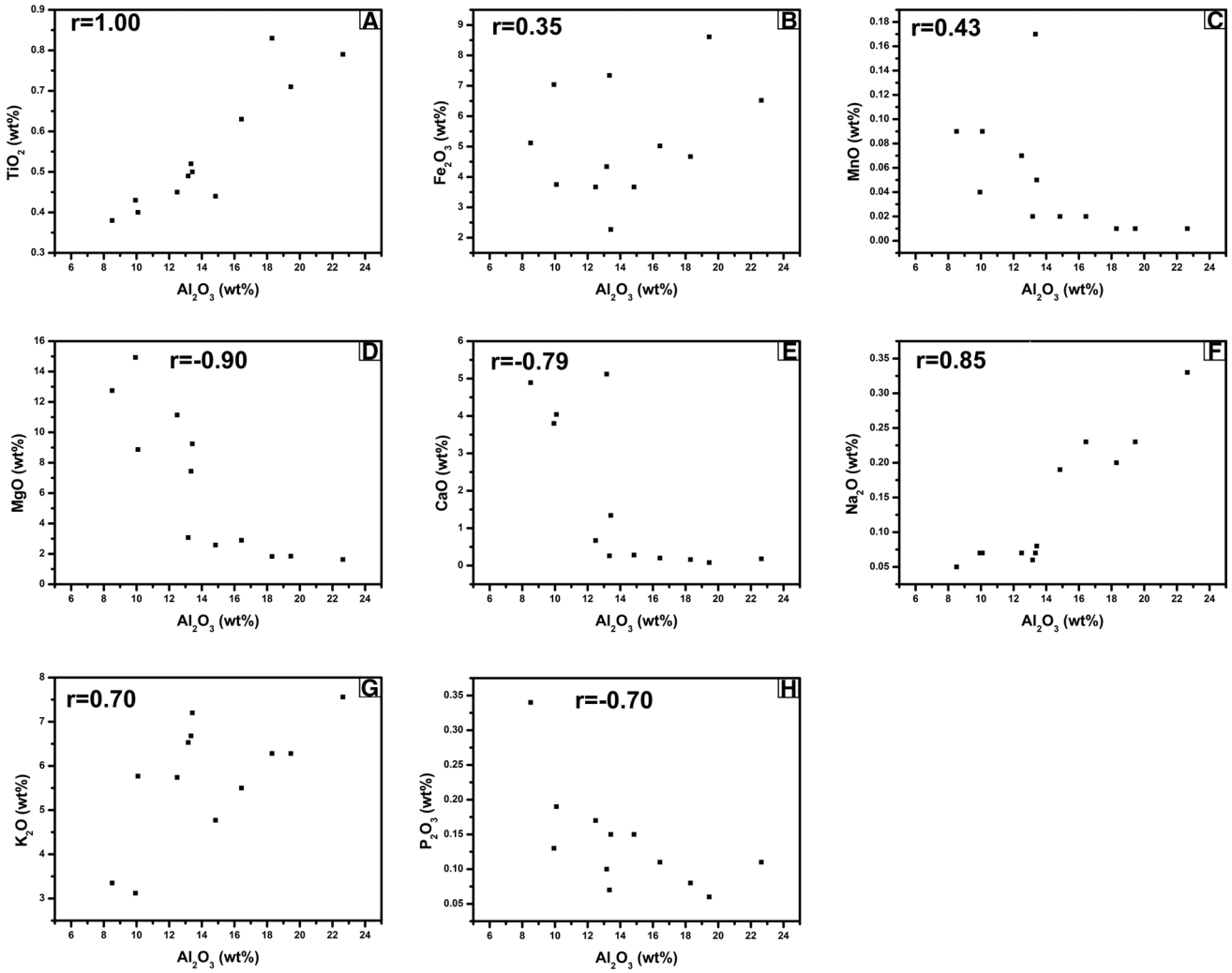


**Fig. 5** Binary plots of the Gulcheru siliciclastic rocks versus $Al_2O_3$

Log ($Fe_2O_3/K_2O$) (Fig. 6; Herron, 1988) shows all samples representing the shale and greywacke composition.

The ternary diagram $Fe_2O_3$–$K_2O$–$Al_2O_3$ (Fig. 7) shows that all shale samples are plotted near the $Al_2O_3$ apex, which indicates the dominance of $Al_2O_3$ in the parent body. The information from $K_2O/Al_2O_3$ proportion suggests clay minerals (0.0–0.3) and feldspar (0.3–0.6) enrichment in the source rock. Gulcheru shales $K_2O/Al_2O_3$ ratio ranges from 0.31to 0.59 and these values are a strong indicator of feldspar dominance in the parent rock.

The CIA calculated for the analysed shales have values ranging between 62.48 and 73.37 (average 68.14). The CIW value of the Gulcheru shale samples ranges from 97.33 to 98.94 (average 98.06). Gulcheru Formation clastic sediments show PIA values with ranges from 93.26 to 96.86 (average 95.18). The ICV value of Gulcheru Formation Shales varies from 0.75 to 3.12 (average 1.57).

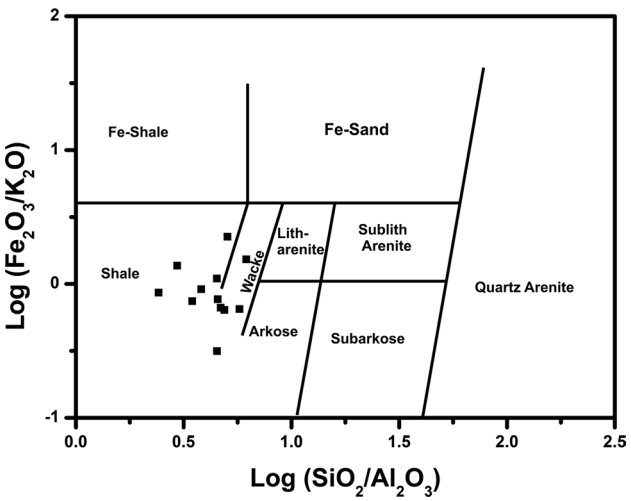


**Fig. 6** Binary diagram: log ($Fe_2O_3/K_2O$) versus log ($SiO_2/Al_2O_3$) diagram of Herron (1988)

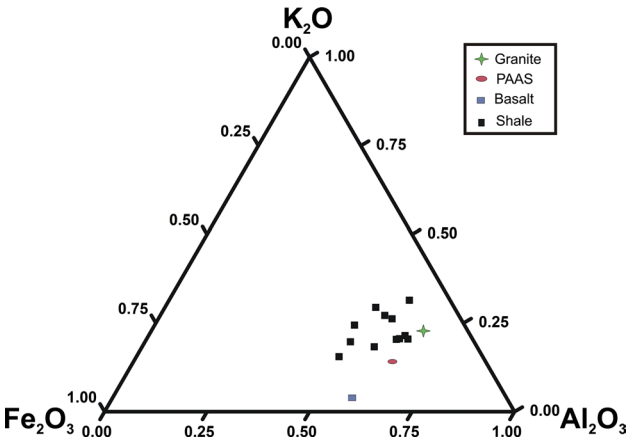


**Fig. 7** Major element distribution in the Gulcheru shales in $K_2O$–$Fe_2O_3$–$Al_2O_3$ ternary diagram. Granite, basalt and PAAS are defined from Condie (1993) and Taylor and McLennan (1985) respectively

## 5.3 Trace element concentrations

The trace elements were normalised with PAAS values (Bhatia & Crook, 1986; Taylor & McLennan, 1995) and show depletion of Cs, Pb, Sr, V, Y, Zr, Nb and Th, and enrichment of Ba, Rb, Cr and U (Fig. 8a). The elements with strong field strength, such as Hf-Zr element pair does not alter after weathering due to the immobility and insolubility nature (Long et al., 2012). The high field strength elements, as Hf–Zr element pair does not differentiate during the weathering process due to their immobility and insolubility nature (Long et al., 2012). Zr/Hf ratio of the Gulcheru shale samples varies from 32.82 to 35.68 with an average 33.83 (Table 4), which is similar to the Zr/Hf ratio (33, Crichton & Condie, 1993; Taylor & McLennan, 1985) of upper continental crust (UCC).

The presence of Sr precipitation in the open marine basin or saline lake indicates high solubility of $SrSO_4$. So, generally the proportion of Sr/Ba steadily increases from the coast to the centre of the lake/seal. The Sr/Ba ratio suggests the salinity of the water, and Sr/Ba ratios < 0.6, 0.6–1.0,

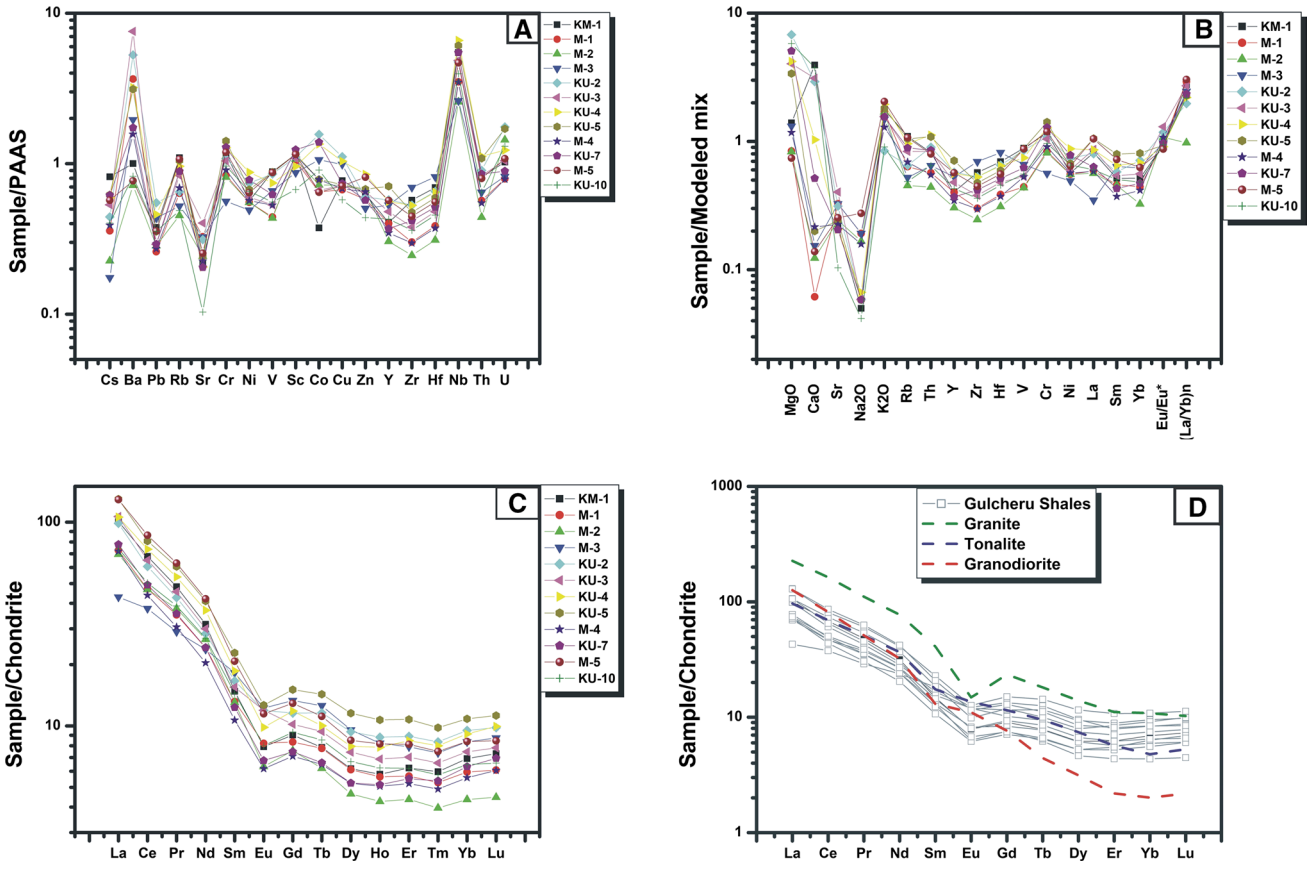


**Fig. 8** **a** PAAS normalized trace element pattern distribution; **b** major and trace elements normalized to modelling mix results (Wang & Zhou, 2013). **c** Chondrite normalized REE elements pattern distribution in Gulcheru shale samples. PAAS and Chondrite normalized values are defined from Taylor and McLennan, (1985); **d** Chondrite-normalized REE pattern of potential source rocks (Granodiorite and tonalite) of Eastern Dharwar Craton with Gulcheru Formation shales

**Table 4** Trace element (ppm) concentration for shales of the Gulcheru Formation, Cuddapah Basin with average composition of PAAS (Taylor & McLennan, 1985)

| | KM-1 | M-1 | M-2 | M-3 | KU-2 | KU-3 | KU-4 | KU-5 | M-4 | KU-7 | M-5 | KU-10 | PAAS (Taylor & McLennan, 1985) |
|---|---|---|---|---|---|---|---|---|---|---|---|---|---|
| Sc | 18.50 | 18.43 | 13.94 | 18.13 | 17.70 | 17.38 | 15.36 | 18.51 | 16.69 | 19.81 | 17.15 | 10.76 | 16 |
| V | 123.85 | 122.21 | 92.39 | 74.22 | 119.58 | 74.60 | 104.20 | 122.96 | 61.90 | 87.27 | 60.94 | 77.89 | 150 |
| Cr | 116.36 | 118.99 | 56.22 | 90.69 | 108.25 | 104.27 | 127.78 | 141.60 | 83.74 | 128.44 | 81.35 | 96.34 | 110 |
| Co | 7.49 | 12.93 | 21.20 | 15.65 | 31.31 | 13.28 | 27.04 | 15.70 | 12.98 | 27.77 | 14.45 | 18.14 | 23 |
| Ni | 33.98 | 38.51 | 29.50 | 34.06 | 44.54 | 35.94 | 52.58 | 40.34 | 33.23 | 46.85 | 33.23 | 39.31 | 55 |
| Cu | 38.60 | 35.58 | 49.47 | 34.08 | 55.59 | 36.04 | 51.92 | 36.31 | 33.58 | 36.89 | 35.94 | 28.77 | 50 |
| Zn | 53.45 | 69.22 | 42.94 | 55.22 | 50.94 | 55.46 | 72.24 | 57.56 | 49.34 | 48.66 | 56.56 | 37.21 | 85 |
| Ga | 15.32 | 18.24 | 8.49 | 11.42 | 20.32 | 12.14 | 18.46 | 17.72 | 9.62 | 17.46 | 9.12 | 13.13 | 17.5 |
| Rb | 175.29 | 171.42 | 83.59 | 110.40 | 104.03 | 133.69 | 153.81 | 167.89 | 101.74 | 142.40 | 72.45 | 78.07 | 160 |
| Sr | 43.57 | 50.80 | 65.22 | 45.02 | 62.56 | 80.69 | 41.20 | 48.21 | 65.45 | 40.95 | 48.53 | 20.67 | 200 |
| Y | 10.94 | 15.37 | 14.31 | 9.35 | 15.51 | 12.96 | 15.11 | 19.12 | 10.83 | 9.99 | 8.22 | 11.57 | 27 |
| Zr | 120.08 | 93.82 | 145.91 | 62.36 | 111.42 | 79.64 | 110.85 | 99.76 | 63.32 | 87.88 | 51.61 | 75.76 | 210 |
| Nb | 10.43 | 8.89 | 4.98 | 6.60 | 9.04 | 9.22 | 12.53 | 11.59 | 6.65 | 10.40 | 4.89 | 7.53 | 19 |
| Cs | 4.91 | 3.43 | 1.05 | 2.34 | 2.66 | 3.20 | 3.56 | 3.72 | 2.15 | 3.70 | 1.36 | 2.42 | 15 |
| Ba | 651.78 | 499.98 | 1271.09 | 1018.80 | 3430.09 | 4922.53 | 2084.29 | 2031.82 | 2376.85 | 1127.72 | 466.58 | 536.10 | 650 |
| Hf | 3.47 | 2.78 | 4.09 | 1.86 | 3.27 | 2.40 | 3.23 | 2.97 | 1.93 | 2.57 | 1.56 | 2.28 | 5 |
| Ta | 0.97 | 0.85 | 0.54 | 0.65 | 0.96 | 0.93 | 1.18 | 1.09 | 0.66 | 0.98 | 0.52 | 0.77 | 1.28 |
| Pb | 7.54 | 7.14 | 8.70 | 5.43 | 11.01 | 5.81 | 9.21 | 7.09 | 5.20 | 5.83 | 5.69 | 7.11 | 20 |
| Th | 11.93 | 11.65 | 9.44 | 8.00 | 13.16 | 12.18 | 16.35 | 15.84 | 8.31 | 12.47 | 6.44 | 9.46 | 14.60 |
| U | 3.18 | 3.35 | 2.55 | 2.44 | 5.44 | 3.24 | 3.81 | 5.29 | 2.46 | 2.77 | 4.46 | 4.04 | 3.1 |
| CIA | 64.44 | 72.02 | 71.30 | 71.00 | 73.37 | 60.90 | 62.48 | 64.13 | 71.94 | 65.96 | 70.95 | 69.18 | 70.38 |
| CIW | 98.52 | 96.25 | 96.57 | 95.59 | 97.73 | 97.76 | 98.07 | 98.3 | 95.95 | 98.18 | 95.42 | 98.1 | 82.72 |
| PIA | 96.86 | 94.35 | 94.68 | 93.26 | 96.6 | 94.34 | 95.53 | 96.36 | 93.93 | 96.46 | 93.01 | 96.74 | 79.05 |
| ICV | 1.49 | 0.91 | 0.75 | 0.88 | 2.96 | 2.27 | 1.54 | 1.68 | 0.80 | 1.74 | 0.75 | 3.12 | 0.88 |
| $K_2O/Al_2O_3$ | 0.49 | 0.49 | 0.33 | 0.33 | 0.31 | 0.31 | 0.53 | 0.53 | 0.32 | 0.59 | 0.33 | 0.36 | 0.20 |
| $Al_2O_3/TiO_2$ | 26.87 | 27.39 | 22.32 | 26.07 | 23.11 | 25.22 | 26.84 | 25.65 | 33.72 | 27.75 | 28.65 | 22.39 | 19.09 |
| La/Sc | 1.68 | 2.17 | 0.95 | 1.23 | 1.72 | 1.90 | 2.13 | 2.17 | 1.35 | 1.21 | 1.25 | 2.13 | 2.39 |
| Th/Sc | 0.64 | 0.63 | 0.67 | 0.44 | 0.74 | 0.70 | 1.06 | 0.85 | 0.49 | 0.62 | 0.37 | 0.87 | 0.91 |
| Co/Th | 0.62 | 1.10 | 2.24 | 1.95 | 2.37 | 1.09 | 1.65 | 0.99 | 1.56 | 2.22 | 2.24 | 1.91 | 1.58 |
| Th/U | 3.75 | 3.48 | 3.70 | 3.27 | 2.42 | 3.75 | 4.28 | 2.99 | 3.37 | 4.50 | 1.44 | 2.33 | 4.76 |
| Cu/Zn | 0.72 | 0.51 | 1.15 | 0.61 | 1.09 | 0.64 | 0.71 | 0.63 | 0.68 | 0.75 | 0.63 | 0.77 | 0.59 |
| Ni/Co | 4.53 | 2.97 | 1.39 | 2.17 | 1.42 | 2.70 | 1.94 | 2.56 | 2.56 | 1.68 | 2.29 | 2.16 | 2.39 |
| V/Cr | 1.06 | 1.02 | 1.64 | 0.81 | 1.10 | 0.71 | 0.81 | 0.86 | 0.73 | 0.67 | 0.74 | 0.80 | 1.36 |

and >1.0 are indicative of freshwater, brackish water, and saline water, respectively (Deng, 1993; Liu et al., 2007). The values of the Sr/Ba ratio of the Gulcheru shale vary from 0.24 to 0.78, which demonstrate the impact of marine transgression restriction with fresh water dominance (Kuscu et al., 2016).

The concentrations of Ba range between 467 ppm to 4923 ppm and shows a positive correlation with $K_2O$ (Table 3). These Ba concentrations can be treated as a proxy of detrital flux (Liguori et al., 2016). Gulcheru shale samples show overall enrichment in Ba. The Gulcheru shale samples are depleted in $Na_2O$, Rb and Sr and generally mildly enriched in $K_2O$ relative to the modelled mixture (Fig. 8b), which indicates intense weathering and little Na–K metasomatism (Wang & Zhou, 2013).

### 5.4 Rare earth element concentrations

REE concentrations of the Gulcheru Shales show a range between 82.99 and 158.71 ppm with an average 112.04 ppm. The concentration of the light earth elements (LREEs = La + Ce + Pr + Nd) is higher than that of the heavy earth elements (HREEs = Ho + Er + Tm + Yb + Lu) and middle earth elements (MREEs = Sm + Eu + Gd + Tb + Dy). The average of 12 samples of the REE, LREE, MREE and HREE values are 112.04, 98.76, 9.29 and 3.99 ppm individually (Table 5). All the samples demonstrate a negative Eu anomaly. The chondrite normalized REE plot (Fig. 8c) of Gulcheru shale samples show moderately inclined LREE (La–Nd part) and nearly flat HREE (Ho-Lu part) pattern with negative Eu anomaly (Fig. 8c). Similarly, Granodiorite and Tonalite show similar chondrite normalized REE and LEE pattern (Fig. 8d). The Gulcheru shales have similar values of $La_N/Yb_N$ (~18.30), $La_N/Sm_N$ (~9.07), $Ce_N/Yb_N$ (~31.34) and Eu/Eu*(~0.73) as compared to PAAS values (Taylor & McLennan, 1985), and depleted value of $Gd_N/Yb_N$ (~2.60).

### 5.5 Effects of weathering, sorting and recycling

The degree of weathering of the source rock depends on the factors such as paleo-climate and properties of the source rocks. The quantitative evaluation of weathering level of source area recorded in sediments can be determined by the CIA (Nesbitt & Young, 1982), PIA (Fedo et al., 1995), ICV (Cox et al., 1995) and CIW (Harnois, 1988).

The CIA values (Fig. 9) for the analysed shales have values ranging from 61to 73. The CIA values of the analyzed rocks indicate moderate chemical weathering in the source area (Khan et al., 2019). The high PIA value represents 100 (Kaolinite, gibbsite) denote intense weathering whereas the value of 50 suggests unweathered plagioclase. Gulcheru Formation clastic sediments show PIA values ranging from 93. to 94, which indicate intense weathering of the source rock.

The ICV values are an indicator of the original composition of the source rock. ICV values of Gulcheru Formation shales vary from 0.68 to 3.12. Lower values of ICV indicate abundance in less weathered detrital minerals. These materials were probably derived from the source area with high relief (Armstrong-Altrin et al., 2012, 2017; Cox et al., 1995). On the other hand, higher values indicate enrichment

**Table 5** REE concentration (ppm) for shales of the Gulcheru Formation, Cuddapah Basin with average composition of PAAS (Taylor & McLennan, 1985)

| | KM-1 | M-1 | M-2 | M-3 | KU-2 | KU-3 | KU-4 | KU-5 | M-4 | KU7 | M-5 | KU10 | PAAS (Taylor & McLennan, 1985; McLennan, 2001) |
|---|---|---|---|---|---|---|---|---|---|---|---|---|---|
| La | 31.20 | 40.01 | 13.30 | 22.31 | 30.60 | 33.05 | 32.82 | 40.22 | 22.54 | 24.09 | 21.58 | 22.97 | 38.00 |
| Ce | 54.94 | 69.69 | 30.44 | 35.35 | 49.01 | 52.59 | 59.52 | 65.34 | 38.03 | 39.76 | 37.82 | 40.69 | 79.60 |
| Pr | 5.89 | 7.68 | 3.54 | 3.73 | 5.21 | 5.57 | 6.57 | 7.39 | 4.28 | 4.34 | 4.59 | 4.73 | 8.83 |
| Nd | 18.93 | 25.25 | 14.26 | 12.24 | 17.04 | 18.01 | 22.17 | 24.61 | 14.52 | 14.54 | 15.97 | 16.17 | 33.90 |
| Sm | 2.89 | 4.05 | 3.56 | 2.08 | 3.24 | 3.02 | 3.63 | 4.46 | 2.57 | 2.41 | 2.55 | 2.82 | 5.55 |
| Eu | 0.58 | 0.84 | 0.90 | 0.45 | 0.88 | 0.88 | 0.72 | 0.93 | 0.60 | 0.50 | 0.46 | 0.59 | 1.08 |
| Gd | 2.34 | 3.35 | 3.45 | 1.84 | 3.00 | 2.64 | 3.07 | 3.90 | 2.16 | 1.93 | 1.96 | 2.41 | 4.66 |
| Tb | 0.37 | 0.53 | 0.60 | 0.31 | 0.55 | 0.45 | 0.48 | 0.68 | 0.37 | 0.31 | 0.29 | 0.41 | 0.77 |
| Dy | 1.99 | 2.74 | 3.08 | 1.69 | 3.02 | 2.40 | 2.56 | 3.72 | 1.96 | 1.69 | 1.49 | 2.15 | 4.48 |
| Ho | 0.42 | 0.59 | 0.59 | 0.36 | 0.63 | 0.49 | 0.56 | 0.77 | 0.40 | 0.37 | 0.31 | 0.45 | 0.99 |
| Er | 1.31 | 1.71 | 1.66 | 1.10 | 1.87 | 1.48 | 1.78 | 2.26 | 1.19 | 1.16 | 0.92 | 1.30 | 2.85 |
| Tm | 0.19 | 0.24 | 0.24 | 0.16 | 0.27 | 0.21 | 0.26 | 0.32 | 0.17 | 0.17 | 0.13 | 0.19 | 0.41 |
| Yb | 1.45 | 1.75 | 1.75 | 1.16 | 1.99 | 1.56 | 1.91 | 2.27 | 1.24 | 1.32 | 0.91 | 1.35 | 2.82 |
| Lu | 0.24 | 0.27 | 0.28 | 0.19 | 0.32 | 0.25 | 0.32 | 0.36 | 0.20 | 0.22 | 0.14 | 0.21 | 0.43 |
| ∑REE | 122.71 | 158.71 | 77.64 | 82.99 | 117.61 | 122.59 | 136.37 | 157.23 | 90.25 | 92.81 | 89.12 | 96.45 | 184.37 |

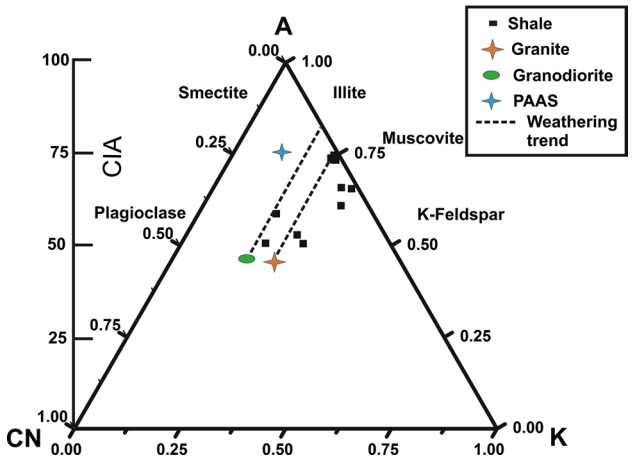


**Fig. 9** Major element compositions of Gulcheru shale samples in molecular proportion triangular diagram of $Al_2O_3$–($Na_2O_3$ + $CaO^*$)–$K_2O$ with the Chemical Index of Alteration (CIA) and Chemical Index of Weathering (CIW) scales shows the idealized weathering trend (after Fedo et al., 1995)

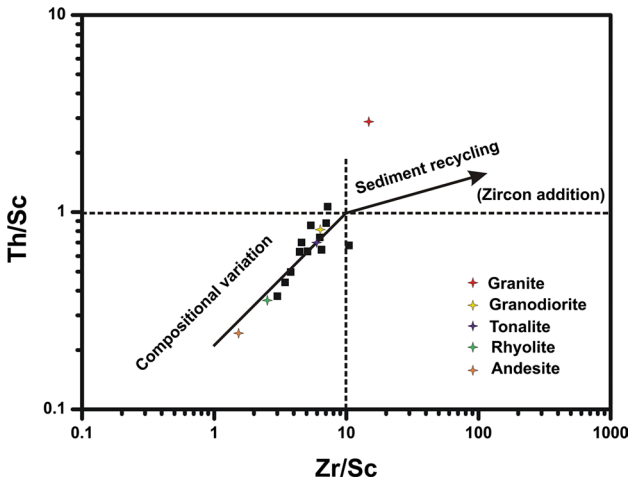


**Fig. 10** Th/Sc versus Zn/Th plot (after McLennan et al., 1993) showing sedimentary sorting for Gulcheru Formation sedimentary rocks. The data on average rock compositions (granodiorite, tonalite, rhyolite, and andesite) are defined from Condie, (1993)

of pyroxene and feldspar (non-clayey minerals) in the source rock (Depetris et al., 2014; Pasquini et al., 2017).

The CIW show values of 80 for un-weathered potassic granite and near to 100 value for clay minerals such as Kaolinite, illite and Gibbsite. The CIW (Fig. 10) value of the Gulcheru shale samples ranges from 95.25 to 98.52 (average 97.20), which indicate an intense weathering of the source rock.

The $Al_2O_3$–($CaO^*$+$Na_2O$)–$K_2O$ (A-CN-K) ternary diagram (Nesbitt & Young, 1984) is an imperative outline that is utilized to demonstrate the weathering attributes of clastic sedimentary rocks. The best possible weathering trend in A-CN-K diagram is indicated by the parallel line to A-CN side. For these Gulcheru Formation shale samples, weathering trend starts from granite (Fig. 9) and from the further weathering continue, the direction advances close to the illite composition (Fedo et al., 1995). Gulcheru shale samples mainly fall on the $Al_2O_3$–$K_2O$ connection line, which is related to illite composition, demonstrating an intense degree of weathering of the source rock (Hessler & Lowe, 2006). Since the pattern of the data does not end on the CN-K line of the A-CN-K diagram where normal groundwater composition lies, this allows us infer that the K—metasomatism shows a critical influence on the formation of the Gulcheru meta-sedimentary rocks (Li et al., 2007; McLennan et al., 1993). Gulcheru shales plot near to A-K line (Fig. 9) with critically high $K_2O$ content; it is a strong indicator of late potassium metasomatism (Li et al., 2015).

Gulcheru Formation has been affected by low grade (green schist facies) and low-grade deformation. The coherent behaviour of U and Th metamorphism is manifested in the rocks by Th/U ratio ranges between 1.44 and 4.28, which is essentially lower than the upper amphibolite facies rocks. This shows that there is no preferential leaching of U during metamorphic dehydration processes (Camire et al., 1993; Li et al., 2008). The possible alteration effects of metamorphism and deformation can further be elucidated from the Harker variation diagrams (Fig. 4) where $SiO_2$ is compatible and positively correlated with $Al_2O_3$, $TiO_2$, $Na_2O$ and $K_2O$ and negatively correlated with MnO, $Fe_2O_3$, CaO, MgO and $P_2O_5$. The low value of $SiO_2$ however might be ascribed to chemical destruction under oxidising states of the source area.

Bivariate plot Th/Sc vs Zr/Sc (Fig. 10) can measure the amount of sedimentary process of sorting and recycling (McLennan et al., 1993). Thorium is enriched in silicic rocks rather than basic rocks whereas Scandium shows more enrichment in basic rocks rather than silicic rocks. The ratio Th/Sc does not vary significantly during sedimentary recycling processes (Cullers, 1995). But, the Zr/Sc proportion will increase gradually during the sediment recycling. So the values of Zr/Sc are useful indicator of zircon enrichment (McLennan, 1989). The Gulcheru Formation clastic sedimentary rocks show variable Th/Sc (0.37–1.06) and Zr/Sc (3.00–10.46) ratio (Table 4). Despite the fact that these rocks have distinctive Th/Sc and Zr/Sc values, they show a solid positive relationship in the Th/Sc–Zr/Sc diagram (Fig. 10). This indicates geochemical variation dominated by the composition of the source materials but not sediment recycling (Cullers, 1995; Li et al., 2015).

### 5.6 Provenance

Geochemical data of clastic sediments is an important tool to characterize the source rock (Cullers, 2000; Mongelli et al.,

1996). Chondrite normalized REE pattern of the Gulcheru shale shows a similar pattern to granodiorite (Jayananda et al., 2000) and tonalite (Allen, 1985) of the Eastern Dharwar Craton (Fig. 9). So it indicates that Gulcheru shale samples should be derived from the mixing of granodiorite and tonalite. As the basement of Cuddapah Group of rocks is the Eastern Dharwar Craton, granodiorite and tonalite of the Eastern Dharwar Craton are possibly considered to be the parent rocks of the Gulcheru Formation (Mitra et al. 2018).

The $SiO_2/Al_2O_3$ ratios a significant tool for indicating the maturity of the sediments (Roser et al., 1996). Gulcheru Formation clastic sedimentary rocks show $SiO_2/Al_2O_3$ ratio ranging between 2.14 and 6.17 (average 4.39), which indicates the presence of mature sediments and quartz enrichment in the source rock (Babu, 2017).

The ratio of $Al_2O_3/TiO_2$ in clastic sediments is generally utilized to depict the character of provenance (Hayashi et al., 1997; Sun et al., 2013). The $Al_2O_3/TiO_2$ ratios vary from mafic (3–8), intermediate (8–21) to felsic (21–70) igneous rocks (Hayashi et al., 1997; Sun et al., 2013). In Gulcheru shale samples, $Al_2O_3/TiO_2$ ratio (Fig. 11a) varies between 22.32 and 33.72 (average of 26.33). In the binary diagram $Al_2O_3$ versus $TiO_2$ (Amajor, 1987) for Gulcheru shale samples (Fig. 11a) are represents the granite field and indicates a felsic source rock for these sediments. Taking into account that $Al_2O_3$ residing in feldspars and $TiO_2$ in mafic minerals, the $Al_2O_3/TiO_2$ ratio of the Gulcheru shales indicates lower $TiO_2$ values than the PAAS (Taylor & McLennan, 1985). This fact strongly indicates the presence of felsic material in the source rock. Gulcheru clastic sediments present high $K_2O/Na_2O$ ratio values (22.90–108.83), which suggests enrichment of feldspar, illite and mica in the source rock (Crook, 1974).

The ternary diagram $K_2O$–$Fe_2O_3$–$Al_2O_3$ (Fig. 7) shows all the shale samples plotted near the $Al_2O_3$ apex, which indicates enrichment of $Al_2O_3$ in the parent rock (Wronkiewicz & Condie, 1987). The $K_2O/Al_2O_3$ proportions of shale samples are useful to understand the original composition of the source rock. The $K_2O/Al_2O_3$ ratio of Gulcheru shale ranges from 0.31 to 0.53 (average 0.39). These proportions indicate the feldspar dominance in the parent body. Additionally $TiO_2$/Ni bivariate diagram (Fig. 11b; Floyd et al., 1989), also indicates that Gulcheru clastic sediments are mainly derived from felsic source rocks. Zr versus $TiO_2$ bivariate plot (Fig. 11c) also demonstrates the felsic source of the Gulcheru sediments.

Chromium and Ni concentrations in siliciclastic rocks are important for the investigation of provenance. In Gulcheru clastic sediments, Cr/Ni ratio varies from 1.9 to 3.5. These values also indicate the felsic provenance of the Gulcheru shales. The triangular plot of $K_2O$–$Fe_2O_3$–$Al_2O_3$ (Fig. 7) of Gulcheru shales suggests derivation from felsic rocks of granite composition.

The REE and Eu anomaly is also a very important tool for delineation of parent rock (Tapia-Fernandez et al., 2017). The Gulcheru clastic sediments show high LREE/HREE values (average 24.74) (Table 4) and negative Eu anomaly pointing towards felsic source for the sediments.

## 5.7 Tectonic setting

Elemental geochemistry of the clastic sediments gives imperative data about structural setting of the parent rock (Armstrong-Altrin & Verma, 2005; Armstrong-Altrin et al., 2017; Bhatia, 1983; Ramakrishnan & Vaidyanadhan, 2008). The discrimination plot of La–Th–Sc and Th–Sc–Zr/10 shows that all of the Gulcheru Formation clastic sediments fall within the continental Island Arcs field (Fig. 12a and b). The sedimentary rock deposited on this continental arc setting is characterised by high LREE/HREE with negative Eu anomaly on chondrite normalized plots. These results are very well correlated with modern geological interpretations about the amalgamation of Columbia Supercontinent (~2 Ga), which clearly states that Papaghni back arc extensional basin (Gulcheru Formation) was formed due to the subduction of the oceanic crust underneath the Dharwarian Craton (Absar et al., 2016).

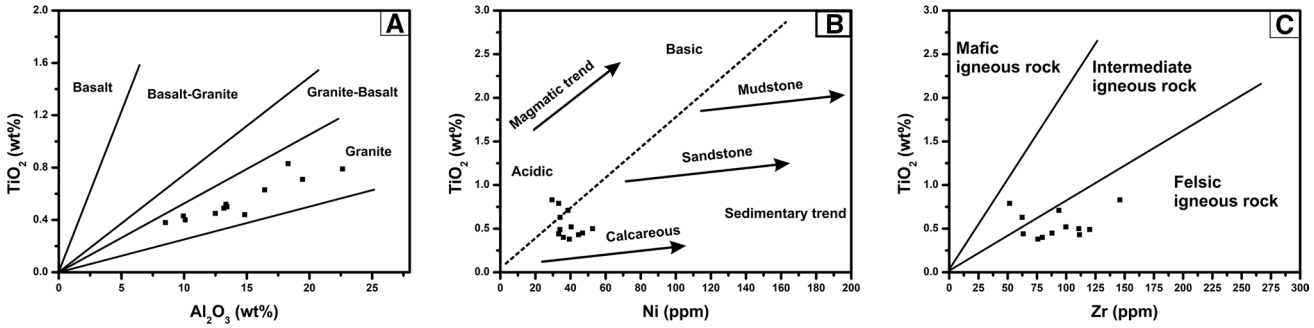


**Fig. 11** Scatter plots of **a** $Al_2O_3$ versus $TiO_2$; **b** Ni versus $TiO_2$; **c** Zr versus $TiO_2$for linear provenance indicators for shale samples from Gulcheru Formation

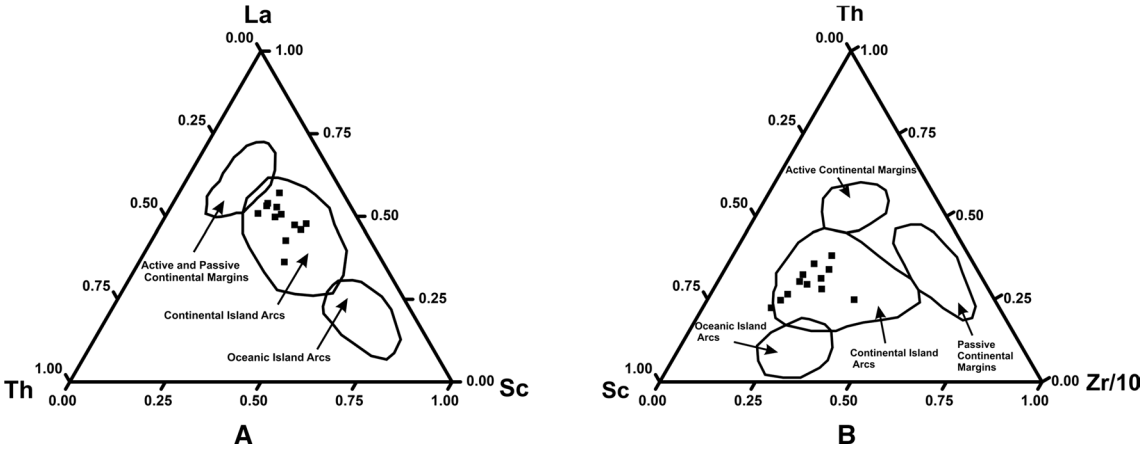


**Fig. 12** Discrimination plots **a** La–Th–Sc and **b** Th-Sc–Zr/10 for tectonic settings (Bhatia & Crook, 1986) for siliciclastic sediments of Gulcheru Formation

## 5.8 Paleo-environment and paleo-climate

The redox conditions of clastic sediment formation are analysed with the help of some geochemical parameters. Some redox-sensitive metals, such as U, Th, V, Ni, Cu, Zn and Cr in clastic sediments gives powerful information about paleoredox condition (Madhavaraju & Ramasamy, 1999). Element proportions, for example, U/Th, Cu/Zn, Ni/Co and V/Cr, have been utilized to assess paleoredox condition (Tribovillard et al., 2006).

Low U content is an indicator of sediments deposited in an oxidising environment, whereas a high concentration of U implies the deposition in the oxygen minimum zone (Armstrong-Altrin et al., 2015; Ramos-Vazquez et al., 2017). So low U concentrations (average 3.59 ppm) of the Gulcheru clastic sediment indicate an oxidizing depositional environment. As weathering increases, U is generally lost due to oxidization.

In addition, low U/Th values (< 1.25) demonstrate oxidising depositional environment and high U/Th values (> 1.25) indicate suboxic to anoxic environmental condition (Nath et al., 1997). The Gulcheru shale samples have U/Th values lower than 1.25 (ranging from 0.22 to 0.69), which indicate oxic depositional conditions (Jones & Manning, 1994). The values of the ratio Cu/Zn also demonstrate depositional conditions of clastic sediment (Pandey et al., 2019). For clastic sediments, high Cu/Zn ratios suggest reducing environment and low Cu/Zn ratios indicate oxidising environment (Hallberg, 1976). In Gulcheru Formation shales the Cu/Zn ratios vary from 0.51 to 1.15 (average 0.74). These values indicate oxic condition during deposition. But wide ranges of this ratio indicate the change in bottom water conditions from oxic to sub-oxidising depositional environment (Mitra et al. 2018).

Major oxides also play an important role in paleo-environmental studies (srivastava & Singh, 2018). The $SiO_2$ versus ($Al_2O_3$ + $Na_2O$ + $K_2O$) diagram (Fig. 13a; Suttner & Dutta, 1986) of the Gulcheru shale samples indicates a semi-arid to arid domain suggesting their depositional climatic condition.

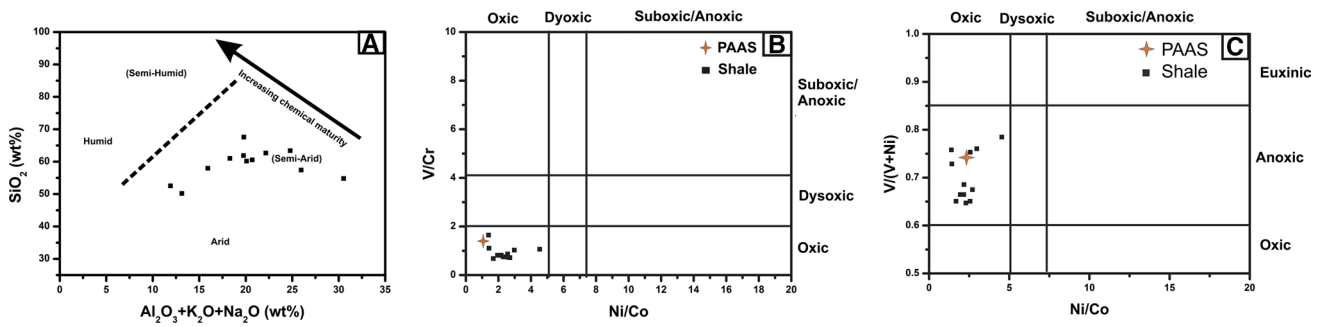


**Fig. 13** Paleo-environment of Gulcheru shales **a** bivariate plot of $SiO_2$ versus ($Al_2O_3 + K_2O + Na_2O$) to discriminate paleo-climatic condition of the Gulcheru sediments (after Suttner & Dutta, 1986); **b** binary plot of Ni/Co versus V/Cr indicates oxic condition during deposition and **c** binary plot of Ni/Co versus V/(V + Ni) indicates oxic to anoxic condition during deposition

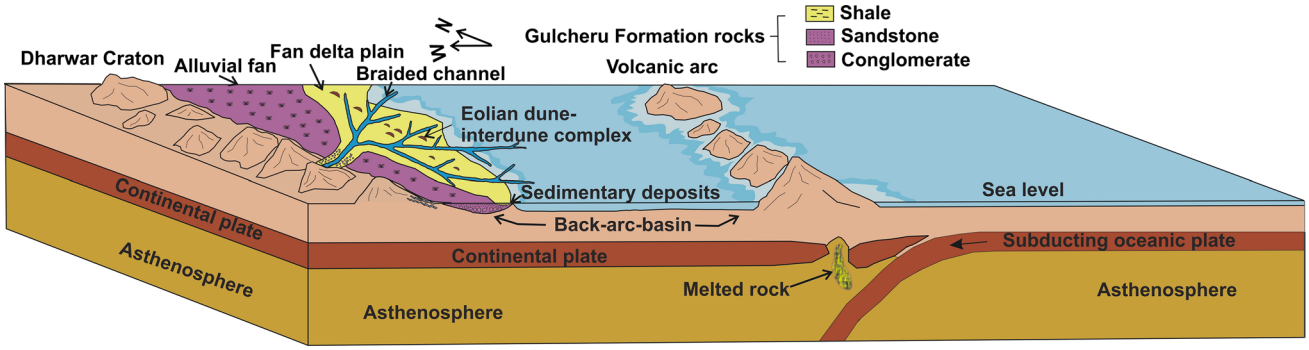


**Fig. 14** Depositional architecture showing a generalised depositional model of Gulcheru Formation rocks, Cuddapah Basin, India

According to Jones and Manning (1994), values of the Ni/Co ratio < 5 represent oxic condition, 5–7 dyoxic condition and > 7 are associated with anoxic to suboxic environmental condition. In Gulcheru shale samples, Ni/Co ratios vary from 1.4 to 4.5, which suggest an oxic depositional condition. In addition, these authors suggested that V/Cr ratios: > 4.25 imply suboxic to anoxic environment; between 2.00 and 4.25 are related to dyoxic condition and; < 2.00 indicate oxic environments. The V/Cr values of Gulcheru shale samples ranging from 0.67 to 1.64 (average 0.9) show oxic condition during deposition. So,V/Cr vesus Ni/Co ratio (Fig. 13b) of Gulcheru shale samples suggest an oxic environment and the Ni/Co versus V/(V+Ni) ratio (Fig. 13c) suggests an oxic to slightly anoxic depositional condition for Gulcheru clastic sediments.

In summary, the following picture (Fig. 14) may emerge from our studies on geochemistry of Gulcheru Formation shale. The Gulcheru clastic sediments were eroded from mixed source rocks of granite, granodiorite and tonalite (felsic igneous rocks) of Eastern Dharwar Craton (EDC) of southern India during late Paleoproterozoic time. These sediments were deposited in a marginal marine environment under continental island arc setting during the process of amalgamation of supercontinent Columbia. This back-arc extensional basin was formed due to the subduction of oceanic crust underneath the Dharwar Craton. The sediments were deposited mostly in an oxic environment under arid to semi-arid condition. The depositional set-up changed occasionally due to fluctuation of sea-level during the post-Archean time.

## 6 Conclusions

1. The Gulcheru Formation rocks were deposited prior to the amalgamation of the Supercontinent Columbia.
2. The discrimination plot La–Th–Sc and Th–Sc–Zr/10 suggest that the Gulcheru Formation rocks were deposited in continental Island arc setting.
3. The $Al_2O_3$ versus $TiO_2$ plot, Ni versus $TiO_2$ plot, Zr versus $TiO_2$ plot, REE pattern and elemental ratio of La, Th, Sc and Co calculated from geochemical data indicates that the Gulcheru clastic sediments are derived from mixed source rocks of granite, granodiorite and tonalite of Eastern Dharwarian Craton (EDC).
4. Some redox-sensitive metal (U, Th, V, Co and Cr) ratios indicate that the Gulcheru clastic sediments were deposited under oxic environmental condition. But wide ranges of Cu/Zn ratios suggest change in depositional setup due to sea level fluctuation in Post Archean time.
5. $SiO_2$ versus $(Al_2O_3 + K_2O + Na_2O)$ ratio indicate an arid to semi-arid environment during deposition of Gulcheru Formation rocks.

**Acknowledgements** Financial assistance was provided by University Grant Commission [Grant no-5-44/2007(BSR)]. Authors are also grateful to the Department of Science and Technology, Government of India, for their financial support for grant no PURSE (Phase II) F4/SC/20/15. The authors are thankful to Jadavpur University, Kolkata for providing infrastructural support. All authors express their profound thanks to the NGRI, Hyderabad particularly C. Manikyamba, senior principal scientist, NGRI for analytical support of ICP-MS study. All the authors are also grateful to the Geological Survey of India, Kolkata and XRF Laboratory, NCESS, Akkulam, Thiruvananthapuram particularly N. Nishanth, Scientific Assistant, NCESS for their analytical support.

## References

Absar, N., Nizamudheen, B. M., Augustine, S., Managave, S., & Balakrishnan, S. (2016). C, O, Sr and Nd isotope systematics of carbonates of Papaghni sub-basin, Andhra Pradesh, India: Implications for genesis of carbonate-hosted stratiform uranium mineralisation and geodynamic evolution of the Cuddapah basin. *Lithos, 263*, 88–100 (In this issue).

Allen, P. (1985). The geochemistry of the Amphibolite-Granulite facies transition in Central South India (Ph.D. thesis). New Mexico Institute of Mining and Technology, Socorro, New Mexico, USA.

Amajor, L. C. (1987). Major and trace element geochemistry of Albian and Turonianshales from the Southern Benue trough, Nigeria. *Journal of African Earth Sciences, 6*, 633–641

Anand, M., Gibson, S. A., Subbarao, K. V., Kelley, S. P., & Dickin, A. P. (2003). Early proterozoic melt generation processes beneath the intra cratonic Cuddapah basin, Southern India. *Journal of Petrology, 44*, 2139–2171

Armstrong-Altrin, J. S., & Verma, S. P. (2005). Critical evaluation of six tectonic setting discrimination diagrams using geochemical data of Neogene sediments from known tectonic setting. *Sedimentary Geology, 177*, 115–129

Armstrong-Altrin, J. S., Verma, S. P., Madhavaraju, J., & Ramaswami, S. (2004). Geochemistry of sandstones from the Upper Miocene Kudankulam Formation, Southern India: Implications for provenance, weathering and tectonic setting. *Journal of Sedimentary Research, 74*(2), 285–297

Armstrong-Altrin, J. S., Lee, Y. I., Kasper-Zubillaga, J. J., Carranza-Edwards, A., Garcia, D., Eby, N., Balaram, V., & Cruz-Ortiz, N. L. (2012). Geochemistry of beach sands along the western Gulf of Mexico, Mexico: Implication for provenance. *Chemie der Erde Geochemistry, 72*, 345–362

Armstrong-Altrin, J. S., Machain-Castillo, M. L., Rosales-Hoz, L., Carranza- Edwards, A., Sanchez-Cabeza, J. A., & Ruíz-Fernández, A. C. (2015). Provenance and depositional history of continental slope sediments in the Southwestern Gulf of Mexico unraveled by geochemical analysis. *Continental Shelf Research, 95*, 15–26

Armstrong-Altrin, J. S., Lee, Y. I., Kasper-Zubillaga, J. J., & Trejo-Ramirez, E. (2017). Mineralogy and geochemistry of sands along the Manzanillo and El Carrizal beach areas, Southern Maxico: Implications for palaeoweathering, provenance and tectonic setting. *Geological Journal, 52*(4), 559–582

Babu, K. (2017). Geochemical characteristics of sandstones from Cretaceous Garudamangalam area of Ariyalur, Tamilnadu, India: Implications of provenance and tectonic setting. *Journal of Earth System Science, 126*(3), 45

Bhatia, M. R. (1983). Plate tectonics and geochemical composition of sandstones. *The Journal of Geology, 91*, 611–627

Bhatia, M. R., & Crook, K. A. W. (1986). Trace element characteristics of graywackes and tectonic setting discrimination of sedimentary basins. *Contributions to Mineralogy and Petrology, 92*, 181–193

Camire, M. E., Zhao, J., & Violette, D. A. (1993). In vitro binding of bile acids by extruded potato peels. *Journal of Agricultural and Food Chemistry, 41*, 2391–2394

Chakrabarti, G., & Shome, D. (2007). Reworked diamictite accumulation as debris flow in aqueous medium—an example from late Palaeoproterozoic basal Gulcheru Formation, Cuddapah Basin, India. *Himalayan Geology, 28*, 87–98

Chakrabarti, G., & Shome, D. (2010). Interaction of microbial communities with clastic sedimentation during Palaeoproterozoic time—an example from basal Gulcheru Formation, Cuddapah basin, India. *Sedimentary Geology, 226*, 22–28

Chakrabarti, G., Shome, D., Bauluz, B., & Sinha, S. (2009). Provenance and weatheringhistory of Mesoproterozoicclastic sedimentary rocks from the basal GulcheruFormation, Cuddapah basin, India. *Geological Society of India, 74*, 119–130

Chakrabarti, G., Eriksson, P. G., & Shome, D. (2015). Chapter 17 sedimentation in the Papaghni group of rocks in the Papaghni sub-basin of the Proterozoic Cuddapah Basin, India. *Geological Society London Memoirs, 43*(1), 255–267

Condie, K. C. (1993). Chemical composition and evolution of the upper continental crust: Contrasting results from surface samples and shales. *Chemical Geology, 104*(1–4), 1–37

Cox, R., Lowe, D. R., & Culleres, R. L. (1995). The influence of sediment recycling and basement composition on evolution of mudrock chemistry in the SW rn United States. *Geochemica Cosmochimica Acta, 59*(14), 2919–2940

Crichton, J. G., & Condie, K. C. (1993). Trace elements as source indicators in cratonic sediments: a case study from the Early Proterozoic Libby Creek Group, Southeastern Wyoming. *Journal of Geology, 101*(1993), 319–332

Crook, K. A. W. (1974). Lithogenesis and geotectonics: The significance of compositional variation in flyscharenites (greywackes). *Society of Economic Paleontologists Mineralogy Special Publications, 19*, 304–310

Cullers, R. L. (1995). The controls on major and trace element evolution of shales, siltstones, and sandstones of Ordovician to Tertiary age in the Wet Mountains region, Colorado, USA. *Chemical Geology, 123*, 107–131

Cullers, R. L. (2000). The geochemistry of shales, siltstones and sandstones of Pennsylvanian-Permian age, Colorado, USA: Implications for provenance and metamorphic studies. *Lithos, 51*, 181–203

Deng, P. (1993). The application of trace amount of elements in the exploration of oil and gas. *Petroleum Exploration and Development, 20*, 27–32 In Chinese with English abstract.

Depetris, P. J., Pasquini, A. I., & Lecomte, K. L. (2014). *Weathering and the riverine denudation of continents*. (p. 95). Springer.

Drury, S. A. (1984). A Proterozoic intracratonic basin, Dyke Swarms and thermal evolution in Southern India. *Journal of the Geological Society of India, 25*(7), 437–444

Fedo, C. M., Nesbitt, H. W., & Young, G. M. (1995). Unraveling the effects of potassium metasomatism in sedimentary rocks and paleosols, with implications for paleoweathering conditions and provenance. *Geology, 23*, 921–924

Floyd, P. A., Winchester, J. A., & Park, R. G. (1989). Geochemistry and tectonic setting of Lewisian clastic metasediments from the Early Proterozoic Loch MareeGroup of Gairloch, NW Scotland. *Precambrian Research, 45*, 203–214

Hallberg, R. O. (1976). A geochemical method for investigation of paleo redox conditions in sediments. *Ambio Special Report, 4*, 139–147

Harnois, L. (1988). The CIW index: a news index of weathering. *Sedimentary Geology, 55*, 319–322

Hayashi, K. I., Fujisawa, H., Holland, H. D., & Ohmoto, H. (1997). Geochemistry of ~ 1.9 Ga sedimentary rocks from northeastern Labrador, Canada. *Geochimica Cosmochimica Acta, 61*(19), 4115–4137

Herron, M. M. (1988). Geochemical classification of terrigenous sands and shales from core or log data. *Journal of Sedimentary Research, 58*(5), 820–829

Hessler, A. M., & Lowe, D. M. (2006). Weathering and sediment generation in the Archean: An integrated study of the evolution of siliciclastic sedimentary rocks of the 3.2 Ga Moodies Group, Barberton Greenstone Belt, South Africa. *Precambrian Research, 151*, 185–210

Hossain, I., Roy, K. K., Biswas, P. K., Alam, M., Moniruzzaman, M., & Deeba, F. (2014). Geochemical characteristics of Holocene sediments from Chuadanga district, Bangladesh: Implications for weathering, climate, redox conditions, provenance and tectonic setting. *Chinese Journal of Geochemistry, 33*(4), 336–350

Jain, S. C., Nair, K. K. K., & Yedekar, D. B. (1995). Tectonic evolution of the Son–Narmada–Tapti lineament zone. *Project Crumansonata Special Publications, 10*, 333–371

Jayananda, M., Moyen, J. F., Martin, H., Peucat, J. J., Auvray, B., & Mahabaleswar, B. (2000). Late Archaean (2550–2520 Ma) juvenile magmatism in the Eastern Dharwar Craton, Southern India: constraints from geochronology, Nd–Sr isotopes and whole rock geochemistry. *Precambrian Research, 99*, 225–254

Jones, B., & Manning, D. A. C. (1994). Comparison of geochemical indices used for the interpretation of palaeoredox conditions in ancient mudstones. *Chemical Geology, 111*(1–4), 111–129

Khan, T., Sarma, D. S., Somasekhar, V., Ramanaiah, S., & Reddy, N. R. (2019). Geochemistry of the Palaeoproterozoic quartzites of Lower Cuddapah Supergroup, South India: Implications for the

palaeoweathering, provenance, and crustal evolution. *Geological Journal, 55*, 1587–1611

Kuscu, M., Ozsoy, R., Ozcelik, O., Altunsoy, M. (2016). Trace and rare earth element geochemistry of black shales in Triassic Kasimlar formation, Anamas-Akseki platform, Western Taurids, Turkey. I : IOP conference series earth and environmental sciences.

Li, Q., Liu, S., Wang, Z., Chu, Z., Song, B., Wang, Y., & Wang, T. (2007). Contrasting provenance of Late Archean metasedimentary rocks from the Wutai Complex, North China Craton: detrtal zircon U–Pb, whole-rock Sm–Nd isotope, and geochemical data. *International Journal of Earth Sciences, 2008*(97), 443–458

Li, Z. L., Yang, S. F., Chen, H. L., Langmuri, C. H., Yu, X., & Lin, X. B. (2008). Chronology and geochemistry of Taxinan basalts from the Tarim Basin: Evidence for Permian plume magmatism. *Acta Petrologica Sinica, 24*, 959–970 In Chinese with English abstract.

Li, Z., Chen, B., Wei, C., Wang, C., & Han, W. (2015). Provenance and tectonic setting of the Pa;eoproterozoic metasedimentary rocks from the Liaohe Group, Jiao-Liao-Ji Belt, North China Craton: Insights from detrital zircon U-Pb geochronology, whole-rock Sm-Nd isotopes, and geochemistry. *Journal of Asian Earth sciences, 111*(2015), 711–732

Liguori, B. T. P., Almeida, M. G. D., & Rezende, C. E. D. (2016). Barium and its importance as an indicator of (Paleo) productivity. *Anais Da Academia Brasileira de Ciências, 88*(4), 2093–2103

Liu, J., Sitaram, A., & Burd, C. G. (2007). Regulation of copper-dependent endocytosis and vacuolar degradation of the yeast copper transporter, Ctr1p, by the Rsp5 ubiquitin ligase. *Traffic, 8*(10), 1375–1384

Long, X. P., Yuan, C., Sun, M., Safonova, I., Xiao, W. J., & Wang, Y. J. (2012). Geochemistry and U–Pb detrital zircon dating of Paleozoic greywackes in Junggar, NW China: Insights into subduction accretion processes in the southern Central Asian Orogenic Belt. *Gondwana Research, 21*, 637–653

Madhavaraju, J., & Ramasamy, S. (1999). Rare earth elements in limestones of Kallankurichchi formation of Ariyalur group, Tiruchirapalli Cretaceous, Tamil Nadu. *Journal of the Geological Society of India, 54*, 291–301

Matin, A. (2015). Tectonics of the Cuddapah basin and a model of its evolution: A review. *Geological Society London Memoir, 43*(1), 231–254

McLennan, S. M. (1989). Rare earth elements in sedimentary rocks: Influence of provenance and sedimentary processes. *Reviews in Mineralogy and Geochemistry, 24*, 169–200

McLennan, S. M., Hemming, S., McDaniel, D. K., & Hanson, G. N. (1993). Geochemical approaches to sedimentation, provenance and tectonics. In M. J. Johnson & A. Basu (Eds.), *Processes controlling the composition of clastic sediments.* (Vol. 284, pp. 21–40). Geological society of America. Special Paper.

Meijerink, A. M. J., Rao, D. P., & Rupke, J. (1984). Stratigraphic and structural development of the Precambrian Cuddapah Basin, S.E, India. *Precambrian Research, 26*, 57–104

Mir, A. R. (2015). Rare earth element geochemistry of Post- to Neoarchean shales from Singhbhum mobile belt, Eastern India: Implications for tectonic setting and paleo-oxidation conditions. *Chinese Journal of Geochemistry, 34*(3), 401–409

Mitra, R., Chakrabarti, G. & Shome, D. (2018). Geochemistry of the Palaeo–Mesoproterozoic Tadpatri shales, Cuddapah basin, India: implications on provenance, paleoweathering and paleoredox conditions. Acta Geochim *37*, 715–733. https://doi.org/10.1007/s11631-017-0254-3

Mongelli, G., Cullers, R. L., & Muelheisen, S. (1996). Geochemistry of Late Cretaceous-Oligocenic shales from the Varicolori Formation, southern Apennines, Italy: Implications for mineralogical, grain-size control and provenance. *European Journal of Mineralogy, 8*, 733–754

Murthy, Y. G. K., Rao, V. B., Guptasarma, D., Rao, J. M., Rao, M. N., & Bhattacharji, S. (1987). Tectonic petrochemical and geophysical studies of mafic dike swarms around the Proterozoic Cuddapah Basin, south India. In H. C. Halls & W. Fahrig (Eds.), *Mafic dykes swarms, special paper no. 34.* (pp. 303–316). Geological Association of Canada.

Nagarajan, R., Madhavaraju, J., Nagendra, R., Armstrong-Altrin, J. S., & Moutte, J. (2007). Geochemistry of Neoproterozoicshales of Rabanpalli formation, Bhima basin, Northern Karnataka, SouthernIndia: implications for provenance and paleo-redox conditions. *Revista Mexicana de Ciencias Geológicas, 24*(2), 150–160

Nagarajan, R., Roy, P. D., Jonathan, M. P., Lozano, R., Kessler, F. L., & Prasanna, M. V. (2014). Geochemistry of Neogene sedimentary rocks from Borneo basin, East Malaysia: Paleo-weathering, provenance and tectonic setting. *Chemie Erde Geochemistry, 74*, 139–146

Nath, B. N., Bau, M., RamalingeswaraRao, B., & Rao, C. H. M. (1997). Trace and rare earth elemental variation in Arabian Sea sediments through a transect across the oxygen minimum zone. *Geochimica et Cosmochimica Acta, 61*(12), 2375–2388

Nesbitt, H. W., & Young, G. M. (1982). Early Proterozoic climates and plate motions inferred from major element chemistry of lutites. *Nature, 299*, 715–717

Nesbitt, H. W., & Young, G. M. (1984). Prediction of some weathering trends of plutonic and volcanic rocks based on thermodynamic and kinetic considerations. *Geochimica et Cosmochimica Acta, 48*, 1523–1534

Pandey, S., Parcha, S. K., & Srivastava, P. K. (2019). Petrography and geochemistry of the Neoproterozoic sedimentary rocks from the Batal Formation of Spiti Basin: Implication on provenance. *Arabian Journal of Geosciences, 12*(2), 61

Pascoe, E. H. (1973). A Manual of the Geology of India and Burma, 3rd ed

Pasquini, A. I., Campodonico, V. A., Rouzaut, S., & Giampaoli, V. (2017). Geochemistry of a soil catena developed from loess deposits in a semiarid environment, Sierra Chica de Córdoba, central Argentina. *Geoderma, 295*, 53–68

Patranabis-Deb, S., Saha, D., & Tripathy, V. (2012). Basin stratigraphy, sealevel fluctuations and their global tectonic connections—evidencefrom the Proterozoic Cuddapah basin. *Geological Journal, 47*, 263–283

Raman, P. K., Murty, V. N. (1997). Geology of Andhra Pradesh (Geological Society of India, Bangalore)

Ramakrishnan, M., & Vaidyanadhan, R. (2008). Geology of India, volume 1. Geological Society of India, Bangalore, 556. Determination of tectonic setting of sandstone-mudstone suites using $SiO_2$ content and $K_2O$–$Na_2O$ ratio. *Journal of Geology, 94*, 635–660

Ramos-Vázquez, M., Armstrong-Altrin, J. S., Rosales-Hoz, L., Machain- Castillo, M. L., & Carranza-Edwards, A. (2017). Geochemistry of deepsea sediments in two cores retrieved at the mouth of the Coatzacoalcos river delta, Western Gulf of Mexico, Mexico. *Arabian Journal of Geosciences, 10*(6), 148

Rao, B. K. N., Rajurkar, S. T., Ramalingaswami, G., & Ravindra Babu, B. (1987). Stratigraphy structure and evolution of cuddapah Basin. In B. P. Radhakrishna (Ed.), *Purana Basins of Peninsular India, no. 6.* (pp. 33–86). Geological Society of India.

Roser, B. P., & Korsch, R. J. (1986). Determination of tectonic setting of sandstone-mudstone suites using $SiO_2$ content and $K_2O/Na_2O$ ratio. *The Journal of Geology, 94*(5), 635–650

Roser, B. P., & Korsch, R. J. (1988). Provenance signature of sandstone-mudstone suite determined using discriminant function analysis of major-element data. *Chemical Geology, 67*, 119–139

Roser, B. P., Cooper, R. A., Nathan, S., & Tulloch, A. J. (1996). Reconnaissance sandstone geochemistry, provenance and tectonic setting of the lower Paleozoicterranes of the West Coast and Nelson,

New Zealand, New Zealand. *Journal of Geology and Geophysics, 39*, 1–16

Saha, D., & Tripathy, V. (2012). Palaeoproterozoic sedimentation in the Cuddapah Basin, south India and regional tectonics—a review. In R. Mazumder & D. Saha (Eds.), *Paleoproterozoic of India.* (Vol. 365, pp. 159–182). Geological Society.

Singh, A. P., & Mishra, D. C. (2002). Tectonosedimentary evolution of Cuddapah Basin and Eastern Ghat Mobile belt (India) as Proterozoic Collision: gravity, seismic and geo dynamic constrains. *Journal of Geodynamics, 33*, 249–267

Srivastava, V. K., & Singh, B. P. (2018). Depositional environments and sources for the middle Eocene Fulra Limestone Formation, Kachchh Basin, western India: Evidences from facies analysis, mineralogy, and geochemistry. *Geological Journal, 54*, 62–82

Sun, L., Gui, H., & Chen, S. (2013). Geochemistry of sandstones from the Neoproterozoic Jinshanzhai Formation in northern Anhui Province, China: Provenance, weathering and tectonic setting. *Chinese Journal of Geochemistry, 32*, 95–103

Suttner, L. J., & Dutta, P. K. (1986). Alluvial sandstones composition and paleoclimate, I, framework mineralogy. *Journal of Sedimentary Petrology, 56*, 329–345

Tapia-Fernandez, H. J., Armstrong-Altrin, J. S., & Selvaraj, K. (2017). Geochemistry and U–Pb geochronology of detrital zircons in the Brujas beach sands, Campeche, Southwestern Gulf of Mexico, Mexico. *Journal of South American Earth Sciences, 76*, 346–361

Taylor, S. R., & Mclennan, S. M. (1985). *The continental crust: Its composition and evolution*. (p. 312p). Blackwell.

Taylor, S. R., & Mclennan, S. M. (1995). The geochemical evolution of the continental crust. *Reviews of Geophysics, 33*, 241–265

Tribovillard, N., Algeo, T. J., Lyons, T., & Riboulleau, A. (2006). Trace metals as paleoredox and paleoproductivity proxies: An update. *Chemical Geology, 232*(1–2), 12–32

Wang, W., & Zhou, M. F. (2013). Petrological and geochemical constraints on provenance, paleoweathering, and tectonic setting of the Neoproterozoic sedimentary basin in the eastern Jiangnan orogen, south china. *Journal of Sedimentary Research, 83*, 974–993

Wronkiewicz, D. J., & Condie, K. C. (1987). Geochemistry of Archean shales from the Witwatersrand Supergroup, South Africa: source area weathering and provenance. Geochim Cosmochim Acta *51*, 2401–2416. https://doi.org/10.1016/0016-7037(87)90293-6

Zachariah, J. K., BhaskarRao, Y. J., Srinivasan, R., & Gopalon, K. (1999). Pb, Sr, Nd isotope systematics of uranium mineralized stromatolitic dolomites from the Proterozoic CuddapahSupergroup, south India: Constraints on age and provenance, chem. *Geology, 162*, 49–64